

Università degli Studi di Torino  
Dipartimento di Fisica Teorica

Dottorato di ricerca in Fisica fondamentale, applicata ed  
astrofisica

XIX Ciclo

**Sneutrino phenomenology in  
supersymmetric models:  
relevance as cold dark matter in  
the light of its cosmological and  
detection properties**

Tesi presentata da:

**Chiara Arina**

Relatore

*Prof. Nicolao Fornengo*

Coordinatore del ciclo

*Prof. Stefano Sciuto*

Anni Accademici 2003/04-2004/05-2005/06-2006/07

Settore scientifico-disciplinare di afferenza: FIS/02



# Overview

The main goal of this thesis is the study of the sneutrino phenomenology in the astroparticle physics framework.

Astroparticle physics links the extremely large scales related to cosmology, with the extremely small scales related to particle physics. From a theoretical point of view we want to emphasize the role of particle physics in explaining one of the most enigmatic puzzle of cosmology, the Dark Matter (DM). The evidence for non-baryonic Dark Matter is compelling at all observed astrophysical scales, and may be explained as a relic from the big bang. We need some new physics in order to explain the presence of such very weakly interacting particles. To the theoretically favored particle candidates for non-baryonic dark matter belong axions, supersymmetric particles, kaluza-klein particles and massive neutrinos. One of the possible framework where to look at is Supersymmetry. In supersymmetric models conserving  $R$ -parity, the lightest non standard particle is stable and may provide a good candidates for DM. We wish to consider supersymmetric models where the lightest supersymmetric particle is the scalar neutrino, the superpartner of the neutrino. We investigate its phenomenology relevant both for Cosmology and for relic particle detection.

The particle physics models we explicitly analyze are the Minimal Supersymmetric Standard Model (MSSM) and extensions of it. Since neutrinos have masses, as is now clearly understood by a host of independent and very robust experimental results and theoretical analyses, we will focus our attention on extensions of the MSSM which contain terms in the supersymmetric lagrangian which can drive neutrino masses. Connection between neutrino physics and the phenomenology of sneutrino DM will therefore arise and we will explicitly consider them whenever relevant. The models which we will consider are therefore natural and direct extensions of the minimal supersymmetric model which incorporate at the same time the new physics required to explain two basic problems of astroparticle physics: the origin of neutrino masses and the nature of dark matter. We do not attempt to be totally exhaustive on the type of supersymmetric models. Instead we concentrate on a number of the most direct extension of the MSSM and derive the phenomenology of sneutrino DM thoroughly.

In Chapter 1 we will briefly discuss the astrophysical observations and the strong evidences of DM at all astrophysical scales from experimental data (Sec. 1.2). A short review on the decoupling of particles from the thermodynamical equilibrium in the early Universe will be given in Chapter 2 in the framework of the cosmological standard model. A particular attention will be paid to the calculation of the relic abundance (Sec. 2.4) without approximations for the thermal averaged cross section. Indeed this latter physical quantity is one of the main building blocks of the numerical code (Sec. 2.6) we developed to evaluate the relic abundance for a generic supersymmetric particle.

Supersymmetry will be presented in Chapter 3: Sections from Sec. 3.1 up to Sec. 3.1.3 report a brief introduction on the superfield formalism; we then proceed by presenting the supersymmetric lagrangian (Sec. 3.2), and the soft supersymmetry breaking lagrangian (Sec. 3.4). In the last Sections (from Sec. 3.3 up to Sec. 3.5) we deal with the minimal supersymmetric extension of the Standard Model (MSSM) conserving  $R$ -parity.

The succeeding Chapter 4 is dedicated to the study of the sneutrino phenomenology as a possible candidate of DM. The first Section is dedicated to the standard MSSM sneutrinos (Sec. 4.1). Next the Sections from Sec. 4.2 to Sec. 4.4 are dedicated to non minimal extensions of the MSSM; the introduction of a right-handed neutrino superfield (LR models) induces mixing in the sneutrino sector and modifies the particle phenomenology, leading to new features as a reduction of the sneutrino Z boson coupling, relevant for the cosmological properties. In Sec. 4.3 we introduce a L-number violating term ( $\mathbb{L}$  models) in the minimal supersymmetric lagrangian with a consequent split of the sneutrino mass eigenstates, which alters the coupling to the Z boson and therefore modifies the sneutrino phenomenology; moreover the L-number violating term introduces one loop contributions to the neutrino mass, which results in a relevant constraint for the sneutrino parameter space. Finally we consider an extension of the MSSM with Majorana mass terms for the neutrino and a right handed neutrino superfield. These models (Sec. 4.4) (Maj models) accommodate both Dirac and Majorana masses for the neutrinos via the see-saw mechanism. For all of these models we discuss the sneutrino phenomenology in terms of the new parameters and by keeping a fixed configuration for the rest of the supersymmetric parameter space, whenever relevant. The results for the different models are shown and compared. When the cosmological properties of the sneutrinos are appealing, we go further in the investigation of the supersymmetric model by including a full scan of the supersymmetric parameter space.

The dark matter particles compose the Milky Way halo, so it is worthwhile from the point of view of both cosmology and particle physics, to explore the possibility to detect them. This can be done directly in terrestrial detectors sensitive to the

nuclear recoil caused by the passing wind of dark matter particles. In Chapter 5 we explore this possible type of detection of sneutrinos, both in the case sneutrinos are the dominant component of the dark matter halo, and in the case of subdominant halo component. It is indeed an interesting feature by itself the possibility of detect relic particles from the early Universe by means of various astrophysical signals even though the relic particle does not fully account for the DM content of the Universe. We begin with a general introduction on the direct detection of Weakly Interacting Massive Particles (WIMPs) (in Secs. 5.1 and 5.3). The former section describes the differential detection rate, while the latter briefly mentions the main experiments currently running and the actual status on upper limits and bounds on direct searches. Section 5.2 summarize the main properties of sneutrino nucleus elastic scattering. Our numerical results, compared with the experimental bounds are presented in sections 5.4, 5.5, 5.6 and 5.7 for MSSM, LR,  $\mathcal{L}$  and Majorana models, respectively.

In the last Chapter 6, we examine the indirect signals which can be produced by sneutrino self-annihilation in the galactic halo or inside celestial bodies. The self annihilation of WIMPs in our Galaxy may produce a bunch of particles, such as antimatter, described in Sec. 6.1, gamma rays, analyzed in Sec 6.2 and neutrino fluxes presented in Sec 6.3. Predictions for antiprotons, antideuterons, gamma rays and neutrino fluxes are provided and discussed. The results for the LR models and Majorana supersymmetric models, which are the more interesting models from a cosmological point of view referring to sneutrino phenomenology, are presented in Sec. 6.4.

Conclusively, in Appendix A we report all the interaction vertices related to the sneutrino phenomenology in the MSSM and in the extended supersymmetric models taken into account, while in Appendix B we briefly mention the experimental constraints which we impose on supersymmetric particles and we discuss the parameter choice for the full scan on the supersymmetric parameter space.

# Contents

<b>Overview</b>	<b>i</b>
<b>1 Observational Cosmology</b>	<b>1</b>
1.1 Cosmological Parameters	1
1.2 Observational hints of Dark Matter	4
1.3 Dark Matter Candidates	9
<b>2 Dark Matter Relic Abundance</b>	<b>11</b>
2.1 Standard Cosmological Model	11
2.2 Thermal evolution of the Universe	14
2.3 Boltzmann Equation	19
2.3.1 Freeze out for a non relativistic species	22
2.4 Full thermal averaged cross section	26
2.5 Coannihilation	29
2.6 Numerical Code	31
<b>3 Supersymmetry</b>	<b>35</b>
3.1 Supersymmetric Algebra and Superfields	38
3.1.1 Chiral supermultiplets	41
3.1.2 Gauge supermultiplets	42
3.1.3 Superspace integration	43
3.2 Supersymmetric Lagrangian	44
3.2.1 Scalar Lagrangian	45
3.2.2 Vector Lagrangian	46
3.2.3 Gauge Invariance	46
3.3 R-parity	48
3.4 Supersymmetry Breaking	49
3.5 Minimal Supersymmetric Standard Model	51
3.5.1 Higgs sector	55
3.5.2 Higgsino and gaugino sectors	58
3.5.3 Sfermion sector	61

<b>4</b>	<b>Sneutrino phenomenology and cosmological relic abundance</b>	<b>64</b>
4.1	MSSM sneutrinos	65
4.2	Right-handed sneutrino models	68
4.3	L-number violating sneutrino models	72
4.4	Majorana models: implications in the sneutrino sector	76
4.4.1	TeV scale Majorana mass term	78
4.4.2	Large scale Majorana mass term	79
<b>5</b>	<b>Sneutrino direct detection properties</b>	<b>97</b>
5.1	Detection rate and differential spectrum	98
5.2	Elastic cross-section on nuclei and nucleon	100
5.3	Present experiments and results	103
5.4	MSSM sneutrinos direct detection	105
5.5	Right-handed model direct detection	106
5.6	L number violating sneutrino direct detection	108
5.7	Majorana models and direct detection rates	109
5.7.1	TeV scale Majorana mass term	110
5.7.2	Large scale Majorana mass term	110
<b>6</b>	<b>Sneutrino in the light of indirect dark matter searches</b>	<b>129</b>
6.1	Antiproton and antideuterium signals	129
6.2	Gamma rays	132
6.3	Neutrino flux	133
6.4	Sneutrino in supersymmetric models and indirect detection signals	134
6.4.1	Indirect detection rates in right-handed models	135
6.4.2	Majorana models and indirect detection rates	138
	<b>Conclusions</b>	<b>154</b>
<b>A</b>	<b>Interaction Lagrangians</b>	<b>157</b>
A.1	Scalar leptons–Higgs bosons	157
A.2	Scalar leptons–Gauge boson vectors	160
A.3	Scalar leptons–Fermions	162
<b>B</b>	<b>The supersymmetric model</b>	<b>164</b>
B.1	Scan over the SUSY parameter space	164
B.2	Experimental constraints	164
	<b>Bibliography</b>	<b>178</b>

# Chapter 1

## Observational Cosmology

The central premise of modern cosmology is that, at least on scales larger than 100 Mpc, the Universe is homogeneous and isotropic. This is borne out by a variety of observations, most outstandingly the nearly identical temperature of microwave background radiation (CMB) coming from different parts of the sky. Despite the belief in homogeneity on large scales, it is all too apparent that in nearby regions the Universe is highly inhomogeneous, with matter clumped into stars, galaxies and galaxy clusters. It is widely believed that these irregularities have grown over through gravitational attraction, from a distribution that was more homogeneous in the past. The large scale behavior of the Universe can be described by assuming an homogeneous and isotropic background, over this background we can superimpose the short-scale irregularities.

From a theoretical point of view the dynamics of the background is described by the Big Bang model, based on the Einstein equations, on the Robertson-Walker (RW) metric and on inflationary models. The inhomogeneities can be considered as small perturbations on the evolution of the background Universe [1].

First we will briefly outline the observational status of some fundamental cosmological parameters, describing the global state of the Universe and the matter content of it. Afterwards, we will introduce the main Dark Matter experimental evidences, candidates and constraints. Exhaustive reviews on the subject are e.g. [2, 3, 4].

### 1.1 Cosmological Parameters

The Universe about 15 billion years ago emerged with a distribution of matter at very high temperature and density and has been expanding and cooling down since then. Hubble was measuring the galaxy radiation and observed that the radiation was red-shifted: the galaxies and clusters of galaxies were moving away one from

the other. The expansion rate is determined by the Hubble constant  $H$ , a tangled quantity to measure accurately; it is common, defining  $H_0 = 100 h$  km Mpc/s as the Hubble constant at present time, to refer to [5]:

$$h = 0.72 \pm 0.08 \quad (1.1)$$

Recently, from high-redshift Type Ia Supernovae (SNIa) [6] data turns out that the Universe is not only in expansion but it is accelerating. An accelerating Universe is currently best explained by a cosmological constant or other form of dark energy with negative pressure. The best fit [5] requires:

$$\Omega_\Lambda = 0.732 \pm 0.018 \quad (1.2)$$

with  $\Omega_\Lambda$  being the fraction of Dark Energy (DE) contributing to the critical energy density in the Universe.

One of the most relevant observables is the cosmic microwave background (CMB), first discovered by Penzias and Wilson in 1965 [7] and predicted by Gamow in the '40s [8]. The CMB radiation looks like a black body radiation at a temperature  $T \simeq 2.73$  K and is extremely isotropic and homogeneous; the small temperature anisotropies measured first by COBE [9] then with high precision by the WMAP [5] satellite are of the order of  $\delta T/T \sim 10^{-5}$  at large angular scales. The position of the first peak in the CMB power spectrum leads to a clearly indication of a flat Universe, namely:

$$\Omega \simeq 1.003 \pm 0.010 \quad (1.3)$$

with  $\Omega$  the fraction density referred to the critical density, that will be introduced in the next chapter 2.2, in accord with the predictions of Inflation.

As for the temperature, also the luminous matter distribution, if observed at very large scale, has an uniform distribution, instead at the cluster or even smaller scales looks highly inhomogeneous, with density differences of the order  $10^2 - 10^5$ . Another important component of the Universe is  $\Omega_b$ , the baryon fraction. Baryons are the matter out of which planets, stars, clouds of gas and possibly "dark" stars are made; some of it could also form black holes. The data on the light element abundances and CMB fluctuations strongly indicate that the baryons contribute only to a small percentage of the critical energy density [5]:

$$\Omega_b h^2 \simeq 0.02186 \pm 0.00068 \quad (1.4)$$

The number of photons per baryons is of the order  $10^9$ . From a theoretical point of view the big bang nucleosynthesis (BBN) [10] makes some predictions on the abundance of light nuclei, confirmed by experiments: the chemical composition

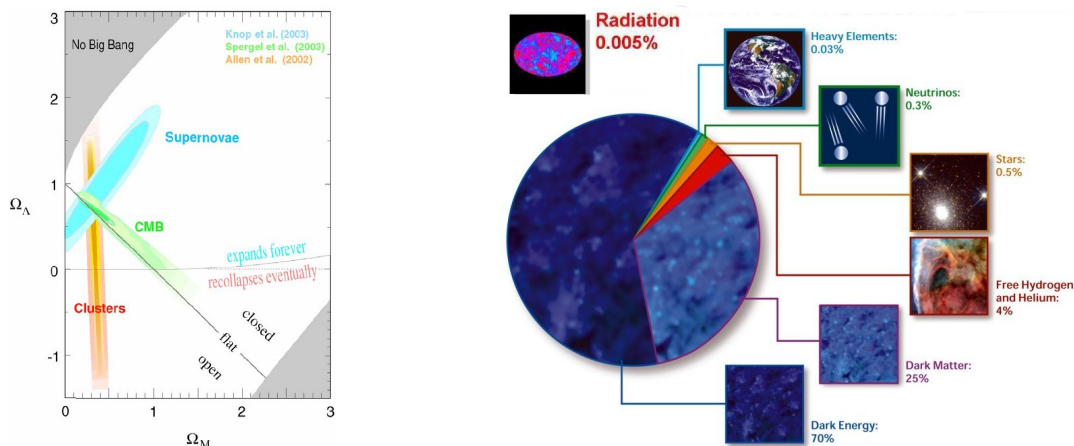


Figure 1.1: Left panel: Confidence regions for  $\Omega_M$  vs  $\Omega_\Lambda$  using Supernova Cosmology Project data with results from CMB and galaxy cluster data added; from [11]. Right panel: Energy density contributions in the Universe, from <http://universe.nasa.gov/be/Library/images-library1.html>.

of baryonic matter is about 75% hydrogen (H), 25% helium ( $\text{He}^3, \text{He}^4$ ) plus trace amounts of heavier elements like deuterium (D) and lithium ( $\text{Li}^6, \text{Li}^7$ ).

Together with a relic photon radiation it is also predicted a relic background of neutrinos at  $T \simeq 1.96$  K. Neutrinos are very abundant in the Universe, in number only slightly smaller than that of relic photons. They influence various cosmological stages, e.g. the evolution of primordial perturbations.

In Fig. 1.1 the combined WMAP, SNIa and galaxy clusters measurements are shown: on cosmological scales the evidence of exotic matter (DM) and exotic energy is compelling, in order to explain  $\Omega \simeq 1$ . The Dark Energy contributes with  $\Omega_\Lambda \sim 0.74$ , and if  $\Omega_b \simeq 0.044$ , from BBN, then the difference must be DM which contributes to the total density with:

$$\Omega_{\text{DM}} \simeq 0.268 \pm 0.018 \quad (1.5)$$

or equivalently, and it will be the reference interval for all our calculations:

$$0.092 \leq \Omega_{\text{DM}} h^2 \leq 0.124 \quad (1.6)$$

Then a satisfactory description of most cosmological observations is obtained by the so called " $\Lambda$ CDM model", which comes out from the best fit of the combined data analysis.

## 1.2 Observational hints of Dark Matter

The definition of Dark Matter comes out from the fact that this kind of matter does not emit or absorb electromagnetic radiation at any wavelength, its gravitational interactions dominate on scales from tiny dwarf galaxies, to large spirals such as the Milky Way, to clusters of galaxies, to the largest scales until now observed.

Actually the first hint of the presence of DM was given by Zwicky in 1933, measuring the rotational velocity of the Coma cluster. On galactic scales and smaller, the classical tests of the mass distribution provided by rotation curves continue to be refined. A compilation of almost 1000 rotation curves led to the conclusion that non-luminous matter indeed is present in large amounts.

For a spiral galaxy, in which the luminous matter has a mass distribution modelled by a disk and a bulge, Newton's laws of gravity give for the rotation velocity of a tracer star, or neutral hydrogen, at distance  $r$  from the center:

$$\frac{v_{rot}^2(r)}{r} = \frac{GM_{tot}(r)}{r^2} \quad (1.7)$$

where  $v_{rot}(r)$  is the rotation velocity at the distance  $r$  and  $M_{tot}(r)$  is the total mass of the galaxy interior to  $r$ . Thus:

$$M_{tot}(r) = \frac{v_{rot}^2(r)r}{G} \quad (1.8)$$

A constant rotation velocity, which is usually observed for spiral galaxies over a large range of  $r$  implies a halo mass which grows linearly with  $r$ , as shown in Fig. 1.2. Realistically, this growth can not extend arbitrarily far. The growth of mass eventually becomes only logarithmic until the halo starts to overlap with one of a nearby galaxy. The mass of a galaxy is 10 times larger than the present bright matter. The Dark Matter is roughly spherically distributed, implying that  $\rho_{DM} \sim r^{-2}$ , at large distances from the galactic center.

Spiral galaxies offer the most robust evidence for the Dark Matter. Moving to larger scales, such as galaxy clusters, the evidence of DM comes from different experimental methods, such as gravitational lensing, X-ray gas temperatures and the motion of cluster member galaxies. In general, depending on the scale to which we look at, different methods of measuring directly or indirectly the presence of Dark Matter are employed (see Fig 1.2):

**Gravitational Lensing** According to the predictions of Einstein's general relativity, the curvature of space-time caused by matter gives rise to a deflection of light rays. Since the deflection angle is proportional to the mass of the object causing the deflection, called lens, one has in principle a good tool for estimating directly the mass of astrophysical objects, from planets and

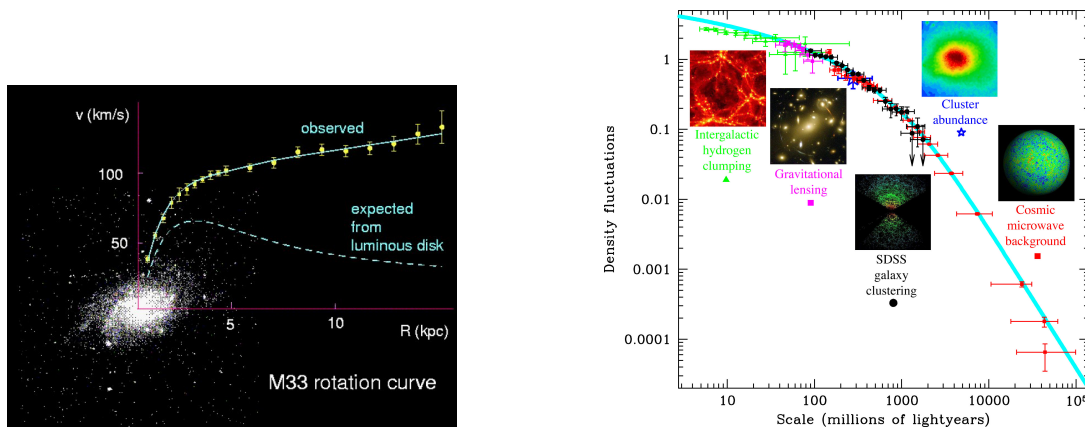


Figure 1.2: Left panel: Observed H I rotation curve of the nearby dwarf spiral galaxy M33 superimposed on an optical image, from [3]. Right panel: Indirect evidences of Dark Matter at all scales [12].

upwards to galaxies and galaxy clusters. In the latter case, distant bright galaxies and galaxy nuclei such as quasars are very useful as sources. Usually they can be considered as being pointlike, and an excellent signature of gravitational lensing is the appearance of multiple images of one and the same quasars. The masses of lensing objects determine the angular separation of images and the frequency of lensing events has a strong dependence on the geometry of the Universe, in particular is sensitive to the presence of vacuum energy. The gravitational lensing analysis, e.g. [13], indicates that there is plenty of Dark Matter.

**Large Scale Structures (LSS)** The galaxy clusters offer another window on Dark Matter properties. The galaxy redshift surveys, such as SDSS and 2dF Galaxy Redshift Survey [14, 15], are taking maps of the Universe at high redshift. It is thus possible to identify the cluster of galaxies, to see their hot gas as hot spots in X-ray maps or cold spots in microwave maps (the so-called Sunyaev-Zel'dovich effect) or to spot their gravitational effects with gravitational lensing. A large scale structure reconstruction of the Universe is viable, by mapping the Universe till the last scattering surface: the filaments, the walls and the voids appear, as it is shown in Fig. 1.3, with an overall homogeneous distributions on large scales.

Theoretically in the structure formation is important the type of particle making up the Dark Matter. Relativistic particles (Hot Dark Matter, HDM) at the time structures start to form will free-stream out over galaxy-sized overdense regions, so that only very large structures can form early. Massive particles (Cold Dark Matter, CDM) will typically move with non-relativistic

velocities and can therefore clump to smaller scales. In between there may exist the Warm Dark Matter (WDM), which could be made up of keV scale neutral particles. There the inverse of the mass scale of the particle defines a length scale of structure formation below which early structure is suppressed. From observational data it is inferred that structures form in a hierarchical fashion, with small clumps merging in larger ones, forming galaxy halos and successively larger structures. From a theoretical point of view the N-body simulations provide a very powerful tool to follow the highly nonlinear dynamics of merging. There is some tension with observation on small scales in the non-linear structure formation regime compared with the numerical simulation, which provide an overabundance of substructures in the halos. Such a discrepancy can be alleviated with WDM hypothesis instead of CDM [16]. Therefore the main contribution to dark matter comes from cold dark matter; however a small mixture of HDM with in a Universe dominated by CDM provides a good agreements with the data.

**Lyman- $\alpha$  Forest** The so-called Lyman- $\alpha$  forest offers an excellent probe of the matter power spectrum at high redshift of the order  $z \sim 2 \div 4$ . The Lyman- $\alpha$  emission line in quasars spectra is produced by the inhomogeneous distribution of a warm ( $T \sim 104\text{K}$ ) and photoionized Inter Galactic Medium (IGM) along the line-of-sight. The opacity fluctuations in the spectra arise from fluctuations in the matter density and trace the gravitational clustering of the matter distribution. The data on the Lyman- $\alpha$  forest collected by the sky surveys are from one side compared with cosmological hydrodynamic simulation of a cold dark matter, namely with the evolution of galaxies surrounded by halos of hot gas, on the other side are combined with the other observable data to constraints the  $\Lambda$ CDM model parameters (see e.g. [17]).

It is fortunate that the most secure evidence for dark matter is in spiral galaxies, since direct searches and indirect annihilation signals can be carried out only in our spiral galaxy. The Milky Way is immersed in a dark halo which outweighs the luminous components by about a factor of ten. Although the DM halo profile at large distances from the galactic center is know, the central structure of the DM halos is far from being well determined. There are many astrophysical uncertainties about the DM galactic velocity distribution and density profile, which can lead to uncertainties in the calculations of direct and indirect detection signals. The shape of the Dark Matter halo takes into account the possible existence and prominence of central cusps or the possible physical extent of a constant density inner core and the possible presence of a population of subhalos. No definitive answer, up to now, can be given to these questions by experimental constraints. Moreover theoretical predictions on the density profiles and velocity distribution



Figure 1.3: 3D model of the galaxies and quasars found by the SDSS. Currently there are 250 000 galaxies and 40 000 quasars. Also included is the cosmic microwave background as mapped by the WMAP; from <http://astro.uchicago.edu/cosmus/projects/sloangalaxies/>

functions differ substantially among themselves or take into account different input parameters.

The modeling of the DM density profile is an open question. It can be addressed through numerical N-body simulations, however the current cosmological simulations are not anyway reliable for radii smaller than a  $r_{min} \simeq 0.1 - 1\text{kpc}$ . Thus the very inner slope of the profile is then usually just extrapolated and does not take into account interactions with baryons which fall in the DM potential well. Many different density profiles have been proposed, compatible with observations. The most commonly used density distributions can be parameterized by the following spherically averaged density profile:

$$\rho_{\text{DM}} = \rho_{\odot} \left( \frac{R_{\odot}}{r} \right)^{\gamma} \left( \frac{1 + (R_{\odot}/a)^{\alpha}}{1 + (r/a)^{\alpha}} \right)^{(\beta-\gamma)/\alpha} \quad (1.9)$$

where  $r = |\vec{r}|$ ,  $R_{\odot} = 8.5\text{kpc}$  is the distance of the Sun from the galactic center,  $a$  is

the scale length and  $\rho_{\odot}$  is the total local (solar neighborhood) dark matter density. In Tab. 1.1 the isothermal, NFW and Moore density profiles are explicitly reported. The two latter profiles in Tab. 1.1, which come out from N-body simulations, differ

Density profile	$\alpha$	$\beta$	$\gamma$
Isothermal	2	2	0
NFW [18]	1	3	1
Moore <i>et al.</i> [19]	1.5	3	1.5

Table 1.1: Isothermal, NFW and Moore density profiles

noticeably in their behavior at small distances from the galactic center:  $r^{-1}$  for the NFW profile [18, 20] and  $r^{-1.5}$  for the Moore *et al.* profile [19, 21], while the isothermal sphere has a constant density core. A key parameter for all density distributions is the value for the total local DM density  $\rho_{\odot}$ . This parameter can be determined for each density profile assuming compatibility with the measurements of rotational curves and the total mass of the Galaxy. For instance a simple modeling of the visible and dark component of the galaxy showed that it is a reasonable assumption to take  $\rho_{\odot}$  having the mean value of  $0.3 \text{ GeVcm}^{-3}$ .

All the profiles in Eq. 1.9 produce rotation curves which are flat at large radii and the local velocity distribution can be approximated by a Maxwell distribution:

$$f(v) = \frac{e^{-v^2/v_0}}{\pi^{3/2}v_0^3} \quad (1.10)$$

The parameter  $v_0$  is simply the rotation speed at large radii. Since the stellar disk density of the Galaxy is thought to drop exponentially at radii much larger than the extent of the disk, this velocity should be due only to the halo. If we assume that the velocity ellipsoid is isotropic, the velocity dispersion is thus given by  $\bar{v} = \sqrt{3/2}v_0 \simeq 270 \text{ km s}^{-1}$ . As well the density profiles need a cut-off at large radii, otherwise leading to a total infinite mass, the velocity distribution, Eq. 1.10, is truncated at a certain escape velocity, usually taken to be  $v_{esc} \simeq 450 \text{ km s}^{-1}$ , see [22].

Observations of the velocity dispersion of high proper motion stars suggest the existence of a Super Massive Black Hole (SMBH) lying at the center of our Galaxy. If a SMBH exists, the process of adiabatic accretion of Dark Matter on it would produce a spike in the dark matter density profile [23, 24, 25, 26]. Also baryon dissipation would alter the halo profile in the galactic center [27, 28].

All the previous models are spherically symmetric with isotropic velocity dispersion. However the departures from the isothermal sphere is interesting and lead to different density profiles and velocity distributions, in which rotation or

axisymmetries are taken into account. Following [22], the most relevant classes of models are the spherically symmetric matter density with non-isotropic velocity dispersion and the axisymmetric models.

In chapter 5, we will refer to these models (A, B, C, NFW and Moore *et al.*) for calculations of direct and indirect detection of DM particles and we will see that they are the source of great uncertainties in the signals evaluations. Indirect detection is sensible to clump effects in the DM halos, and in general the production of antimatter particles and gamma rays from DM annihilation is very sensitive on the density profile of the innermost region of the Galaxy, namely it can lead to expected rates spanning several orders of magnitude.

### 1.3 Dark Matter Candidates

It is natural to ask what is the Dark Matter made of. Potentially the only indication compatible with the cosmological measurements is that it is composed of non-baryonic, neutral and weakly interacting particles. In the literature several candidates were proposed, the most relevant are:

**Standard Model Neutrinos** The existence of a relic sea of neutrinos in number only slightly below that of relic photons that constitute the CMB, is a generic prediction of the standard hot Big Bang model. Their contribution to the matter density of the Universe is:

$$\Omega_\nu = \frac{\sum_i m_i}{93.14 h^2 \text{eV}} \quad (1.11)$$

The requirement that  $\Omega_\nu \lesssim \Omega_m \simeq 0.3$  imposes stringent limits on their masses. Indeed dark matter particles with a large velocity dispersion such as that of the neutrinos (HDM) affect the evolution of the cosmological perturbations. This leads to a top-down scenarios which is not supported by the present observations, as mentioned before, since the galaxies seems older than clusters.

**Heavy Neutrinos** belong, together with charged heavy leptons, to standard  $SU(2)_L$  doublets, that may be added to the SM particle content. The allowed mass range is bounded from below from the Lee-Weinberg limit [29],  $m_\nu > 2 \text{ GeV}$ . A more stringent bound comes from colliders: neutrinos lighter than  $45 \text{ GeV}$  are excluded by the total decay width of the Z boson. For very heavy neutrinos the Yukawa coupling to the Higgs boson would be so strong that perturbative calculation become non-reliable [30] and partial waves unitarity has to be imposed [31], leading to a stringent mass upper

bound,  $m_\nu \lesssim 3 \text{ TeV}$ . In the allowed mass range the cosmological properties can be interesting, however their interactions are quite strong, therefore they are mainly excluded by direct detection bounds and lead to a low relic abundance.

**Sterile Neutrinos** are similar to SM neutrinos, but without SM interactions, apart from mixing [32]. Stringent cosmological and astrophysical constraints on sterile neutrinos come from the analysis of their cosmological abundance and the study of their decay products [33].

**Axions** have been introduced to explain the so called strong CP violation problem [34, 35]. From different searches, it is expected that axions are very light and extremely weakly interacting with ordinary particles, which implies that they were not in thermal equilibrium in the early Universe. The calculation of the relic density is uncertain, nevertheless it is possible to find some range where axions satisfy the present constraints and represent a possible DM candidate [36].

**Supersymmetric Particles:** in models conserving  $R$ -parity the lightest non standard particle (LSP), such as the neutralino, sneutrino, gravitino or axino could provide the right amount of Dark Matter density in the Universe. Which particle is the LSP, it depends on the supersymmetric models and on how supersymmetry is broken.

**Kaluza-Klein states** are excitations of the Standard Model fields which appears in models with extra dimensions, see e.g. [37, 38, 39, 40].

**Super-heavy dark matter** is composed by heavy stable particles with a mass in the range  $10^{12}$  to  $10^{16}$  GeV. These particles leads to scenarios for production of nonthermal dark matter [41].

**Light scalar dark matter:** considering fermionic dark matter candidates, Lee and Weinberg concluded that relic density arguments preclude such a WIMP with a mass less than a few GeV, see e.g.[42]. If the dark matter is made up by other types of particles, however, this limit could be evaded, leading to light dark matter particles.

**Dark matter from Little Higgs models** These models have been proposed in order to stabilize the weak scale and to solve the hierarchy problem as alternative to the Standard Model. This class of models possess discrete symmetries which result in the existence of stable weakly interacting particles, see for definiteness [43, 44].

# Chapter 2

## Dark Matter Relic Abundance

The Dark Matter is a relic from the Big Bang and is made off non-baryonic particles. The early Universe was in local thermal equilibrium, guaranteed by the interactions between the plasma constituents. It is the decoupling of a species from the thermal bath which gives rise to the relic particles, like the CMB, the neutrinos and the DM.

The main constraint is the requirement that the relic mass density of the dark matter be compatible with present observations. In the early Universe, these particles would have been present in a large numbers in thermal equilibrium, and as the Universe cooled down they could reduce their density only through pair annihilation. As their density decreases, however, it becomes more and more difficult for particles to find others with which to annihilate, and the co-moving density become constant, namely the species “freeze-out” from the primordial plasma and turns into a relic in the expanding Universe.

In this chapter we will first present the Cosmological Standard Model [2.1](#) and a brief thermal history of the Universe [2.2](#). Then we will focus on dark matter relic, for which the decoupling from the primordial plasma is studied in section [2.3](#). The subsequent sections contain technical details for precise numerical computation of the relic abundance, see [2.4](#) and [2.5](#). Finally in [2.6](#) we present the numerical code developed with the aim of computing the relic abundance of a generic dark matter candidate.

### 2.1 Standard Cosmological Model

The fundamental picture of the Standard Cosmological Model is the Big Bang scenario, which describes the Universe as a system evolving from a highly compressed state existing around  $10^{10}$  years ago. It establishes its theoretical basis on three main building blocks:

**Cosmological Principle** which assumes on large scales an homogeneous and isotropic Universe, namely there are no privileged directions and the density is constant.

**Einstein Equations** which describe the dynamics of the Universe.

**Equation of state** specifying the physical properties of the matter, radiation and vacuum energy content.

The properties of isotropy and homogeneity imply a specific form for the metric, which needs to be spatially maximally symmetric, namely the line element can be expressed as:

$$d\tau^2 = dt^2 - R^2(t) \left( \frac{dr^2}{1 - kr^2} + r^2 d\theta^2 + r^2 \sin^2 \theta d\phi^2 \right) \quad (2.1)$$

with  $t$  being the cosmological time,  $r, \theta, \phi$  are the comoving coordinates.  $R(t)$  is the scale factor, the only parameter that depends on time. Finally  $k$  is the spatial curvature, which can take the values  $+1, 0, -1$  depending on whether the geometry is open, flat or closed. These are the Robertson-Walker-Friedman (RWF) models. For the simplest case  $k = 0$  we see that the metric describes ordinary Euclidean three-space with the scale factor  $R$  giving the overall normalization of physical distances.

Actually the metric describes the kinematics of the Universe; it can be used to write the Einstein equations:

$$R_{\mu\nu} - \frac{1}{2} R g_{\mu\nu} = 8\pi G T_{\mu\nu} + \Lambda g_{\mu\nu} \quad (2.2)$$

where  $T_{\mu\nu}$  is the stress energy tensor for all the fields present, like matter, radiation, etc., and  $\Lambda$  is the cosmological constant.

To be consistent with the symmetries of the metric, the total stress energy tensor must be diagonal and by isotropy the spatial components must be equal. The simplest realization of such a stress energy tensor is that of a perfect fluid characterized by a time dependent energy density  $\rho(t)$  and pressure  $p(t)$ :

$$T_{\nu}^{\mu} = \text{diag}(\rho, -p, -p, -p) \quad (2.3)$$

The 0 component of the  $T_{\nu}^{\mu}$  conservation implies that the change in energy in a comoving volume  $d(\rho R^3)$  is equal to minus the pressure times the change of volume,  $-pd(R^3)$ , conversely the first law of thermodynamics. The equation of state of the matter, radiation, cosmological constant has the form  $p = w\rho$  (with  $w = 1/3, 0, -1$

for radiation, matter and cosmological constant respectively), therefore the energy density evolves as:

$$\rho \propto R^{-3(1+w)} \Rightarrow \begin{cases} p = \frac{1}{3}\rho & \rightarrow \rho \propto R^{-4} & \text{(Radiation)} \\ p = 0 & \rightarrow \rho \propto R^{-3} & \text{(Matter)} \\ p = -\rho & \rightarrow \rho \propto \text{const} & \text{(Vacuum Energy)} \end{cases} \quad (2.4)$$

The early Universe was radiation dominated, the latter matter dominated and in a very recent phase is kept in acceleration by the cosmological constant. If the Universe underwent inflation there was a very early period when the energy density was dominated by the vacuum energy. Inflation has been proposed in order to solve some open issues in the standard cosmological models, like the horizon problem, the flatness problem and the origin of primordial density fluctuations.

The dynamical equations that describe the evolution of the scale factor  $R(t)$  follow from the Eq. 2.2:

$$\begin{aligned} \frac{\dot{R}^2}{R^2} + \frac{k}{R^2} &= \frac{8\pi G}{3}\rho \\ \frac{\ddot{R}}{R} &= -\frac{4\pi G}{3}(\rho + 3p) \end{aligned} \quad (2.5)$$

The first equation is the so called Friedmann equation and describes the evolution of the expansion rate of the Universe, namely the Hubble parameter  $H \equiv \dot{R}/R$  (see Eq. 1.1 for the present value). Instead the second equation provides the acceleration of  $\dot{R}$ . Today  $\dot{R} \geq 0$ ; if in the past  $(\rho + 3p)$  was always positive, then  $\ddot{R}$  was always negative and thus at some finite time in the past  $R$  must have been equal to zero. This event, referred to as Big Bang, is usually defined at time  $t = 0$  and implies  $R = 0$ . The Hubble parameter is not constant and in general varies as  $H \propto t^{-1}$ , therefore the Hubble time  $H^{-1}$  sets the time scale for the expansion.

The Friedmann equation can be recast into the form:

$$\frac{k}{H^2 R^2} = \Omega - 1 \quad (2.6)$$

where  $\Omega$ , mentioned qualitatively in section 1.1, is the ratio of the density to the critical density  $\rho_c$ :

$$\Omega \equiv \frac{\rho}{\rho_c} \quad \rho_c \equiv \frac{3H^2}{8\pi G} \quad (2.7)$$

At present time  $\rho_c = 1.88 \times 10^{-29} h^2 \text{gcm}^{-3}$ .

Since  $R^2 H^2 \geq 0$  there is a correspondence between the spatial curvature  $k$  and  $\Omega$ :

$$\begin{cases} k = +1 & \Rightarrow \Omega > 1 & \text{Closed} \\ k = 0 & \Rightarrow \Omega = 1 & \text{Flat} \\ k = -1 & \Rightarrow \Omega < 1 & \text{Open} \end{cases} \quad (2.8)$$

We remark that the geometry of the Universe is determined by the energy content of it.

For a flat Universe, which is strongly favored by the data [5], the time dependence of the scale factor is, from Eq 2.8:

$$R \propto t^{2/3(1+w)} \Rightarrow \begin{cases} w = \frac{1}{3} & \rightarrow R \propto t^{1/2} & \text{(Radiation)} \\ w = 0 & \rightarrow R \propto t^{2/3} & \text{(Matter)} \\ w = -1 & \rightarrow R \propto e^{H_0 t} & \text{(Vacuum Energy)} \end{cases} \quad (2.9)$$

Our description of the Universe is based on extrapolation of known physics back to the Planck epoch, when the Universe was only  $t = 10^{-43}$  sec old, or equivalently up to energies of the order of the Planck mass ( $M_P = 10^{18}$  GeV) at which the gravitational interaction becomes strong.

## 2.2 Thermal evolution of the Universe

Most of the constituents of the Universe were in thermal equilibrium, thereby making an equilibrium description a good approximation. Actually there have been a number of very notable departures from thermal equilibrium: neutrino, background radiation and relic massive particle decoupling.

The number density  $n_i$  and the energy density  $\rho_i$  of a dilute weakly-interacting gas of particle with  $g_i$  internal degrees of freedom and mass  $m_i$  is given in term of its phase space distribution function  $f(\vec{p})$ :

$$\begin{cases} n_i = \frac{g_i}{(2\pi)^3} \int f_i(\vec{p}) d^3p \\ \rho_i = \frac{g_i}{(2\pi)^3} \int E(\vec{p}) f_i(\vec{p}) d^3p \end{cases} \quad (2.10)$$

where  $E^2 = |\vec{p}|^2 + m_i^2$ . For a species in kinetic equilibrium the phase space occupancy  $f_i$  is given by the familiar Fermi-Dirac or Bose-Einstein distributions:

$$f_i(\vec{p}) = \frac{1}{e^{(E-\mu_i)/T} \pm 1} \quad (2.11)$$

where  $\mu_i$  is the chemical potential of the species and +1 pertains to Fermi-Dirac statistic while  $-1$  to Bose-Einstein species. The quantities in Eqs. 2.10 get simple expressions in two limiting cases. First of all, for relativistic particles ( $m_i \ll T$ ):

$$n_i = \begin{cases} \left(\frac{\zeta(3)}{\pi^2}\right) g_i T^3 & \text{(Bose)} \\ \left(\frac{3}{4}\right) \left(\frac{\zeta(3)}{\pi^2}\right) g_i T^3 & \text{(Fermi)} \end{cases} \quad (2.12)$$

$$\rho_i = \begin{cases} \left(\frac{\pi^2}{30}\right) g_i T^4 & \text{(Bose)} \\ \left(\frac{7}{8}\right) \left(\frac{\pi^2}{30}\right) g_i T^4 & \text{(Fermi)} \end{cases} \quad (2.13)$$

Here  $\zeta(3) = 1.20206\dots$  is the Riemann zeta function of 3.

In the non-relativistic limit ( $m_i \gg T$ ) the number density and the energy density are the same for Bose and Fermi species:

$$\begin{cases} n_i = g_i \left( \frac{m_i T}{2\pi} \right)^{3/2} e^{-\frac{m_i}{T}} \\ \rho_i = m_i n_i \end{cases} \quad (2.14)$$

Notice that non relativistic particles are depleted by the exponential factor, arising from the Maxwell-Boltzmann statistic.

The total energy density of all species in equilibrium in the Universe can be expressed in term of the photon temperature  $T$ :

$$\rho = \sum_i \rho_i = \frac{\pi^2}{30} g_*(T) T^4 \quad (2.15)$$

where:

$$g_*(T) = \sum_i \left( \frac{T_i}{T} \right)^4 \frac{g_i}{2\pi^2} \int_{x_i}^{\infty} du \frac{(u^2 - x_i^2)^{1/2} u^2}{e^{(u-y_i)} \pm 1} \quad (2.16)$$

with  $x_i \equiv m_i/T$  and  $y_i \equiv \mu_i/T$ . We have taken into account the possibility that the species  $i$  may have a thermal distribution, but with a different temperature than that of the photons. Since the energy density for a non-relativistic species, Eq. 2.14, is exponentially smaller than that of relativistic particles, it is a very good approximation to include only the relativistic species in Eq. 2.16:

$$g_*(T) = \sum_{i=\text{bosons}} g_i \left( \frac{T_i}{T} \right)^4 + \frac{7}{8} \sum_{i=\text{fermions}} g_i \left( \frac{T_i}{T} \right)^4 \quad (2.17)$$

The relative factor of 7/8 accounts for the different statistics, see Eq. 2.12. Notice that  $g_*$  counts the total number of effectively massless degrees of freedom at a certain temperature  $T$ , hence at a certain epoch in the Universe expansion, as reported in Tab. 2.1.

The entropy in a comoving volume is defined as:

$$S = \frac{(\rho + p)}{T} R^3 \quad (2.18)$$

thus the entropy density is, with  $R^3 \equiv V$ :

$$s \equiv \frac{S}{V} = \frac{(\rho + p)}{T} \quad (2.19)$$

Since the evolution of the Universe can be described by subsequent stages in which local thermal equilibrium is maintained, the entropy in a comoving volume is constant:

$$dS = 0 \tag{2.20}$$

and the expansion of the Universe is adiabatic, see [10, 45].

The entropy density is dominated by the contribution of relativistic particles, so that a very good approximation is:

$$s = \frac{2\pi^2}{45} g_{*s} T^3 \tag{2.21}$$

where

$$g_{*s}(T) = \sum_{i=bosons} g_i \left(\frac{T_i}{T}\right)^3 + \frac{7}{8} \sum_{i=fermions} g_i \left(\frac{T_i}{T}\right)^3 \tag{2.22}$$

When the thermal equilibrium breaks down, the particle species decouples, its entropy and the entropy of the other particles (which continue to interact) are separately conserved. In particular, if a massive species annihilates and reheats the interacting particles, the decoupled species will not share in the released energy and so will differ in temperature from the interacting particles. It is important to underline that the temperature of the relic particle may differ from that of the photons. The temperature of the decoupled particles is calculated from conservation of entropy and is then used to find their contributions to  $g_*(T)$  and  $g_{*s}(T)$ . For most of the history of the Universe all particles have a common temperature, and  $g_{*s}$  is equivalent to  $g_*$ . Thus the two functions, Eqs. 2.16, 2.22 have different values, namely  $g_* = 3.36$  and  $g_{*s} = 3.91$ , as it is shown in Fig. 2.1.

Actually, a constant comoving entropy,  $S = g_{*s} R^3 T^3 = \text{const}$  implies that the temperature of the Universe evolves as:

$$T \propto g_{*s}^{-1/3} R^{-1} \tag{2.23}$$

Whenever  $g_{*s}$  is constant, it follows  $T \propto R^{-1}$ . The factor of  $g_{*s}^{-1/3}$  enters because when a particle species becomes non-relativistic and disappears its entropy is transferred to the other relativistic particle species still present in the thermal plasma, causing  $T$  to decrease slightly less slowly. Massless particles that are decoupled from the heat bath will not share in the entropy transfer as the temperature drops below the mass thresholds of a species; instead the temperature of a massless decoupled particle scales as  $T \propto R^{-1}$ . If we consider a massive particle species, the number density scales as  $R^{-3}$  and the kinetic energy is redshifted as  $R^{-2}$ . Summing the two effects such a decoupled species will have precisely an equilibrium phase space distribution characterized by temperature  $T \propto R^{-2}$ .

T less than	Particles in equilibrium	$g_*(T)$
1 eV	$\gamma$	2
$m_e$	$\gamma, e^+, e^-$	$\frac{11}{2}$
$m_\mu$	$\gamma, e^+, e^-, \nu_e, \nu_\mu, \nu_\tau$	$\frac{43}{4}$
$m_\pi$	$\gamma, e^\pm, \nu_e, \nu_\mu, \nu_\tau, \mu^\pm$	$\frac{57}{4}$
$\Lambda_{QCD}$	$\gamma, e^\pm, \nu_e, \nu_\mu, \nu_\tau, \mu^\pm, \pi^\pm, \pi^0$	$\frac{69}{4}$
$m_s$	$\gamma, e^\pm, \nu_e, \nu_\mu, \nu_\tau, \mu^\pm, u, \bar{u}, d, \bar{d}, g$	$\frac{205}{4}$
$m_c$	$\gamma, e^\pm, \dots, u, \bar{u}, d, \bar{d}, g, s, \bar{s}$	$\frac{247}{4}$
$m_\tau$	$\gamma, e^\pm, \dots, u, \bar{u}, d, \bar{d}, g, s, \bar{s}, c, \bar{c}$	$\frac{289}{4}$
$m_b$	$\gamma, e^\pm, \dots, d, \bar{d}, g, s, \bar{s}, c, \bar{c}, \tau^\pm$	$\frac{303}{4}$
$m_t$	$\gamma, e^\pm, \dots, d, \bar{d}, g, s, \bar{s}, c, \bar{c}, \tau^\pm, b, \bar{b}$	$\frac{345}{4}$
$m_W$	$\gamma, e^\pm, \dots, s, \bar{s}, c, \bar{c}, \tau^\pm, b, \bar{b}, t, \bar{t}$	$\frac{387}{4}$
$T > m_Z$	$\gamma, e^\pm, \dots, s, \bar{s}, c, \bar{c}, \tau^\pm, b, \bar{b}, t, \bar{t}, W^\pm, Z$	$\frac{423}{4}$

Table 2.1: Effective massless degrees of freedom of the Universe at different epochs.  $\Lambda_{QCD}$  is taken to be of the order  $\mathcal{O}(100)$  MeV.

The Universe evolves and cools down, therefore it is interesting to relate the time evolution with the temperature:

$$\begin{cases} t = 0.301 g_*^{-1/2} \frac{M_P}{T^2} & T > T_{eq} \\ t = 0.402 g_*^{-1/2} \frac{M_P}{T^{3/2} T_{eq}^{1/2}} & T \leq T_{eq} \end{cases} \quad (2.24)$$

where  $T_{eq} \simeq 5.5$  eV is the equivalence temperature at which the matter density equals the radiation density, namely it ends the radiation dominated epoch and starts the matter dominated period. As shown in the previous section, the Hubble parameter depends on time, therefore on the temperature:

$$\begin{cases} H = 1.66 g_*^{1/2} \frac{T^2}{M_P} & T > T_{eq} \\ H = 1.66 g_*^{1/2} \frac{T^{3/2} T_{eq}^{1/2}}{M_P} & T \leq T_{eq} \end{cases} \quad (2.25)$$

The key to understand the thermal history of the Universe is the comparison of the particle interaction rates and the expansion rate. Ignoring the temperature variation of  $g_*$ ,  $T \propto R^{-1}$  and the rate of change of the temperature  $\dot{T}/T$  is just set by the expansion rate,  $\dot{T}/T = -H$ . So long as the interactions necessary for the particle distribution functions to adjust to the changing temperature are rapid compared to the expansion rate, the Universe will, to a good approximation, evolve through a succession of nearly thermal states with temperature decreasing as  $R^{-1}$ .

In a standard description of the early Universe, the Big Bang was followed by an inflationary epoch which ended in a period of reheating and particle production.

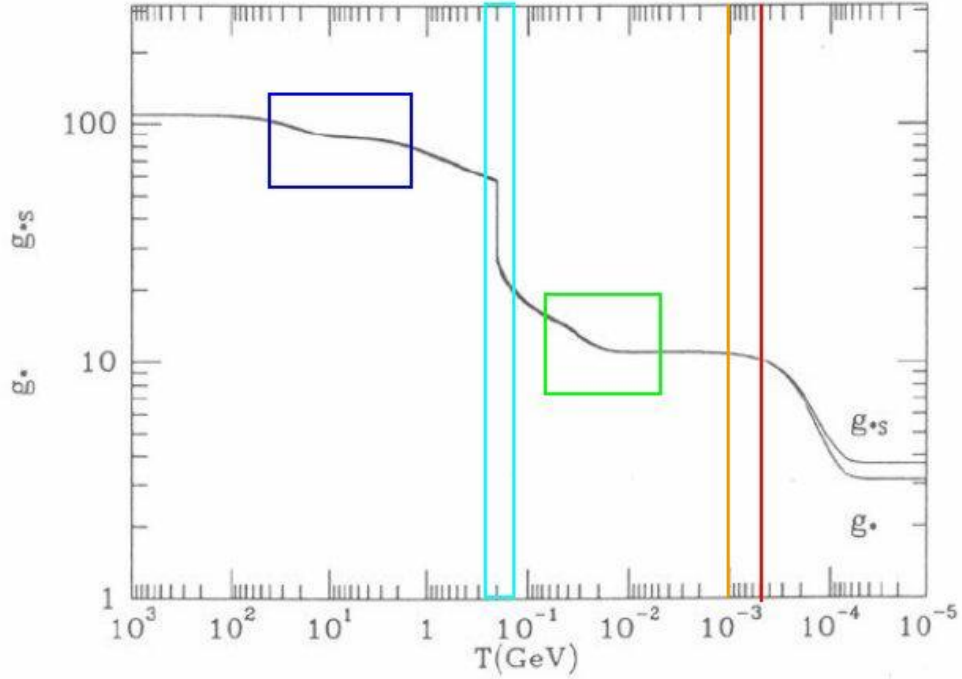


Figure 2.1: Behavior of  $g_*$  (Eq. 2.16) and  $g_{*s}$  (Eq 2.22) with respect to the temperature [46]. Relevant departures from thermal equilibrium and phase transitions are underlined: the blue area denotes the transition to the non relativistic regime of heavy quarks and bosons, the cyan area represents the QCD transition, the green area refers to mesons and baryons freeze, which become non relativistic, the orange line marks the neutrino decoupling and finally the red line denote the electron transition to non relativistic behavior.

Therefore at the earliest time the Universe was a plasma of relativistic particles, including the quarks, the leptons, gauge bosons and Higgs bosons. A number of Spontaneous Symmetry Breaking (SSB) phase transitions should take place during the course of the early history of the Universe. They include the grand unification (GUT) phase transition at a temperature of  $10^{16}$  GeV and the electroweak symmetry breaking at  $T \sim 300$  GeV. At a temperature of about 100 and 300 MeV the Universe should undergo a transition associated with chiral symmetry breaking and color confinement, after which the strongly interacting particles are confined into baryons and mesons.

The epoch of primordial nucleosynthesis follows when  $t \sim 10^{-2}$  to  $10^2$  sec and  $T \sim 10$  to 0.1 MeV. At a time about  $10^{11}$  sec and  $T \sim 1$  eV the matter density becomes equal to that of the radiation. This marks the beginning of

the matter dominated epoch. Finally at time about  $10^{13}$  sec and  $T \sim 0.2$  eV the hydrogen recombination takes place: ions and electrons combine to form atoms and CMB decouples from matter, ending the long epoch of near thermal equilibrium that existed in the Universe. The surface of last scattering for the microwave background radiation is the Universe itself at decoupling. The cosmic plasma becomes practically neutral and the photons propagate freely. After recombination neutral hydrogen is not resisted by the radiation pressure against forming cosmic structures and baryons start infalling into already evolved seeds of structures made of dark matter. At the epoch of reionization, at a redshift  $z \sim 10$  the first stars start to form.

The main transition phases in the early Universe are illustrated in Fig. 2.1, where the respective changes in the degrees of freedom of the Universe are shown.

## 2.3 Boltzmann Equation

The kinetic and chemical equilibrium of a species  $\chi$  is maintained by its mutual interactions (annihilation processes and pair creation, Eq. 2.26) and by frequently scattering with the cosmic background (Eq. 2.27):

$$\chi + \bar{\chi} \leftrightarrow A + \bar{A} \quad (2.26)$$

$$\chi + A \leftrightarrow \chi + A \quad (2.27)$$

The expansion of the Universe involves a decrease of the temperature, see Eq. 2.23. The rough criterion for a particle species to be either coupled or decoupled involves the comparison of the interaction rate of the particle,  $\Gamma \propto n^2 \sigma v$ , that keeps the species in thermal equilibrium, with the expansion rate of the Universe,  $H$ , since the dilution of a species is proportional to  $Hn$ . At a certain time after the Big Bang the interactions become too small compared to the dilution due to the expansion:

$$\begin{aligned} \Gamma > H &\longrightarrow \text{coupled} \\ \Gamma < H &\longrightarrow \text{decoupled} \end{aligned} \quad (2.28)$$

As the temperature goes down, the processes are not enough rapid to maintain equilibrium; light particles have a kinetic energy lower than the threshold for the production of a pair of  $\chi$  particles, and the reaction Eq. 2.27 stops to go backward and proceeds only forward, depleting the number density of the  $\chi$  species.

If a massive particle species remains in thermal equilibrium until the present, its abundance, Eq. 2.14, would be absolutely negligible because of the exponential factor. If the interactions of the species freeze out at a temperature such that  $m/T$  is much larger than 1, the species can have a significant relic abundance today.

Suppose we are working with stable particles, so only annihilation and inverse annihilation processes may let change the number of the species. In addition we assume that there is no asymmetry between particles and anti-particles.

The evolution of the phase space distribution of a species which is in thermal equilibrium or is completely decoupled is simple. It is the evolution of particle distribution around the epoch of decoupling that is challenging. The Boltzmann equation describes exactly the evolution of the spatial density of a species in the early Universe and is defined as:

$$\mathbf{L}[f] = \mathbf{C}[f] \quad (2.29)$$

where  $\mathbf{L}$  is the Liouville operator, giving the net rate of change in time of the particle phase-space density, and  $\mathbf{C}$  is the collision operator representing the number of particles per phase space volume that are lost or gained per unit time under collisions with other particles. In order to properly treat decoupling one must follow the microscopic evolution of the particle phase space distribution function  $f(p^\mu, x^\mu)$  [47].

The form of the Boltzmann equation depends on which kind of phase space distribution we choose: non relativistic particles,  $T \ll m$ , obey to MB statistic (Maxwell-Boltzmann), relativistic particles,  $T \gg m$ , are described by Fermi-Dirac (FD) or Bose-Einstein statistic (BE).

The phase space distribution in a Robertson-Walker metric is spatially homogeneous and isotropic:

$$\begin{aligned} f(p^\mu, x^\mu) &= f(|\vec{p}|, t) \\ &= f(E, t) \end{aligned} \quad (2.30)$$

Since the Universe evolved from a tiny, extremely dense, singular state one may ask for what epochs should a phase space description be possible. Presumably it should be possible so long as the de Broglie wavelength of the particles is small compared to the observable size of the Universe. Using dimensional arguments we expect to be able to use the phase space description so long as  $T < M_P$ , where  $M_P$  is the Plank mass.

The definition of the Liouville operator  $\mathbf{L}$  appropriate to the flat space RWF cosmology, using the isotropy of the phase space distribution, reads [47]:

$$\mathbf{L}[f] = \frac{\partial f}{\partial t} - 2\frac{\dot{R}}{R}p\frac{\partial f}{\partial p} \quad (2.31)$$

In comoving coordinates, namely introducing the "local momentum"  $\vec{p} \equiv R\vec{p}$ ,  $\mathbf{L}$  assumes the simple expression:

$$\mathbf{L}[f(E, t)] = E\left\{\frac{\partial f}{\partial t} - pH\frac{\partial f}{\partial p}\right\} \quad (2.32)$$

Using the definition of the number density, Eq. 2.10:

$$n(t) = \int dn = \frac{g}{(2\pi)^3} \int d^3p f(E, t) \quad (2.33)$$

the Boltzmann equation, Eq. 2.29 becomes:

$$\frac{dn}{dt} + 3Hn = \frac{g}{(2\pi)^3} \int d^3p \mathbf{C}[f(E, t)] \quad (2.34)$$

If the particles do not interact Eq. 2.29 reduces to:

$$\mathbf{L}[f] = 0 \quad (2.35)$$

actually the particles are sensible only to the Universe expansion and therefore the species undergoes dilution.

As noticed before the function  $f$  is determined by the microscopic behavior of the system, the inter-particle collisions. The collision operator in Eq. 2.29 includes the elastic and inelastic collision operators:

$$\mathbf{C}[f(E, t)] = \mathbf{C}_{el}[f(E, t)] + \mathbf{C}_{ann}[f(E, t)] \quad (2.36)$$

The elastic collisions  $\mathbf{C}_{el}$  are responsible for maintaining the kinetic equilibrium and do not change the number of particles of the considered species, instead the inelastic collisions  $\mathbf{C}_{ann}$  vary the number of particles.

In the most general case, the Boltzmann equations are a coupled set of integral-partial differential equations for the phase space distributions of all the species present in the process. Fortunately, in problems of interest to us, all but one (or two) species will be nearly the decoupling phase at a certain temperature, reducing the problem to a single partial-integral differential equation for the one species of interest.

For solving the decoupling Boltzmann equation it is useful to introduce a new quantity, the number density per comoving volume:

$$Y \equiv \frac{n}{s} \quad (2.37)$$

and the dimensionless variable  $x \equiv m/T$ , with  $T$  being the photon temperature. If the number of particles is not changing, i.e. particles are not created nether destroyed,  $Y$  remains constant, namely the comoving number density is the density in a unit volume which expand with the Universe. Its physical volume increases but it is still called a unit volume.

The solution of the Boltzmann equation for hot relics is trivial. For relativistic particles ( $x \ll 1$ ) the freeze out occurs when the species are still relativistic and

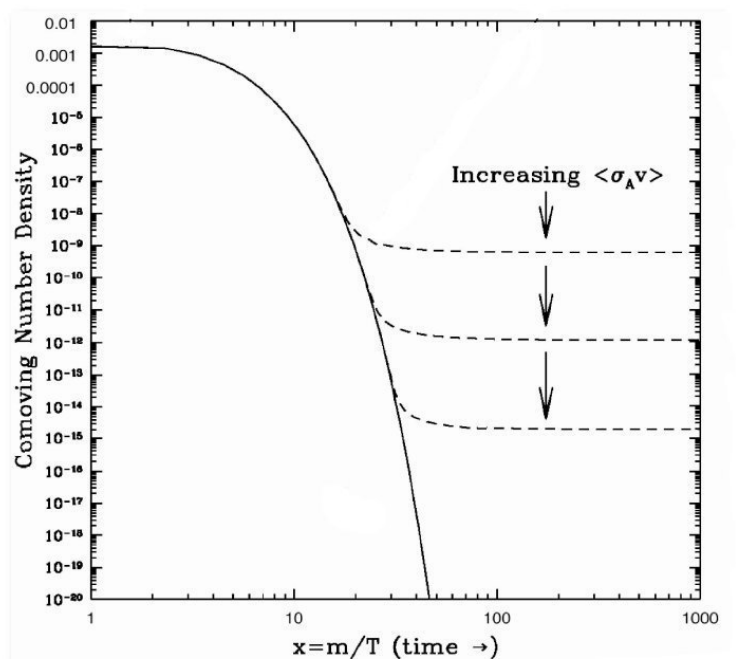


Figure 2.2: The comoving number density for non relativistic particle versus  $x = m/T$  is shown. The solid line represent the equilibrium number density distribution  $Y_{eq}$  and the dashed lines are the today  $Y_0$  comoving number density. The value at present time depends on the range of the annihilation interactions.

the number density in a comoving volume  $Y_{eq}$  is not changing with time. Since  $Y_{eq}$  is constant the final value of  $Y$  is insensitive to the details of freeze out and the asymptotic value of  $Y_0$  today (i.e. the value of  $x$  when decoupling takes place) is just the equilibrium value at freeze out. Thus the species decouple with order unity abundance relative to the number density of photons.

### 2.3.1 Freeze out for a non relativistic species

Non relativistic particles ( $x \gg 1$ ) are subject to a more involved decoupling history. The evolution of the comoving number density from the equilibrium distribution  $Y_{eq}$  to the today value  $Y_0$  is shown in Fig 2.2.

Qualitatively the relic abundance for a non relativistic species, which freezes out at  $x_f$ , is given, using an approximate solution of the evolution equation [45],

by:

$$\Omega h^2 \propto \frac{10^{-38} \text{cm}^2}{\langle \sigma v_{Mol} \rangle} \quad (2.38)$$

Notice that the interactions of the particles need to be extremely weak in order to have a relic abundance of the order  $\mathcal{O}(10^{-1})$ ; such particles are called by definition WIMPs. The inverse proportionality between  $\Omega$  and the thermal averaged cross section is clearly understood: stronger is the interaction rate, more depleted is the number density of the species and as a consequence the relic abundance is low; viceversa for weakly interacting particles the annihilation processes are less efficient, the particle freeze out at early time and at present time have a significant abundance, see Fig. 2.2.

We will now discuss in detail the non relativistic particle decoupling. The phase-space distribution can be properly described by the Maxwell-Boltzmann statistic. This is a safe approximation, using qualitative arguments: the particle species density will begin to differ from its equilibrium value only after  $T$  falls below the freezing temperature  $T_d$ . Typically  $T_d \sim \frac{1}{20}m$ , so that at these temperatures where it is a very good approximation to take the phase space distribution to be a MB distribution regardless of the statistics of the particles. This is a great simplification.

We will solve the Boltzmann equation for two generic species, 1 and 2, annihilating into the particle species 3 and 4. The Liouville operator is given by the left-hand side of Eq. 2.34, while the right side of the equation represents the collision operator, defined in Eq. 2.36. In general if the collision term is integrated over the momenta of the incoming particle only the inelastic contributions  $\mathbf{C}_{ann}$  survive:

$$g_1 \int \frac{d^3 p_1}{(2\pi)^3} \mathbf{C}[f(E_1, t)] = - \sum_{spins} \int d\mathcal{P} (2\pi)^4 \delta^4(p_1 + p_2 - p_3 - p_4) \times \\ \times (f_1 f_2 (1 \pm f_3)(1 \pm f_4) |\mathcal{M}_{12 \rightarrow 34}|^2 - f_3 f_4 (1 \pm f_1)(1 \pm f_2) |\mathcal{M}_{34 \rightarrow 12}|^2) \quad (2.39)$$

where the  $(1 \pm f)$  refers to the statistical factors, the  $+$ ( $-$ ) sign applies to bosons (fermions), the  $\mathcal{M}$  are the invariant amplitudes obtained with the usual Feynman rules, the sum is over the initial and final spins and:

$$d\mathcal{P} = \frac{d^3 p_1}{(2\pi)^3 2E_1} \frac{d^3 p_2}{(2\pi)^3 2E_2} \frac{d^3 p_3}{(2\pi)^3 2E_3} \frac{d^3 p_4}{(2\pi)^3 2E_4} \quad (2.40)$$

The Eq. 2.39 is valid even if the particles 1 and 2 are identicals (as in the case of Majorana fermions). No additional factors of  $\frac{1}{2}$  are needed since there is a factor of  $\frac{1}{2}$  to avoid double counting of the particle states and a factor of 2 due to the disappearance of two particles in each annihilation. For massive particles which

decouple in the early Universe while they are a non degenerate gas, we can neglect the statistical mechanical factors.

It is necessary to assume that the annihilation products go quickly into equilibrium with the thermal background. This is certainly true if these particles are electrically charged, since they interact with the many thermal photons present in the thermal bath, but it is still true for neutral particles. Since 3 and 4 are in thermal equilibrium we can write:

$$f_i = \exp(-E_i/T) \quad i = 3, 4 \quad (2.41)$$

Here we have neglected the chemical potential of the species. Actually if we have a group of particles  $A, B, C, \dots$  which enter a reaction producing particles  $A', B', C', \dots$  and if these particles are in chemical equilibrium then it should be:

$$\mu_A + \mu_B + \mu_C + \dots = \mu_{A'} + \mu_{B'} + \mu_{C'} + \dots \quad (2.42)$$

where the  $\mu_s$  are the chemical potential of the particles. Eq. 2.42 enable us to draw some conclusions about the chemical potential of various particles in chemical equilibrium:

- the photon chemical potential is necessarily zero  $\mu_\gamma = 0$ . This is traceable to the fact that the photon number is not conserved, i.e. a bremsstrahlung reaction like  $e + e \rightarrow e + e + \gamma$  would violate Eq. 2.42, unless  $\mu_\gamma$  were zero;
- particle and antiparticle  $X, \bar{X}$  can annihilate into photons  $X + \bar{X} \rightarrow \gamma + \gamma$ , so it follows that  $\mu_X = -\mu_{\bar{X}}$ , meaning that particle and antiparticle have opposite chemical potential;
- suppose there is a particle  $L$  described by an equilibrium FD statistical distribution of the form  $f_L = 1/[\exp(\mu_L + E_L/T) + 1]$ , thus it follows that for the antiparticle  $\bar{L}$ ,  $f_{\bar{L}} = 1/[\exp(\mu_{\bar{L}} + E_{\bar{L}}/T) + 1]$ . Hence, unless  $\mu_L$  is zero  $N_L \neq N_{\bar{L}}$ . For some  $L$  particles, such as electrons, we know from charge neutrality that, in the early Universe, prior to electron-positron annihilation,  $N_{e^-} \simeq N_{e^+}$ . Hence we shall take  $\mu_{e^-} = 0$ ;
- the neutrino chemical potential is a much more elusive quantity, and could be quite large in some regimes, but we set it to zero, in absence of a reason of the contrary. The neutrino–antineutrino asymmetry is constrained from cosmological observable as BBN and CMB and leads to stringent bounds for the neutrino chemical potential, see ref. [48]:  $-0.06 \leq \xi_e \leq 1.1$  for  $\nu_e$  and  $|\xi_{\mu,\tau}| \leq 5.6 - 6.9$  for  $\nu_{\mu,\tau}$ , with  $\xi = \mu/T$  is the degeneracy parameter. The bounds are stronger for electron neutrinos, since they are directly involved in neutron to proton conversion processes, which eventually fix the total amount of  $\text{He}^4$  produced in nucleosynthesis, while  $\xi_{\mu,\tau}$  only enters via their contribution to the expansion rate of the Universe.

The unpolarized Lorentz invariant cross section  $\sigma_{12\rightarrow 34}$ , using CP invariance, can be written as:

$$\sum_{spins} \int \frac{d^3p_3}{(2\pi)^3 2E_3} \frac{d^3p_4}{(2\pi)^3 2E_4} |\mathcal{M}_{12\rightarrow 34}|^2 (2\pi)^4 \delta^4(p_1 + p_2 - p_3 - p_4) = 4F g_1 g_2 \sigma_{12\rightarrow 34} \quad (2.43)$$

where F is  $F = \sqrt{(p_1 \cdot p_2)^2 - m_1^2 m_2^2}$ , while the spin factors  $g_1$  and  $g_2$  come from the average over the initial spins. The inclusion of all possible annihilation channels is trivial:

$$\sigma = \sum_{i=allSM}^{particles} \sigma_{12\rightarrow X_i \bar{X}_i} \quad (2.44)$$

The interaction term can be written in terms of the number density of the species  $n_1, n_2$  and  $n_i^{eq}$ , the number density the particles 1, 2 would have in thermal equilibrium at temperature  $T$ :

$$g_1 \int \frac{d^3p_1}{(2\pi)^3} \mathbf{C}[f_1(E_1, t)] = - \int \sigma v_{M\phi l} (dn_1 dn_2 - dn_1^{eq} dn_2^{eq}) \quad (2.45)$$

The Møller velocity  $v_{M\phi l} \equiv F/E_1 E_2$  represents the relative velocity of the particles in the comoving frame. The product  $v_{M\phi l} n_1 n_2$  is invariant under Lorentz transformations.

From symmetry considerations, the phase space distributions in kinetic equilibrium are proportional to those in chemical equilibrium, with a proportionality factor independent of momentum. This is true if species 1 and 2 are maintained in kinetic equilibrium through scattering with other particles and the thermal bath during all their evolution, even after decoupling when they are out of chemical equilibrium. Thus, before and after the decoupling, we can rewrite Eq. 2.45 as:

$$g_1 \int \frac{d^3p_1}{(2\pi)^3} \mathbf{C}[f_1(E_1, t)] = - \langle \sigma v_{M\phi l} \rangle (n_1 n_2 - n_1^{eq} n_2^{eq}) \quad (2.46)$$

where the thermally averaged total annihilation cross section times Møller velocity is defined by:

$$\langle \sigma v_{M\phi l} \rangle = \frac{\int \sigma v_{M\phi l} dn_1^{eq} dn_2^{eq}}{\int dn_1^{eq} dn_2^{eq}} \quad (2.47)$$

The last term in the right hand side of Eq. 2.46 is positive and describes the deviation from the exact thermal equilibrium.

Equating the collision term and the integrated Liouville the Boltzmann equation becomes:

$$\frac{dn_1}{dt} + 3Hn_1 = - \langle \sigma v_{M\phi l} \rangle (n_1 n_2 - n_1^{eq} n_2^{eq}) \quad (2.48)$$

There is an analogous equation for  $n_2$  with the same right-hand side. If particles 1 and 2 are identical, the density of the species  $n = n_1 = n_2$  satisfies:

$$\frac{dn}{dt} + 3Hn = - \langle \sigma v_{M\phi l} \rangle (n^2 - n_{eq}^2) \quad (2.49)$$

If 2 is the antiparticle of 1, the density of the species is  $n = n_1 + n_2$ . If the species have negligible chemical potential then  $n_1 = n_2$  and  $n = 2n_1$ . The equation for the particle (or antiparticle) density  $n_1$  is still Eq. 2.49, but the equation for  $n$  contains a factor of 1/2 in front of the cross section. Thus there is a factor of 1/2 in front of  $\sigma$  for non-identical initial particles, and no extra factor for identical initial particles.

Using the  $Y$  (Eq. 2.37) and  $x$  Eq. 2.49 takes the form:

$$\frac{dY}{dx} = - \left( \frac{45G}{\pi} \right)^{-1/2} \frac{\sqrt{g_*} m}{x^2} \langle \sigma v_{M\phi l} \rangle (Y^2 - Y_{eq}^2) \quad (2.50)$$

where for the definition of the Hubble parameter  $H$  we have used Eq. 2.5 with  $k = 0$ , and the quantity  $g_*$  differs slightly from the definition in Eq 2.16:

$$\sqrt{g_*} = \frac{g_{*s}}{\sqrt{g_*}} \left( 1 + \frac{1}{3} \frac{T}{g_{*s}} \frac{dg_{*s}(T)}{dT} \right) \quad (2.51)$$

since we have retained terms related to the change of  $g_{*s}(T)$  with temperature. They have to be taken into account if the relic particles decouple near the quark-hadron transition, otherwise, if there is no entropy production it is a good approximation to set  $dg_{*s}(T)/dT = 0$ . Notice that the results of the relic abundance may depend on assumptions made about the quark-hadron transition. At present there are no reliable models from which to obtain the value of  $g_*(T)$  and  $g_{*s}(T)$  in the region between the free hadron phase and the free quark phase [45]. It is believed that the quark-hadron transition takes place between 100 MeV and 400 MeV with the lower end favored by recent results on lattice gauge theory.

## 2.4 Full thermal averaged cross section

The thermal averaged cross section  $\langle \sigma v_{M\phi l} \rangle$  is the key quantity in the determination of the cosmic relic abundance of a species. Usually it is approximate by

expanding the cross section at low relative velocity, namely in power of  $x^{-1}$  [45]:

$$\langle \sigma v_{M\phi l} \rangle = a + \frac{3}{2}bx^{-1} + \dots \quad (2.52)$$

Notice in the expansion, the lowest order is given by a s-wave term, while to the first order it contributes as usual the p-wave term.

Indeed most species are not completely non-relativistic at decoupling: when  $x$  is of the order 20 – 25 relativistic corrections are expected. The low velocity approximation fails when the cross section is poor approximated by its expansion, as near the formation of a resonance or when its expansion diverges, as at the opening of a new annihilation channel.

Therefore if the cross section varies rapidly with the energy [49], it is compelling a general formula for the thermal average in the relativistic context, which involves a single integration and does not require expansion at low energies.

In the cosmic comoving frame, where the gas is assumed at rest as a whole, the thermal averaged cross section in Eq.2.47 turns out to be:

$$\langle \sigma v_{M\phi l} \rangle = \frac{\int \sigma v_{M\phi l} e^{-E_1/T} e^{-E_2/T} d^3 p_1 d^3 p_2}{\int e^{-E_1/T} e^{-E_2/T} d^3 p_1 d^3 p_2} \quad (2.53)$$

with 1 and 2 being the colliding particles. After some simply algebraic manipulations and changes of variables, we lead to a single integral expression for the thermal averaged cross section [49]:

$$\langle \sigma v_{M\phi l} \rangle = \frac{1}{8m^4 T K_2^2(m/T)} \int_{4m^2}^{\infty} \sigma(s - 4m^2) \sqrt{s} K_1(\sqrt{s}/T) ds \quad (2.54)$$

where the special functions  $K_i$  are the second order modified Bessel functions.

This equation has been obtained for particles with Maxwell-Boltzmann statistics. However if in the freeze-out calculations the relevant temperatures are less than the particle mass  $m$ , we can safely use the equation for all statistics, namely the final abundance of heavy relic is insensitive on the statistic of the particles, provided that  $T \lesssim 3m$ .

In the laboratory frame ( $lab$ ), Eq 2.54 becomes:

$$\langle \sigma v_{M\phi l} \rangle = \int_0^{\infty} d\epsilon \mathcal{K}(x, \epsilon) \sigma v_{lab} \quad (2.55)$$

The thermal kernel is defined as:

$$\mathcal{K}(x, \epsilon) \equiv \frac{2x}{K_2^2(x)} \sqrt{\epsilon} (1 + 2\epsilon) K_1(2x\sqrt{1 + \epsilon}) \quad (2.56)$$

where  $\epsilon$  is the dimensionless kinetic energy per unit,  $\epsilon = (s - 4m^2)/4m^2$ , and the velocity results to be  $v_{lab} = 2\sqrt{\epsilon}\sqrt{1+\epsilon}/(1+2\epsilon)$ . The derivation of the above formula follows the lines of [49].

As an alternative, rewriting Eq. 2.47 in the center of mass ( $cm$ ) frame, the thermal average of the annihilation process has the following expression:

$$\langle \sigma v_{M\phi l} \rangle = \int_0^\infty d\epsilon \sigma \mathcal{K}_{cm}(x, \epsilon) \quad (2.57)$$

$\mathcal{K}_{cm}(x, \epsilon)$  is this time the thermal kernel in the  $cm$  frame:

$$\mathcal{K}_{cm}(x, \epsilon) = \frac{2x}{K_2^2(x)} \left[ 1 + \frac{K_1^2(x)}{K_2^2(x)} \right] \sqrt{\epsilon + 1} \epsilon K_1(2x\sqrt{\epsilon + 1}) \quad (2.58)$$

where we have used the relations:

$$\langle \sigma v_{M\phi l} \rangle = \langle \sigma v_{lab} \rangle^{lab} = \langle \sigma v_{cm} \rangle^{cm} \frac{1}{2} \left[ 1 + \frac{K_1^2(x)}{K_2^2(x)} \right] \quad (2.59)$$

Notice that the thermal kernel is the probability distribution of the momentum or velocity of the particles at freeze out. Due to phase-space suppression, contained in the Bessel functions, only few particles will be at rest or almost at rest. Most of the particles will have low and intermediate velocities, while the abundance of high velocity particles will be strongly depleted. The Boltzmann suppression sets in at lower velocity when the temperature is decreased, i.e. the peak of the distribution is shift to the left.

All the calculations for the annihilation cross sections in this thesis have been done using Eqs. 2.57 and 2.58. Subsequently we briefly report some useful definitions for the cross section. In the center of mass frame, where the total three-momentum vanishes, the differential cross section is defined as:

$$\frac{d\sigma}{d\Omega} = \frac{1}{2E_1 2E_2 |\vec{v}_1 - \vec{v}_2|} \frac{|\vec{p}_3|}{(2\pi)^2 4E_{cm}} |\mathcal{M}_{12 \rightarrow 34}|^2 \quad (2.60)$$

where  $|\vec{v}_1 - \vec{v}_2|$  is the velocity in the  $cm$  frame. The following relation is verified:

$$2E_1 2E_2 |\vec{v}_1 - \vec{v}_2| = 4\sqrt{(p_1 \cdot p_2)^2 - m_1^2 m_2^2} \quad (2.61)$$

Rewriting the amplitude square and the differential cross section in terms of the Mandelstam invariants  $s, t$  and  $u$ :

$$\frac{d\sigma}{dt} = \frac{1}{64 |p_{cm}|^2 s} |\mathcal{M}(s, t)|^2 \quad (2.62)$$

where  $|p_{cm}|^2 s = (p_1 \cdot p_2)^2 - m_1^2 m_2^2$ . After integration over  $t$  or equivalently over the solid angle, Eq. 2.62 leads to the total cross section.

Therefore the so obtained expression for the thermal averaged cross section should be inserted in the Boltzmann equation, Eq. 2.50, to get the relic abundance of the considered species.

## 2.5 Coannihilation

In theories like supersymmetry under  $R$ -parity, it may occur that the relic particle is the lightest of a set of similar particles whose masses are nearly degenerate. The relic abundance of the lightest particle is determined not only by its annihilation cross section, but also by the annihilation of the heavier particles, which later decay into the lightest; this is the definition of coannihilation. Therefore, when coannihilation is included, the application of the standard methods in computing the thermal averaged cross section, Eq 2.54 and the Boltzmann Eq. 2.49, fails to give correct results and a modified treatment is required. First of all we will briefly rewrite the Boltzmann equations considering all the possible annihilation processes [50] and then we will present a modified expression for calculating the thermal average whether coannihilation is included [51].

Particles are presumed to exist which are nearly degenerate with, but have masses slightly greater than the relic one, denoted by  $\chi_1$ . If the mass difference  $\delta m \equiv m - m_1$  is large compared to the temperature  $T_f$ , when  $\chi_1$  annihilations freeze-out, then the extra particles play no significant role. However if  $\delta m \simeq T_f$  the extra particles are thermally accessible, namely they are nearly as abundant as the relic species and their annihilations processes can play an important role in determining the relic abundance.

Consider the evolution in the early Universe of a class of particles  $\chi_i$ ,  $i = 1, \dots, N$ , which differ from standard model particles by a discrete conserved quantum number. We assume that the particles are labeled such that  $m_i < m_j$ , when  $i < j$ ; that is,  $\chi_1$  has a mass  $m_1$  and is the lightest, while  $\chi_2$  is the second lightest, etc. The only allowed reactions that change the  $\chi_i$  number densities and determine their relic abundance in the early Universe are:



where  $A, A'$  denote any standard model particles. As long as reactions of type 2.65 take place at a reasonable rate, we expect that all the  $\chi_j$  ( $j > 1$ ) particles to have decayed into  $\chi_1$  particles by today.

The abundances of the  $\chi_i$  are determined by a set of  $N$  Boltzmann equations:

$$\begin{aligned} \frac{dn_i}{dt} = & -3Hn_i - \sum_{j=1}^N \langle \sigma_{ij} v_{ij} \rangle (n_i n_j - n_i^{eq} n_j^{eq}) - \sum_{j \neq i} [\Gamma_{ij}(n_i - n_i^{eq}) - \Gamma_{ji}(n_j - n_j^{eq})] \\ & - \sum_{j \neq i} [\langle \sigma'_{Aij} v_{ij} \rangle (n_i n_A - n_i^{eq} n_A^{eq}) - \langle \sigma'_{Aji} v_{ij} \rangle (n_j n_A - n_j^{eq} n_A^{eq})] \end{aligned} \quad (2.66)$$

The first term, as noticed in Eq. 2.49 is as usual the dilution due to the expansion of the Universe. The second term refers to the annihilation reactions as Eq. 2.63, while the third to Eq. 2.65 and finally the last term represents conversion by scattering on the cosmic thermal background, Eq. 2.64. The relative velocity is denote by  $v_{ij}$  and was defined in Eq. 2.61. We have defined the cross section of the different reactions and the decay rates as:

$$\sigma_{ij} = \sum_{A,A'} \sigma(\chi_i \chi_j \rightarrow AA') \quad (2.67)$$

$$\Gamma_{ij} = \sum_A \Gamma(\chi_i \rightarrow \chi_j A) \quad (2.68)$$

$$\sigma'_{Aij} = \sum_{A'} \sigma(\chi_i A \rightarrow \chi_j A') \quad (2.69)$$

Since all the  $\chi_i$  which survive annihilation eventually decay into  $\chi_1$ , the relevant quantity is the total density of  $\chi_i$  particle,  $n = \sum_{i=1}^N n_i$ . Substituting in Eq. 2.66 we find:

$$\frac{dn}{dt} - 3Hn = \sum_{i,j=1}^N \langle \sigma_{ij} v_{ij} \rangle (n_i n_j - n_i^{eq} n_j^{eq}) \quad (2.70)$$

We have retained in the equation only the main reaction which determine the freeze-out from the plasma. Indeed reactions of type 2.64 and 2.65 occur at a rate larger by a factor of  $10^9$  respect to the annihilation processes 2.63. In this case the  $\chi_i$  remain in thermal equilibrium and in particular their ratios are equal to the equilibrium values:

$$\frac{n_i}{n} \simeq \frac{n_i^{eq}}{n^{eq}} \quad (2.71)$$

We then get:

$$\frac{dn}{dt} = -3Hn - \langle \sigma_{eff} v \rangle (n^2 - n_{eq}^2) \quad (2.72)$$

where

$$\langle \sigma_{eff} v \rangle = \sum_{ij} \langle \sigma_{ij} v_{ij} \rangle \frac{n_i^{eq} n_j^{eq}}{n^{eq} n^{eq}} \quad (2.73)$$

is the thermal average of the effective cross section. It can be accommodated into an expression very similar to the case without coannihilation, Eq. 2.54, the only differences being the denominator and the replacement of the annihilation rate with the effective annihilation rate [49]:

$$\langle \sigma_{eff} v \rangle = \frac{\int_0^\infty dp_{eff} p_{eff}^2 W_{eff} K_1 \left( \frac{\sqrt{s}}{T} \right)}{m_1^4 \left[ \sum_i \frac{g_i}{g_1} \frac{m_i^2}{m_1^2} k_2 \left( \frac{m_i}{T} \right) \right]^2} \quad (2.74)$$

In the absence of coannihilation Eq 2.74 reduces to Eq. 2.54. The effective annihilation rate is defined as:

$$\begin{aligned} W_{eff} &= \sum_{ij} \frac{p_{ij}}{p_{11}} \frac{g_i g_j}{g_1^2} W_{ij} \\ &= \sum_{ij} \sqrt{\frac{[s - (m_i - m_j)^2] [s - (m_i + m_j)^2]}{s (s - 4m_1^2)}} \frac{g_i g_j}{g_1^2} W_{ij} \end{aligned} \quad (2.75)$$

where  $g_i, g_j$  are the particle degrees of freedom,  $W_{ij}$  is the annihilation rate for a single process summed over all possible final states and averaged over initial the particle spins. Notice that  $W_{ij}(s) = 0$  for  $s \leq (m_i + m_j)^2$ . Finally  $p_{ij}$  is the center of mass momentum, in particular  $p_{11} = p_{eff} = 1/2\sqrt{s - 4m_1^2}$ . In the effective annihilation rate coannihilations appear as thresholds at  $\sqrt{s}$  equal to the sum of the masses of the coannihilating particles. At high  $p_{eff}$  the Boltzmann suppression factor, contained in  $K_1$ , dominates.

The effective annihilation rate does not depend on the temperature, thus it can be calculated once and for all in a supersymmetric model.

## 2.6 Numerical Code

This is a technical section describing how we deal with the annihilation cross section calculations and the numerical methods we use to evaluate the thermal average and the integration of the Boltzmann equation.

The main ingredients characterizing the sneutrino phenomenology, given a specific supersymmetric model, are the relic abundance, the direct detection cross sections and the indirect annihilation signals. In all of these relevant physical quantities the particle properties of the sneutrino are of fundamental significance.

In particular the key building blocks in all the phenomenological calculations of this thesis are the Lorentz invariant squared amplitudes  $|\mathcal{M}_{ann}(\tilde{\nu}\tilde{\nu} \rightarrow f)|^2$ . The index *ann* refers to processes of annihilation of two sneutrinos in all possible final states  $f$  (these are listed in Tab. 4.1 and Tab. 4.2, depending on the supersymmetric model). We computed analytically the tree level amplitudes in the unitary gauge, using the HIP [52] package for Mathematica [53].

Considering the process  $p_1 p_2 \rightarrow p_3 p_4$ , we wrote all the possible annihilation processes in the  $s, t, u$  and interference channels that involve two incoming scalar particles, with different masses and quantum numbers, in the initial states. The final states are parameterized as follows:

- generic fermions  $f_1, f_2$
- generic vector bosons  $V_1, V_2$

- generic Higgs particles  $h_1, h_2$
- mixed final states with a generic Higgs boson  $h$  and a vector boson  $V$

Keeping fixed the Lorentz structure of each interaction vertex we multiplied it by a generic coupling constant, with real and imaginary part, to take into account the particle coupling constants and quantum numbers. The fermionic, vector boson and scalar boson propagators are expressed in terms of generic masses and decay widths. The cross section for each channel are obtained by analytically integrating over  $\cos\theta$ , where  $\theta$  is the angle between the momenta of the incident particle  $p_1$  and the produced particle  $p_3$  in the annihilation center of mass frame.

Therefore all the annihilation processes for the sneutrino are obtained by taking the viable channels and inserting in the vertices the desired couplings. The total effective cross section results by summing over all possible final states. We checked all the sneutrino squared amplitudes with the one produced by the package CompHep [54], in the framework of the minimal supersymmetric standard model.

It is clear that the subsequent calculations arise automatically:

**coannihilation** : the charged leptons are as well scalar particles, therefore in the sneutrino annihilation cross sections it suffices to substitute the correct vertices in order to get, e.g. the selectron annihilation channels, with the addition of the processes involving photons in the final states, absent in the sneutrino case. Clearly the same holds for  $\tilde{\nu}_L \tilde{l}_L$  coannihilation channels.

**extended supersymmetric models** : the sneutrino phenomenology changes, if we extend the content of the MSSM. As we will see, the main modifications are in the vertex couplings. Therefore we just insert in the squared amplitudes the desired interaction vertices, listed in Appendix A, in order to describe the annihilation processes in any supersymmetric model.

As a further improvement, we have repeated the procedure leading to the general expressions of the squared amplitudes also in the case of fermionic initial states, which can be applied e.g. to the neutralino, and of mixed initial states, which can arise in processes such as sneutrino neutralino coannihilation.

We have to pay attention when diagrams involve Majorana fermions, such as neutralinos, in the initial state or in the propagator. In the Feynman rules, Dirac fermions are denoted by a straight solid line and an arrow: the direction of the arrow is set by convention and indicate the flow of some quantum number. For Majorana fermions the direction of the arrow is arbitrary, since there is no distinction between particle and antiparticle, therefore they do not carry a conserved additive quantum number. The correct procedure is to first choose a direction for the arrow for a given Majorana fermion line, then one may unambiguously use the

Feynman rules for Majorana fermion presented in Ref [55]; respect to the Feynman rules for Dirac fermion there are additional constraints on the fermionic spinors  $u(k, s) = C\bar{v}^T(k, s)$  and  $v(k, s) = C\bar{u}^T(k, s)$  that arise from the definition of a Majorana fermion. These constraints are important when dealing with spin sums. The ambiguity in the fermionic line (namely we can chose which line denotes a particle and than fix consequently the line denoting an antiparticle) leads to ambiguity in the interference terms, where we have to be careful in dealing with the relative sign between two diagrams. If the Majorana particles are in the initial or final state, we have to multiply by a factor of 1/2 for avoiding double counting of identical particles. Example on how to deal with Majorana fermions are given in Ref [55].

The relic abundance is obtained by solving numerically the Boltzmann equation, Eq. 2.72. We generate FORTRAN routines for the numerical adaptive gaussian integration over  $p_{eff}$  of the thermal averaged cross section, Eq. 2.74, which takes into account coannihilation. The calculation of the effective invariant rate  $W_{eff}$  is the most time-consuming part. Fortunately it does not depend on the temperature  $T$  and it can be tabulated once for each model [49]. We have to make sure that the maximum  $p_{eff}$  in the table is large enough to include all important resonances, thresholds and coannihilation thresholds. In the thermal average, the effective invariant rate is weighted by  $K_1 p_{eff}$ : the fast exponential decay of the Bessel function at high  $p_{eff}$  suppresses resonances and thresholds, therefore we are safe enough to truncate the integration around  $p_{eff} = 20m_{\tilde{\nu}}$ . The tables are more densely populated in the important low  $p_{eff}$  region than elsewhere.

To perform the thermal average in Eq. 2.74, we integrate over  $p_{eff}$  by means of adaptive gaussian integration, using a spline to interpolate over the  $(p_{eff}, W_{eff})$  table. We finally integrate the Boltzmann equation using an implicit trapezoidal method with adaptive step size; the numerical integration starts when the second condition of Eq. 2.28 is met, namely the species begins to decouple.

In Fig 2.3 we show, as an example, the relic abundance obtained by the previous procedure for the annihilation of two neutralinos into a  $b\bar{b}$  pair, through  $s$  channel exchange of the A CP-odd Higgs boson. The solid [red] curve refers to our numerical results for Eq. 2.57, since we do not consider coannihilation, and the dashed [black] curve to the approximated thermal average, reported in Eq. 2.52. Notice that at the A pole, the red curve is well defined, while the expansion fails to give a finite result. An example of thresholds opening clearly appears in Fig. 4.1, where it is plotted the relic abundance of the sneutrino. The sharp drop at  $m_1 \sim 80$  GeV denotes the threshold of the  $W^+W^-$  channel. In this case the relic abundance is computed using Eq. 2.74, since coannihilation is included.

The thermal average does not contribute directly to the scattering cross section off nuclei for direct searches, but enters in the  $\xi$  factor, through the  $\Omega h^2$  factor,

Eq. 5.23. Instead the  $(p_{eff}, W_{eff})$  tables are very useful for indirect detection signals, since the differential production rate for photons, antimatter and neutrinos are proportional to  $\langle \sigma_{ann} v \rangle_0$ . The subscript 0 refers to a thermal average at present time over the velocity distribution of the relic WIMPs in the galactic halo; the velocity distribution is nearly a Maxwell-Boltzmann with  $\beta = v/c \simeq 10^{-3}$ , leading to a temperature  $T_{WIMP} \sim v^2$ . Performing the numerical integration of Eq. 2.57 (notice that at present time the coannihilating particles are no longer present subsequently their decays into the dark matter particles) at this temperature is equivalent to keep in the approximate formula Eq. 2.52 the s wave contributions, namely the  $a$  terms. Therefore, once we numerically evaluate the annihilation cross section as a function of the effective momentum  $p_{eff}$ , we are able to perform both the thermal average in the early Universe, for prediction on the present relic abundance (at temperature around  $T \sim m_{\tilde{\nu}}/20$ ), and at the temperature  $T_{WIMP}$ , for predictions on the annihilation signals in the galaxy.

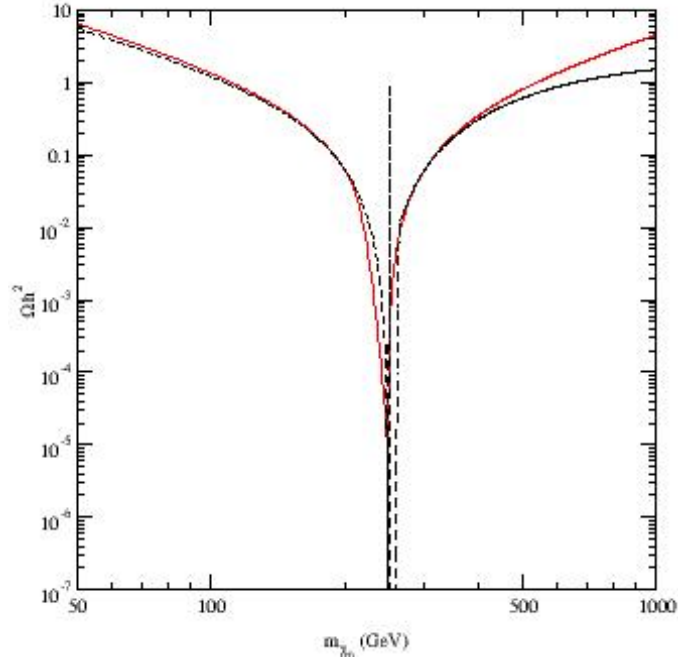


Figure 2.3: Relic abundance  $\Omega h^2$  of neutralino vs its mass  $m_{\tilde{\chi}^0}$  for the single process  $\tilde{\chi}^0 \tilde{\chi}^0 \rightarrow b\bar{b}$  in the  $s$  channel mediated by the CP-even Higgs boson  $A$ . The solid [red] curve refers to our numerical solution for the relic abundance, the dashed [black] curve corresponds to the  $a$  term, Eq. 2.52, of the thermal average expansion.

# Chapter 3

## Supersymmetry

The Standard Model (SM) of elementary particle physics [56, 57, 58], based on the  $SU(3)_C \times SU(2)_W \times U(1)_Y$  gauge symmetry, provides a remarkably successful theory in describing the strong and electroweak interactions. Despite experiments at energies of the order 100 GeV confirm no deviations from SM predictions there are few unambiguous hints of additional structure and a number of theoretical and phenomenological issues that the SM fails to address adequately:

**Hierarchy problem** Phenomenologically the mass of the Higgs boson associated with electroweak symmetry breaking must be in the electroweak range,  $\mathcal{O}(100 \text{ GeV})$ . The Higgs potential is given by:

$$V = m_H^2 |H|^2 + \lambda |H|^4 \quad (3.1)$$

The SM requires a non-vanishing vacuum expectation value  $\langle \text{VEV} \rangle$  for  $H$  at the minimum of the potential. This will occur if  $m_H^2 < 0$ , resulting in  $\langle H \rangle = \sqrt{-m_H^2/2\lambda}$ . Since we know experimentally that  $\langle H \rangle = 174 \text{ GeV}$  from measurements of the properties of the weak interactions, it must be that  $m_H^2$  is of the order of the electroweak symmetry breaking scale. However, radiative corrections to the Higgs mass are quadratically dependent on the UV cutoff  $\Lambda$ , since the masses of fundamental scalar fields are not protected by chiral or gauge symmetries. Namely let consider a Dirac fermion  $f$ , with a mass  $m_f$  and coupling  $-\lambda_f H \bar{f} f$  to the Higgs. Its loop contribution to  $m_H^2$  yields:

$$\Delta m_H^2 = \frac{|\lambda_f|^2}{16\pi^2} \left\{ -2\Lambda^2 + 6m_f^2 \ln\left(\frac{\Lambda}{m_f}\right) + \dots \right\} \quad (3.2)$$

The largest correction comes from the top quark, whose Yukawa coupling is of the order  $\lambda_{top} \sim 1$ . Therefore, the “natural” value of the Higgs mass is of  $\mathcal{O}(\Lambda)$ , leading to a destabilization of the hierarchy of the mass scales in the

SM. On the one hand if we choose the cut-off scale  $\Lambda$  to be the GUT scale ( $M_{\text{GUT}}^2 \sim 10^{16}$  GeV), or the Planck scale ( $M_P^2 \sim 10^{18}$  GeV), the Higgs boson mass will prefer to be close to the very high scale and thus huge. For the SM Higgs boson to stay relatively light, at least  $m_H < 1$  TeV for unitarity and perturbativity reasons, we need to add a counterterm to the mass squared and adjust it with a precision of  $\mathcal{O}(10^{-30})$ , which seems highly unnatural and fine-tuned. On the other hand the question why  $\Lambda \gg m_Z$  arises.

**Electroweak symmetry breaking (EWSB)** In the SM, electroweak symmetry breaking is parameterized by the Higgs boson  $H$  and its potential  $V(H)$ , see Eq. 3.1. However, the Higgs sector must be put into the theory by hand.

**Gauge coupling unification** The model is based on the direct product of three simple groups with different coupling constants and, in this sense, does not provide a true unification of the electroweak and strong interactions. Therefore, one may expect the existence of a more fundamental Grand Unified Theory (GUT), able to describe the three forces within a single group, such as  $SU(5)$  or  $SO(10)$ , with just one coupling constant. However, given the high-precision measurements at LEP and the particle contents of the SM, the renormalization group evolution of the gauge coupling constants is such that they fail to meet at a common point, the GUT scale.

**Family structure and fermion masses** The SM does not explain the existence of three families and can only parameterize the strongly hierarchical values of the fermion masses. Massive neutrinos imply that the theory has to be extended, since in the SM the neutrinos are strictly left-handed and massless. Right-handed neutrinos can be added, but achieving ultralight neutrino masses from the see-saw mechanism requires the introduction of a new scale which may be much larger than  $\mathcal{O}(100$  GeV).

**Cosmological challenges** Several difficulties are encountered when trying to build cosmological models based solely on the SM particle content. The baryon asymmetry generated at the electroweak phase transition is too small. The SM does not have a viable candidate for the CDM, nor viable inflaton.

SM is widely believed to be an effective theory valid only at presently accessible energies. Certainly a new framework will be required at the reduced Planck scale  $M_P = (8\pi G_N)^{-1/2} \sim 10^{18}$  GeV, where quantum gravitational effects become important. Theories with low energy supersymmetry have emerged as one of the strongest candidates for physics beyond the SM.

Supersymmetry (SUSY) is a symmetry relating fermions and bosons: each particle has a superpartner which differs in spin by  $1/2$ . Therefore a supersymmetric transformation turns a bosonic state into a fermionic state and viceversa.

The main reason why SUSY is considered the best-motivated possibility for new physics at the TeV scale is that it can solve simultaneously the above mentioned open issues:

**Naturalness problems** Suppose the existence of a complex scalar particle  $S$  with mass  $m_S$  and trilinear coupling to the Higgs given by  $-\lambda_S$ . The leading contributions to the Higgs self-energy are:

$$\Delta m_H^2 = \frac{\lambda_S}{16\pi^2} \left\{ \Lambda^2 - 2m_S^2 \ln\left(\frac{\Lambda}{m_S}\right) + \dots \right\} \quad (3.3)$$

If one assume that the Higgs coupling of the scalar particle is related to the Higgs-fermion coupling in such a way that  $\lambda_f^2 = \lambda_S$ , once one add Eqs. 3.2 and 3.3, the quadratic divergences disappear. The logarithmic divergence is still present, but even for values  $\Lambda \sim M_P$  of the cut-off, the contribution is rather small. This logarithmic divergence vanishes if, in addition, the fermion and the scalar have the same mass  $m_S = m_f$ . The conclusion is that, if there are scalar particles with a symmetry which relates their couplings to the fermion couplings there are no quadratic divergences to the Higgs boson mass: the hierarchy and naturalness problems are solved. If in addition there exists exact “supersymmetry”, which enforces the scalar having the same mass as the fermion, there are no divergences at all and the Higgs mass is protected. Generalizing the argument to the other SM fields, the introduction of fermionic partners to the gauge bosons and adjusting their couplings to the Higgs, all the quadratically divergent corrections are canceled. If the symmetry is badly broken and the masses of the scalar particles are much larger than the fermion and Higgs masses, the hierarchy and naturalness problems would be reintroduced again in the theory, coming from radiative terms proportional to  $(m_f^2 - m_S^2) \ln(\Lambda/m_S)$ . Such a term becomes large again and  $m_H$  will have the tendency to exceed the unitarity and perturbativity limit of  $\mathcal{O}(1 \text{ TeV})$ . Therefore to keep the Higgs mass in the range of electroweak symmetry breaking scale, one may make small the mass difference between the SM and the new particles. For the radiative corrections to be of the same order of the tree level Higgs mass, the new particles should not be much heavier than the TeV scale. For further references see e.g. [59, 60, 61, 62, 63, 64].

**Radiative EWSB** Electroweak symmetry breaking can thus take place in a natural way in the SUSY theories via a radiative mechanism, see e.g. [65, 66, 67].

**Gauge coupling unification** The new SUSY particle spectrum contributes to the renormalization group evolution of the three gauge coupling constants and alters their slopes so that they can meet at an energy scale slightly above  $10^{16} \text{ GeV}$ , see e.g. [68, 69, 70, 71].

**CDM** In supersymmetric theories the lightest superpartner (LSP) may be stable. The LSP provides a nice heavy, non baryonic Dark Matter candidate.

Until yet none of the superpartners of the Standard Model particles have been discovered. Therefore Supersymmetry, if it exist, is a broken symmetry in nature. In the lagrangian we distinguish two contributions:  $\mathcal{L}_{\text{SUSY}}$ , described in the next section 3.2, is the supersymmetric lagrangian, and  $\mathcal{L}_{\text{soft}}$ , of which we will talk about in section 3.4, breaks Supersymmetry and contains many free parameters, characterizing the masses and additional couplings of the supersymmetric particles.

However the sparticle spectrum is constrained by the negative results for searching SUSY at colliders [72]. In particular the sneutrino lower mass bound will be discussed in the chapter 4.

The aim of this chapter is not to provide a full supersymmetric theory description, instead it only sketch the SUSY outstanding marks leading to the superparticle phenomenology; for exhaustive and complete reviews see e.g. [55, 73, 74, 75]. A brief outline of the minimal extension of the Standard Model (MSSM) particle contents and properties is given in section 3.5. We will first introduce the supersymmetric algebra 3.1, the superfield formalism, see sections 3.1.1 and 3.1.2, and the superspace 3.1.3.

## 3.1 Supersymmetric Algebra and Superfields

In particle physics the S-matrix and the underlying theory possess various symmetries:

- Poincaré invariance, the semi-direct product of translations, with generator  $P_\mu$ , and Lorentz rotations,  $M_{\mu\nu}$ . The generators satisfy the algebra:

$$\begin{aligned} [P_\mu, P_\nu] &= 0 \\ [P_\beta, M_{\mu\nu}] &= i(g_{\beta\mu}P_\nu - g_{\beta\nu}P_\mu) \\ [M_{\alpha\beta}, M_{\mu\nu}] &= i(g_{\alpha\nu}M_{\beta\mu} + g_{\beta\mu}M_{\alpha\nu} - g_{\alpha\mu}M_{\beta\nu} - g_{\beta\nu}M_{\alpha\mu}) \end{aligned} \quad (3.4)$$

where  $g_{\mu,\nu}$  is the usual metric tensor (+,-,-,-).

- Internal global symmetries, related to conserved quantum numbers such as the electric charge and isospin. The symmetry generators  $B_l$  are Lorentz scalars and for gauge theories generate a Lie algebra, with structure constants  $C_{lm}^k$ :

$$\begin{aligned} [B_l, B_m] &= iC_{lm}^k B_k \\ [B_l, P_\mu] &= 0 \\ [B_l, M_{\mu\nu}] &= 0 \end{aligned} \quad (3.5)$$

- Discrete symmetries: charge conjugation C, parity P and time reversal T.

As a consequence of Eqs. 3.5 the Poincaré algebra has two Casimir operators, the mass operator  $P^2 = P_\mu P^\mu$ , with eigenvalues  $m^2$ , and the square of the Pauli-Ljubanski vector:

$$W_\sigma = \frac{1}{2} \epsilon_{\sigma\alpha\beta\gamma} P^\alpha M^{\beta\gamma} \quad (3.6)$$

where  $\epsilon_{\alpha\beta\mu\nu}$  is the antisymmetric Levi-Civita tensor.  $W^2$  has eigenvalues  $-m^2 s(s+1)$  for massive states and  $W_\sigma = \lambda P$  for massless states, where  $\lambda$  is the helicity.

Coleman and Mandula [76] demonstrated that the previous ones are the only possible symmetries of the S-matrix, basically assuming that the symmetric algebra can involve only commutators.

As mentioned before, both for phenomenological and technical reasons, a symmetry connecting fermions and bosons is appealing. The generators  $Q$  of this symmetry must turn a bosonic state into a fermionic one and viceversa. Therefore the generators themselves carry half-integer spin, i.e. are anticommuting spinors and represent not an internal symmetry but a spacetime symmetry.

Haag, Lopuzanski and Sohnius [77] proved that the assumption of having only commuting generators may be weakened, yielding possible Supersymmetry as a symmetry of a gauge theory. Rather they demonstrated that Supersymmetry is the only possible extension of the known spacetime symmetries of particle physics.

The simplest choice of SUSY generators is a two-dimensional Weyl spinor  $Q_\alpha$  with its conjugate; it is possible to extend in a consistent way the number of generators up to  $N = 8$ , however we will always refer to  $N = 1$  SUSY models.

Since these generators are fermionic, their algebra can most easily be written in term of anticommutators:

$$\begin{aligned} \{Q_\alpha, Q_\beta\} &= \{\bar{Q}_{\dot{\alpha}}, \bar{Q}_{\dot{\beta}}\} = 0 \\ \{Q_\alpha, \bar{Q}_{\dot{\beta}}\} &= 2\sigma_{\alpha\dot{\beta}}^\mu P_\mu \\ [Q_\alpha, P_\mu] &= [\bar{Q}_{\dot{\alpha}}, P_\mu] = 0 \\ [Q_\alpha, M_{\mu\nu}] &= \frac{1}{2} \sigma_{\mu\nu\alpha}^\beta Q_\beta \\ [\bar{Q}_{\dot{\alpha}}, M_{\mu\nu}] &= -\frac{1}{2} \bar{Q}_{\dot{\beta}} \sigma_{\mu\nu\dot{\alpha}}^{\dot{\beta}} \end{aligned} \quad (3.7)$$

where  $\sigma_\alpha^{mn\beta}$  are the  $SL(2, C)$  generators. The operators  $Q_\alpha$  and  $\bar{Q}_{\dot{\alpha}}$  belong respectively to the  $(1/2, 0)$  and  $(0, 1/2)$  representation of the Lorentz group.  $Q_\alpha$  behaves like a left-handed Weyl spinor (with an undotted index), while  $\bar{Q}_{\dot{\alpha}}$  as a right-handed Weyl spinor (with a dotted index). If applied to a field with spin  $j$ , they let transform it into a field with spin  $j \pm 1/2$ .

For SUSY,  $P^2$  is still a Casimir operator, since  $Q$  and  $\bar{Q}$  commute with  $P$ , but  $W^2$  is not. One can define a new Casimir operator  $C^2$ :

$$\begin{aligned} C^2 &= C_{\mu\nu}C^{\mu\nu} \\ C_{\mu\nu} &= B_\mu P_\nu - B_\nu P_\mu \\ B_\mu &= W_\mu - \frac{1}{4}\bar{Q}_{\dot{\alpha}}\bar{\sigma}_\mu^{\dot{\alpha}\beta}Q_\beta \end{aligned} \tag{3.8}$$

Eqs. 3.7 and 3.8 let deduce important properties of SUSY multiplets: particles belonging to the same irreducible SUSY representation should not have the same spin ( $W^2$  is not an invariant quantity), however need to have the same mass. The Casimir operator  $C^2$  points out that in a supermultiplet the bosonic and fermionic degrees of freedom should be the same, says  $n_F = n_B$ .

A compact description of a supersymmetric field theory requires the introduction of fermionic coordinates  $\theta, \bar{\theta}$ . These are anticommuting Grassman variables:

$$\{\theta^\alpha, \theta^\beta\} = \{\bar{\theta}_{\dot{\alpha}}, \bar{\theta}_{\dot{\beta}}\} = \{\theta^\alpha, \bar{\theta}_{\dot{\beta}}\} = 0 \tag{3.9}$$

Of course the objects on which these SUSY transformations act must then also depend on  $\theta$  and  $\bar{\theta}$ . These objects are the so called *superfields*, functions of the *superspace*  $(x^\mu, \theta, \bar{\theta})$ , where  $x^\mu$  are the spacetime coordinates.

It is clear that Supersymmetry doubles the spacetime coordinates, due to the introduction of  $\theta, \bar{\theta}$  as two component spinors. A generic global supersymmetric transformation is defined as:

$$S(x, \theta, \bar{\theta}) = e^{i(-x_\mu P^\mu + \theta Q + \bar{\theta} \bar{Q})} \tag{3.10}$$

The composition of two supersymmetric transformations  $S(x, \theta, \bar{\theta})S(y, \zeta, \bar{\zeta})$  is a translation in the superspace:

$$(x, \theta, \bar{\theta}) \rightarrow (x + y + i\theta\sigma^\mu\bar{\zeta} - i\zeta\sigma^\mu\bar{\theta}, \theta + \zeta, \bar{\theta} + \bar{\zeta}) \tag{3.11}$$

This equation leads to a differential definition of the  $Q_\alpha$  and  $\bar{Q}_{\dot{\alpha}}$  operators:

$$\begin{aligned} Q_\alpha &= \frac{\partial}{\partial\theta^\alpha} - i\sigma_{\alpha\dot{\beta}}^\mu\bar{\theta}^{\dot{\beta}}\partial_\mu \\ \bar{Q}_{\dot{\alpha}} &= -\frac{\partial}{\partial\bar{\theta}^{\dot{\alpha}}} + i\theta^\beta\sigma_{\beta\dot{\alpha}}^\mu\partial_\mu \end{aligned} \tag{3.12}$$

with  $P_\mu = -i\partial_\mu$ .

We can now define the general scalar superfield  $\Phi(x, \theta, \bar{\theta})$ : it has a finite Taylor expansion in power of  $\theta^\alpha, \bar{\theta}_{\dot{\alpha}}$ , called component expansion, therefore it may contain

fields with different statistic. The series is truncated due to the anticommuting nature of the variables, namely powers higher than  $\theta^2$  and  $\bar{\theta}^2$  are null:

$$\begin{aligned} \Phi(x, \theta, \bar{\theta}) = & f(x) + \theta\phi(x) + \bar{\theta}\bar{\psi}(x) + \theta\theta m(x) + \bar{\theta}\bar{\theta}n(x) \\ & + \theta\sigma^\mu\bar{\theta}v_\mu(x) + \theta\theta\bar{\theta}\bar{\lambda}(x) + \bar{\theta}\bar{\theta}\theta\xi(x) + \theta\theta\bar{\theta}\bar{\theta}d(x) \end{aligned} \quad (3.13)$$

From Eqs. 3.12 it is possible to obtain the mass dimension of  $\theta$ , which is  $-1/2$ . Therefore the superfield components have increasing mass dimension, starting from  $[f]$ , which has the same dimension of  $\Phi$ , up to  $[d] + 2$ .  $\psi, \chi, \lambda, \xi$  carry a spinorial index, hence describe fermions, while  $f, m, n, v_\mu, d$  are bosonic fields. In nature a physical boson has mass dimension 0 or 1 and a fermion  $3/2$ : from Eq. 3.13 we can construct chiral superfield, where the fermionic field and the scalar field have the right dimensions and vector superfield, where the vector field is the physical one. The components having dimensions different from the physical ones are called auxiliary fields: they have no dynamics and can be easily removed from the lagrangian using their trivial equation of motions.

A supersymmetric transformation change the components of  $\Phi$  with dimension  $\mathcal{D}$  into the components with dimension immediately higher  $[\mathcal{D} + \infty/ \epsilon]$  and in the derivative of the components immediately lower  $[\mathcal{D} + \infty/ \epsilon]$  [78]. The highest dimension of the superfield  $d$  transforms as a total space time derivative; this properties will be useful in defining the invariant supersymmetric action.

The superfield expression in Eq. 3.13 is a reducible representation. Imposing some constraints on  $\Phi$ , the superfield will have the right particle field contents.

### 3.1.1 Chiral supermultiplets

The name chiral superfield comes from the fact that the SM fermions are chiral, namely their left-handed and right-handed components transform differently under  $SU(2)_W \times U(1)_Y$ . We therefore need superfields with only two physical fermionic degrees of freedom, which can then describe the left or right handed component of a SM fermion. Of course, the same supermultiplets carry the bosonic partners, the sfermions.

The chiral superfields can describe spin 0 bosons and spin 1/2 fermions, i.e. they can accommodate the Higgs bosons and the quarks and leptons.

The superfield expression in Eq. 3.13 is a reducible representation. Imposing some constraints on  $\Phi$ , the superfield will have the right particle field contents. A chiral superfield arises from Eq. 3.13 imposing the condition:

$$\bar{D}_{\dot{\alpha}}\Phi = 0 \quad (3.14)$$

where  $\bar{D}_{\dot{\alpha}}$  is the covariant derivative, defined as:

$$\begin{aligned}\bar{D}_{\dot{\alpha}} &= -\bar{\partial}_{\dot{\alpha}} - i\theta^{\beta}\sigma_{\beta\dot{\alpha}}^m\partial_m \\ D_{\alpha} &= \partial_{\alpha} + i\sigma_{\alpha\dot{\beta}}^m\bar{\theta}^{\dot{\beta}}\partial_m\end{aligned}\tag{3.15}$$

Defining new bosonic coordinates  $y^{\mu} = x^{\mu} + i\theta\sigma^{\mu}\bar{\theta}$  in the superspace, any function  $\Phi(y, \theta)$  of  $y^{\mu}$  and  $\theta^{\alpha}$ , but not  $\bar{\theta}_{\dot{\alpha}}$ , satisfying the constraint Eq. 3.14, gets the simple expression:

$$\Phi(y, \theta) = \phi(y) + \sqrt{2}\theta\psi(y) + \theta\theta F(y)\tag{3.16}$$

where  $\phi(y)$ ,  $F(y)$  are complex scalar fields, while  $\psi^{\alpha}(y)$  is a complex left-handed Weyl spinor. There are  $4 + 4 = 8$  real off-shell field components. Assigning the usual mass dimension 1 to the scalar field  $\phi$ , which results to be the same as for the superfield, the fermionic field, as mentioned before, has the correct physical dimension; instead the field  $F$  has the unusual mass dimension 2, therefore is an auxiliary field.

Antichiral superfields  $\Phi^{\dagger}$ , i.e. right-handed superfields, are defined as the conjugates of chiral fields  $\Phi(y, \theta)$ , functions of the coordinates  $y^{\dagger} = x^{\mu} - i\theta\sigma^{\mu}\bar{\theta}$  and  $\bar{\theta}$ . They satisfy:

$$\begin{aligned}D_{\alpha}\Phi^{\dagger} &= 0 \\ \Phi^{\dagger} &= \phi^*(y^{\dagger}) + \sqrt{2}\bar{\theta}\bar{\psi}(y^{\dagger}) + \bar{\theta}\bar{\theta}F^*(y^{\dagger})\end{aligned}\tag{3.17}$$

Since  $D_{\alpha}$  and  $\bar{D}_{\dot{\alpha}}$  obey the chain rule, any product of chiral (antichiral) superfields is also a chiral (antichiral) superfield. Instead  $\Phi\Phi^{\dagger}$  and  $\Phi + \Phi^{\dagger}$  are not superfields, however the latter turn out to be a special case of a vector superfields.

### 3.1.2 Gauge supermultiplets

We have to describe the gauge sector of the SM, which contains the spin 1 vector bosons. They are introduced by vector superfield.

A vector supermultiplet is defined to be self-conjugate:

$$V(x, \theta, \bar{\theta}) \equiv V^{\dagger}(x, \theta, \bar{\theta})\tag{3.18}$$

In form of components, Eq. 3.18 leads to the following expression for  $V$ :

$$\begin{aligned}V(x, \theta, \bar{\theta}) &= (1 + \frac{1}{4}\theta\theta\bar{\theta}\bar{\theta}\partial_{\mu}\partial^{\mu})C(x) + (i\theta + \frac{1}{2}\theta\theta\sigma^{\mu}\bar{\theta}\partial_{\mu})\chi(x) - \theta\sigma_{\mu}\bar{\theta}A^{\mu}(x) \\ &\quad + i\theta\theta\bar{\theta}\bar{\lambda}(x) - i\bar{\theta}\bar{\theta}\theta\lambda(x) + \frac{1}{2}\theta\theta\bar{\theta}\bar{\theta}D(x) - \frac{i}{2}\bar{\theta}\bar{\theta}[M(x) - iN(x)] \\ &\quad + \frac{i}{2}\theta\theta[M(x) + iN(x)] + (-i\bar{\theta} + \frac{1}{2}\bar{\theta}\bar{\theta}\sigma^{\mu}\theta\partial_{\mu})\bar{\chi}(x)\end{aligned}\tag{3.19}$$

We end up with seven components: 4 real scalars, two Weyl spinor and the vector field  $A^\mu$ . We now have many more gauge degrees of freedom than in non supersymmetric theories, since now the gauge parameters are themselves superfields. Any superfield action invariant under abelian gauge transformation will also be independent of several component fields of  $V(x, \theta, \bar{\theta})$ . This transformation rule can be written as:

$$V \rightarrow V + i(\Lambda - \Lambda^\dagger) \quad (3.20)$$

with  $\Lambda(x, \theta, \bar{\theta})$  is a chiral superfield. Remembering that a chiral superfield contains four scalar degrees of freedom as well as one Weyl spinor, it achieves the possibility of using Eq. 3.20 to fix:

$$\chi(x) = C(x) = M(x) = N(x) \equiv 0 \quad (3.21)$$

This is well-known as Wess-Zumino (WZ) gauge-fixed superfield [79]. The WZ gauge is in some sense the SUSY analog of the unitarity gauge in field theory, since it removes many unphysical degrees of freedom and let unchanged the gauge freedom.

Assigning the usual mass dimension 1 to  $A^\mu$ ,  $V(x, \theta, \bar{\theta})$  describes a vector boson, a fermion field  $\lambda$  and has an auxiliary field  $D$ , with trivial equations of motion and mass dimension 2.

### 3.1.3 Superspace integration

Before going on and present the supersymmetric Lagrangian in 3.2, a brief detour into the technical details of the integration in the superspace is needed.

We begin with the Berezin integration for a single Grassmann parameter  $\theta$ :

$$\begin{aligned} \int d\theta\theta &= 1 \\ \int d\theta &= 0 \\ \int d\theta f(\theta) &= f_1 \end{aligned} \quad (3.22)$$

where we have used the Taylor expansion of a function of a single Grassmann variable,  $f(\theta) = f_0 + f_1\theta$ . Two integration properties emerge from Eqs. 3.22:

- translationally invariant

$$\begin{aligned} \int d(\theta + \xi) f(\theta + \xi) &= \int d\theta f(\theta) \\ \int d\theta \frac{d}{d\theta} f(\theta) &= 0 \end{aligned} \quad (3.23)$$

- equivalent to differentiation

$$\frac{d}{d\theta}f(\theta) = f_1 = \int d\theta f(\theta) \quad (3.24)$$

We introduce the Grassmann delta function:

$$\delta(\theta) \equiv \theta \quad (3.25)$$

The important notations are:

$$\begin{aligned} d^2\theta &= -\frac{1}{4}d\theta^\alpha d\theta^\beta \epsilon_{\alpha\beta} \\ d^2\bar{\theta} &= -\frac{1}{4}d\bar{\theta}_{\dot{\alpha}} d\bar{\theta}_{\dot{\beta}} \epsilon^{\dot{\alpha}\dot{\beta}} \\ d^4\theta &= d^2\theta d^2\bar{\theta} \end{aligned} \quad (3.26)$$

Using these notations and the spinor summation convention, one gets:

$$\begin{aligned} \int d^2\theta\theta\theta &= 1 \\ \int d^2\bar{\theta}\bar{\theta}\bar{\theta} &= 1 \end{aligned} \quad (3.27)$$

## 3.2 Supersymmetric Lagrangian

The next attempt, after the definition of the superspace and the superfield properties, is the construction of a supersymmetric field theory. By definition, one requires the action to be invariant under SUSY transformations:

$$\delta_S \int d^4x \mathcal{L}(x) = 0 \quad (3.28)$$

This is satisfied if  $\mathcal{L}$  itself transforms into a total derivative. As noticed in the section 3.1, the highest components of the chiral and vector superfields meet this requirement. They can therefore be used to construct the Lagrangian. Thus the action  $S$  turns out to be:

$$\begin{aligned} S &= \int d^4x \left( \int d^2\theta \mathcal{L}_F + \int d^2\theta d^2\bar{\theta} \mathcal{L}_D \right) \\ &= \int d^4x \{ (\mathcal{L}_F)_{\theta\theta} + (\mathcal{L}_D)_{\theta\theta\bar{\theta}\bar{\theta}} \} \end{aligned} \quad (3.29)$$

$\mathcal{L}_F$  and  $\mathcal{L}_D$  are general chiral and gauge superfields, giving rise to the so-called "F-terms" and "D-terms", respectively.

### 3.2.1 Scalar Lagrangian

In order to construct a renormalizable SUSY theory, the Lagrangian can carry only terms with mass dimension up to 4. Therefore, the only available terms contains at most three powers of chiral superfields. As stated before, the product of left (right)-handed superfields is a left (right)-handed superfield :

$$\mathcal{L}_\Phi = (\Phi_i \Phi_i^\dagger)_{\theta\theta\bar{\theta}\bar{\theta}} + \left[ \left( \lambda_i \Phi_i + \frac{1}{2} m_{ij} \Phi_i \Phi_j + \frac{1}{3} g_{ijk} \Phi_i \Phi_j \Phi_k \right)_{\theta\theta} + h.c. \right] \quad (3.30)$$

The kinetic term is given by  $\Phi_i \Phi_i^\dagger$ , while in the bracket the interaction terms are shown, with  $m_{ij}$  and  $g_{ijk}$  generic index symmetric couplings. The meaning of the different terms becomes manifest rewriting Eq. 3.30 into the various components:

$$\begin{aligned} \mathcal{L}_\Phi &= i\partial_\mu \bar{\psi}_i \sigma^\mu \psi_i + \phi_i^* \square \phi_i + F_i^* F_i \quad (3.31) \\ &+ \left[ m_{ij} \left( \phi_i F_j - \frac{1}{2} \psi_i \psi_j \right) + g_{ijk} (\phi_i \phi_j F_k - \psi_i \psi_j \phi_k) + \lambda_i F_i + h.c. \right] \end{aligned}$$

The  $F$  fields have no kinetic term, since they are auxiliary fields and can be eliminated using their trivial equation of motions, given by:

$$\partial \mathcal{L} / \partial F_j = 0 \quad (3.32)$$

In order to illustrate how the  $F$  fields can be removed from  $\mathcal{L}_\Phi$ , let define the superpotential  $V$  as:

$$V(\Phi_i) = \frac{1}{2} \sum_{i,j} m_{ij} \Phi_i \Phi_j + \frac{1}{3} \sum_{ijk} g_{ijk} \Phi_i \Phi_j \Phi_k \quad (3.33)$$

The Lagrangian in Eq. 3.31 can be rewritten as:

$$\mathcal{L}_\Phi = F_i^* F_i + \phi_i^* \square \phi_i - i\partial_\mu \bar{\psi}_i \sigma^\mu \psi_i + \left[ \frac{\partial V(\phi_i)}{\partial \phi_j} F_j - \frac{1}{2} \frac{\partial^2 V(\phi_i)}{\partial \phi_j \partial \phi_k} \psi_j \psi_k + h.c. \right] \quad (3.34)$$

Using Eq. 3.32, the auxiliary fields are integrated out:

$$F_i = - \left[ \frac{\partial V(\phi_i)}{\partial \phi_j} \right]^* \quad (3.35)$$

This last expression, substituted into Eq. 3.34, leads to:

$$\mathcal{L}_\Phi = \mathcal{L}_{kin} - \left[ \frac{\partial^2 V(\phi_i)}{\partial \phi_j \partial \phi_k} \psi_j \psi_k + h.c. \right] - \left| \frac{\partial V(\phi_i)}{\partial \phi_j} \right|^2 \quad (3.36)$$

Here  $\mathcal{L}_{kin}$  stands for the second and third terms of Eq. 3.34. The first bracket describes fermion masses and Yukawa interactions, while the last term describes scalar mass terms and scalar interactions. Since both terms are determined by the single function  $V$ , there are clearly many relations between coupling constants.

### 3.2.2 Vector Lagrangian

A supersymmetric invariant kinetic term for gauge fields is carried out by the  $W_\alpha$  and  $\bar{W}_{\dot{\alpha}}$  spinors, defined as:

$$\begin{aligned} W_\alpha &= -\frac{1}{4}\bar{D}\bar{D}D_\alpha V(x, \theta, \bar{\theta}) \\ \bar{W}_{\dot{\alpha}} &= -\frac{1}{4}DD\bar{D}_{\dot{\alpha}} V(x, \theta, \bar{\theta}) \end{aligned} \quad (3.37)$$

Notice that  $\bar{D}_{\dot{\alpha}}W_\alpha = 0$  and  $D_\alpha\bar{W}_{\dot{\alpha}} = 0$ , therefore they are a left-handed and right-handed chiral superfield, respectively. While  $V$  is a vector superfield. The Lagrangian for a vector superfield is simply:

$$\mathcal{L}_V = \frac{1}{4}(W^\alpha W_\alpha)_{\theta\theta} + (\bar{W}^{\dot{\alpha}}\bar{W}_{\dot{\alpha}})_{\bar{\theta}\bar{\theta}} \quad (3.38)$$

In the ‘‘Wess-Zumino’’ gauge:

$$\mathcal{L}_V = -\frac{1}{4}F_{\mu\nu}F^{\mu\nu} - i\lambda\sigma^\mu\partial_\mu\bar{\lambda} + \frac{1}{2}D^2 \quad (3.39)$$

They reproduce exactly the strength for a vector boson  $A_\mu$ ,  $F_{\mu\nu} = \partial_\mu A_\nu - \partial_\nu A_\mu$ . Notice that the D term does not propagate, as well as the F-term. In this case there are no interaction terms, therefore  $D = 0$ . In a gauge theory, it can be removed from the lagrangian and leads to quartic bosonic interactions.

### 3.2.3 Gauge Invariance

Up to now, the theory we have constructed in 3.2.1 and 3.2.2 is invariant under SUSY transformations. In order to build a supersymmetric extension of the SM, the lagrangian needs to be invariant under gauge transformations. We can proceed as usual, first defining gauge transformations for the bosonic and fermionic chiral superfield components, then introducing vector fields, belonging to vector superfields, which transform exactly in such a way to keep the lagrangian gauge invariant. This procedure leads moreover to the implementation in the lagrangian of the gauge interactions.

If we consider the abelian gauge group  $U(1)$ , the transformation for the chiral superfield reads:

$$\begin{aligned} \Phi &\rightarrow \Phi' = e^{-ig\Lambda}\Phi \\ \Phi^\dagger &\rightarrow \Phi'^\dagger = e^{ig\Lambda^\dagger}\Phi^\dagger \end{aligned} \quad (3.40)$$

with  $g$  the  $U(1)$  charge. The parameter  $\Lambda$  has to be a left-handed superfield, in order to end up still with chiral superfields.

If the gauge transformation is global, namely does not depend on the space coordinates, the only term in Eq. 3.30 which is not invariant is  $\lambda_i \Phi_i$ ; thus this kind of terms can not appear in the lagrangian. If the gauge transformation is local, even the kinetic term does not preserve the gauge invariance. It is needed the introduction of a vector superfield, which transforms as:

$$V \rightarrow V' = V + i(\Lambda - \Lambda^\dagger) \quad (3.41)$$

The kinetic lagrangian  $\mathcal{L}_{kin}$  therefore has the minimal coupling:

$$\Phi_i^\dagger \Phi_i \rightarrow \Phi_i^\dagger e^{gV} \Phi_i \quad (3.42)$$

This leads to the right transformation laws for the physical fields:

$$A_\mu \rightarrow A'_\mu = A_\mu - i\partial_\mu(a^* - a) \quad (3.43)$$

with  $a$  the scalar component of the  $\Lambda$  left-handed superfield. Instead  $\lambda$  and  $D$  are gauge invariant quantities:

$$\begin{aligned} \lambda &\rightarrow \lambda' = \lambda \\ D &\rightarrow D' = D \end{aligned} \quad (3.44)$$

The most general supersymmetric lagrangian, invariant under abelian gauge transformation is:

$$\mathcal{L}_{\text{SUSY}} = \frac{1}{4}(W^\alpha W_\alpha)_{\theta\theta} + (\bar{W}^{\dot{\alpha}} \bar{W}_{\dot{\alpha}})_{\bar{\theta}\bar{\theta}} + \Phi_i^\dagger e^{g\Lambda} \Phi_i + V(\Phi_i) \quad (3.45)$$

where  $V(\Phi_i)$  is the superpotential, defined in Eq. 3.56, an holomorphic function of the superfield and constituted only by gauge invariant interactions.

If the gauge group is non abelian the situation is quite similar, there are just technical modifications. The chiral superfield has the same transformation law as in Eq. 3.40, however  $\Lambda$  is now a matrix:

$$\Lambda_{ij} = T_{ij}^a \Lambda_a \quad (3.46)$$

with  $T^a$  being the gauge group generators, in the same representation of the superfield  $\Phi$ . Therefore we may introduce as many vector superfields  $V_a$  as the number of generators:

$$V_{ij} = T_{ij}^a V_a \quad (3.47)$$

The transformation rule in Eq. 3.42 becomes:

$$e^{gV} \rightarrow e^{gV'} = e^{-ig\Lambda^\dagger} e^{gV} e^{ig\Lambda} \quad (3.48)$$

The coupling choice is always the minimal coupling of Eq. 3.42

The spinor  $W_\alpha$  transforms as:

$$W_\alpha = -\frac{1}{4}\bar{D}\bar{D}e^{-gV}D_\alpha e^{gV} \quad (3.49)$$

with the generators in the adjoint group representation.

Notice that the scalar superfield  $\Phi$  contains the matter content of the theory and belong to the chiral representation of the supersymmetric group and to the fundamental representation of the gauge group. Instead the vector field belongs to the real representation of the SUSY transformations and to the adjoint representation of the gauge group.

### 3.3 R-parity

As mentioned in section 3.1, a generic field theory has internal symmetries, with generators  $B_l$ . Let's take an abelian group, for a supersymmetric theory one gets the following commutators:

$$\begin{aligned} [Q_\alpha, B_l] &= Q_\alpha \\ [\bar{Q}_{\dot{\alpha}}, B_l] &= -\bar{Q}_{\dot{\alpha}} \end{aligned} \quad (3.50)$$

Clearly only one independent combination of the abelian generators actually has a nonzero commutator with  $Q_\alpha$  and  $\bar{Q}_{\dot{\alpha}}$ ; let us denote this U(1) generator by  $R$ :

$$\begin{aligned} [Q_\alpha, R] &= Q_\alpha \\ [\bar{Q}_{\dot{\alpha}}, R] &= -\bar{Q}_{\dot{\alpha}} \end{aligned} \quad (3.51)$$

Thus SUSY in general possesses an internal global U(1) symmetry known as  $R$ -symmetry. Notice that the supersymmetric generators have  $R$ -charge +1 and -1 respectively.

The supersymmetric lagrangian may contains renormalizable, gauge invariant terms which violate the lepton number  $L$  or the baryon number  $B$ . In addition, as we will see in the next sections, the SUSY particle spectrum contains majorana fermions, leading to  $L$ -violating processes. Since such a reactions have never been observed in experiments, no fermion number violation would seem to occur. Concerning the baryon number violation, the most obvious experimental constraint comes from the non-observation of proton decay. If the majorana particles were massless then a generalization of fermion number conservation could be defined. However these particles cannot have a zero mass, since supersymmetric particles have not yet been observed, in which case the continuous  $R$ -symmetry of Eq. 3.51 must be broken [55]. It turns out that despite this breaking a discrete  $R$ -symmetry

remains, described by the  $Z_2$  group. This leads to the multiplicatively conserved quantum number called  $R$ -parity.

Formally one can define the  $R$ -parity of any particle of spin  $j$ , baryon number  $B$  and lepton number  $L$  to be:

$$R = (-1)^{2j+3(B-L)} \quad (3.52)$$

Particles within the same supermultiplet do not have the same  $R$ -parity: all ordinary particles are assigned a  $R$ -parity  $+1$ , whereas the supersymmetric partners have a  $R$ -parity of  $-1$ . If  $R$ -parity is exactly conserved, then there can be no mixing between the SUSY and ordinary particles and every interaction vertex will contain an even number of  $R = -1$  particles.

The  $R$ -parity assignment is very useful for phenomenology, since it leads to three important consequences:

- supersymmetric particles can be produced only in pairs;
- there must be a lightest supersymmetric particle (LSP): such a particle could not decay, must be stable. If the LSP is electrically neutral, it is weakly interacting with ordinary matter and can make an interesting candidate for CDM;
- each sparticle other than the LSP must eventually decay into a state which contains an odd number of LSP (usually just one).

We will consider supersymmetric models conserving  $R$ -parity.

## 3.4 Supersymmetry Breaking

A realistic phenomenological model must contain supersymmetry breaking: the supersymmetric lagrangian in Eq. 3.45 assigns identical masses to the ordinary SM particles and their superpartners. This is clearly not realistic, if supersymmetry exists.

We expect that supersymmetry should be an exact symmetry which is spontaneously broken, namely the ultimate model should have a lagrangian density which is invariant under SUSY transformations, but a vacuum state which is not. Unfortunately it is not easy to break supersymmetry spontaneously. One problem follows directly from the definition of the SUSY algebra in Eq. 3.7:

$$\frac{1}{4} (\bar{Q}_1 Q_1 + Q_1 \bar{Q}_1 + \bar{Q}_2 Q_2 + Q_2 \bar{Q}_2) = P^0 \equiv H \quad (3.53)$$

where  $H$  is the Hamiltonian. If supersymmetry is unbroken in the vacuum state, it follows that  $H|0\rangle = 0$  and the vacuum has zero energy. Conversely, if SUSY is

spontaneously broken in the vacuum state, then the vacuum must have positive energy, since  $\langle 0|H|0\rangle > 0$  from Eq. 3.53. Therefore supersymmetry will be broken if  $F_i$  and/or  $D^a$  does not vanish in the ground state, namely we are looking for models in which the equations  $F_i = 0$  and  $D^a = 0$  can not be simultaneously satisfied for any values of the fields.

Many models of spontaneous symmetry breaking have indeed been proposed: these always involve extending the minimal supersymmetric model to include new particles and interactions at very high energy scales and there is no consensus on exactly how this should be done.

Supersymmetry breaking through non zero  $D$ -terms is achieved by the Fayet-Iliopoulos mechanism [80]. These models have troublesome problems, such as breaking color,  $U(1)_{em}$  charge or can not give rise to the correct mass scale for the gaugino sector.

Models where supersymmetry breaking is due to non zero  $F$ -terms, called O’Raifeartaigh models [81], determine the mass scale for SUSY breaking of a dimensionful parameter introduced by hand. At the end these models seem to be *ad hoc*.

Supersymmetry breaking may then be best described in terms of the effective dynamics of the strongly coupled theory, which naturally generate the right scale for the gauginos and scalar masses. These terms arise indirectly or radiatively rather than from tree-level renormalizable couplings to the supersymmetric breaking order parameters. Supersymmetry breaking evidently occurs in a ”hidden sector” of particles which have no (or only very small) direct coupling to the ”visible sector” chiral supermultiplets of the minimal supersymmetric model. However the two sectors do share some interactions which are responsible for mediating supersymmetry breaking from the hidden sector to the visible sector, where they appear as calculable terms. There are two main competing proposal for what the mediating interaction might be. The first is that they are gravitational, associated to the new physics, which appears at the Planck scale; this is the so called gravity-mediated supersymmetry breaking scenario. The second possibility is that the flavor-blind mediating interactions for supersymmetry breaking are the ordinary electroweak and QCD gauge interactions. In this gauge-mediated scenario the effective terms arise from loop diagrams involving some messenger particles.

From a practical point of view it is extremely useful to simply parameterize the effects of the hidden sector by just introducing extra terms which break supersymmetry explicitly in the effective minimal supersymmetric lagrangian. The new couplings should be soft in order to naturally maintain a hierarchy between the electroweak scale and the Planck mass scale. Namely the introduction of dimensionless supersymmetry breaking couplings is forbidden.

In the most general SUSY breaking lagrangian  $\mathcal{L}_{soft}$ , the allowed terms turn

out to be:

- scalar masses  $-m_i^2|\phi_i|^2$
- gaugino masses  $-\frac{1}{2}m_l\bar{\lambda}_l\lambda_l + h.c.$
- trilinear scalar interactions  $-a_{ijk}\phi_i\phi_j\phi_k + h.c.$
- bilinear scalar terms  $-b_{ij}\phi_i\phi_j + h.c.$

Gauge symmetry always let to introduce masses for gauginos. The  $m_{ij}^2$  terms are allowed for  $i, j$  such that  $\phi_i, \phi_j^*$  transform in complex conjugate representation of each other under all gauge symmetry; in particular this is true if  $i = j$ , so every scalar is eligible to get a mass. The other terms may be present depending on the lagrangian symmetries: the  $a_{ijk}$  and  $b_{ij}$  are allowed by gauge symmetry only if the corresponding terms are considered in the superpotential.

Possible soft terms for the chiral supermultiplets fermions could always be reabsorbed into a redefinition of the superpotential and the scalar masses and trilinear couplings. It has been shown rigorously that a softly-broken supersymmetric theory is indeed free from quadratic divergences to all orders in perturbation theory [82].

It is clear that  $\mathcal{L}_{soft}$  breaks supersymmetry, since it involves only gauginos and sfermions and not their respective superpartners. The soft terms are capable of giving masses to all of the scalars and gauginos even if the gauge bosons and chiral fermions are massless or relatively light.

Most of we do not already know about a SUSY model has to deal with  $\mathcal{L}_{soft}$ .

## 3.5 Minimal Supersymmetric Standard Model

We will present the minimal supersymmetric extension of the Standard Model, the MSSM, starting from the generic supersymmetric lagrangian, Eq. 3.45, and the soft breaking lagrangian introduced in section 3.4.

The minimal supersymmetric lagrangian is the sum of the supersymmetric lagrangian  $\mathcal{L}_{SUSY}$  and the soft SUSY breaking lagrangian  $\mathcal{L}_{soft}$ :

$$\mathcal{L}_{MSSM} = \mathcal{L}_{SUSY} + \mathcal{L}_{soft} \quad (3.54)$$

The first term of the right hand side is defined as:

$$\mathcal{L}_{SUSY} = \mathcal{L}_{gauge} + \mathcal{L}_{chiral} \quad (3.55)$$

The chiral lagrangian is given in Eq. 3.34, while the gauge part is reported in Eq. 3.38. The soft lagrangian will be described in the succeeding discussion, see Eq. 3.59.

“Minimal” extension means that we want to keep the number of superfields and interactions as small as possible. Since the SM matter fermions reside in different representations of the gauge group than the gauge bosons, we have to place the minimal numbers of different superfields. One generation of the SM is therefore described by five left-chiral superfields:  $\hat{Q}$  contains the (s)quark  $SU(2)$  doublets,  $\hat{D}$  and  $\hat{U}$  contain the up and down (s)quark singlet,  $\tilde{L}$  describes the (s)lepton doublets and finally  $\hat{R}$  contains the (s)lepton singlets. Of course we need three generations to describe the matter content of the Standard Model. We have to introduce vector superfields to describes the gauge sector. In particular we need eight gluinos  $\tilde{g}$  as partners of the gluons, three winos  $\tilde{W}$  as partners of the  $SU(2)$  gauge bosons and a bino  $\tilde{B}$  as  $U(1)_Y$  gaugino. The only subtlety in the field content of the MSSM is in the choice of the Higgs sector. As in the SM we want to break  $SU(2)_W \times U(1)_Y$  invariance by  $SU(2)$  doublet scalar with hypercharge  $|Y| = 1/2$ . Looking through the fields that have already been introduced, the slepton doublets fulfill this requirement. Unfortunately the sneutrino can not play the role of the Higgs boson: if sneutrino would acquire a VEV, the lepton number would be explicitly broken. The masses of chiral fermions must originate from terms in the superpotential. Thus the superpotential has to be an analytic function of the scalar superfields. This means that we are not allowed to introduce the hermitian conjugate of a Higgs superfield in  $W_{\text{MSSM}}$ . It would then be impossible to introduce  $U(1)_Y$  invariant term that give masses to both up-type and down-type quark if there is only one Higgs superfield. We need at least two  $SU(2)$  Higgs doublets. All the standard model particles with their supersymmetric partners are shown in Tab. 3.1.

The MSSM superpotential is given by:

$$W_{\text{MSSM}} = \epsilon_{ij} \left( \mu \hat{H}_i^1 \hat{H}_j^2 - Y_e^{IJ} \hat{H}_1^I \hat{L}_j^J \hat{R}^J - Y_d^{IJ} \hat{H}_1^I \hat{Q}_j^J \hat{D}^J + Y_u^{IJ} \hat{H}_1^I \hat{Q}_j^J \hat{U}^J \right) \quad (3.56)$$

while the scalar potential is computed as:

$$V = \frac{1}{2} (D^a D^a + (D')^2) + F_i^* F_i \quad (3.57)$$

where:

$$\begin{aligned} F_i &= \frac{\partial W}{\partial A_i} \\ D^a &= \frac{1}{2} g A_i^* \sigma_{ij}^\mu A_j \\ D' &= \frac{1}{2} e A_i^* A_j \end{aligned} \quad (3.58)$$

In the above expressions,  $A_i$  collectively denotes all scalar fields appearing in the theory.

SM	Particles/Fields	SUSY Partners			Supermultiplets
Symbol	Name	Interaction eigenstates	Name	Mass eigenstates	Symbol
$q$	quark	$\tilde{q}_L, \tilde{q}_R$	squark	$\tilde{q}_1, \tilde{q}_2$	$\hat{Q}, \hat{U}, \hat{D}$
$l$	lepton	$\tilde{l}_L, \tilde{l}_R$	slepton	$\tilde{l}_1, \tilde{l}_2$	$\hat{L}, \hat{R}$
$\nu$	neutrino	$\tilde{\nu}_L$	sneutrino	$\tilde{\nu}_L$	$\hat{L}$
$g$	gluon	$\tilde{g}$	gluino	$\tilde{g}$	$\hat{g}$
$W^\pm$	W boson	$\tilde{W}^\pm$	wino	$\tilde{\chi}_i^\pm$	$\hat{W}$
$H^-$	H boson	$\tilde{H}_1^-$	higgsino	chargino	$(\hat{H}_1^0, \hat{H}_1^-)$
$H^+$	H boson	$\tilde{H}_2^+$	higgsino	$i = 1, 2$	$(\hat{H}_2^+, \hat{H}_2^0)$
$B$	B field	$\tilde{B}$	bino	$\tilde{\chi}_i^0$	$\hat{B}$
$W^3$	$W^3$ field	$\tilde{W}^3$	wino	neutralino	$\hat{W}$
$H_1^0$	H boson	$\tilde{H}_1^0$	higgsino	$i = 0, 1, 2, 3$	$(\hat{H}_1^0, \hat{H}_1^-)$
$H_2^0$	H boson	$\tilde{H}_2^0$	higgsino		$(\hat{H}_2^+, \hat{H}_2^0)$
$H_3^0$	H boson				

Figure 3.1: The MSSM particle content, with both interactions and the mass eigenstates. The corresponding superfields are reported.

The dimensionless Yukawa couplings  $Y_u^{IJ}, Y_d^{IJ}, Y_e^{IJ}$  are  $3 \times 3$  matrices in family space, which we will consider real and diagonal in flavor space. They determine the masses and CKM mixing angle of the ordinary quarks and leptons, after EWSB. Since the top, the bottom and the tau are the heaviest fermions in the SM usually the approximation that only the third family components are important.

Since the Yukawa interactions in a general supersymmetric theory must be completely symmetric, these terms imply not only Higgs-quark-quark and Higgs-lepton-lepton interactions, but also i.e. squark-Higgsino-quark and slepton-Higgsino-lepton interactions. In general, from  $R$ -parity conservation it follows that in each vertex there must be an even number of sparticles. As a consequence, for each SM vertex one can construct the corresponding MSSM vertices by changing two of the particles into their superpartners. In addition, the superpotential in Eq. 3.56 introduces new interactions, such as scalar quartic couplings.

The term proportional to  $\mu$  is dimensionful and provides for higgsinos mass terms as well as Higgs (mass)<sup>2</sup> terms. Since it is positive definite, it is clear that we cannot understand electroweak symmetry breaking without including supersymmetry breaking (mass)<sup>2</sup> soft term for the Higgs scalars, which can be negative.

The most physical relevant interaction vertices in the MSSM are typically dom-

inated by the supersymmetric interactions of gauge-coupling strength. The couplings of the  $Z, W, \gamma$  and gluons to the MSSM particles are determined completely by gauge invariance of the kinetic terms in the lagrangian.

Thus the structure of the MSSM Lagrangians allows very little arbitrariness. In fact all of the dimensionless couplings and all but one mass term,  $\mu$ , correspond directly to some parameters in the ordinary SM which were already measured by experiment. In contrast, the supersymmetric breaking lagrangian apparently show a considerable amount of arbitrariness:

$$\begin{aligned}
 \mathcal{L}_{soft}^{MSSM} = & -\frac{1}{2} \left( M_3 \tilde{g}\tilde{g} + M_2 \tilde{W}\tilde{W} + M_1 \tilde{B}\tilde{B} \right) + h.c. \\
 & - \epsilon_{ij} \left( \Lambda_u^{IJ} \tilde{U}^{J*} \tilde{Q}_j^I H_i^2 - \Lambda_d^{IJ} \tilde{D}^{J*} \tilde{Q}_j^I H_i^1 + \Lambda_e^{IJ} \tilde{R}^{J*} \tilde{L}_j^I H_i^1 \right) + h.c. \\
 & - (M_Q^2)^{IJ} \tilde{Q}_i^{J*} \tilde{Q}_j^I - (M_U^2)^{IJ} \tilde{U}^I \tilde{U}^{J*} - (M_D^2)^{IJ} \tilde{D}^I \tilde{D}^{J*} \\
 & - (M_L^2)^{IJ} \tilde{L}_i^{J*} \tilde{L}_j^I - (M_R^2) \tilde{R}^I \tilde{R}^{J*} \\
 & - m_{H_2}^2 H_2^* H_2 - m_{H_1}^2 H_1^* H_1 - (b H_1 H_2 + h.c.)
 \end{aligned} \tag{3.59}$$

In Eq. 3.59  $M_1, M_2$  and  $M_3$  are the bino, wino and gluino mass parameters. Each of  $\Lambda_e^{IJ}, \Lambda_u^{IJ}, \Lambda_d^{IJ}$  is in general a complex  $3 \times 3$  matrix in family space. The third line of Eq. 3.59 consist of squark and sleptons mass terms:  $(M^2)^{IJ}$  are hermitian matrices in family space. Finally in the last line we have supersymmetry breaking contributions to the Higgs potential. All the  $M_i^2$  are of the order  $\mathcal{O}(m_{soft}^2)$ , while  $M_i$  and  $\Lambda_i$  are defined at the mass scale  $m_{soft}$ , with  $m_{soft}$  not much larger than  $\mathcal{O}(1 \text{ TeV})$ .  $\mathcal{L}_{soft}^{MSSM}$  introduces more than 100 real parameters with no counterpart in the ordinary SM.

From the experiments it is possible to derive many organizing hints, leading to a drastic reduction in the number of free parameters. Most of the soft parameters involves flavor mixing, flavor changing neutral current (FCNC) and CP violation of the type which is already severely restricted by observational data. All of these effects in the MSSM can be evaded if one assume a soft-breaking universality:

$$\begin{aligned}
 M_Q^2 = m_Q^2 \mathbf{1} \quad M_U^2 = m_U^2 \mathbf{1} \quad M_D^2 = m_D^2 \mathbf{1} \quad M_L^2 = m_L^2 \mathbf{1} \quad m_R^2 = m_R^2 \mathbf{1} \\
 \Lambda_U = A_{u0} Y_u \quad \Lambda_D = A_{d0} Y_d \quad \Lambda_e = A_{e0} Y_e \\
 \arg(M_1), \arg(M_2), \arg(M_3), \arg(A_{u0}), \arg(A_{d0}), \arg(A_{e0}) = 0 \quad \text{or} \quad \pi
 \end{aligned} \tag{3.60}$$

From Eqs. 3.60 it follows that the scalar mass parameters should be real and that the soft terms do not introduce new complex phases. The matrices  $\Lambda_i^{IJ}$  are therefore real and diagonal in flavor space. For the Higgs sector, in order to avoid complex phases and a non-hermitian lagrangian, the  $\mu$  parameter and  $m_{H_i}^2$  should set to be real.

The soft breaking universality relations are presumed to be the result of some specific model for the origin of supersymmetry breaking. Even if it is rather

unknown what the specific mechanism should actually be. Therefore there are in general two different approaches for reducing the parameter freedom arising from the soft breaking potential. In the so-called high-energy approach one impose a particular structure on the supersymmetry breaking terms at a common high energy scale, such as the Planck scale or the Grand Unification Scale (GUT,  $M_{GUT} = 10^{16}$  GeV) scale. Using the renormalization group equations, one can then derive the low-energy MSSM parameters relevant for collider physics. The initial conditions (at the appropriate high-energy scale) for the renormalization group equations depend on the mechanism by which supersymmetry breaking is communicated to the effective low energy theory. Examples of this scenario are provided by models of gravity-mediated and gauge-mediated supersymmetry breaking. An alternative approach is a low-energy approach, in which the soft breaking parameters are fixed at the electroweak scale.

The supersymmetric model we adopt here in this thesis belongs to this second type of approach, and is the so-called effective MSSM scheme at the electroweak scale. The free independent parameters at low energy are: the SU(2) gaugino mass parameter  $M_2$ , the ratio between the U(1) and SU(2) gaugino mass parameters  $R \equiv M_1/M_2$  (in GUT-induced case  $R = 5/3 \tan^2 \theta_W \simeq 0.5$ ). The Higgs sector (Sec 3.5.1) will be described in addition by the Higgs mixing parameter  $\mu$ ,  $\tan \beta = v_2/v_1$  and the mass of the CP-odd Higgs  $m_A$ , the masses of the other Higgs bosons are calculated from  $m_A$  by employing two-loop corrections. We will have a common soft-mass for all the squarks (Sec 3.5.3),  $m_Q$  (both right-handed and left-handed), and a common dimensionless trilinear parameter for the third family  $A$  ( $A_{\tilde{t}_0} = A_{\tilde{b}_0} \equiv Am_{\tilde{Q}}$  and  $A_{\tilde{\tau}_0} \equiv Am_{\tilde{L}}$  and the trilinear parameters for the other families being set equal to zero). Therefore we end up with few free parameters, to which the free sneutrino parameters (presented in Chapter 4 and in Section 3.5.3) will add up. In our calculations we will present first a fixed configuration in the SUSY parameter space and we will scan the sneutrino mass parameters, then we will present the results for a full scan of the supersymmetric parameter space as reported in Appendix B.

### 3.5.1 Higgs sector

The two Higgs-doublets have opposite hypercharge,  $H_1$  with  $T_3 = -1$  and  $H_2$  with  $T_3 = 1$ , and are defined as:

$$H_1 = \begin{pmatrix} H_1^0 \\ H_1^- \end{pmatrix} \quad H_2 = \begin{pmatrix} H_2^+ \\ H_2^0 \end{pmatrix} \quad (3.61)$$

The Higgs potential gets contribution from the scalar potential and from the

soft breaking potential,  $V_{Higgs} = V + V_{soft}$ :

$$V = \frac{1}{8}g_2^2 \left( 4|H_1^{I*} H_2^J|^2 - 2(H_1^{i*} H_1^i)(H_2^{j*} H_2^j) + (H_1^{i*} H_1^i)^2 + (H_2^{i*} H_2^i)^2 \right) + \frac{1}{8}g_1^2 (H_2^{i*} H_2^i - H_1^{i*} H_1^i)^2 + |\mu|^2 (H_2^{i*} H_2^i + H_1^{i*} H_1^i) \quad (3.62)$$

$$V_{soft} = m_1^2 H_1^{i*} H_1^i + m_2^2 H_2^{i*} H_2^i - (B\mu\epsilon_{ij} H_1^i H_2^j + h.c.) \quad (3.63)$$

Notice that in the MSSM the strength of the quartic interactions is determined by the gauge coupling, instead this is not the SM case, where it is an unknown free parameter.

We now have to demand that the minimum of this potential should break electroweak symmetry down to electromagnetism  $SU(2)_W \times U(1)_Y \rightarrow U(1)_{EM}$ . From Eq 3.62 it comes out that at the minimum of the potential the charged components of the Higgs scalars can not acquire VEVs, so we can set  $\langle H_1^- \rangle = \langle H_2^+ \rangle = 0$ . The neutral components of the Higgs fields acquires non null vacuum expectation values,  $v_i = \langle H_i^0 \rangle$ , which can be taken real and non negative:

$$H_1 = \begin{pmatrix} v_1 + \frac{1}{\sqrt{2}}(S_1 + iP_1) \\ H_1^- \end{pmatrix} \quad H_2 = \begin{pmatrix} H_2^+ \\ v_2 + \frac{1}{\sqrt{2}}(S_2 + iP_2) \end{pmatrix} \quad (3.64)$$

For details of electroweak symmetry breaking see [83].

We need to require that VEVs reproduce the correct EWSB. The expectations values can be connected to the known masses of the W, Z gauge bosons and with the gauge couplings:

$$\begin{aligned} v_1^2 + v_2^2 &= \frac{2m_Z^2}{g_2^2 + g_1^2} \\ v_1^2 + v_2^2 &= \frac{m_W^2}{g_2^2} \end{aligned} \quad (3.65)$$

As a consequence,  $v_1$  and  $v_2$  are not independent parameters, but they are constrained to get the value  $v \approx 174 \text{ GeV}$ , with  $v^2 = v_1^2 + v_2^2$ . It is usual to define a new free parameter:

$$\tan \beta = \frac{v_2}{v_1} \quad (3.66)$$

The value of  $\tan \beta$  is not fixed by present experiments, but  $\tan \beta > 1$  is required from EWSB. Instead of the parameters  $|\mu|$  and  $B$ , it is common to keep as free parameters  $\tan \beta$  and the sign of  $\mu$ .

Notice that the  $H_1$  field gives mass to the down type fermions, while  $H_2$  to the up type ones, being the fermion mass matrices proportional to  $\mathcal{M}^u = y^u v_2$ ,  $\mathcal{M}^d =$

$y^d v_1$  and  $\mathcal{M}^l = y^l v_1$ . In the same way the Higgs provide the sfermion masses, see 3.5.3.

The Higgs scalar fields consist of two complex  $SU(2)_W$  doublets, namely eight real degrees of freedom. When electroweak symmetry is broken, three of them are the Nambu-Goldstone bosons which becomes the longitudinal modes of the Z and  $W^\pm$  massive vector bosons. We are left with five degrees of freedom: they represent the mass eigenstates of the five Higgs scalar fields in the MSSM. There is one CP-odd neutral scalar A, two CP-even neutral scalars, h, H and two charged fields  $H^\pm$ :

$$\begin{cases} A = \sin \beta P_1 + \cos \beta P_2 \\ h = -S_1 \sin \alpha + S_2 \cos \alpha \\ H = S_1 \cos \alpha + S_2 \sin \alpha \\ H^+ = (H_1^-)^* \sin \beta + H_2^+ \cos \beta \\ H^- = (H^+)^* \end{cases} \quad (3.67)$$

The tree level masses are:

$$\begin{cases} m_A^2 = m_1^2 + m_2^2 + 2\mu^2 \\ m_{h,H}^2 = \frac{1}{2} \left( m_A^2 + m_Z^2 \mp \sqrt{(m_A^2 + m_Z^2)^2 - 4m_Z^2 m_A^2 \cos^2 2\beta} \right) \\ m_{H^\pm}^2 = m_A^2 + m_W^2 \end{cases} \quad (3.68)$$

being h the lightest CP-even Higgs, by definition. In terms of the masses the mixing angle  $\alpha$ , which appears in Eqs. 3.67, is determined by:

$$\cos 2\alpha = \frac{(m_Z^2 - m_A^2) \cos 2\beta}{\sqrt{(m_A^2 + m_Z^2)^2 - 4m_Z^2 m_A^2 \cos^2 2\beta}} \quad (3.69)$$

and the definition range is  $-\pi/2 < \alpha < 0$ . In the Higgs interaction lagrangian all the couplings are determined by the relation between the two angles,  $\alpha$  and  $\beta$ : the Higgs-fermion-fermion coupling turn out to be proportional to the ratio of trigonometric functions of  $\alpha$  and  $\beta$ , while Higgs-gauge bosons vertices are dependent on  $(\alpha - \beta)$ , and finally the Higgs self interactions contain the  $\sin(\alpha + \beta)$  or  $\cos(\alpha + \beta)$  combinations.

Notice that the masses of the Higgs are all connected one to each other. The Higgs sector, at tree level is completely determined by two free parameters,  $\tan \beta$  and  $m_A^2$ . The following relationships hold at tree level:

$$\begin{aligned} m_h &\leq |\cos 2\beta| m_Z \\ m_{H^\pm} &\geq m_W \\ m_h &< m_A < m_H \\ m_h^2 + m_H^2 &= m_A^2 + m_Z^2 \end{aligned} \quad (3.70)$$

As a consequence,  $H$  turn out to be bounded from below, its mass should be greater than the  $Z$  mass. The tree level mass formulas, Eqs. 3.68, are subject to significant quantum corrections, which are especially important for  $h$ , since they weaken the upper bound on the mass of the lightest Higgs. The dominant one loop contributions are due to top and stop loop diagrams: the quark top is heavy, therefore its coupling with the Higgs may get large values; moreover supersymmetry is broken and the stop has a different mass respect to the top and the divergences in the top and stop loops are not exactly cancelled. The loop contributions increase the scalar masses. The one loop  $h$  mass is given by:

$$m_h^2 \lesssim m_Z^2 + \frac{3g_2^2 m_t^4}{8\pi^2 m_W^2} \left( \ln \frac{m_S^2}{m_t^2} + \frac{X_t^2}{m_S^2} \left( 1 - \frac{X_t^2}{12m_S^2} \right) \right) \quad (3.71)$$

where  $m_S^2$  is the average of the two stop masses  $m_{\tilde{t}_1}$  and  $m_{\tilde{t}_2}$  and  $X_t = A_t - \mu \cos \beta$  is the top-squark mixing factor. Notice that the corrections are proportional to the top mass. The lightest CP-even Higgs mass is still bounded from above but may take values greater than  $m_Z$ . Actually  $m_h$  may run up to 114 GeV (for a SM-like light Higgs) [84, 85] or up to several hundreds of GeV (depending on naturalness assumptions). Nevertheless it is lighter than about 140 – 150 GeV [86, 87] for  $m_t = 175$  GeV and  $m_S \simeq 1$  TeV. The absolute lower bound for the lightest Higgs  $h$  is of 90 GeV (which occurs for specific values of the Higgs mixing angle). Eq. 3.71 represents also the lower bound for the  $H$  mass.

If  $h$  saturates the bounds of Eq. 3.71,  $A$ ,  $H$  and  $H^\pm$  would be heavy and nearly degenerate and  $\alpha = \beta - \pi/2$ . In this limit  $h$  has the same couplings as the SM Higgs boson. Namely, depending on the set of model parameters,  $h$  might turn out to deviate from a standard -model like Higgs boson or behaves in a way nearly indistinguishable.

### 3.5.2 Higgsino and gaugino sectors

The higgsinos and electroweak gauginos mix with each other because of the effects of electroweak symmetry breaking. The neutral higgsinos ( $\tilde{H}_1, \tilde{H}_2$ ) and the neutral gauginos ( $\tilde{B}, \tilde{W}^3$ ) combine to form four neutral mass eigenstates called neutralinos. We will denote the neutralino mass eigenstates by  $\chi_i$  ( $i = 0, 1, 2, 3$ ), by convention they are labelled in ascending order, so that  $\chi^0$  is the lightest mass eigenstate. The charged higgsinos ( $\tilde{H}^\pm$ ) and winos ( $\tilde{W}^\pm$ ) mix to form two mass eigenstates with charge  $\pm 1$ , called charginos. We will denote the charginos mass eigenstates by  $\tilde{\chi}_i^\pm$  ( $i = 1, 2$ ). As well as the neutralino case we define  $m_{\tilde{\chi}_1^\pm} < m_{\tilde{\chi}_2^\pm}$ .

Here we will present the mass spectrum and mixing, whereas the main interaction lagragians are reported in the Appendix A.

### Neutralinos

In the gauge-eigenstates basis  $\psi^0 = (\tilde{B}, \tilde{W}^3, \tilde{H}_1, \tilde{H}_2)$  the neutralino mass lagrangian is:

$$-\mathcal{L}_\chi = \frac{1}{2} (\psi^0)^T \mathcal{M}_\chi (\psi^0) + h.c. \quad (3.72)$$

where:

$$\mathcal{M}_\chi = \begin{pmatrix} M_1 & 0 & -m_Z \cos \beta \sin \theta_W & m_Z \sin \beta \sin \theta_W \\ 0 & M_2 & m_Z \cos \beta \cos \theta_W & -m_Z \sin \beta \cos \theta_W \\ -m_Z \cos \beta \sin \theta_W & -m_Z \cos \beta \cos \theta_W & 0 & -\mu \\ m_Z \sin \beta \sin \theta_W & -m_Z \sin \beta \cos \theta_W & -\mu & 0 \end{pmatrix} \quad (3.73)$$

The entries  $M_i$  come directly from the MSSM soft breaking lagrangian, Eq. 3.59, while the  $\mu$  terms are the supersymmetric higgsino mass term, Eq 3.62. The terms proportional to  $m_Z$  are the result of the Higgs-higgsino-gaugino coupling, with the Higgs getting their VEVs, Eq 3.65.

Notice that in general  $\mathcal{M}_\chi$  is a complex symmetric matrix. Only one diagonalizing matrix  $N$  is required. We define the two-component mass-eigenstates using:

$$\chi_i^0 = N_{ij} \psi_j^0 \quad i, j = 1, \dots, 4 \quad (3.74)$$

whit  $N$  a unitary matrix satisfying:

$$N^* \mathcal{M}_\chi N^{-1} = N_D = \text{diag}(m_{\chi_1}, m_{\chi_2}, m_{\chi_3}, m_{\chi_4}) \quad (3.75)$$

where  $N_D$  is the diagonal neutralino mass matrix. One can choose  $N$  such that the elements of the diagonal matrix  $N_D$  are real and non-negative. The proper four-component neutralino mass-eigenstates are given by:

$$\tilde{\chi}^0 = \begin{pmatrix} \chi_i^0 \\ \chi_i^0 \end{pmatrix} \quad i = 1, \dots, 4 \quad (3.76)$$

Note that the neutralinos are Majorana fermions. The condition of real and positive eigenvalues is not necessary, it is possible to diagonalize the matrix of Eq. 3.73 using a new rotation matrix  $Z$ , leading to:

$$Z^* \mathcal{M}_\chi Z^{-1} = N'_D = \text{diag}(\epsilon_1 m_{\chi_1}, \epsilon_2 m_{\chi_2}, \epsilon_3 m_{\chi_3}, \epsilon_4 m_{\chi_4}) \quad (3.77)$$

where the  $\epsilon_i$  are the mass-eigenvalue signs. The two rotation matrices are connected by the relation:

$$N_{ij} = \sqrt{\epsilon_i} Z_{ij} \quad (3.78)$$

Hence the four neutralino mass-eigenstates are defined by:

$$\chi_i = Z_{i1}\tilde{B} + Z_{i2}\tilde{W}^3 + Z_{i3}\tilde{H}_1 + Z_{i4}\tilde{H}_2 \quad i = 1, \dots, 4 \quad (3.79)$$

It is usual to define the superpartners of the SM photon and  $Z$ , the photino  $\tilde{\gamma}$  and the zino  $\tilde{z}$ , as a rotation in the bino and wino space by the Wienberg angle  $\theta_W$ :

$$\begin{cases} \tilde{\gamma} = +\cos\theta_W\tilde{B} + \sin\theta_W\tilde{W}^3 \\ \tilde{z} = -\sin\theta_W\tilde{B} + \cos\theta_W\tilde{W}^3 \end{cases} \quad (3.80)$$

### Charginos

The chargino spectrum is analyzed in a similar way as for the neutralinos. In the gauge-eigenstates basis  $\psi^\pm = (\tilde{W}^+, \tilde{H}_2^+, \tilde{W}^-, \tilde{H}_1^-)$ , the chargino mass term is given by:

$$-\mathcal{L}_{\chi^\pm} = \frac{1}{2}(\psi^\pm)^T \mathcal{M}_{\chi^\pm}(\psi^\pm) + h.c. \quad (3.81)$$

where, in  $2 \times 2$  block form:

$$\mathcal{M}_{\chi^\pm} = \begin{pmatrix} 0 & X^T \\ X & 0 \end{pmatrix} \quad \mathcal{X} = \begin{pmatrix} M_2 & m_W\sqrt{2}\sin\beta \\ m_W\sqrt{2}\sin\beta & \mu \end{pmatrix} \quad (3.82)$$

Again, the  $M_2$  term comes from the soft breaking lagrangian, Eq. 3.59, while the  $\mu$  term from the higgsinos sector, Eq. 3.62. The terms proportional to  $m_W$  come from EWSB and Eqs. 3.65.

We define two-component mass-eigenstate via:

$$\chi_i^+ = V_{ij}\psi_j^+ \quad \chi_i^- = U_{ij}\psi_j^- \quad i, j = 1, 2 \quad (3.83)$$

where  $U$  and  $V$  are unitary matrices chosen such that:

$$U^* X V^{-1} = M_D = \text{diag}(m_1, m_2) \quad (3.84)$$

$M_D$  being the diagonal chargino mass matrix. In particular  $U$  and  $V$  can be chosen so that the elements of the diagonal matrix  $M_D$  are real and non-negative. The proper two components definition of the charginos are:

$$\chi_1^+ = \begin{pmatrix} \chi_1^+ \\ \chi_1^- \end{pmatrix} \quad \chi_2^+ = \begin{pmatrix} \chi_2^+ \\ \chi_2^- \end{pmatrix} \quad (3.85)$$

Since they are only  $2 \times 2$  matrices it is easy to solve for the masses explicitly:

$$\begin{aligned} m_{1,2}^2 &= \frac{1}{2} (M_2^2 + \mu^2 + 2m_W^2 \mp \Delta) \\ \Delta &= \sqrt{(M_2^2 + \mu^2 + 2m_W^2)^2 - 4|\mu M_2 - m_W^2 \sin 2\beta|^2} \end{aligned} \quad (3.86)$$

### 3.5.3 Sfermion sector

The sfermion sector includes all the superpartners of the leptons and quarks, namely to each SM fermionic field  $f$  is associated a complex scalar field  $\tilde{f}$ . We will widely discuss the slepton sector, since it contains the sneutrino phenomenology. All the sneutrino interaction lagrangians are reported in Appendix A, while here the mass terms are illustrated.

The mass and interaction terms arise from three source: the gauge interaction  $D$ -terms, the  $F$ -terms coming from the superpotential  $W$  and the most general set of soft supersymmetry breaking terms. From Eqs. 3.56 to 3.58:

$$V = V_F + V_D + V_{soft} \quad (3.87)$$

with:

$$\begin{aligned} V_F = & (-\mu^* H_2^{i*} + yL^{i*} \bar{e}^*) (-\mu H_2^i + yL^i \bar{e}) + y^2 |\epsilon_{ij} H_1^i L^j|^2 + y^2 |\epsilon_{ij} H_2^i L^j|^2 \\ & + (yH_1^{i*} \bar{e}^*) (yH_1^i \bar{e}) + (-\mu^* H_1^{i*} + y_2 Q^{i*} \bar{u}^*) (-\mu H_1^i + y_2 Q^i \bar{u}) \\ & + (-\mu^* H_2^{i*} + y_1 Q^{i*} \bar{d}^*) (-\mu H_2^i + y_1 Q^i \bar{d}) + y_1^2 |\epsilon_{ij} H_1^i Q^j|^2 \\ & + y_2^2 |\epsilon_{ij} H_2^i Q^j|^2 + (y_1 H_1^{i*} \bar{d}^* - y_2 H_2^{i*} \bar{u}^*) (y_1 H_1^i \bar{d} - y_2 H_2^i \bar{u}) \end{aligned} \quad (3.88)$$

$$\begin{aligned} V_D = & \frac{1}{8} g_2^2 \left( 4|H_1^{i*} Q^i|^2 + 4|H_2^{i*} Q^i|^2 - 2Q^{i*} Q^i (H_1^{i*} H_1^i + H_2^{i*} H_2^i) + (Q^{i*} Q^i)^2 \right) \\ & + \frac{1}{8} g_1^2 \left( H_2^{i*} H_2^i - H_1^{i*} H_1^i + f_q Q^{i*} Q^i + f_u \bar{u}^* \bar{u} + f_d \bar{d}^* \bar{d} \right)^2 \\ & + \frac{1}{8} g_2^2 \left( 4|H_1^{i*} L^i|^2 + 4|H_2^{i*} L^i|^2 - 2L^{i*} L^i (H_1^{i*} H_1^i + H_2^{i*} H_2^i) + (L^{i*} L^i)^2 \right) \\ & + \frac{1}{8} g_1^2 \left( H_2^{i*} H_2^i - H_1^{i*} H_1^i + f_L L^{i*} L^i + f_e \bar{e}^* \bar{e} \right)^2 \end{aligned} \quad (3.89)$$

$$\begin{aligned} V_{soft} = & m_Q^2 Q^{i*} Q^i + m_u^2 \bar{u}^* \bar{u} + m_d^2 \bar{d}^* \bar{d} + (\epsilon_{ij} y_1 A_d H_1^i Q^j \bar{d} - \epsilon_{ij} H_2^i Q^j \bar{u}) \\ & + m_L^2 L^{i*} L^i + m_e^2 \bar{e}^* \bar{e} + (\epsilon_{ij} y_1 A_e H_1^i L^j \bar{e}) \end{aligned} \quad (3.90)$$

with  $y, y_{1,2}$  being the Yukawa couplings and  $f_q = 1/3, f_u = -4/3, f_d = 2/3, f_L = 1, f_e = 2$ . Obviously  $Q$  and  $L$  refers to the  $SU(2)_L$  (s)quark and (s)leptons doublets, while  $\bar{u}, \bar{d}$  and  $\bar{e}$  to the right-handed fields.

First of all, we assume that the interactions are flavor-blind, therefore the squark and slepton families can not mix with each other. The Yukawa couplings, from  $V_F$ , are negligible for all the family except the  $t$  and  $b$  squark and the tau slepton.

The second term of Eqs. 3.88 comes from gauge interactions  $D$ -term. It leads to a splitting in the mass spectrum produced by electroweak symmetry breaking. Each slepton and squark will get a contribution  $\Delta_\Phi$  to its (mass)<sup>2</sup>, coming

from the  $SU(2)_W$  and  $U(1)_Y$  D-term quartic interactions. These terms are model-independent, for a given value of  $\tan \beta$ , and are given by:

$$\Delta_\Phi = (T_{3\Phi} - e_\Phi \sin^2 \theta_W) \cos 2\beta m_Z^2 \quad (3.91)$$

where  $T_{3\Phi}$  and  $e_\Phi$  are the third component of weak isospin and the electric charge of the scalar superfield  $\Phi$ .

To each fermion  $f_L$  and  $f_R$  corresponds a complex scalar field  $\tilde{f}_L$  and  $\tilde{f}_R$ . The four component notation is as follows:

$$\begin{aligned} Q &= \begin{pmatrix} \tilde{u}_L \\ \tilde{d}_L \end{pmatrix} & \bar{u} &= \tilde{u}_R & \bar{d} &= \tilde{d}_R \\ L &= \begin{pmatrix} \tilde{\nu}_L \\ \tilde{e}_L \end{pmatrix} & \bar{e} &= \tilde{e}_R \end{aligned} \quad (3.92)$$

Considering a generic sfermion, the mass lagrangian is defined to be:

$$\mathcal{L}_{mass} = \frac{1}{2} (\tilde{f}_L^* \quad \tilde{f}_R^*) \mathcal{M}^2 \begin{pmatrix} \tilde{f}_L \\ \tilde{f}_R \end{pmatrix} \quad (3.93)$$

In particular the mass matrix has the form:

$$\mathcal{M}^2 = \begin{pmatrix} m_L^2 + D_{\tilde{L}} + m_f^2 & m_f (A_f + \mu \tan \beta) \\ m_f (A_f + \mu \tan \beta) & m_R^2 + D_{\tilde{R}} + m_f^2 \end{pmatrix} \quad (3.94)$$

with  $D_{\tilde{L}}$  and  $D_{\tilde{R}}$  the left and right handed expression of Eq. 3.91, respectively. In the next chapters we will unify the soft mass terms for all the sleptons and for all the squarks,  $m_L^2$  and  $m_R^2$  and  $m_Q^2$ . Here we have presented the lagrangian at the electroweak scale, the unification can be done at the GUT scale, as in gravity-mediated supersymmetric models, or at low energy, called effective MSSM. As mentioned before we will adopt this second type of approach in fixing the parameters of the supersymmetric models.

Thus the mass eigenstate are:

$$\begin{cases} \tilde{f}_1 = +\cos \theta \tilde{f}_L + \sin \theta \tilde{f}_R \\ \tilde{f}_2 = -\sin \theta \tilde{f}_L + \cos \theta \tilde{f}_R \end{cases} \quad (3.95)$$

while the mass eigenvalues are obtained diagonalizing the  $2 \times 2$  matrix in Eq. 3.94.

Depending on the choice of the Yukawas, the mass squark eigenstates can be a superposition of right and left handed states. The same holds in the case of the tau lepton; for the  $\mu$  and  $e$  sleptons, the Yukawas are negligible, therefore the mass eigenstates coincide with the right and left handed states.

Especially, the sneutrino and the selectron lagrangians are defined by:

$$\begin{aligned}
-\mathcal{L}_{m_{\tilde{\nu}}} &= \tilde{\nu}_L^* \tilde{\nu}_L \left\{ m_{\tilde{\nu}}^2 + \frac{1}{2} m_Z^2 \cos 2\beta \right\} \\
-\mathcal{L}_{m_{\tilde{e}_L}} &= \tilde{e}_L^* \tilde{e}_L \left\{ m_{\tilde{e}_L}^2 - m_Z^2 \cos 2\beta \left( \frac{1}{2} + e_L \sin^2 \theta_W \right) + m_f^2 \right\} \\
-\mathcal{L}_{m_{\tilde{e}_R}} &= \tilde{e}_R^* \tilde{e}_R \left\{ m_{\tilde{e}_R}^2 + m_Z^2 \cos 2\beta e_R \sin^2 \theta_W + m_f^2 \right\}
\end{aligned} \tag{3.96}$$

From Eq. 3.91, it turns out that the sneutrino is lighter than the corresponding charged slepton, since  $\cos 2\beta$  is negative:

$$m_{\tilde{e}_L}^2 - m_{\tilde{\nu}_L}^2 = -\cos 2\beta m_W^2 \tag{3.97}$$

At most they would be degenerate if the soft term is very large compared with the  $D$ -term,  $m_{\tilde{e}_L}^2 \gg \sin^2 \theta_W \cos 2\beta m_Z^2$ .

The above presented is the sneutrino sector in the standard minimal supersymmetric model. We will extend Eqs. 3.88 with the introduction of new mass and interaction terms for the sneutrino in the superpotential and in the soft breaking potential. The arising modified phenomenology will be widely discussed in the next chapter 4.

## Chapter 4

# Sneutrino phenomenology and cosmological relic abundance

The sneutrino,  $\tilde{\nu}$ , is a scalar supersymmetric particle and belongs to the same superfield of the neutrino, as discussed in section 3.5.3. Therefore it shares with the neutrino the same quantum numbers: both are electrically neutral, colorless, have same hyper-charge but different masses, since supersymmetry is broken, and obviously different spins.

Actually sneutrinos may provide a good candidate for the solution of the missing matter in the Universe, depending on the supersymmetric model taken into account. They enclose all the main features of a CDM particle: by assumption they are LSP, thus stable, they do not interact with light and are WIMPs.

All the calculations of the relic abundance are done using the code described in Section 2.6, and solving the Boltzmann equation, where we assume that sneutrino were thermally produced in the early Universe.

First of all we will discuss the cosmological sneutrino properties in the framework of the standard MSSM in Sec. 4.1 and we will call this model “STD model”. Then we will introduce a right handed neutrino superfield 4.2, so the arising models are called “LR models”. The third typology of SUSY models, called “ $\mathcal{L}$  violating models”, contains L flavour violating terms in the lagrangian, Sec. 4.3. Finally in Section 4.4 the last class of models, called “Maj models”, contain right handed sneutrino fields and  $\mathcal{L}$  violating terms simultaneously. For these models, we will explicitly write down only terms that contribute to the masses and not the gauge interaction terms involving neutrino superfields in the superpotential and in the soft supersymmetry breaking potential. All the considered supersymmetric models are low energy supersymmetric extensions of the Standard Model, supposing a soft or spontaneous SUSY breaking in an hidden sector and conserve R-parity. All the experimental constraints involving these supersymmetric models are discussed in Appendix B.

Sneutrinos in connection with the dark matter problem have also been discussed in different frameworks some of which may be found in Refs. [88, 89, 90, 91, 92, 93, 94, 95].

## 4.1 MSSM sneutrinos

Sneutrinos in the Minimal Supersymmetric Standard Model have been studied in the past: light sneutrinos ( $m_{\tilde{\nu}} \leq m_W$ ) have been considered in [96, 97, 98] while heavy sneutrinos have been investigated by [99, 100].

In the MSSM there are three left-handed  $\tilde{\nu}_L$  sneutrinos, superpartners respectively of the  $\nu_e, \nu_\mu$  and  $\nu_\tau$ . From the first equation in Eqs. 3.96, it follows that the three sneutrinos are degenerate mass eigenstates with squared masses  $m_1^2 = m_L^2 + 1/2m_Z^2 \cos 2\beta$ . Here and thereafter we will denote by  $m_1$  the mass of the lightest sneutrino mass eigenstate. The phenomenology of the sneutrino is only slightly sensitive to  $\tan\beta$ , the main free parameter being  $m_L$ . The interaction terms get contributions from the superpotential  $W_{\text{MSSM}}$ , Eq 3.56, and from the SUSY breaking potential  $V_{\text{soft}}$ , Eq. 3.88, and are reported in Appendix A.

The experimental bounds on MSSM sneutrinos come from searches for supersymmetry at colliders and from studies of width and decays of the Z boson. Regarding the accelerator bound, it is induced by the non observation of the corresponding charged sleptons. As it is shown in Eqs. 3.96, these latter possess both left handed and right handed components: for equal masses, namely  $m_{\tilde{l}_R} = m_{\tilde{l}_L}$ , the cross section for the right handed field is smaller than for the left handed state, so limits are set conservatively for the production of  $\tilde{l}_R$  type particles. For selectrons, current limits are 73 GeV for  $\tilde{e}_R$  and 107 GeV for  $\tilde{e}_L$  [72, 101], while we have 94 GeV for  $\tilde{\mu}_R$  and 81.9 GeV for a generic mixing of  $\tilde{\tau}_L$  and  $\tilde{\tau}_R$ . Let us consider Eqs. 3.96, where the mass lagrangians of the slepton sector are reported: notice that there are two mass parameters,  $m_L$  for the left handed SU(2) doublets, and  $m_R$  for the right handed singlets. Here and thereafter we will assume that the parameters  $m_L$  and  $m_R$ , which usually are matrices in flavour space, are diagonal and common over the three leptonic families. The sneutrino mass phenomenology is thus related to the left handed charged component behavior and independent on the value of  $m_R$ . Therefore, in general, a bound to the mass of the lightest charged sleptons does not directly transfer to a mass limit to the corresponding sneutrino. For instance in mSUGRA scenarios the values of the parameters at the electroweak scale are induced by the renormalization group evolution equations from the GUT scale; referring to the slepton squared masses they lead to:

$$\begin{aligned} m_R^2 &= m_0^2 + 0.15m_{1/2}^2 \\ m_L^2 &= m_0^2 + 0.52m_{1/2}^2 \end{aligned} \tag{4.1}$$

where  $m_0$  and  $m_{1/2}$  are defined at the GUT scale and are the common values of the gauginos and scalar masses in the soft supersymmetric breaking potential. In this framework the lower bound on the sneutrino mass is 84 GeV [72, 101]. The low energy MSSM model does not necessarily invoke mSUGRA relations for the parameters, therefore we assume that in this minimal version of the MSSM all the soft mass parameters of the charged and neutral leptons are common at the electroweak scale and we set  $m_L = m_R$ . In this case the collider limit can be weakened, depending on the value of  $\tan\beta$ , until to become as low as the limit coming from the invisible Z decay width. Sneutrinos lighter than  $m_Z/2$  contribute to the invisible Z width with:

$$\Delta\Gamma_Z = \frac{\Gamma_\nu}{2} \left[ 1 - \left( \frac{2m_1}{m_Z} \right)^2 \right]^{3/2} \theta(m_Z - 2m_1) \quad (4.2)$$

where  $\Gamma_\nu = 167$  MeV is the Z invisible decay width into one neutrino species. We consider  $\Delta\Gamma_Z < 2$  MeV [72], which translates into a sneutrino mass limit of 43.7 GeV for one sneutrino species and of 44.7 GeV for three degenerate sneutrinos [72]. We will assume these latter as the sneutrino lower mass bounds in the subsequent phenomenological analysis.

Let us now turn to the sneutrino phenomenology relevant for the dark matter. The sneutrino annihilation channels are reported in Tab. 4.1, at the end of the chapter, for definiteness for the first family only. In these minimal MSSM models, the three sneutrinos are degenerate in mass: they therefore must be considered jointly in the calculations of the relevant processes. Sneutrinos lighter than  $m_W$  can annihilate into all possible fermionic final states, except the top quark, and the dominant process is the t-channel neutralinos exchange, as we will discuss later. Heavier sneutrinos ( $m_1 > m_W$ ) can annihilate into a much greater set of final states and the total annihilation cross section is dominated by gauge boson channels, in particular by the process  $\tilde{\nu}\tilde{\nu} \rightarrow W^+W^-$ .

We include coannihilation processes, listed in Tab. 4.1, which may arise when the sleptons are close in mass to the sneutrinos. Although one might expect that this case results in a relic abundance three times larger than the case without coannihilation, in fact it is a little more complicated. Some annihilation channels, namely  $\tilde{\nu}_i\tilde{\nu}_j \rightarrow \nu_i\nu_j$ ,  $\tilde{\nu}_i\tilde{e}_{Lj} \rightarrow \nu_ie_{Lj}$  and  $\tilde{e}_{Li}\tilde{e}_{Lj} \rightarrow e_{Li}e_{Lj}$ , with  $i, j$  flavor indices, can now occur in nine different ways, whereas all the others possible channels can occur in three different ways. For general values of the parameter space of the model, sneutrinos may eventually also coannihilate with neutralinos and/or charginos, but this case is more accidental than the one with sleptons, due to the relation in Eq. 3.97: if  $m_L$  is increased, the sneutrino and the charged slepton masses become more and more close to each other, up to being degenerate for  $m_L$  at the TeV scale. In the models presented here we have explicitly neglected coannihilation

with the gaugino and higgsino sectors, by considering configurations which possess neutralinos at least 30% heavier than the lightest sneutrino.

An example of sneutrino relic abundance  $\Omega h^2$  in the standard MSSM is shown in Fig 4.1 as a function of the sneutrino mass  $m_1$ . In this plot all the parameters of the low energy MSSM model are fixed, except  $m_L$ , which is kept running in the range from 1 GeV up to 1 TeV. The Higgs masses are  $m_h = 120$  GeV, while H, A and the charged higgs  $H^\pm$  are degenerate with a common mass  $m_H \simeq m_A \simeq m_{H^\pm} \simeq 400$  GeV. Finally  $\tan\beta$  has been fixed at 20 and the widths of all the Higgs bosons at 1 GeV: indeed the Higgs widths become experimentally significant, of the order of  $\Gamma_{Higgs} \simeq 10$  GeV, for large values of  $\tan\beta$  and for heavy masses of h, H, A and  $H^\pm$ , see Ref. [102]. The lightest neutralino mass is  $m_{\tilde{\chi}^0} = \min(294 \text{ GeV}, 1.3m_1)$  for the solid curve, and  $m_{\tilde{\chi}^0} = 1.3 m_1$  for the dashed curve. This latter case, which possess light neutralinos, requires gaugino–non universality [103, 104, 105] in order to evade the neutralino mass lower bound of about 50 GeV, derived for gaugino universal models. We have considered two different neutralino configurations because the  $t$ -channel neutralino exchange is the dominant channel for light sneutrinos. We remark that the  $t$ -channel is proportional to  $1/m_{\tilde{\chi}^0}^2$  (for the channel  $\tilde{\nu}\tilde{\nu} \rightarrow \nu\nu$ ) and to  $1/m_{\tilde{\chi}^0}^4$  (for the channel  $\tilde{\nu}\tilde{\nu} \rightarrow \nu\bar{\nu}$ ): if the neutralino is taken to be heavy compared with the sneutrino mass the annihilation rate gets reduced, while if the neutralino is taken to be light the cross section gets enhanced and the relic abundance is much lower, leading to a larger sets of viable sneutrino configurations. In the MSSM models this distinction between the two neutralino behavior is not relevant, since sneutrino are excluded in the interested mass range, however it will turn out to be very useful in the extended SUSY models, as we will see. The dashed-dotted line represents the invisible Z width lower mass bound: we have plotted the relic abundance in a larger interval for sake of comparison with the modified models discussed later on.

The relic abundance of the sneutrino is typically very small [96, 97], much lower than the cosmological range for CDM derived by WMAP, see Eq. 1.6. We conclude that sneutrinos in the standard MSSM are not good dark matter candidates, except for masses in a narrow range which we determine to be 600-700 GeV, consistent with previous analyses [99]. In all the mass range from  $m_Z/2$  up to 600 GeV the sneutrino as LSP are cosmologically viable, namely their relic abundance is below the WMAP bound, but they are underabundant.

In Fig. 4.1 notice the three dips represent the pole of the Z boson, at  $m_1 = m_Z/2$ , the h pole, around  $m_1 \simeq 60$  GeV, and the degenerate H, A and  $H^\pm$  pole ( $H^\pm$  and A are exchanged in the coannihilation processes). Obviously the higgs poles may move in the allowed mass range, see Eqs. 3.68 and 3.70, since the higgs masses are not fixed. At a sneutrino mass of the order of  $m_W$ , the deep drop is due to the opening of the  $W^+W^-$  annihilation channel.

## 4.2 Right-handed sneutrino models

In this class of models the superfield content of the standard minimal supersymmetric model is extended by the introduction of right handed neutrino superfields  $N^I$ , one for each family generation  $I$ . These models possess a rich sneutrino phenomenology and may account for a neutrino mass of Dirac type. Past studies and references about these models can be found in [106, 107, 108, 109, 110, 111].

The superpotential in Eq. 3.56 gets an additional contribution:

$$W = \epsilon_{ij}(\mu \hat{H}_i^1 \hat{H}_j^2 - Y_l^{IJ} \hat{H}_i^1 \hat{L}_j^I \hat{R}^J + Y_\nu^{IJ} \hat{H}_i^2 \hat{L}_j^I \hat{N}^J) \quad (4.3)$$

where  $Y_\nu^{IJ}$  is a matrix in flavor space, which we again choose real and diagonal in flavor space, from which the Dirac mass of neutrinos are obtained  $m_D^I = v_2 Y_\nu^{II}$ . Also the soft-breaking potential gets modified:

$$V_{\text{soft}} = (M_L^2)^{IJ} \tilde{L}_i^{I*} \tilde{L}_j^J + (M_N^2)^{IJ} \tilde{N}^{I*} \tilde{N}^J - [\epsilon_{ij}(\Lambda_l^{IJ} H_i^1 \tilde{L}_j^I \tilde{R}^J + \Lambda_\nu^{IJ} H_i^2 \tilde{L}_j^I \tilde{N}^J) + \text{h.c.}] \quad (4.4)$$

where we take both the matrices  $M_N^2$  and  $\Lambda_\nu^{IJ}$  real and diagonal. The diagonal common entries for  $M_N^2$  are denoted as  $m_N^2$ .

The sneutrino mass-term potential is now:

$$V_{\text{mass}} = \left[ m_L^2 + \frac{1}{2} m_Z^2 \cos(2\beta) + m_D^2 \right] \tilde{\nu}_L^* \tilde{\nu}_L + [m_N^2 + m_D^2] \tilde{N}^* \tilde{N} + F^2 (\tilde{\nu}_L^* \tilde{N} + \tilde{N}^* \tilde{\nu}_L) \quad (4.5)$$

The parameter  $F^2$ , which mixes the left and right handed sneutrino fields is:

$$F^2 = v \Lambda_\nu \sin \beta - \mu m_D \cot \beta \quad (4.6)$$

In the basis defined by the vector  $\Phi^\dagger = (\tilde{\nu}_L^*, \tilde{N}^*)$ , we can define the sneutrino mass potential as:

$$V_{\text{mass}} = \frac{1}{2} \Phi_{LR}^\dagger \mathcal{M}_{LR}^2 \Phi_{LR} \quad (4.7)$$

where the squared-mass matrix  $\mathcal{M}_{LR}^2$  is:

$$\mathcal{M}_{LR}^2 = \begin{pmatrix} m_L^2 + \frac{1}{2} m_Z^2 \cos(2\beta) + m_D^2 & F^2 \\ F^2 & m_N^2 + m_D^2 \end{pmatrix} \quad (4.8)$$

The Dirac neutrino mass is small, and can be safely neglected. The parameter  $m_N$  in general does not depend on the other mass parameters, in particular is not linked to  $m_L$ , which instead is related to the charged leptons masses, as discussed in the previous section 4.1. We are therefore allowed to vary freely  $m_N$ , and whenever

$m_N$  is small enough, sneutrinos lighter than those encountered in the standard MSSM models are in principle viable. As long as the left-handed mass  $m_L$  is compatible with the mass lower bounds on the charged leptons (which occurs for  $m_L \gtrsim 80 - 90$  GeV)  $m_1$  can be small, provided that  $m_N \ll m_L$ , without entering in conflict with accelerator bounds. In this case, light sneutrinos may arise, and the only relevant limit which remains is the one provided by the invisible  $Z$ -width, which we discuss in a moment. Moreover the  $F^2$  term provides an additional source of splitting between the sneutrino and charged slepton masses.

The off diagonal term  $F^2$  is relevant for the mixing among the mass eigenstates, obtained by diagonalizing  $\mathcal{M}_{LR}^2$ . For  $\Lambda_\nu$  aligned along the Yukawa matrix  $Y_\nu$ , *i.e.* for  $\Lambda_\nu = \eta Y_\nu$ ,  $F^2$  is necessarily very small as compared to the diagonal entries (especially the element  $(\mathcal{M}_{LR}^2)_{11}$  of the matrix), because in that case  $F^2$  is proportional to the neutrino mass  $m_D$ , and is therefore negligible since both  $v$  and  $\mu$  are electroweak scale parameters. However,  $\Lambda_\nu$  is in general a free parameter. In this case  $F^2 \simeq v\Lambda_\nu \sin\beta$  may naturally be of the order of the other entries of the matrix, and induce a sizeable mixing of the lightest sneutrino in terms of left handed and right handed fields. We define the mixing as follows:

$$\begin{cases} \tilde{\nu}_1 = -\sin\theta \tilde{\nu}_L + \cos\theta \tilde{N} \\ \tilde{\nu}_2 = +\cos\theta \tilde{\nu}_L + \sin\theta \tilde{N} \end{cases} \quad (4.9)$$

where  $\theta$  is the LR mixing angle. Sizeable mixings reduce the coupling to the  $Z$ -boson, which couples only to left handed fields, and therefore have relevant impact on all the sneutrino phenomenology, as recognized in Refs. [106, 107, 108, 109, 110]. The right handed sneutrino is a sterile component respect to all the supersymmetric fields except the Higgs bosons, as we can see from the superpotential Eq. 4.3 and the soft breaking potential Eq. 4.4. The modified interaction vertices are reported in Appendix A.

Due to the mixing between left and right sneutrino states, the lightest sneutrino  $\tilde{\nu}_1$  coupling with the  $Z$  boson is reduce by a factor  $\sin\theta$ . If  $\tilde{\nu}_1$  is light enough to be produced in  $Z$  decay its contribution to the  $Z$  width is given by:

$$\Delta\Gamma_Z = \sin^4\theta \frac{\Gamma_\nu}{2} \left[ 1 - \left( \frac{2m_1}{m_Z} \right)^2 \right]^{3/2} \theta(m_Z - 2m_1) \quad (4.10)$$

The main consequence is that sneutrinos light than  $m_Z/2$  are now viable: as we will show sneutrinos of the order  $\mathcal{O}(1 \text{ GeV})$  are possible for small values of the mixing angle. Actually a small  $\sin\theta$  means that the sneutrino is essentially a right handed sneutrino with a small fraction of active component.

The free parameters in the sneutrino sector for the LR model are therefore  $m_L$ ,  $m_N$  and  $F^2$ . We will vary freely  $m_L$ , which is not linked to slepton masses by

gauge invariance, and  $F^2$ , while we will take  $m_L$  in the range from 100 GeV up to the TeV scale, in order to be compatible with the collider limits for charged sleptons.

In Figs. 4.4.2, 4.2 and 4.3, we show the correlation between the mixing angle  $\sin \theta$ , the right handed soft mass  $m_N$  and the sneutrino mass  $m_1$ , for different values of the  $F^2$  parameter and for two different values of the scalar soft mass  $m_L$ . In Fig 4.4.2  $m_L$  is fixed at 120 GeV: for  $m_N \lesssim m_L$  the sneutrinos turn out to be light and largely mixed with the right handed component  $\tilde{N}$ , namely  $\sin \theta$  has very small values, as can be noticed in Fig. 4.2, and the Z width bound may be avoided. All the curves start from a value of  $m_N$  below which the negative mass squared eigenvalue  $m_1^2$  occurs. If we increase  $m_L$ , as in Fig 4.3, up to 1 TeV the tachionic bound is met for small values of  $m_N$  and the mixing angle diminishes. For large values of  $m_L$  and  $F^2$  small mixing can occur also for heavy sneutrinos.

In Figs 4.4, 4.4.2 and 4.5 a full scan over the sneutrino parameter  $m_N$  and  $m_L$  is done, for  $F^2 = 10^2 \text{ GeV}^2, 10^3 \text{ GeV}^2$  and  $10^4 \text{ GeV}^2$  respectively. The remaining set of parameters of the supersymmetric model is fixed as described in section 4.1. The solid [blue] region in the right corner is forbidden from the Z-width bound: notice that light sneutrinos are allowed in these supersymmetric models provided a small mixing angle,  $|\sin \theta| \lesssim 0.4$ . In the plane  $m_1 - \sin \theta$  we plot the phenomenological viable sneutrino configurations: the black regions are allowed by collider limits, the red regions have acceptable relic abundance and finally the light blue regions are compatible with the bounds of direct searches of dark matter. These latter will be exhaustively considered in the next chapter 5. Consider small values of  $F^2$ : for small  $m_N$  the mixing angles are typically very small for light sneutrinos, almost vanishing, namely the lightest sneutrino is already mostly right handed. For  $m_N \simeq m_L$  large mixing are still allowed, while when  $m_N > m_L$  the sneutrino is very similar to the standard MSSM sneutrino, since the left handed component dominates the mixing. The increase in value of the parameter  $F^2$  leads to a more rich and interesting phenomenology, since large mixing angles are viable also for light sneutrinos and, as shown in Figs. 4.4.2 and 4.5 the Z width bound is important.

A large mixing with the right handed field  $\tilde{N}$  is important for the cosmological properties of the sneutrino: the interactions are reduced and the corresponding relic abundance gets enhanced. The dependence of the relic abundance on the sneutrino parameters is plotted versus  $m_1$  in Figs. 4.4.2, 4.6 and 4.7; the other parameters are fixed at the same values used in the previous section. All the models shown in the plot are acceptable from a point of view of all experimental constraints, including the invisible Z width. The horizontal solid and dotted line delimit the WMAP interval for cold dark matter. In the first two plots we have varied the value of the mixing angle in the range  $\sin \theta = 0.1$  up to  $\sin \theta = 1$  (blue

region), which corresponds to a pure left handed sneutrino, at fixed  $m_L = 120$  GeV and  $m_L = 1$  TeV respectively. For a small  $m_L$  the phenomenological acceptable configurations are not as different as the standard case for light sneutrinos, while the relic abundance increases for heavy sneutrinos. A TeV scale  $m_L$  is more interesting: light sneutrinos are not only viable but can be dominant (in a mass range from few GeV up to 10 GeV) if the left right mixing is large, indeed the heavy sneutrinos are less sensible and behave similarly to the previous case. In Fig. 4.7 it is shown the relic abundance for LR models for a full variation of the sneutrino parameter space:  $120 \text{ GeV} < m_L < 1 \text{ TeV}$ ,  $1 \text{ GeV} < m_N < 1 \text{ TeV}$  and  $10 \text{ GeV}^2 < F^2 < 10^4 \text{ GeV}^2$ . The points with an acceptable relic abundance at masses below 10 GeV are obtained for models with light neutralinos, assuming gaugino non universality. The  $t$ -channel neutralino exchange is sensitive to neutralino masses: if neutralinos are heavy the cross section gets reduced, while taking light neutralinos will enhance the corresponding annihilation channels and lead to acceptable relic abundance for small  $\sin \theta$ .

Contrary to the standard MSSM sneutrino, in LR models sneutrinos may represent the dominant dark matter component for a wide range of masses, spanning from few GeV up to approximately 300 GeV. When  $F^2$  is small, as in Fig. 4.4, the mixing angles have values much lower than  $10^{-2}$ , thus the sneutrinos are practically pure right handed fields and get high values for the relic abundance, above the WMAP bounds. In this case only heavy sneutrinos with  $m_1 \geq m_W$  have acceptable  $\Omega h^2$  values, since the annihilation channel into  $W^+W^-$  opens and produces a sharp drop in the relic abundance and maintain it in the WMAP range until  $m_1 \simeq 200$  GeV. When  $F^2$  increases, like in Figs 4.4.2 and 4.5, the cosmologically allowed parameter space opens up. The mixing angles are typically larger than the previous case and may reach values of the order of 0.3. Light sneutrino, with mass of 10 or few GeV for  $F^2 = 10^3$  and  $F^2 = 10^4$  respectively, become acceptable. The  $F^2$  term does not modify significantly the phenomenology of the heavy sneutrino: also in the two latter case, sneutrinos are compatible with the WMAP observations for masses up to 200-300 GeV.

The analysis presented until now has been done for a specific set of supersymmetric parameters, with fixed Higgs masses and peculiar neutralino and chargino masses. We now go further and analyse with a full scan all the SUSY parameter space. The parameter space is defined in Appendix B with the inclusion of the experimental constraints. For instance the sneutrino parameters are varied in the following ranges:  $100 \text{ GeV} < m_L < 3 \text{ TeV}$ ,  $1 \text{ GeV} < m_N < 1 \text{ TeV}$  and  $1 \text{ GeV}^2 < F^2 < 10^6 \text{ GeV}^2$ .

In Fig. 4.4.2 we show  $F^2$  as a function of  $m_N$ ; the crosses [red] refer to sneutrinos with relic abundance in the cosmological relevant range, while the dots [blue] denote underabundant sneutrinos. As we noticed, for low values of  $m_N$ , which turns

out to drive the sneutrino masses, there is a correlation between the off diagonal term and the soft right handed mass; at high values of  $m_N$ , the phenomenological viable sneutrino configuration are spread in all the parameters range. Fig 4.8 shows the correlation between  $m_L$  and  $m_N$ , with the same notation as the previous picture. Again, the lightest sneutrino mass eigenstates is composed mainly by the right handed  $\tilde{N}$  for  $m_N \leq m_L$ , while for  $m_N > m_L$  it holds the opposite. Finally in Fig 4.4.2 we plot the the viable LR models in the plane  $m_1 - \sin\theta$ : small mixing angles, namely  $\sin\theta \lesssim 3 \times 10^{-2}$ , correspond to heavy sneutrinos ( $m_1 \simeq \mathcal{O}(100 \text{ GeV})$ ), while for  $\sin\theta \gtrsim 0.1$ , the parameter space allows light sneutrinos as dominant dark matter component. This is clear in Fig 4.9, where the relic abundance versus  $m_1$  is reported, for the full scan in the SUSY parameter space. The most relevant new feature is that, respect to Figs. 4.6 and 4.7, the mass range allowed by the cosmological constraints is enlarged up to 800 GeV and all the interval above the Z pole may lead to strongly subdominant sneutrinos, due either to the occurrence of the Higgs poles in the annihilation cross section or to the mixing with the right handed sneutrino field.

We conclude that for a full scan in the parameter space in LR models, after all experimental constraints are imposed, sneutrino dark matter is perfectly viable, both as dominant and as subdominant component, for the whole mass range  $15 \text{ GeV} \lesssim m_1 \lesssim 800 \text{ GeV}$ . The lower limit of 15 GeV represents therefore a cosmological bound on the sneutrino mass in LR models.

### 4.3 L–number violating sneutrino models

In the presence of L-number violation, sneutrinos can mix with anti-sneutrinos because there are no other quantum numbers which forbids the mixing. These models have the same superfield content of the MSSM but in the superpotential and in the soft breaking potential  $\mathcal{L}$  terms are introduced, leading to a non renormalizable lagrangian. Sneutrino mixing phenomena have been discussed [46, 106, 107, 108, 109, 110, 112, 113, 114], in connection also to the problem of the neutrino masses.

The simplest approach for the neutrino to acquire a Majorana mass term, is to introduce a gauge invariant five dimensional operator [106, 113, 115, 111] that violate lepton number by two units ( $\Delta L = 2$ ):

$$\mathcal{L}_5 = \frac{g_{IJ}}{\Lambda} (\epsilon_{ij} L_i^I H_j) (\epsilon_{kl} L_k^J H_l) + h.c. \quad (4.11)$$

where the indices  $I, J$  label the three slepton generations. The neutrino Majorana mass term is generated after electroweak symmetry breaking, by the neutral components of the doublet Higgs fields, which acquires VEVs. The five dimensional

term is generated by new physics at the scale  $\Lambda$ , which turns out to be of the order  $\Lambda \gtrsim 10^{13}$  GeV from current bound on light neutrino masses. Such a parameter close to the GUT scale provides a neutrino mass of the order  $m_M \sim g_2 v^2 / \Lambda$ , where  $g_2$  and  $v$  have been defined in section 3.5.1.

This extension of the MSSM superpotential allows L-number violating terms in the sneutrino lagrangian, the effect of the  $\Delta L = 2$  operator is to introduce a mass splitting and mixing into the sneutrino-antisneutrino sector; the sneutrino and the antisneutrino will then no longer be mass eigenstates. Therefore the mass potential is modified as:

$$V_{\text{mass}} = \left[ m_L^2 + \frac{1}{2} m_Z^2 \cos(2\beta) \right] \tilde{\nu}_L^* \tilde{\nu}_L + \frac{1}{2} m_B^2 (\tilde{\nu}_L \tilde{\nu}_L + \tilde{\nu}_L^* \tilde{\nu}_L^*) \quad (4.12)$$

where  $m_B$  is a mass parameter that makes the mass lagrangian no longer diagonal in the  $(\tilde{\nu}_L \tilde{\nu}_L^*)$  basis. In this basis the squared–mass matrix reads:

$$\mathcal{M}_{\tilde{\nu}}^2 = \begin{pmatrix} m_L^2 + \frac{1}{2} m_Z^2 \cos(2\beta) & m_B^2 \\ m_B^2 & m_L^2 + \frac{1}{2} m_Z^2 \cos(2\beta) \end{pmatrix} \quad (4.13)$$

and it may be conveniently diagonalized by a rotation into a basis defined by the CP–even  $\tilde{\nu}_+$  and CP–odd  $\tilde{\nu}_-$  sneutrino eigenstates [106]:

$$\begin{cases} \tilde{\nu}_+ = \frac{1}{\sqrt{2}} (\tilde{\nu} + \tilde{\nu}^*) \\ \tilde{\nu}_- = \frac{-i}{\sqrt{2}} (\tilde{\nu} - \tilde{\nu}^*) \end{cases} \quad (4.14)$$

The states  $\tilde{\nu}_+$  and  $\tilde{\nu}_-$  are also mass eigenstates. The squared–mass eigenvalues are easily computed:

$$m_{1,2}^2 = m_L^2 + \frac{1}{2} m_Z^2 \cos(2\beta) \pm m_B^2 \quad (4.15)$$

which implies  $\Delta m^2 \equiv m_2^2 - m_1^2 = 2m_B^2$ . The mixing angle is fixed at the value  $\theta = \pi/4$ .

The  $Z$  coupling to sneutrinos is non–diagonal in the  $(\tilde{\nu}_+, \tilde{\nu}_-)$  basis, which are now non–degenerate in mass. The first consequence is that the invisible  $Z$ –width decay occurs via the process  $Z \rightarrow \nu_1 \nu_2$  and is therefore modified as:

$$\Delta\Gamma_Z = \frac{\Gamma_\nu}{2} \left[ 1 - \left( \frac{m_1 + m_2}{m_Z} \right)^2 \right]^{3/2} \theta(m_Z - m_1 - m_2) \quad (4.16)$$

Therefore the bound of the  $Z$  invisible width is weakened depending on the size of the splitting  $\Delta m$ . We let run the scalar mass  $m_L$  from 80 GeV, to be safe regarding the collider limit for charged sleptons. If  $m_B$  is taken to be large enough, close to its upper limit, which prevents tachionic sneutrinos,  $m_1$  may be small and  $m_2$  large.

Thus the sum of the two never get smaller than  $m_Z$ : in this case the Z invisible width does not impose limits on light sneutrinos. We will see that sneutrinos of the order of 10 GeV are now allowed. Thus the parameters relevant for the sneutrino sector are  $m_L$  and  $m_B$ .

In Fig 4.4.2 it is shown the correlation between the one loop correction of the neutrino mass and the lightest sneutrino mass eigenstate: we see that sneutrinos light as 10 GeV are perfectly viable in L-number violating models.

The neutrino mass and the sneutrino mass splitting are related as a consequence of the lepton number violating interactions and supersymmetry breaking. Thus we can use upper bounds on neutrino masses to set bounds on the sneutrino mass splitting. In general the existence of a sneutrino mass splitting generates a one loop contribution to the neutrino mass. This effect is generic and is independent of the mechanism that generates the sneutrino mass splitting. Similarly the existence of a Majorana neutrino mass generates a one loop contribution to the sneutrino mass splitting. However the latter effect can be safely neglected since it is of the order  $\Delta m_{\bar{\nu}} \sim (g_2^2/16\pi^2) m_\nu$  [110]. In contrast the one loop correction to the neutrino mass is potentially significant and may dominate the tree level mass. These one loop effects introduce a direct connection of the sneutrino phenomenology to the neutrino physics. Sneutrino dark matter phenomenology will therefore be bounded by neutrino physics in a non trivial way.

The one loop contribution to the neutrino mass comes from the neutralino-sneutrino loop in Fig. 4.4.2 and is given by [111]:

$$\Delta m_{\text{neutrino}}^{\text{1loop}} \simeq -\frac{1}{32\pi^2} \sum_{ik} m_{\tilde{\chi}_i^0} (g_2 Z_{2i} - g_1 Z_{1i})^2 (z_{1k}^2 - z_{2k}^2) \left( \frac{\Delta B_0}{\Delta m^2} \right)_{ik} \quad (4.17)$$

where the  $Z_{ij}$  are the neutralino mass eigenvalues, defined in Eq. 3.79, while the  $z_{kl}$  are the sneutrino mass eigenvalues, obtained by diagonalizing the mass matrix Eq. 4.13 and:

$$\left( \frac{\Delta B_0}{\Delta m^2} \right)_{ik} \equiv \frac{\partial B_0(m_{\tilde{\chi}_i^0}, m_{\bar{\nu}k})}{\partial m_{\bar{\nu}k}^2} \quad (4.18)$$

where  $B_0$  is the standard 2 point loop integral evaluated at  $p^2 = 0$  [116].

The one loop correction is basically proportional to the mass difference between the two sneutrino mass eigenstates  $\Delta m = m_2 - m_1$ , as one can see from Fig. 4.10. The horizontal dashed lines represent the current kinematical neutrino mass bounds: 2 eV for electron type neutrinos, 0.2 MeV for muon type neutrinos and 18 MeV for tau type neutrinos, from [72]. We will consider the bound on the  $\nu_e$  mass as the more reliable limit on the neutrino mass and all our conclusions will be referred to this limits. Indeed the data from atmospheric oscillations, from cosmological observations disagree with the kinematical bounds unless more than

three families are present and/or additional sterile neutrinos are introduced with special mixing patterns with active neutrinos.

Actually, if we consider a neutrino mass bound of 2 eV, Fig 4.10 shows a strong degeneracy in the sneutrino mass eigenstates and allows very small mass splittings, therefore the phenomenology is very similar to the one of the MSSM models, there are no significant modifications. Instead if the upper neutrino mass bound comes from the muon type neutrinos, sizeable splittings arise in the sneutrino mass eigenstates, of the order of 100 MeV; even large mixings are allowed for tau type neutrinos, of the order of 30 GeV. The latter cases provide light sneutrinos, which were forbidden in the MSSM due to the Z invisible width bound.

In the calculations of the relic abundance there are some differences respect to the standard minimal model. The mixing changes some couplings of the sneutrinos, first of all, as noticed, the off diagonal Z coupling, and therefore the annihilation channels. The new interaction vertices are reported in Appendix A: as an example notice that the sneutrino-sneutrino-Higgs couplings A.1 are diagonal in the  $(\tilde{\nu}_+, \tilde{\nu}_-)$  basis, while the sneutrino-neutralino-neutrino A.6 are no more diagonal. In the calculations of the relic abundance we have now to include the coannihilation between the two sneutrino mass eigenstates  $\tilde{\nu}_1$  and  $\tilde{\nu}_2$ , as reported in Tab 4.2. When the mass splitting is large the coannihilation cross section gets reduced and the relic abundance may increase: in fact in the "STD model" the Z boson s channel exchange and the neutralino t channel are very efficient, leading to high values for the cross section. Instead the greater the splitting in mass between the coannihilating particles, the less efficient is the annihilation process. Obviously the coannihilation with the corresponding charged sleptons is taken into account as in the standard case, see Tab 4.1.

In Fig. 4.11 is shown the relic abundance with a scan over both parameters. The remaining values of the parameters are the same as for the standard MSSM model, Sec. 4.1. The resulting relic abundance for a mass bound on the neutrino mass of 18 MeV is plotted (blue band). This would correspond to the case of a tau sneutrino dark matter, since we are applying the tau neutrino kinematical mass bound. We see that the relic abundance increases and light sneutrinos down to 10 GeV are acceptable. Instead if we consider the mass bound of 2 eV on the electron neutrino, the relic abundance reduces to the standard case of the MSSM, discussed in the previous section 4.1.

## 4.4 Majorana models: implications in the sneutrino sector

In this section we will discuss see-saw extend MSSM models, which accommodate sneutrino mixing phenomena and Majorana masses for the neutrinos compatible with the observed neutrino mass pattern. These models may be built by adding to the minimal MSSM right handed neutrino superfields  $\hat{N}$  and L-number violating terms; they therefore share the properties of both LR models and  $\mathcal{Y}$  models and provide a rich sneutrino phenomenology.

The most general and renormalizable superpotential that contribute to the masses and non gauge interactions of the neutrinos and sneutrinos is given by [106, 110]:

$$W = \epsilon_{ij}(\mu \hat{H}_i^1 \hat{H}_j^2 - Y_l^{IJ} \hat{H}_i^1 \hat{L}_j^I \hat{R}^J + Y_\nu^{IJ} \hat{H}_i^2 \hat{L}_j^I \hat{N}^J) + \frac{1}{2} M^{IJ} \hat{N}^I \hat{N}^J \quad (4.19)$$

where the matrices  $M^{IJ}$ ,  $Y_l^{IJ}$  and  $Y_\nu^{IJ}$  are chosen to be real and diagonal, namely we do not consider flavor mixings. We assume  $M^{IJ} = M \delta^{IJ}$ ; this last term is a Majorana mass term and a source of L-number violation. The general form of the soft supersymmetry breaking potential may be written as [111]:

$$V_{\text{soft}} = (M_L^2)^{IJ} \tilde{L}_i^{I*} \tilde{L}_j^J + (M_N^2)^{IJ} \tilde{N}^{I*} \tilde{N}^J - [(m_B^2)^{IJ} \tilde{N}^I \tilde{N}^J + \epsilon_{ij}(\Lambda_l^{IJ} H_i^1 \tilde{L}_j^I \tilde{R}^J + \Lambda_\nu^{IJ} H_i^2 \tilde{L}_j^I \tilde{N}^J) + \text{h.c.}] \quad (4.20)$$

where we assume again that the matrices  $(M_L^2)^{IJ}$ ,  $(M_N^2)^{IJ}$ ,  $(m_B^2)^{IJ}$ ,  $\Lambda_l^{IJ}$  and  $\Lambda_\nu^{IJ}$  are diagonal in the flavor space.

Let us consider the properties of the neutrino masses generated via the see-saw mechanism [117, 118, 119, 120, 121, 122]. A Dirac mass for the neutrinos is obtained through the Yukawa interaction as  $m_D^I = v_2 Y_\nu^{II}$ , but it is not chosen as a free parameter. It is instead derived by the condition that the neutrino masses are determined by the see-saw. The terms quadratic in the neutrino fields are given in terms of two component fermion fields by:

$$-\mathcal{L}_\nu = \frac{1}{2} \begin{pmatrix} \nu_L^T & \nu_L^{cT} \end{pmatrix} \mathcal{M}_\nu \begin{pmatrix} \nu_L \\ \nu_L^c \end{pmatrix} + \text{h.c.} \quad (4.21)$$

with:

$$\mathcal{M}_\nu = \begin{pmatrix} 0 & m_D \\ m_D^T & M \end{pmatrix} \quad (4.22)$$

Provided that  $M \gg m_D$ , this matrix is of see-saw type. The neutrino masses are obtained by diagonalizing Eq. 4.22, neglecting terms of the  $1/M$ : we get one light

neutrino with  $m_\nu \simeq m_D^I/M^2$  and one heavy neutrino, decoupled from the MSSM spectrum with a mass roughly at the  $M$  scale, for each generation. In our analyses we will fix, for definiteness, the neutrino mass to be 2 eV, in order to saturate the bound which comes from the radiative contribution to the neutrino masses discussed in the section 4.3.

We now turn to the sneutrino sector. Sneutrinos are superposition of the left handed  $\tilde{\nu}_L$  fields and the right handed  $\tilde{N}$  fields. Since in the superpotential and in the soft breaking potential there are L-number violating terms, it is convenient to work in the CP eigenstate basis, as we did for the  $\mathcal{L}$  models. The sneutrino masses are therefore obtained by diagonalizing a  $4 \times 4$  squared matrix, given by:

$$\mathcal{M}_{Maj}^2 = \begin{pmatrix} m_L^2 + D + m_D^2 & F^2 + m_D M & 0 & 0 \\ F^2 + m_D M & m_N^2 + M^2 + m_D^2 + m_B^2 & 0 & 0 \\ 0 & 0 & m_L^2 + D + m_D^2 & F^2 - m_D M \\ 0 & 0 & F^2 - m_D M & m_N^2 + M^2 + m_D^2 - m_B^2 \end{pmatrix} \quad (4.23)$$

having defined in accord with Eq. 4.14 the vector basis as  $\Phi^\dagger = (\tilde{\nu}_+^* \tilde{N}_+^* \tilde{\nu}_-^* \tilde{N}_-^*)$ .  $D$  stands for the D-term, defined in Eq. 3.94 and  $F^2$  is defined as Eq. 4.6. Notice that the sneutrino squared mass matrix separate into CP-even and CP-odd blocks. In general the terms  $F^2 \pm m_D M$  induce a left-right mixing of the sneutrino eigenstates, while  $m_B$  is responsible for CP splitting. The new mass parameter  $M$  is responsible for the left-right mixing, since it appears in the off diagonal elements of the squared mass matrix  $\mathcal{M}_{Maj}^2$ . If it is large it can lead two light sneutrinos and two very heavy sneutrinos decoupled from the low energy scale spectrum, since it enters also in the diagonal terms. A sizeable splitting occurs when  $m_D M \simeq F^2$ .

The sneutrino eigenstates may be defined as:

$$\tilde{\nu}_i = Z_{i1}\tilde{\nu}_+ + Z_{i2}\tilde{N}_+ + Z_{i3}\tilde{\nu}_- + Z_{i4}\tilde{N}_- \quad i = 1, 2, 3, 4 \quad (4.24)$$

Notice that sneutrinos are now superpositions of CP eigenstates of both the left handed and right handed neutrino superfield: these models add the properties of mixing with the right handed component together with an off diagonal Z coupling in a natural way.

The sneutrino sector is now characterized by the following parameters:  $m_L$ ,  $m_N$ ,  $M$ ,  $m_B$  and  $F^2$ . The parameter  $m_L$  is linked by gauge invariance to the charged slepton sector, therefore it has to be necessarily larger than about 80-100 GeV to fulfill the charged slepton mass bounds. The other parameters are free and not directly related to the electroweak symmetry breaking scale. We will vary freely  $m_N$ ,  $m_B$  and  $F^2$  as we did in the previous sections.  $M$  is related to the Majorana neutrino mass: typically, in see-saw models, a natural scale for  $M$  is an high energy scale of the order of  $10^9$  GeV, which accommodate a neutrino mass below the eV scale and a Dirac mass term of the

order of the GeV scale. However another possibility is to consider  $M \simeq 1 \text{ TeV}$ , leading to a eV neutrino mass with  $m_D \simeq 1 \text{ MeV}$ , since  $m_D$  is a Dirac mass term arising from a Yukawa interaction of unknown strength. We therefore will analyse two different Majorana models: the first one has a TeV scale Majorana mass term, so it is a low scale model, which we will call Maj[A], while in the second one, called Maj[B], we choose  $10^9 \text{ GeV}$  to be the scale for the Majorana mass parameter. We will see that the choice of the parameter scale changes strongly the phenomenology.

The models have been analyzed with a scan on all the SUSY parameter space, as reported in Appendix B; the choice of the sneutrino parameters is indeed discussed when necessary.

#### 4.4.1 TeV scale Majorana mass term

We consider a see-saw mass scale  $M$  of the order of TeV scale. As noticed before the radiative contribution to the neutrino mass can impose strong bounds on the splitting of the sneutrino masses. The absolute one loop contribution to the neutrino mass are shown in Fig. 4.4.2 as a function of  $\Delta m$ , varying the free parameters as:  $10^2 \text{ GeV} < m_N < 10^3 \text{ GeV}$ ,  $1 \text{ GeV} < m_B < 10^3 \text{ GeV}$  and  $1 \text{ GeV}^2 < F^2 < 10^4 \text{ GeV}^2$ . In this case we see that large mass splittings are possible even if we fix the electron type neutrino mass limit as bound, contrary to the L-number violating case. This is a consequence of the mixing with the right handed field  $\tilde{N}$ , naturally induced in the Maj models: the couplings with the other MSSM fields are reduced and therefore the radiative contributions to the neutrino masses are suppressed. This is manifest in Fig. 4.12, where the sterile components of the sneutrino eigenstates are plotted as a function of the mass splitting  $\Delta m$ . The correlation is of direct proportionality, more the sneutrinos are mixed with the sterile fields  $\tilde{N}$ , the larger the allowed splittings between the mass eigenstates are.

The relic abundance arising from these models is shown in Fig 4.4.2 versus the lightest sneutrino mass  $m_1$ . Notice that Maj[A] models provide sneutrinos as dark matter dominant component in the whole range spanning from 5 GeV to 1 TeV. Especially heavy sneutrinos, with a mass greater than  $m_W$ , can be also underabundant. This is a consequence of the efficient  $W^+W^-$  annihilation channel and of the Higgs poles. As compared to the pure LR case, heavy sneutrinos have a more interesting phenomenology from a cosmological point of view, because of the presence of L-number violating terms.

The distribution of the cosmological acceptable models is shown in Figs. 4.13, 4.4.2 and 4.14. Light sneutrinos typically require small  $F^2$  values, contrary to the LR models, as denoted in Fig. 4.13. Regarding the  $m_N$  parameter, light sneutrinos are strongly correlated to it respect to sneutrino heavier than 100 GeV, Fig 4.4.2. Light sneutrinos are practically pure right-handed fields, while the CP splitting play an important role for heavy sneutrinos; indeed, as we can see in Fig 4.14, sneutrino with  $m_1 > m_W$  may be either strongly mixed with the right components (this is the case for mainly dominant dark matter sneutrinos) or the sterile components are subleading and they present a left handed behavior (typically they are subdominant dark matter halo components).

### 4.4.2 Large scale Majorana mass term

The so called Maj[B] model is a large scale Majorana mass parameter model. The mass term is fixed at  $M = 10^9$  GeV. In this case the large value of  $M$  splits the four sneutrino mass eigenstates into the sets of almost degenerate mass eigenstates: two sneutrinos at the electroweak scale and two at the  $M$  scale respectively arise. The latter sneutrinos result to be very heavy and decoupled from the particle spectrum. Diagonalizing the mass matrix  $\mathcal{M}_{Maj}$ , Eq. 4.23, to first order in  $1/M$ , since it is the largest mass parameter, the two lightest sneutrino eigenstates have squared masses given by:

$$m_{\tilde{\nu}_{1,2}}^2 = m_L^2 + 1/2 m_Z^2 \cos 2\beta \mp \frac{1}{2} \Delta m_{\tilde{\nu}}^2 \quad (4.25)$$

where the squared mass difference  $\Delta m^2 \equiv m_{\tilde{\nu}_2}^2 - m_{\tilde{\nu}_1}^2$  is of the order  $1/M$ . Thus in the large  $M$  limit we recover the two degenerate sneutrino states of the MSSM, usually chosen to be  $\tilde{\nu}, \bar{\tilde{\nu}}$ . For finite  $M$ , these two states mix with a  $45^\circ$  mixing angle and we are reconduced to the L-number violating case.

These class of models are less rich from a phenomenological point of view compared with the Majorana low scale models.

In Fig. 4.4.2 it is shown the contributions of the sneutrino mass difference to the absolute value of one loop neutrino mass. Actually we see that large mass splittings, up to 10 MeV, are allowed, compared with the  $\mathcal{Z}$  and Maj[A] models. As in the previous cases, a full scan in the SUSY parameter space have been done: the arising relic abundance is plotted in Fig. 4.15, as a function of the sneutrino mass  $m_1$ . Cosmological relevant sneutrinos are present only in the range 80 – 90 GeV and 500 – 600 GeV. In the range from 90 GeV up to 500 GeV sneutrinos are strongly subdominant, while sneutrinos heavier than 600 GeV are excluded by the WMAP experimental limits.

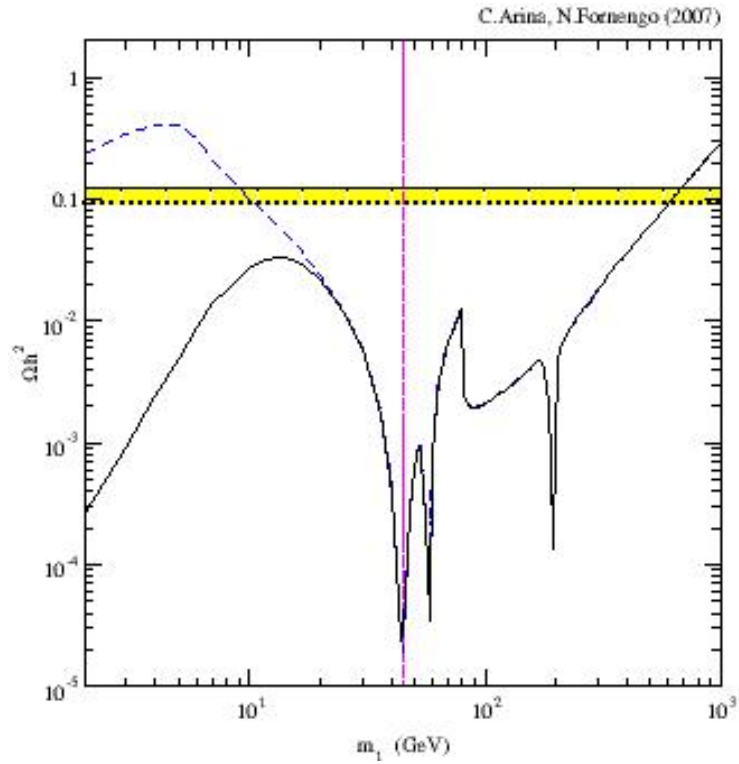


Figure 4.1: STD model – Sneutrino relic abundance  $\Omega h^2$  as a function of the sneutrino mass  $m_1$ . The higgs masses for the lightest CP-even higgs is 120 GeV, for the heaviest CP-even  $H$  and the CP-odd  $A$  is 400 GeV. The solid (dashed) curves refer to models with (without) gaugino universality. The vertical line denotes the lower bound on the sneutrino mass coming from the invisible  $Z$ -width. The horizontal solid and dotted lines delimit the WMAP interval for cold dark matter.

Initial States	Annihilation Products	Available Channels
$\tilde{\nu}_L \tilde{\bar{\nu}}_L$	$\nu \bar{\nu}$ $l \bar{l}$ $q \bar{q}$ $W^+ W^-$ $ZZ$ $hh, HH, hH$ $AA$ $Ah, AH$ $H^+ H^-$ $W^+ H^-$ $Zh, ZH$ $ZA$	$Z(s), \tilde{\chi}_i^0(t, u) \quad i = 1, 4$ $Z(s), h(s), H(s), \tilde{\chi}_i^\pm(t, u) \quad i = 1, 2$ $Z(s), h(s), H(s)$ $Z(s), h(s), H(s), \tilde{e}_L(t), 4\text{-point}$ $h(s), H(s), \tilde{\nu}_L(t, u), 4\text{-point}$ $h(s), H(s), \tilde{\nu}_L(t), 4\text{-point}$ $h(s), H(s), 4\text{-point}$ $Z(s)$ $Z(s), h(s), H(s), \tilde{e}_L(t), 4\text{-point}$ $h(s), H(s), \tilde{e}_L(t, u)$ $Z(s), \tilde{\nu}_L(t, u)$ $h(s), H(s)$
$\tilde{\nu}_L \tilde{\nu}_L$	$\nu \nu$	$\tilde{\chi}_i^0(t, u) \quad i = 1, 4$
$\tilde{e}_L \tilde{e}_L$	$\nu \bar{\nu}$ $l \bar{l}$ $q \bar{q}$ $W^+ W^-$ $ZZ$ $\gamma \gamma$ $Z \gamma$ $hh, HH, hH$ $AA$ $Ah, AH$ $H^+ H^-$ $W^+ H^-$ $Zh, ZH$ $ZA$	$Z(s), \tilde{\chi}_i^\pm(t, u) \quad i = 1, 2$ $\gamma(s), Z(s), h(s), H(s), \tilde{\chi}_i^0(t, u) \quad i = 1, 4$ $\gamma(s), Z(s), h(s), H(s)$ $\gamma(s), Z(s), h(s), H(s), \tilde{\nu}_L(t), 4\text{-point}$ $h(s), H(s), \tilde{e}_L(t, u), 4\text{-point}$ $\tilde{e}_L(t, u), 4\text{-point}$ $\tilde{e}_L(t, u), 4\text{-point}$ $h(s), H(s), \tilde{e}_L(t, u), 4\text{-point}$ $h(s), H(s), 4\text{-point}$ $Z(s)$ $\gamma(s), Z(s), h(s), H(s), \tilde{\nu}_L(t), 4\text{-point}$ $h(s), H(s), \tilde{\nu}_L(t)$ $Z(s), \tilde{e}_L(t, u)$ $h(s), H(s)$
$\tilde{e}_L \tilde{e}_L$	$ll$	$\tilde{\chi}_i^0(t, u) \quad i = 1, 4$
$\tilde{\nu}_L \tilde{e}_L$	$\nu \bar{e}$ $W^+ Z$ $W^+ \gamma$ $W^+ h, W^+ H$ $W^+ A$ $ZH^+$ $\gamma H^+$ $AH^+$	$W^+(s), \tilde{\chi}_i^0(t, u) \quad i = 1, 4$ $W^+(s), \tilde{e}_L(t), \tilde{\nu}_L(t), 4\text{-point}$ $W^+(s), \tilde{e}_L(t), 4\text{-point}$ $W^+(s), H^+(s), \tilde{e}_L(t), \tilde{\nu}_L(t)$ $H^+(s)$ $H^+(s), \tilde{e}_L(t), \tilde{\nu}_L(t)$ $H^+(s), \tilde{e}_L(t)$ $W^+(s), 4\text{-point}$
$\tilde{\nu}_L \tilde{e}_L$	$\nu_l l$	$\tilde{\chi}_i^0(t, u) \quad i = 1, 4$

Table 4.1: Summary of the sneutrino annihilation and coannihilation channels. For definiteness, we report here the case of the first family.

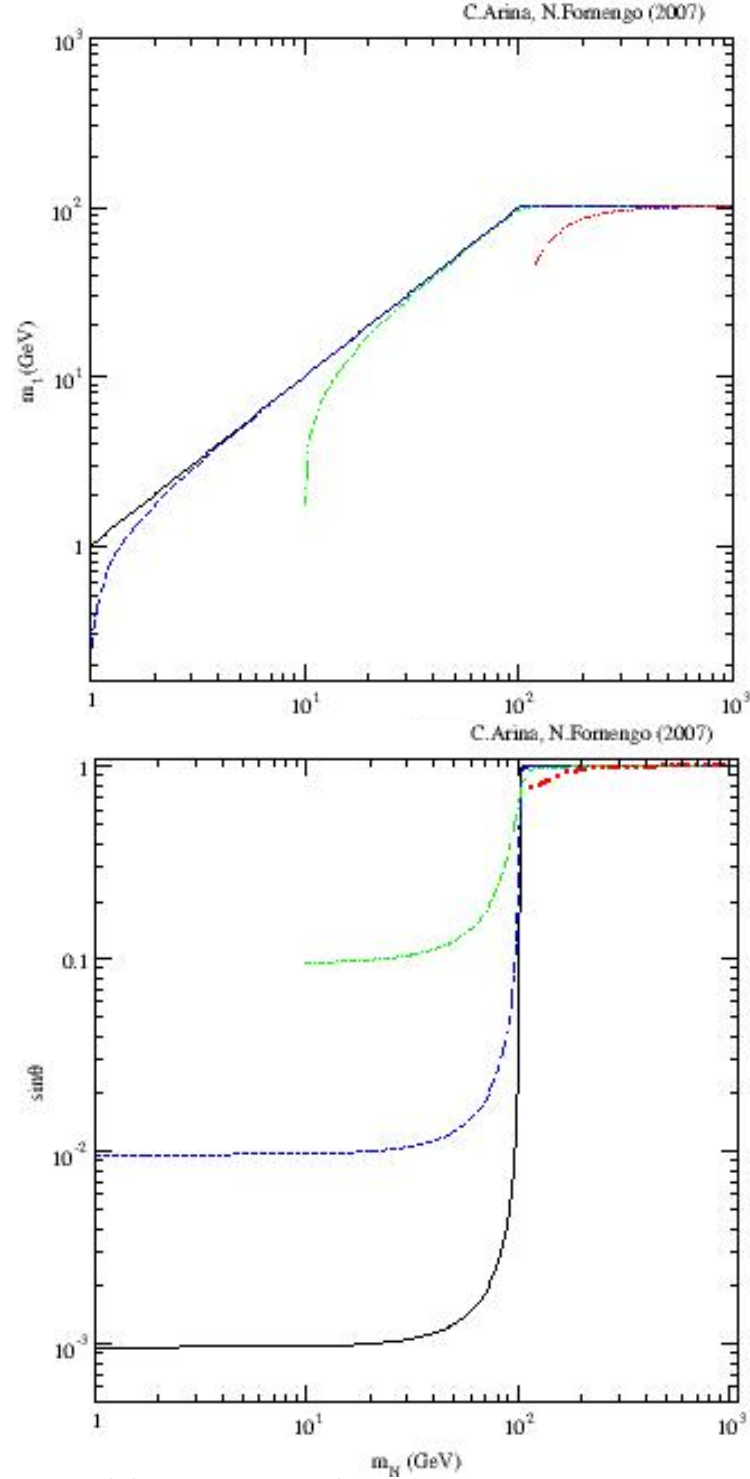


Figure 4.2: LR model – Upper panel: Lightest sneutrino mass eigenstate  $m_1$  as a function of the right handed soft mass parameter  $m_N$  for different values of the off diagonal  $F^2$  term. The solid [black], dashed [blue], dot-dashed [green] and dot-dot-dashed [red] lines denote  $F^2 = 10, 10^2, 10^3, 10^4$  respectively. The soft mass parameter  $m_L$  is fixed at the value of 120 GeV. Lower panel: Sneutrino left-right mixing angle  $\theta$  as a function of the right handed soft mass parameter  $m_N$  for different values of the off diagonal  $F^2$  term. The solid [black], dashed [blue], dot-dashed [green] and dot-dot-dashed [red] lines denote  $F^2 = 10, 10^2, 10^3, 10^4$  respectively. The soft mass parameter  $m_L$  is fixed at the value of 120 GeV.

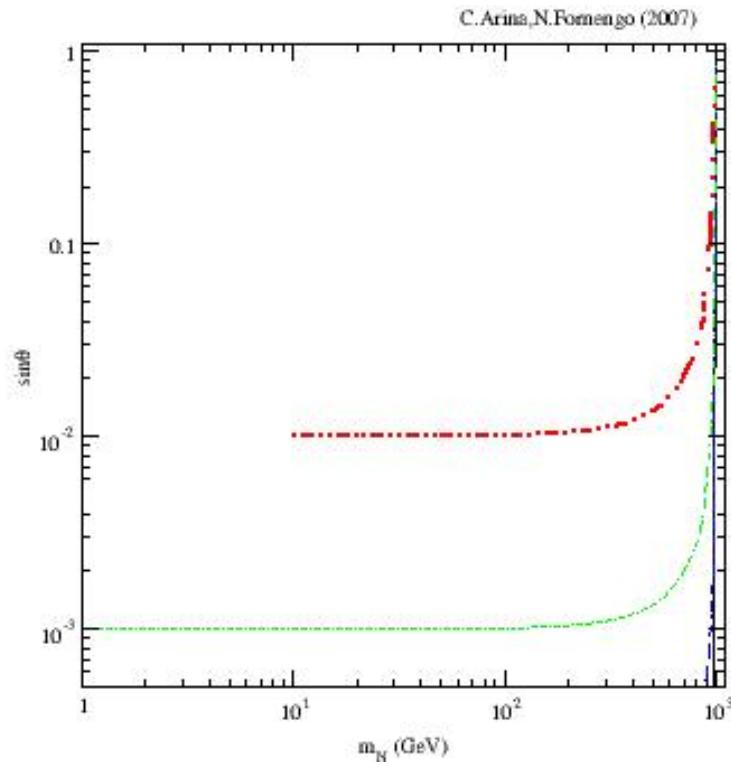


Figure 4.3: LR model – Sneutrino left–right mixing angle  $\theta$  as a function of the right handed soft mass parameter  $m_N$  for different values of the off diagonal  $F^2$  term. The solid [black], dashed [blue], dot–dashed [green] and dot–dot–dashed [red] lines denote  $F^2 = 10, 10^2, 10^3, 10^4$  respectively. The soft mass parameter  $m_L$  is fixed at the value of 1 TeV.

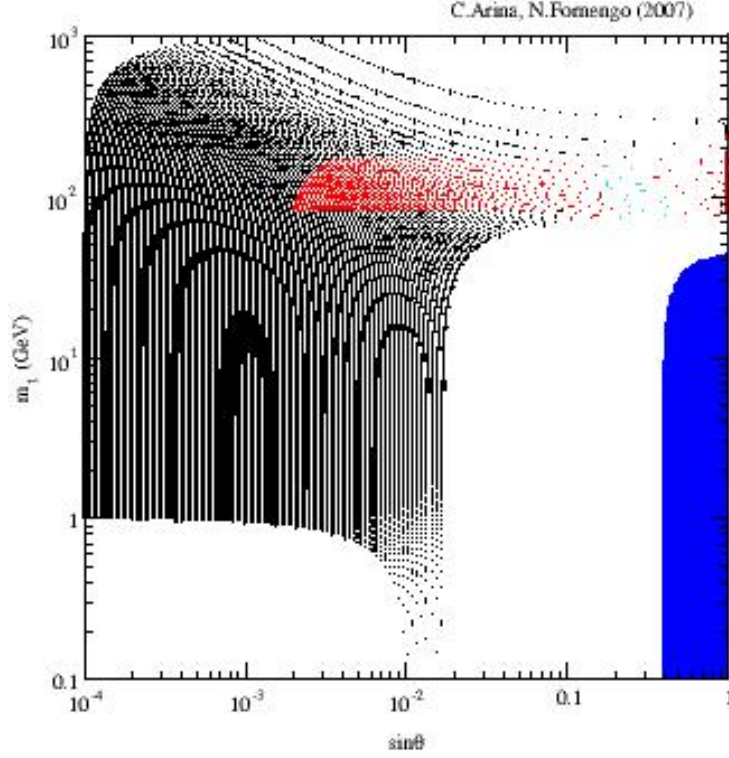


Figure 4.4: LR model – Sneutrino mass  $m_1$  as a function of the sneutrino left–right mixing angle  $\theta$  with  $F^2$  fixed at the value  $10^2 \text{ GeV}^2$  and for a scan of the  $m_L$  and  $m_N$  soft parameters in the ranges:  $120 \text{ GeV} < m_L < 1 \text{ TeV}$  and  $1 \text{ GeV} < m_N < 1 \text{ TeV}$ . The down right [blue] region is excluded by the  $Z$  invisible width bound, the black area denotes the regions where the sneutrino has a relic abundance out of the WMAP limits, the red area refers to cosmological viable sneutrinos while the light [light blue] dots are in accord with the direct detection experimental bounds of DAMA, see next chapter 5.3. The white areas are not covered by the models for the choice of the parameters adopted here.

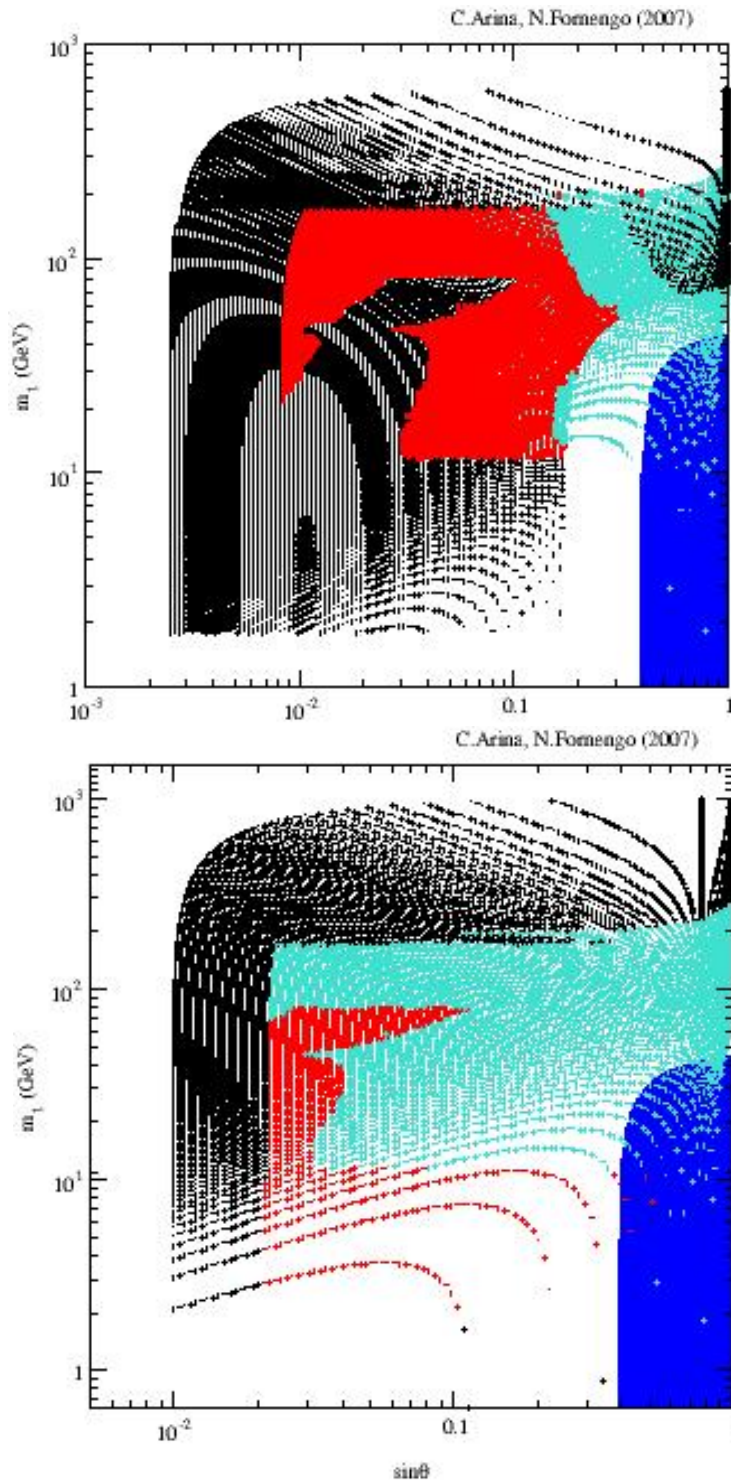


Figure 4.5: LR model – Upper panel: Sneutrino mass  $m_1$  as a function of the sneutrino left–right mixing angle  $\theta$  with  $F^2$  fixed at the value  $10^3 \text{ GeV}^2$ . Lower panel: Sneutrino mass  $m_1$  as a function of the sneutrino left–right mixing angle  $\theta$  with  $F^2$  fixed at the value  $10^4 \text{ GeV}^2$ . The scan on the  $m_L$  and  $m_N$  soft parameters is in the ranges:  $120 \text{ GeV} < m_L < 1 \text{ TeV}$  and  $1 \text{ GeV} < m_N < 1 \text{ TeV}$ . The down right [blue] region is excluded by the Z invisible width bound, the black area denotes the regions where the sneutrino has a relic abundance out of the WMAP limits, the red area refers to cosmological viable sneutrinos while the light [light blue] dots are compatible with the direct detection limits of CDMS, see next chapter 5.3. The white areas are not covered by the models for the choice of the parameters adopted here.

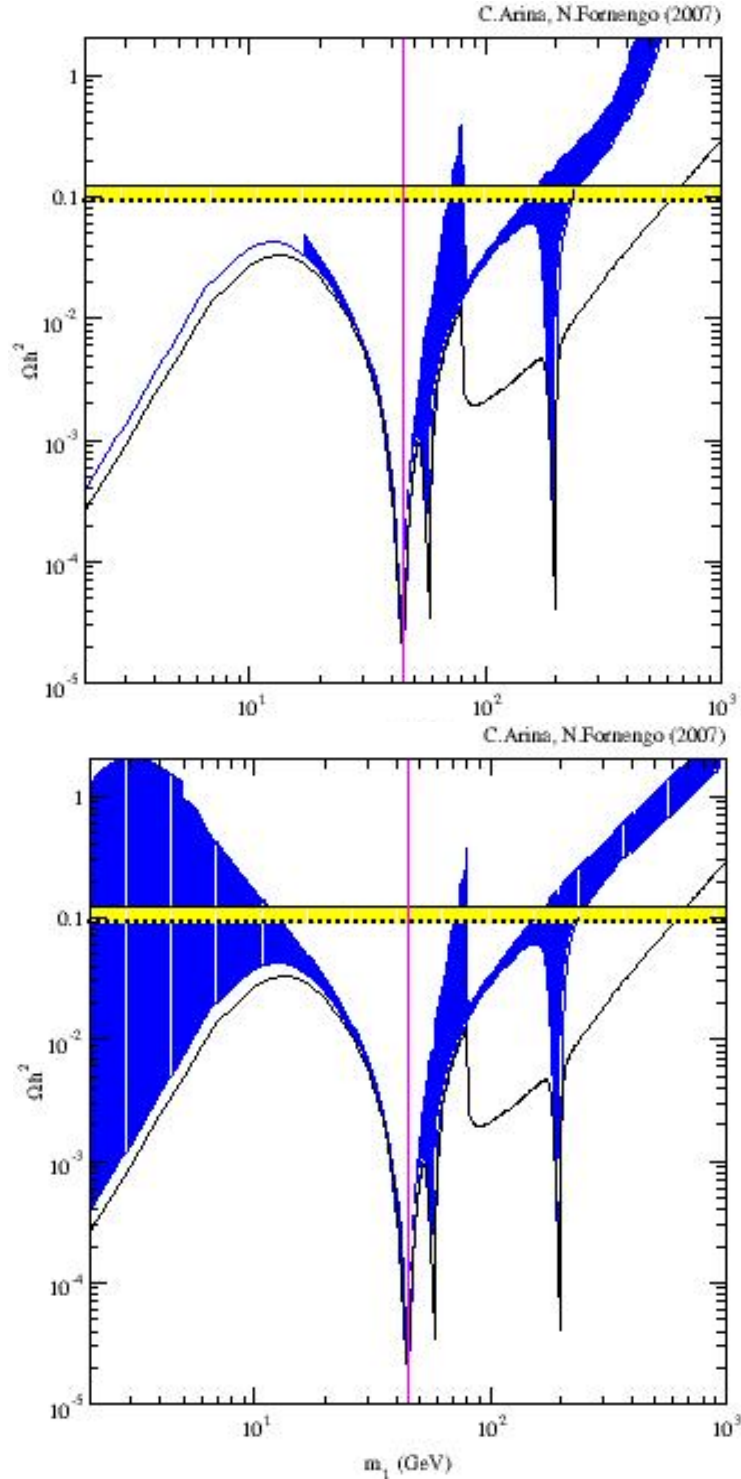


Figure 4.6: LR model – Upper panel: Sneutrino relic abundance  $\Omega h^2$  as a function of the sneutrino mass  $m_1$  at fixed  $m_L = 120$  GeV. Lower panel: Sneutrino relic abundance  $\Omega h^2$  as a function of the sneutrino mass  $m_1$  at fixed  $m_L = 1$  TeV. The solid [black] curve denotes the standard MSSM relic abundance, while the band [blue] refers to all viable sneutrino configurations varying the sneutrino left–right mixing angle  $\theta$  in the range  $0.1 < \sin \theta < 1$ . The higgs and neutralino masses are defined as Fig. 4.1. The horizontal solid and dotted lines [yellow band] delimit the WMAP interval for dark matter.

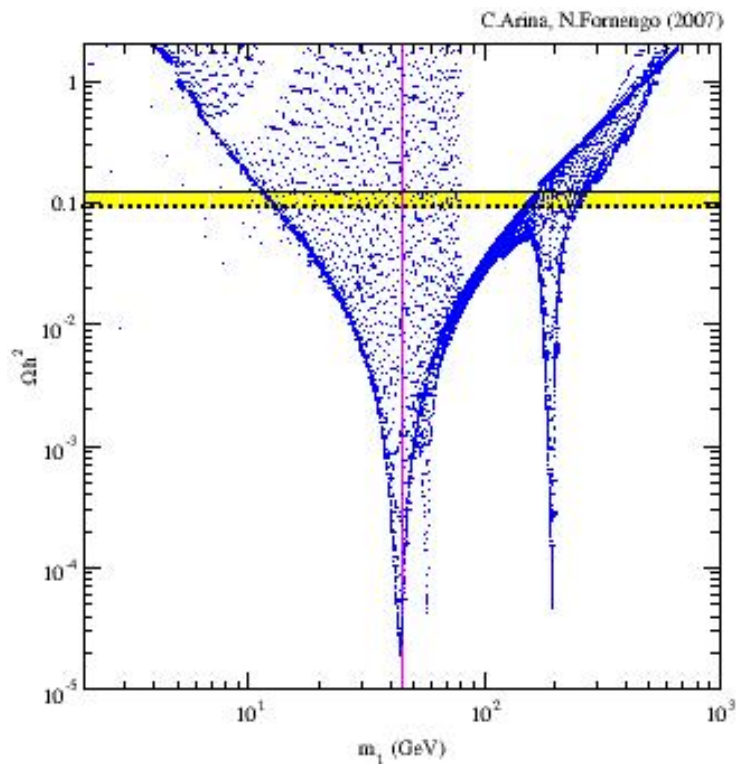


Figure 4.7: LR model – Scatter plot of the sneutrino relic abundance  $\Omega h^2$  as a function of its mass  $m_1$  with a scan over the  $F^2$ ,  $m_N$  and  $m_L$  parameters in the following ranges:  $10 \text{ GeV}^2 < F^2 < 10^4 \text{ GeV}^2$ ,  $1 \text{ GeV} < m_N < 1 \text{ TeV}$  and  $120 \text{ GeV} < m_L < 1 \text{ TeV}$ . The higgs and neutralino masses are defined as Fig. 4.1. All the models shown in the plot are acceptable from the point of view of the all experimental constraints. The horizontal solid and dotted lines [yellow band] delimit the WMAP interval for dark matter.

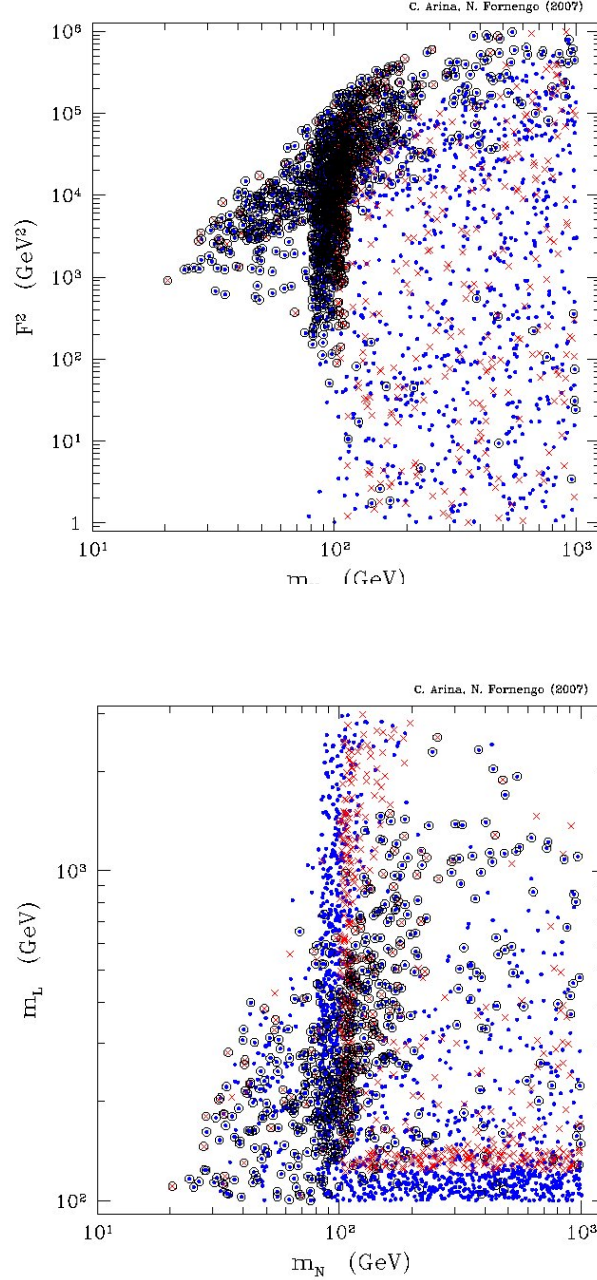


Figure 4.8: LR model – Upper panel:  $F^2$  off diagonal term as a function of the right handed soft mass parameter  $m_N$  for a full scan of the supersymmetric parameter space. The sneutrino parameters are varied as follows:  $100 \text{ GeV} < m_L < 3 \text{ TeV}$ ,  $1 \text{ GeV} < m_N < 1 \text{ TeV}$  and  $1 \text{ GeV}^2 < F^2 < 10^6 \text{ GeV}^2$ . The ranges of the other relevant parameters is described in the text. Lower panel: Soft left mass parameter  $m_L$  as a function of the right soft mass  $m_N$  for a full scan of the supersymmetric parameter space. Crosses [red] refer to models with sneutrino relic abundance in the cosmologically relevant range, dots [blue] refer to cosmologically underabundant sneutrinos and open circles [black] denote configurations which have direct detection cross section in the current sensitivity range.

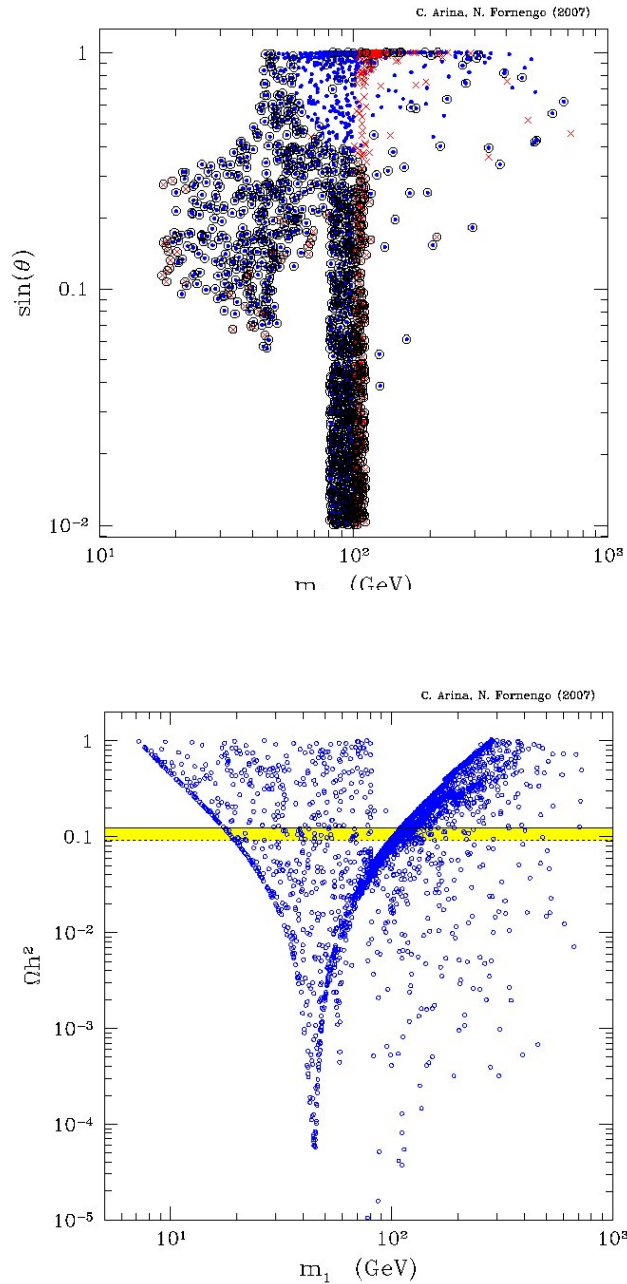


Figure 4.9: LR model – Upper panel: Sneutrino left–right mixing angle  $\theta$  as a function of the sneutrino mass  $m_1$  for a full scan of the supersymmetric parameter space. The sneutrino parameters are varied as Fig 4.4.2. Crosses [red] refer to models with sneutrino relic abundance in the cosmologically relevant range, dots [blue] refer to cosmologically underabundant sneutrinos and open circles [black] denote configurations which have direct detection cross section in the current sensitivity range. Lower panel: Sneutrino relic abundance as a function of the sneutrino mass  $m_1$  for a full scan of the supersymmetric parameter space. The sneutrino parameters are varied as Fig 4.4.2. Dots [blue] refers to all the models acceptable from the point of view of the all experimental constraints. The horizontal solid and dotted lines [yellow band] delimit the WMAP interval for dark matter.

Initial States	Annihilation Products	Available Channels
$\tilde{\nu}_i \tilde{\nu}_i \quad i = 1, 2$	$l\bar{l}$ $q\bar{q}$ $W^+W^-$ $ZZ$ $hh, HH, hH$ $AA$ $H^+H^-$ $W^+H^-$ $Zh, ZH$ $ZA$	$h(s), H(s)$ $h(s), H(s)$ $h(s), H(s), \tilde{\nu}_L(t), 4\text{-point}$ $h(s), H(s), \tilde{\nu}_L(t, u), 4\text{-point}$ $h(s), H(s), \tilde{\nu}_L(t), 4\text{-point}$ $h(s), H(s), 4\text{-point}$ $h(s), H(s), \tilde{\nu}_L(t), 4\text{-point}$ $h(s), H(s), \tilde{\nu}_L(t, u)$ $\tilde{\nu}_L(t, u)$ $h(s), H(s)$
$\tilde{\nu}_1 \tilde{\nu}_2$	$\nu_l \nu_l$ $\bar{l}l$ $\nu \bar{\nu}$ $q\bar{q}$ $W^+W^-$ $Ah, AH$ $H^+H^-$ $Zh, ZH$ $\bar{l}l$	$\tilde{\chi}_i^0(t, u) \quad i = 1, 4$ $Z(s), \tilde{\chi}_i^\pm(t, u) \quad i = 1, 2$ $Z(s), \tilde{\chi}_i^0(t, u) \quad i = 1, 4$ $Z(s)$ $Z(s)$ $Z(s)$ $Z(s)$ $Z(s)$ $\tilde{\chi}_i^\pm(t, u) \quad i = 1, 2$

Table 4.2: Summary of the  $\tilde{\nu}_1 \tilde{\nu}_1$  and  $\tilde{\nu}_2 \tilde{\nu}_2$  annihilation and  $\tilde{\nu}_1 \tilde{\nu}_2$  coannihilation channels in  $\mathcal{L}$  models.

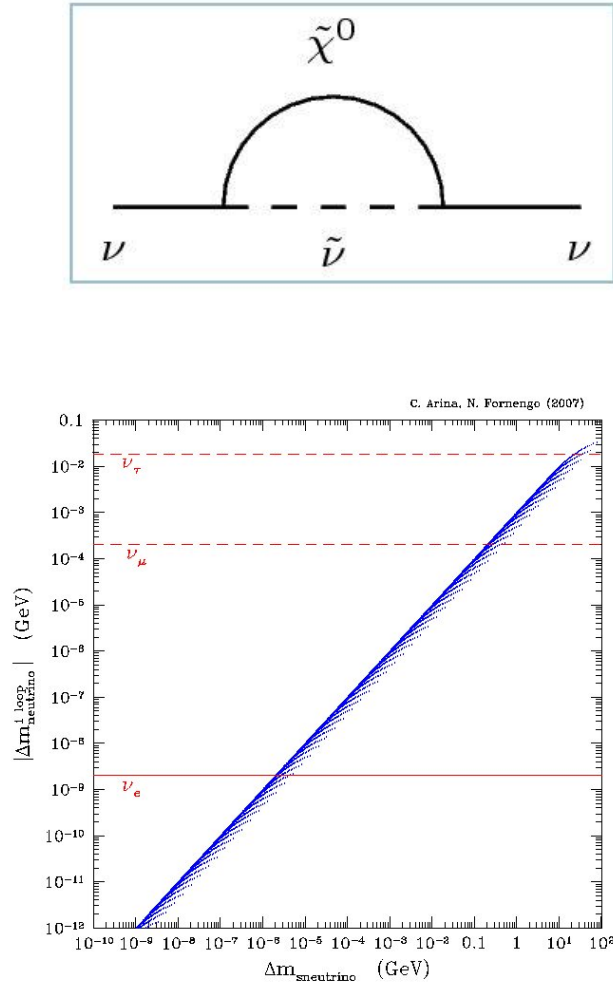


Figure 4.10:  $\mathcal{U}$  model – Upper panel: Neutralino-sneutrino loop diagram contributing to the one loop corrections to the neutrino mass. Lower panel: Correlation between  $\Delta m_{\text{neutrino}}^{\text{1loop}}$  and  $\Delta m$  for a scan of the sneutrino mass parameters varied in the interval:  $80 \text{ GeV} < m_L < 1000 \text{ GeV}$  and  $10^{-4} \text{ GeV} < m_B < 10^2 \text{ GeV}$ . The lightest neutralino is a pure bino of 1 TeV mass. The dashed [red] horizontal lines represents the current  $\nu_e$ ,  $\nu_\mu$  and  $\nu_\tau$  mass bounds, respectively.

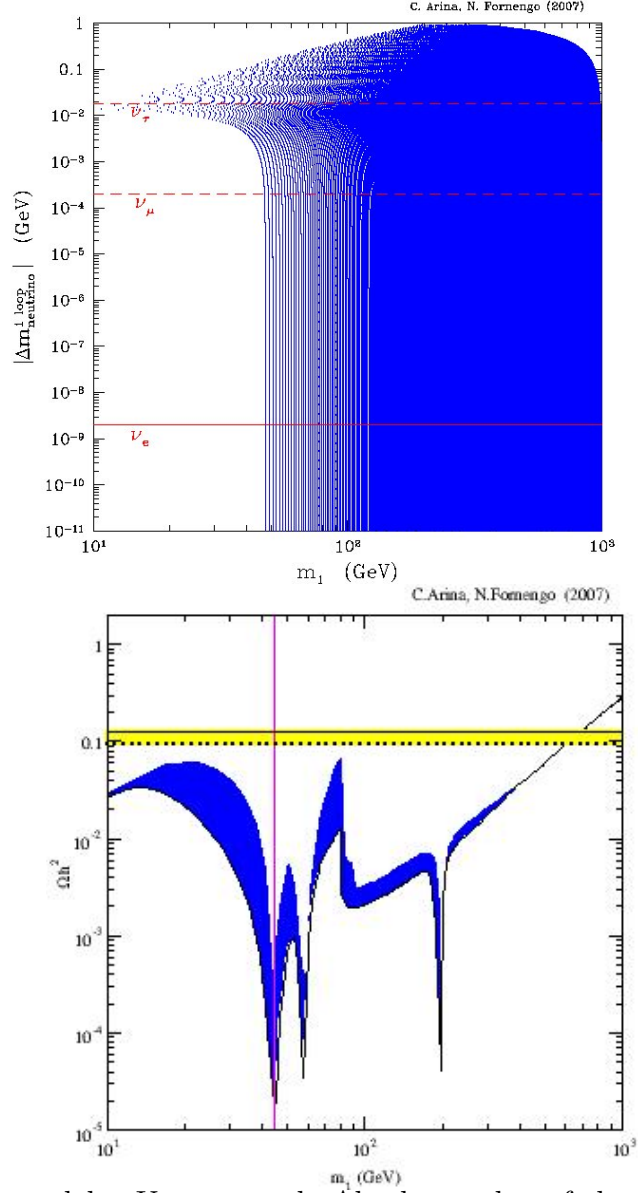


Figure 4.11:  $\mathcal{L}$  model – Upper panel: Absolute value of the one loop correction to the neutrino mass vs the lightest sneutrino mass eigenstate. The parameters are as in Fig. 4.10. The horizontal dashed [red] lines denote upper limits on neutrino masses, as labelled. Lower panel: Sneutrino relic abundance  $\Omega h^2$  as a function of the sneutrino mass  $m_1$ . The solid [black] curve is the standard MSSM relic abundance, while the [blue] band represents the viable values of the relic abundance for a scan of the sneutrino parameters,  $10^{-4} \text{ GeV} < m_B < 10^2 \text{ GeV}$  and  $80 \text{ GeV} < m_L < 1000 \text{ GeV}$ . All the other parameters have been defined in Fig. 4.1. The horizontal solid and dotted lines delimit the WMAP interval for cold dark matter.

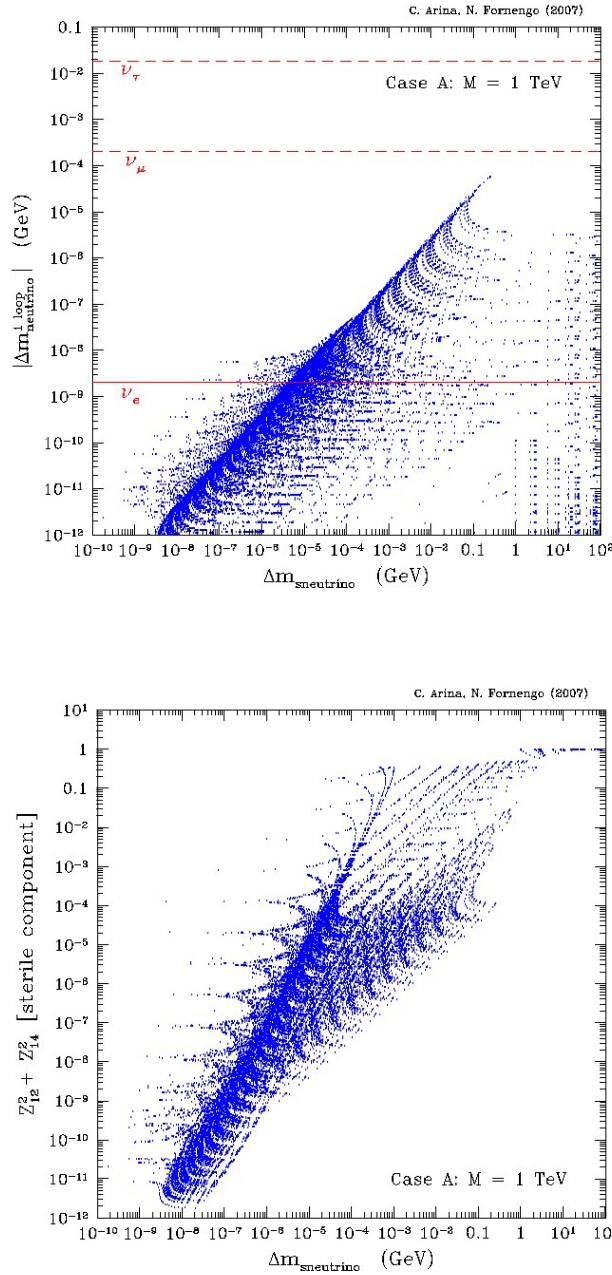


Figure 4.12: Maj[A] model – Upper panel: Absolute one loop contributions to the sneutrino mass  $|\Delta m_{\text{sneutrino}}^{1\text{loop}}|$  versus the mass splitting of the two lightest sneutrino CP eigenstates  $\Delta m$  for a Majorana mass  $M = 1$  TeV. The scan over the sneutrino mass parameters covers the range:  $10^2 \text{ GeV} < m_N < 10^3 \text{ GeV}$ ,  $1 \text{ GeV}^2 < F^2 < 10^4 \text{ GeV}^2$  and  $1 \text{ GeV} < m_B < 10^3 \text{ GeV}$ . The horizontal lines denote the neutrino experimental mass bounds, as labelled. Lower panel: Sterile component of the lightest sneutrino field as a function of the mass splitting of the two lightest sneutrino CP eigenstates, for the low scale Majorana model,  $M = 1$  TeV.

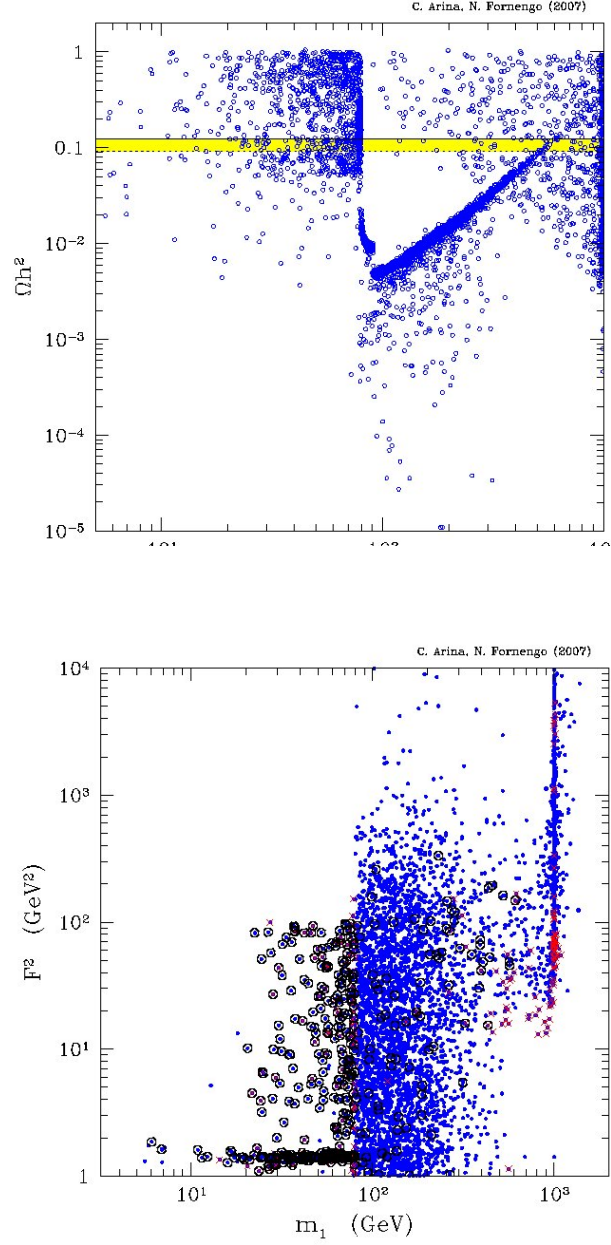


Figure 4.13: Maj[A] model – Upper panel: Sneutrino relic abundance  $\Omega h^2$  as a function of the lightest sneutrino CP mass eigenstate  $m_1$  for a Majorana mass parameter fixed at  $M = 1$  TeV. All the models shown in the plot are acceptable from the point of view of all experimental constraints. The horizontal solid and dashed lines denote the WMAP interval for cold dark matter. Lower panel:  $F^2$  off diagonal term as a function of the lightest sneutrino mass  $m_1$  for a full scan of the supersymmetric parameter space in the Majorana low scale model class,  $M = 1$  TeV. The other sneutrino parameters are varied as in Fig. 4.4.2. Crosses [red] refer to models with sneutrino relic abundance in the cosmologically relevant range, dots [blue] refer to cosmologically underabundant sneutrinos and open circles [black] denote configurations which have direct detection cross section in the current sensitivity range.

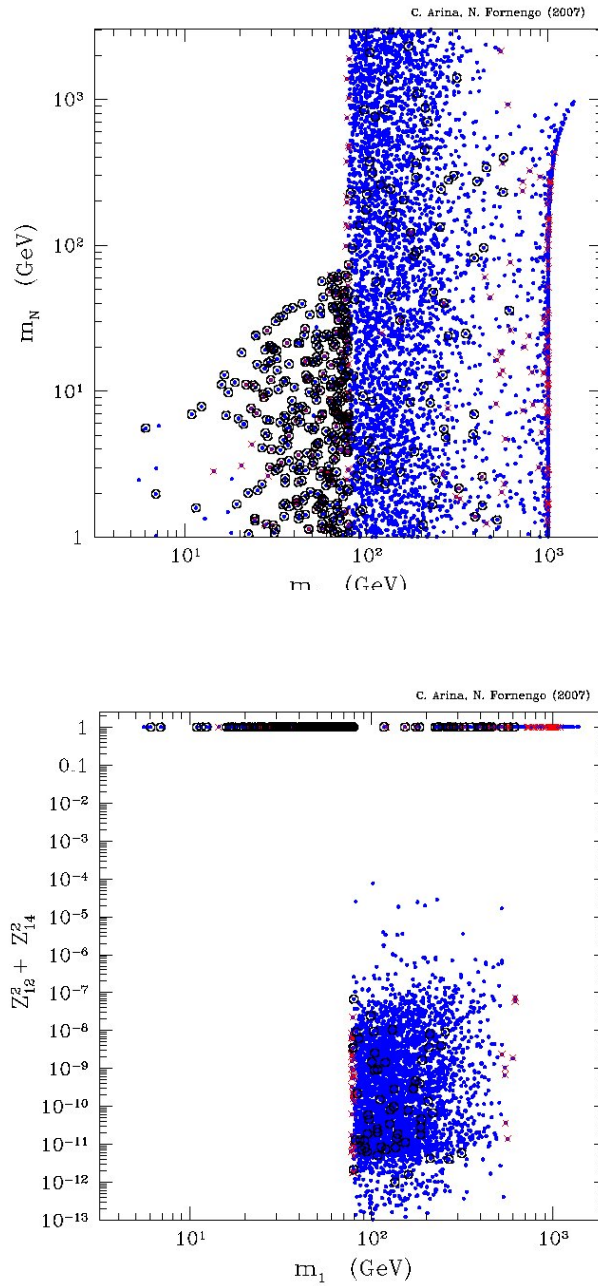


Figure 4.14: Maj[A] model – Upper panel: Right handed soft mass parameter  $m_N$  as a function of the lightest sneutrino mass  $m_1$  for a full scan of the supersymmetric parameter space. Lower panel: Sterile component of the lightest sneutrino field as a function of the lightest sneutrino mass  $m_1$ . The low scale Majorana mass is fixed at  $M = 1$  TeV. The remaining sneutrino parameters are varied as in Fig. 4.4.2. Crosses [red] refer to models with sneutrino relic abundance in the cosmologically relevant range, dots [blue] refer to cosmologically underabundant sneutrinos and open circles [black] denote configurations which have direct detection cross section in the current sensitivity range.

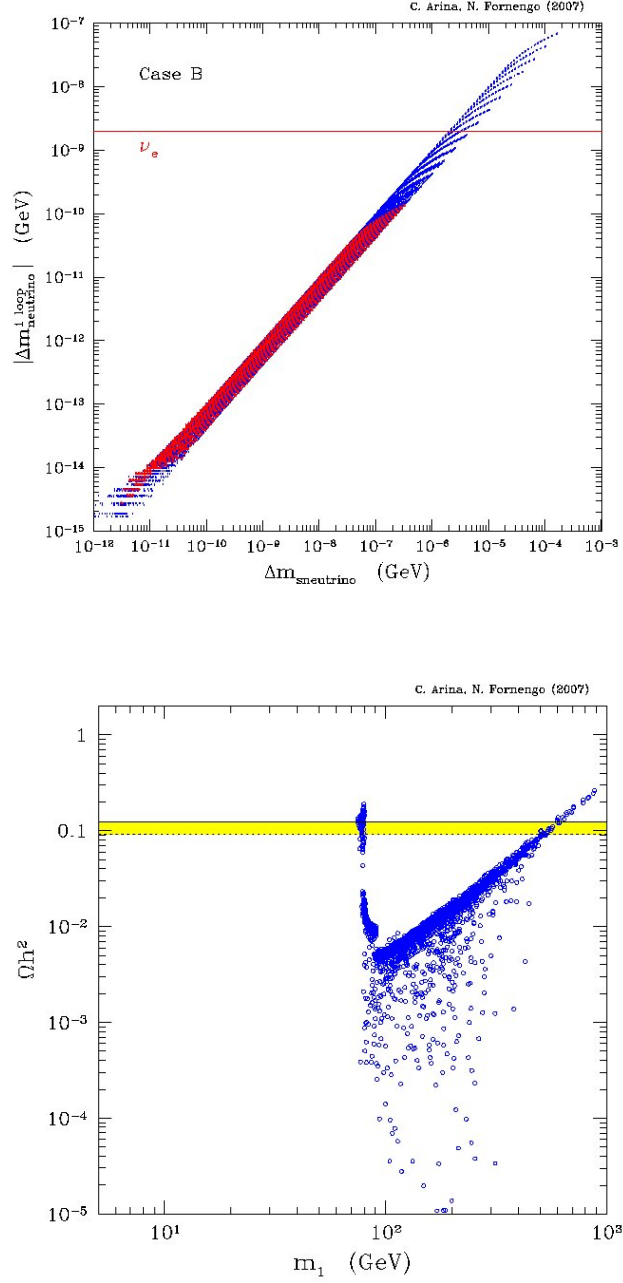


Figure 4.15: Maj[B] model – Upper panel:  $|\Delta m_{\text{sneutrino}}^{1\text{-loop}}|$  versus the mass splitting of the two lightest sneutrino CP eigenstates  $\Delta m$ . Lower panel: Sneutrino relic abundance  $\Omega h^2$  as a function of the lightest sneutrino CP mass eigenstate  $m_1$ . The Majorana mass parameter is fixed at  $M = 10^9$  GeV. The sneutrino parameters are in the same range of Fig. 4.4.2. All the models shown in the plot are acceptable from the point of view of all experimental constraints. The horizontal solid and dashed lines denote the WMAP interval for cold dark matter.

# Chapter 5

## Sneutrino direct detection properties

The dark matter particles move in the Milky Way halo, so it is worthwhile from the point of view of both cosmology and particle physics, to explore the possibility to detect them. This can be done directly in terrestrial detectors sensitive to the nuclear recoil caused by the passing wind of dark matter particles. If sneutrinos are indeed the CDM constituents, there should be a flux of these particles in the Galaxy and of course in the solar neighborhoods.

The most important direct detection process is elastic scattering off nuclei, although inelastic processes [123] and scattering on electrons [124] have also been suggested in the literature.

The recoil energy transferred in a collision between an incident particle of mass  $m$  and velocity  $v$  and a nucleus of mass  $m_{\mathcal{N}}$  in the detector upon the scattering angle  $\theta$  is given by:

$$E_R = \frac{m^2 m_{\mathcal{N}}}{(m + m_{\mathcal{N}})^2} v^2 (1 - \cos \theta) \quad (5.1)$$

Therefore the mean energy of the process is of the order:

$$\langle E_R \rangle \simeq \text{KeV} \left( \frac{m_{\mathcal{N}}}{\text{GeV}} \right) \left( \frac{m}{(m + m_{\mathcal{N}})} \right)^2 \quad (5.2)$$

where we have considered a WIMP mean velocity in the Galactic halo to be  $v \simeq 10^{-3} c \simeq 300 \text{Km/s}$ . The recoils have energy of the order of a few KeV, so detectors should in principle have high sensitivity to heavy nuclei recoils and a good background rejection, in order to deal with such a low energy and rare signals. Moreover notice that particle detectability depends upon the particle mass and velocity and on the choice of the target material.

We will first discuss, in Sec. 5.1, the main properties of the direct detection rates and the astrophysical uncertainties that may affect the predictions. Then referring to

the sneutrino particles, we will discuss their elastic cross section properties, Sec. 5.2. The major current experiments are presented in section 5.3. Finally in the last sections we present the results of the various supersymmetric models: we will see that standard sneutrino, Sec 5.4 are almost completely ruled out by direct detection limits, the same holds for sneutrino in L-number violation models 5.6. Instead LR models, Sec 5.5 and Maj models, Sec. 5.7, provide viable signals for direct detection.

## 5.1 Detection rate and differential spectrum

The rate of CDM particles detection can be obtained by folding in the flux of the WIMPs with the probability of their interactions in the detector. For particles with speed  $w$  with respect to the Earth and mass  $m$  and a detector with threshold energy  $E_{th}$  the differential event rate is given by [125, 126]:

$$\frac{d\mathcal{R}}{dE_R} = \sum_i N_{T,i} \frac{\rho_\odot}{m} \int d\vec{w} f(\vec{w}) \frac{d\sigma_i}{dE_R}(w, E_R) \quad (5.3)$$

where  $N_{T,i}$  is the number of the target nuclei of the  $i$  species per unit of mass, since the detector can be monoatomic like Ge detectors, but in general may be built by different types of nuclei, like NaI.  $f(\vec{w})$  denotes the WIMP distribution function in the Earth frame ( $w = |\vec{w}|$ ), usually defined as in Eq. 1.10 to be an isotropic Maxwell-Boltzmann distribution for an isothermal non rotating halo.  $d\sigma_i/dE_R$  is the WIMP-nucleus differential cross section, with  $E_R$ , the energy of the nuclear recoil, defined in Eq. 5.1.  $\rho_\odot$  is the local value of the total non baryonic dark matter density, defined in Sec. 1.2. Notice that the direct detection rate is proportional to  $\rho_\odot$ , therefore only the parameters in the neighborhoods of the sun are outstanding.

The WIMP velocities in the galactic halo are small, typically of the order of  $\beta = v/c \simeq 10^{-3}$ . Therefore the WIMP nucleus interactions is a low energy process and can be simplified in the following way:

$$\frac{d\sigma_i}{dE_R}(w, E_R) = \frac{d\sigma_i}{dE_R}(w, 0) F_i^2(E_R) \quad (5.4)$$

where  $F_i$  is the nucleus form factor, which takes into account the finite dimension of the nucleus. For coherent interaction it is usually parameterized by the Helm form [127]:

$$F(q^2) = \frac{3j_1(r_0)}{qr_0} e^{(-1/2q^2s^2)} \quad (5.5)$$

where  $s \simeq 1$  fm is the thickness of the nucleus surface,  $r_0 = (r^2 - 5s^2)^{1/2}$  with  $r = 1.2A^{1/3}$  fm being the mean nucleus radius and finally  $j_1(r_0)$  is the first kind spherical Bessel function.

At low energy,  $q^2 \rightarrow 0$ , the WIMP-nucleus differential cross section is isotropic, thus is holds:

$$\frac{d\sigma_i}{dE_R}(w, 0) = \frac{\sigma_i}{E_R^{max}} \quad (5.6)$$

where  $\sigma_i$  is the total elastic scattering cross section on pointlike nucleus, and  $E_R^{max}$  is the maximum recoil energy:

$$E_R^{max} = \frac{2m^2 m_{\mathcal{N}}}{(m + m_{\mathcal{N}})^2} w^2 \quad (5.7)$$

Therefore the differential event rate can be rewritten as:

$$\frac{d\mathcal{R}}{dE_R} = \sum_i \frac{R_i}{\langle E_R^{max} \rangle} F_i^2(E_R) I_i(E_R) \quad (5.8)$$

where  $\langle E_R^{max} \rangle$  is the maximum recoil energy mediated over the velocity in the Earth frame,  $R_i$  contains the contributions from the WIMP nucleus interactions and from the local density distribution of the dark matter particles:

$$R_i = N_{T,i} \frac{\rho_{\odot}}{m} \sigma_i \langle w \rangle \quad (5.9)$$

and:

$$I_i(E_R) = \frac{\langle w^2 \rangle}{\langle w \rangle} \int_{w_R^{min}}^{w^{max}} dw \frac{f(w)}{w} \quad (5.10)$$

with  $w_R^{min}$  is the minimum detectable velocity, given by:

$$w_{min}^2 = \frac{E^{th} (m + m_{\mathcal{N}})^2}{2m m_{\mathcal{N}}} \quad (5.11)$$

while  $w^{max}$  is the escape velocity of the WIMPs, usually taken to be 500 – 600 km/s for a truncated Maxwell-Boltzmann velocity distribution.

The total event rate is given by:

$$\mathcal{R} = \int_{E_R^{th}}^{E_R^0} \frac{d\mathcal{R}}{dE_R} \quad (5.12)$$

where the threshold recoil energy  $E_R^{th}$  depends on the detector characteristics and  $E_R^0$  is usually chosen to maximize the signal to noise ratio. As we have seen, the recoil energies are of the order of few KeV; instead of measuring directly the nuclei recoil, the detectors are based on different techniques, which are sensible to the effects of the recoil, like scintillation, heat production and ionization. In order to deal with the experimental data we define the electron equivalent energy  $E^{ee}$ :

$$E^{ee} = Q E_R \quad (5.13)$$

where  $Q$  is the quenching factor and depends on the detector properties. Typical values for the quenching factor are of the order of the percent.

The direct searches are affected by many uncertainties of nuclear and astrophysical source. Regarding the particle physics the main problem comes from the WIMP–nucleus differential cross section at low energy: sizeable uncertainties are due to the estimate

of the hadronic matrix elements, which describes the quark density contents in the nucleon. In the calculation of the hadronic matrix element the so called pion–nucleon sigma term is crucial in the determination of the quark couplings: the determination of its numerical value from experimental data is rather involved, see Refs. [128, 129]. From an astrophysical point of view, coming back to Eq. 5.3, we stress that extracting an information about the WIMP nucleus cross section from the experimental data requires the use of a specific expression for the velocity distribution function  $f(\vec{w})$ . The main problem arises from the velocity distribution of WIMPs in the galactic halo [22]. We have poor indications on the velocity distribution profile: different kind of halo models may change drastically the exclusion regions in the experimental data. Usually the velocity distribution function is dependent not only on the halo density profile but also on the density distribution of all the other galactic components. The bulge can be described by using a spheroidal distribution which gives a sizeable contribution inside the first kpc from the galactic center, and is truncated at about  $r \simeq 2\text{kpc}$ . The disk has an exponential distribution which in most of the models dies away at about 4 kpc from the galactic center. Therefore we will assume that in the solar neighborhood  $\rho_{vis} \ll \rho_{DM}$  [130]. The key parameters for direct detection searches are the local mean velocity  $v_0 \simeq 220\text{ km/s}$  in the galactic rest frame, leading to  $\langle w \rangle \simeq 300\text{ km/s}$  in the Earth frame, and the local density, usually assumed  $\rho_\odot \simeq 0.3\text{ GeV/cm}^3$ .

## 5.2 Elastic cross-section on nuclei and nucleon

Dark matter particles scatter off of the detector nuclei with elastic cross section given by [131]:

$$\sigma_{\mathcal{N}} = \left( \frac{m^2 m_{\mathcal{N}}}{\pi(m + m_{\mathcal{M}})^2} \right) |\mathcal{M}|^2 \quad (5.14)$$

where  $\mathcal{M}$  is the invariant amplitude, constant at low energy.

The invariant amplitude can receive contributions from three different sources: weak Spin Independent (SI) interactions, weak Spin Dependent interactions (SD) and strong interactions. The sneutrino interaction with the nucleus is purely SI, namely the sneutrinos undergo coherent interactions proportional to the nucleon number or to the mass of the nucleus. The dominant channel is a  $t$  channel  $Z$  boson exchange, while a sub-leading contribution comes from the Higgs mediated  $t$  channel. Thus the sneutrino elastic cross section is the sum of the two contributions:

$$\sigma_{\mathcal{N}} = \sigma_{\mathcal{N}}^Z + \sigma_{\mathcal{N}}^{\text{h,H}} \quad (5.15)$$

Let us first consider the  $Z$  mediated channel. The scattering rate in the non relativistic limit for any particle that scatters off of nuclei by  $Z$  exchange was computed by Goodman and Witten [131]. Sneutrinos have a vector couplings to  $Z$  bosons, since for such particles the axial couplings, which only produce small spin-dependent effects, can

be neglected. At low energy ( $q^2 \rightarrow 0$ ), the weak scattering amplitude is:

$$\mathcal{M}_Z = \frac{g_1^2 + g_2^2}{m_Z^2} J_\nu^0 J_T^0 \quad (5.16)$$

where  $J_\nu^0$  and  $J_T^0$  are the zero components of the weak neutral currents of the sneutrino and the target nucleus. For the sneutrino,  $J_\nu^0$  depends only on the hypercharge,  $J_\nu^0 = \bar{Y}/2$ , with  $\bar{Y} = 1/2(Y_R + Y_L)$ . For a nucleus with  $N$  neutron and  $Z$  protons, we define  $\bar{N} = N - (1 - 4\sin^2\theta_W)Z$ ; then  $J_T^0 = \bar{N}/4$ . Hence the scattering amplitude is:

$$\mathcal{M}_Z = G_F \frac{\bar{Y}\bar{N}}{\sqrt{2}} \quad (5.17)$$

with  $G_F$  the Fermi constant. Substituting in Eq. 5.14 the cross section through  $Z$  exchange reads:

$$\sigma_{\mathcal{N}}^Z = G_F^2 \bar{Y}^2 \bar{N}^2 \left( \frac{m^2 m_{\mathcal{N}}^2}{2\pi(m + m_{\mathcal{N}})^2} \right) \quad (5.18)$$

The result applies to all particles with vector couplings to the  $Z$  boson. Especially it holds in the case of massive Dirac neutrinos [125], nevertheless the annihilation phenomenology is very different from that of sneutrinos.

Hereafter rewriting Eq. 5.18, using  $Y = 1$  the coherent  $Z$  exchange scattering for the sneutrino becomes:

$$\sigma_{\mathcal{N}}^Z = \frac{G_F^2}{2\pi} \frac{m^2 m_{\mathcal{N}}^2}{(m + m_{\mathcal{N}})^2} (A + 2(2\sin^2\theta_W - 1)Z)^2 \quad (5.19)$$

The parameter  $A$  refers to the atomic number of a nucleus of mass  $m_{\mathcal{N}}$ .

For a general LSP, scalar Higgs exchange contributes to the coherent scattering amplitude [132]. The Higgs bosons couple to light ( $u, d, s$ ) quarks, whose masses and nucleonic matrix elements  $\langle \mathcal{N} | q\bar{q} | \mathcal{N} \rangle$  have to be taken from non perturbative model estimates. Moreover they couple to heavy quarks, whose abundance in the nucleon can be calculated perturbatively and may be determined using an effective lagrangian approach, which amounts to keeping only the leading term in an expansion in the inverse quark mass. These latter contributions can be understood as being due to an effective LSP gluon interaction, multiplied with the matrix element  $\langle \mathcal{N} | F_{\mu\nu} F^{\mu\nu} | \mathcal{N} \rangle$  related to the nucleon mass ( $F_{\mu\nu}$  is the gluon field strength tensor). Therefore, the Higgs-bosons exchange cross section is derived in analogy to the neutralino scattering cross section mediated by the Higgs bosons, following [133, 134]. The sneutrino coherent cross section mediated by the Higgs bosons turns out to be:

$$\sigma_{\mathcal{N}}^{h,H} = \frac{m_{\mathcal{N}}^2}{4\pi(m_1 + m_{\mathcal{N}})^2} (f_p Z_{\mathcal{N}} + f_n (A_{\mathcal{N}} - Z_{\mathcal{N}}))^2 \quad (5.20)$$

where  $f_p$  and  $f_n$  denote the effective coupling of the sneutrino to the nucleus, whose determination (like in the case of neutralino-nucleus scattering) is rather involved and

we do not reproduce it here. Details may be found for instance in Refs. [128, 129]. For the case of sneutrinos, the effective couplings may be written as:

$$f_i = m_N \left( \sum_q^{u,d,s} k_q + \sum_Q^{c,b,t} k_Q \right) \quad i = n, p$$

where  $k_q$  and  $K_Q$  are defined as:

$$\begin{aligned} k_q &= f_{T_q} \sum_{j=1,2} \frac{c_{\nu}^j c_q^j}{m_{h_j}^2} \\ k_Q &= \frac{2}{27} f_{T_G} \sum_{j=1,2} \frac{c_{\nu}^j c_Q^j}{m_{h_j}^2} \end{aligned} \quad (5.21)$$

where  $c_{\nu}^j$  denote the sneutrino-Higgs couplings,  $c_q^i$  and  $c_Q^i$  the quark-Higgs couplings,  $f_{T_q}$  is the nucleon mass fraction due to light quark  $q$  and  $f_{T_G} = 1 - \sum_q^{u,d,s} f_{T_q}$ . From the analyses of Refs. [128, 129] we derive the following numerical values:  $f_{T_u} = 0.023$ ,  $f_{T_d} = 0.034$  and  $f_{T_s} = 0.14$  for the proton and  $f_{T_u} = 0.019$ ,  $f_{T_d} = 0.041$  and  $f_{T_s} = 0.14$  for the neutron. We remind that these quantities are affected by a sizeable uncertainty which can increase the direct detection cross section up to a factor of a few [128].

To compare theoretical expectations with experimental data, and experimental data of different detectors among themselves, it is useful to convert the WIMP–nucleon cross section to the WIMP–nucleus cross section. This procedure is feasible independently of the nuclear model and of the specific nature of the WIMP only under the hypothesis that the coherent cross section is dominant and the WIMPs couple equally to protons and neutrons. Under this assumption, the sneutrino nucleon cross section and the sneutrino nucleus cross section is given by:

$$\sigma_{nucleon}^{(scalar)} = \sigma_{\mathcal{N}} A^2 \frac{m_N^2}{m_{\mathcal{N}}^2} \frac{(1 + m_{\mathcal{N}}/m)^2}{(1 + m_N/m)^2} \quad (5.22)$$

where  $m_N$  is the nucleon mass (proton or neutron mass). Actually in the theoretical predictions for the sneutrino nucleon scattering and in the comparison with the experimental data we will use a slightly different definition of the elastic cross section. Let us introduce  $\xi$  as the fractional amount of local non-baryonic DM density:

$$\xi = \min\left(1, \frac{\Omega_{\nu} h^2}{\Omega_{CDM} h^2}\right) \quad (5.23)$$

therefore the effective cross section will be  $\xi \sigma_{nucleon}^{(scalar)}$ , namely we take into account the possibility that the sneutrinos may be subdominant in the dark matter halo.

In Fig. 5.2 we compare the Z mediated and the Higgs mediated elastic channels for the sneutrino in the standard minimal model of Sec 4.1; as previously mentioned, the Z t channel is very efficient, compared to the Higgs channels, which are two order

of magnitude lower than the Z channel for light sneutrinos ( $m_1 < m_Z/2$ ) and become almost six order lower for heavy sneutrinos,  $m_1 \simeq 1$  TeV. The dips in the  $\xi\sigma_{nucleon}^{(scalar)}$  are due to the  $\xi$  factor, which is proportional to  $\Omega h^2$ . The dependence on the relic abundance introduces a dependence on  $\langle\sigma_{ann}v\rangle$  in the rescaling factor: clearly we see that the dips corresponds to the resonant Z and Higgs annihilation  $s$  channels. The elastic scattering cross section by itself would not present a resonant behavior, since it is a  $t$  channel process.

### 5.3 Present experiments and results

Many deep underground experiments have been designed or are planned for direct detection of non baryonic dark matter. We will briefly comment two of them: DAMA/NaI at Laboratori Nazionali del Gran Sasso (I) and CDMS at the Soudan Underground Laboratory (USA). These two experiments deal with different target nuclei and detection techniques and are representative of the two classes of experiments that are currently running. For an exhaustive and detailed description of the present and future direct detection experiments see e.g. [135, 136].

To obtain a reliable signature for WIMPs it is convenient to follow a model independent approach. In principle three main possibilities exist, based on the correlation between the distribution of the events and the galactic motion of the Earth:

- correlation of the recoil direction with that of the Earth velocity due to the distribution of dark matter particles velocities; it is very hard to realize;
- correlation of the time occurrence of each events with the diurnal rotation of the Earth: this effect can be appreciable only for relatively high cross section candidates;
- the annual modulation signature: it is able to test a wide range of cross sections and of WIMP halo densities.

The annual modulation of the signal rate is induced by the Earth revolution around the sun, see Fig. 5.1; as a consequence, the Earth is crossed by a larger WIMP flux in June (when its rotational velocity is summed to the one of the solar system with respect to the galactic frame) and by a smaller one in December (when the two velocity are subtracted). The relation between the WIMP velocity  $\vec{w}$  in the Earth frame and  $\vec{v}$  respect to the galaxy, is given by:

$$\begin{aligned}\vec{v} &= \vec{v}_{\oplus} + \vec{w} \\ \vec{v}_{\oplus} &= \vec{v}_{\odot} + \vec{v}_{\oplus rot}\end{aligned}\tag{5.24}$$

where  $\vec{v}_{\oplus}$  and  $\vec{v}_{\odot}$  denote the velocities of the Earth and the Sun in the Galactic rest frame ( $|\vec{v}_{\odot}| \simeq v_0 + 12\text{km/s}$ ), and  $\vec{v}_{\oplus rot}$  is the Earth's orbital velocity around the sun ( $|\vec{v}_{\oplus rot}| \simeq 30\text{km/s}$ ). Projecting Eq. 5.24 in the galactic plane, we get:

$$|\vec{v}_{\oplus}| = |\vec{v}_{\odot}| + |\vec{v}_{\oplus rot}| \cos \gamma \cos\{\omega(t - t_0)\}\tag{5.25}$$

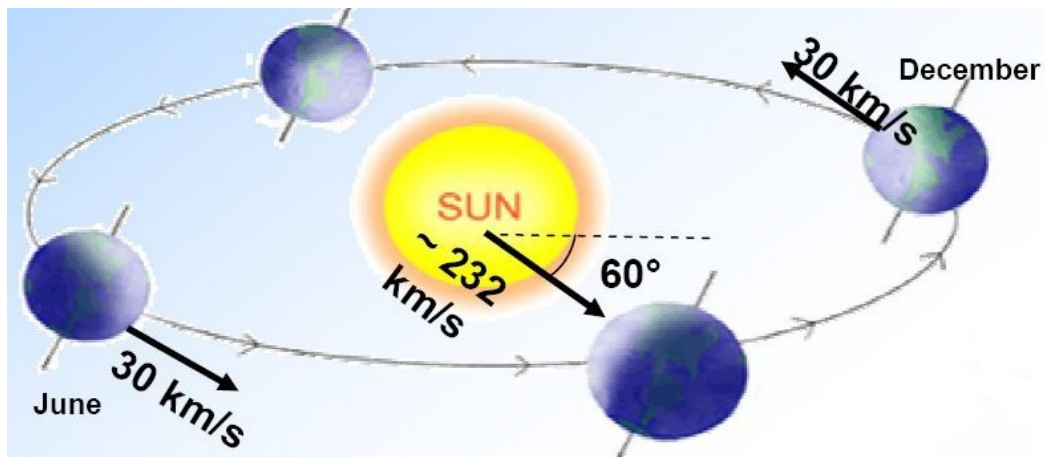


Figure 5.1: Earth frame projected on the galactic plane, where the rotational velocity  $v_{\oplus}$  of the sun in the Galaxy is shown and the relative motion of the Earth around the sun,  $w$ ; from [135].

where  $\gamma$  is the inclination of the plane of rotation with respect to the galactic one,  $\omega = 2\pi/T$  with  $T = 1$  year, and  $t_0 \simeq 2$ nd June. The change in the reference frame of Eq. 5.24 to Eq. 5.25 introduces a time dependence in the expected rate.

DAMA/NaI [137, 138, 139, 140, 141] is a highly radio-pure 100 Kg NaI scintillation experiment, and is designed to detect the annual modulated signature of a WIMP. The Na and I nuclei have a non zero spin value, therefore they are sensitive both to SI and SD couplings. The purely SI scenario represents only a particular case of the more general framework of a WIMP candidate with mixed SI and SD interactions. The model independent approach on the data offers an evidence of an annual modulation signal. The 7 annual cycle data favor the presence of a modulated cosine-like behavior, which is inferred to the annual modulation of the signal, at  $6.3 \sigma$  C.L., compatible with different WIMP models and elastic couplings. In the figures which report the theoretical predictions for sneutrino detection in the various SUSY models, the allowed DAMA region is interpret as due to particle interaction, see e.g. Fig 5.3. The region has been calculated [22] by analysing the annual modulation signal present in the DAMA/NaI data in terms of relic WIMP with purely coherent interactions and by taking into account the astrophysical uncertainties arising from galactic halo modeling. Further insight into the annual modulation signature are expected from the upcoming results of the DAMA/LIBRA experiment, which is currently running with a mass of 250 Kg [142].

The second class of experiments do not attempt to exploit the annual modulation signature, but instead rely on the development of background rejection techniques in order to reduce the background signals to the sum of low neutrons plus dark matter recoils. This type of experiments provide upper bounds on the scattering cross section of nuclei.

CDMS [143, 144] is designed to detect recoils of atomic nuclei that have been scattered by incident WIMPs in Germanium (Ge) and Silicon (Si) crystals (72 Kg x day with a 1.5 Kg Ge plus 0.6 Kg Si detector). The search is most sensitive to spin-independent DM-nucleon scattering amplitudes. Coherent superposition of SI cross sections gives Ge better sensitivity than Si, except for small WIMP masses, where the kinematics increase the Si sensitivity. The experiment discriminates nuclear recoil from electron recoils by measuring both the ionization and phonon energies of interactions within the cryogenic detectors. The data analysis discard all the possible events, therefore up to now no signals have been detected. Hence the bounds set by CDMS should be regarded as an exclusion upper limits on the WIMP-nucleon SI elastic cross section. The upper bound strongly depends on the WIMP model and on the halo velocity distribution. In the figures comparing the sneutrino nucleon elastic scattering with the CDMS results, see e.g. Fig 5.4, we can see three different curves, which have been calculated taking into account three different galactic halo model: the upper curve is the more conservative limit and is obtained from a spherical density distribution by non isotropic velocity dispersion, the central curve denotes the standard isothermal sphere, while the lower curve is calculated using an axisymmetric density distribution  $\rho_{DM}$  [22].

We briefly mention the recent results from the XENON10 Collaboration (15 Kg active liquid Xe) [145]. They have been presented with an exposure of 136 Kg x day and appear more stringent than the CDMS bounds by a factor which ranges from 2 to 10, depending on the WIMP mass. These upper bounds refer to a isothermal density halo model only.

## 5.4 MSSM sneutrinos direct detection

The experimental results, namely the positive indication in the DAMA/NaI data versus the upper limits of CDMS, have different nature and there is no solid criterion to consistently combine the various experimental results, therefore we will present our direct detection analyses by comparing separately our results with the DAMA/NaI region and with the CDMS upper bounds.

Let us turn now to the standard MSSM sneutrino results, shown in Figs. 5.3 and 5.4. The sneutrino nucleon elastic cross section on nucleon is compared with the DAMA/NaI annual modulation region in the former plot. Notice that minimal supersymmetric sneutrinos as dark matter are strongly constrained [99] but some very specific configurations are still viable and could explain the annual modulation effect. The predictions match with the experimental data only in regions of the parameter space where the sneutrinos are highly subdominant. Indeed MSSM sneutrino are still viable, when the sneutrino mass matches the pole condition for annihilation through a light Higgs. However, since the masses of the Higgs bosons may vary, the dips in  $\xi\sigma_{nucleon}^{(scalar)}$  may occur at any value of the sneutrino mass above  $m_h/2$ , where  $m_h$  is the lightest CP-even Higgs, bounded from below at  $m_h \gtrsim 93$  GeV [72]. Thus sneutrinos in a mass range from  $m_Z/2$  up to 200 GeV may be compatible with the DAMA/NaI annual modulation region. In principle

this may appear a fine tuned condition, but it is not as different as the case of relic neutralinos in mSUGRA models, where the relic abundance is typically acceptable only in very specific regions of the parameter space, where strong coannihilation occurs or the pole of the A-boson is met [104, 105, 146].

On the contrary, the mass range 600-700 GeV, where sneutrinos are dominant components of the dark matter halo, is clearly excluded by direct detection.

In Fig. 5.4 minimal standard sneutrinos scalar cross section  $\xi\sigma_{nucleon}^{(scalar)}$  are compared with the CDMS bounds. We see that there are three different curves, see Sec. 5.3, regarding the experimental limits: the dotted curve denotes the upper bound for a standard isothermal halo and excludes totally sneutrinos as dark matter. The dashed line refers to the more conservative upper bounds and leads to some very marginal room for MSSM sneutrinos, when the sneutrinos stay on the CP-even light Higgs pole. In the dot-dashed curve an axisymmetric halo model is taken into account and sneutrinos are completely excluded by this stringent upper limit.

The analyses agree with previous results which excluded the standard minimal sneutrino as a dominant component of dark matter [99, 147]. But still we consider the subdominant sneutrinos as viable relic particles and we have shown that there is, in very limited and restricted mass ranges, a possibility for the MSSM sneutrinos.

Sneutrinos are subdominant or excluded by direct detection since the t channel Z boson exchange in the elastic cross section off nuclei is very efficient and some orders of magnitude greater than the Higgs channel exchange. The extended supersymmetric models present a more rich phenomenology in the direct detection analyses, since the sneutrino coupling to the Z gauge boson is reduced or is off diagonal.

## 5.5 Right-handed model direct detection

The main feature of these extended SUSY models is that sneutrinos are mixed eigenstates of the left  $\tilde{\nu}_L$  field and of the right handed sterile  $\tilde{N}$  field. Therefore the coupling of the sneutrino with the Z gauge boson is reduced proportionally to the left-right mixing angle  $\sin\theta$  and consequently the elastic cross section on nucleon through Z exchange, see Eq. 5.19, is reduced by a factor  $\sin^4\theta$ . Also the Higgs mediated cross section, see Eq. 5.20, results modified as:

$$\xi\sigma_{nucleon}^h \propto \xi (F^2 \sin 2\theta - \cos 2\beta \sin^2 \theta)^2 \quad (5.26)$$

using the LR interaction vertices in Appendix A.

Let us discuss first the LR models scanned over the sneutrino mass and mixing parameters with fixed SUSY Higgs, neutralinos and charginos sectors, as described in Sec 4.2. In Figs. 5.5, 5.6 and 5.7 the sneutrino nucleon cross section  $\xi\sigma_{nucleon}^{(scalar)}$  is reported as a function of the sneutrino mass  $m_1$  for progressively larger values of  $F^2$ . The direct detection bounds, although relevant for many configurations, now is easily evaded. Most of the configurations are allowed and a large fraction of these would be a candidate to explain the DAMA/NaI annual modulation signal and/or are not excluded by the CDMS

upper bounds. The compatibility with sneutrino dark matter and the annual modulation signal increases when  $F^2$  is increased, especially for light sneutrinos. Fig 5.5 shows a lower mass bound of 80 GeV, which is due to the relic abundance bound, as discussed previously in relation with Fig 4.4: most of the cosmological viable configurations are compatible with the direct detection bounds. When  $F^2$  is increased, lighter sneutrinos become possible configurations, as it is shown in Fig 5.6. Here we see that the sneutrinos mass can span from 10 GeV up to 200 GeV respect to the CDMS conservative upper limit, and sneutrino in the mass range from 10 GeV up to 60 GeV can account for the DAMA annual modulation signal. In Fig 5.7, for  $F^2 = 10^4 \text{ GeV}^2$  the situation is even better, the sneutrino in all the whole mass range are compatible with direct detection searches, without invoking fine tuned conditions for the parameters.

In Figs. 5.8 and 5.9 we report a scan over the left right mixing angle for  $m_L = 120$  GeV and  $m_L = 1$  TeV, respectively. The black solid curve represent the value of the standard sneutrino elastic scattering through Z exchange and the blue band denote all the allowed configurations for a scan of  $\sin \theta$  in the range from 0.1 (lower band limit) up to 0.9 (upper limit of the band). For small mixing, namely large  $\sin \theta$ ,  $\xi \sigma_{nucleon}^{(scalar)}$  is not that sensible to the mixing and the reduction is small, therefore these LR models need some fine tuning in the sneutrino parameters to be compatible with the experimental constraints. If  $\sin \theta$  gets small a large compatibility range open up leading to viable sneutrino configurations in the mass range from few GeV up to the TeV. In these cases the elastic scattering through Z exchange is almost completely suppressed and the only contributions arise from the Higgs t channel.

Let us now turn to the full scan on the SUSY parameter space, as described in Appendix B, for a more general analysis. Only points which are accepted by cosmological constraint are shown, namely cosmologically dominant sneutrinos are denoted by red crosses and subdominant dark matter halo component by blue dots.

In Fig 5.10 we show the dependence of the sneutrino nucleon cross section on the left right mixing angle  $\sin \theta$ . The green band denotes the sensitivity of the current experiment for direct searches. As discussed before, except for some configurations with values of  $\sin \theta \gtrsim 0.5$  which are excluded, both dominant and subdominant sneutrinos with mixing angle in the range 0.1 to 0.5 are at the current sensitivity of the direct detection experiments. For small values of  $\sin \theta$  the predicted cross section is some order of magnitude lower than the present sensitivities. In Fig 5.11 the sneutrino nucleon cross section as a function of  $m_1$  is shown. The presence of the mixing with the right handed  $\tilde{N}$  field allows the possibility to have viable sneutrino cold dark matter. A fraction of configurations are excluded by direct detection, but contrary to the standard MSSM models, a large portion of the SUSY parameter space is compatible with the direct detection bounds, both for dominant and for subdominant sneutrinos. The occurrence of sneutrinos which are not in conflict with direct detection limits and that could account for the annual modulation effect in DAMA/NaI is a very interesting feature of these models. We plotted in Fig 5.12 the direct detection relevant cross section  $\xi \sigma_{nucleon}^{(scalar)}$  and the sneutrino relic abundance  $\Omega h^2$ , with the yellow vertical band representing the WMAP interval for cold dark matter. Notice that cosmologically dominant (or slightly

subdominant) sneutrinos are compatible with the direct detection bounds and may be detected in the near future and can account for the annual modulation signature in the DAMA data. As before, there are configurations of the parameters which lead to dominant sneutrino with a low elastic scattering cross section: these sneutrinos correspond to almost pure right handed sneutrino. Moreover we see that there are configurations which are at the right level of experimental sensitivities but are strongly subdominant; in this case the dark matter halo is composed mainly of different DM candidates but nevertheless represents a relic species from the early Universe potentially detectable in the experiment sites.

## 5.6 L number violating sneutrino direct detection

The  $\mathcal{L}$  models allow for L-number violating terms in the superpotential and in the soft supersymmetry breaking potential, as described in Sec. 4.3. The main feature of such terms is the introduction of a splitting in the sneutrino masses and a rotation of the sneutrino eigenstates into a CP basis. In this new basis the resulting sneutrino Z boson coupling is no longer diagonal. Therefore the elastic scattering through t channel exchange of a Z becomes an inelastic reaction, namely instead of the process  $\tilde{\nu} + \mathcal{N} \rightarrow \tilde{\nu} + \mathcal{N}$  one has to produce the heaviest state,  $\tilde{\nu}_1 + \mathcal{N} \rightarrow \tilde{\nu}_2 + \mathcal{N}$ . It is a simple kinematical constraint that  $\tilde{\nu}_1$  can only scatter inelastically off of a nucleus with a mass  $m_{\mathcal{N}}$  if:

$$\Delta m < \frac{\beta^2 m_1 m_{\mathcal{N}}}{2(m_1 + m_{\mathcal{N}})} \quad (5.27)$$

with  $\Delta m = m_2 - m_1$ , as defined in Sec. 4.3. This effect needs to be taken into account in the calculations for the direct detection cross section. The inelasticity effect produces a suppression in the direct detection rates, which depends on the energy of the recoil, the type of nucleus and on the energy threshold of the detector, as discussed in Sec. 5.1. We define a suppression factor for direct detection as:

$$\mathcal{S} = \frac{\mathcal{R}(E_1, E_2; \Delta m)}{\mathcal{R}(E_1, E_2; 0)} \quad (5.28)$$

where  $\mathcal{R}(E_1, E_2; \Delta m)$  and  $\mathcal{R}(E_1, E_2; 0)$  denote the direct detection rate integrated in the energy range  $(E_1, E_2)$  and calculated for a sneutrino mass splitting  $\Delta m$  and for the standard MSSM case ( $\Delta m = 0$ ) respectively. We chose the quenched energies to be  $E_1^{ee} = 2$  KeV and  $E_2^{ee} = 10$  KeV for the Iodine at DAMA/NaI and  $E_1^{ee} = 10$  KeV and  $E_2^{ee} = 100$  KeV for the Germanium, in the CDMS detectors. These  $E^{ee}$  values correspond to the threshold energy for the two experiments. Instead of modifying the experimental results (since we can not do separately for each configuration of the model parameter space) in order to introduce the effects of the suppression factors, as done in [107, 108, 109], we compare the standard experimental curves with a suppressed

scattering process. Thus we redefine the scattering cross section as:

$$\left[ \xi \sigma_{\text{nucleon}}^{(\text{scalar})} \right]_{\text{eff}} = \mathcal{S}(\xi \sigma_{\text{nucleon}}^{(\text{scalar})})^Z + (\xi \sigma_{\text{nucleon}}^{(\text{scalar})})^{h,H} \quad (5.29)$$

where the Z mediated scattering incorporates the suppression factors.

In Fig 5.7.2 we show the ratio of the suppression factors for the case of the Iodine and Germanium nuclei, which are more sensitive to coherent scattering respect to Na and Si nuclei. Notice that for sneutrinos lighter than 200 GeV the detection rates in CDMS can be much more suppressed than in the DAMA/NaI experiment. This is a consequence of the different responses of the two detectors to the dark matter distribution function and mass, as a consequence of the different quenching factors and thresholds energies. Thus  $\mathcal{L}$  models can provide a realization of inelastic dark matter models, proposed in Refs. [107, 108, 109]: if the dark matter can only scatter by making a transition into a slightly heavier state the CDMS and DAMA/NaI are no longer in conflict, since in DAMA there could be some significant regions of sensitivity that are inaccessible to the existing Ge experiments.

In Fig 5.13 the suppression factors are plotted as function of the one loop contribution to the neutrino mass. As we did in the last section, if we consider 2 eV as the neutrino mass bound, the suppression factors are close to one, so we could not expect great differences respect to the standard MSSM case. If instead we consider the tau neutrino mass bound, we notice that the scattering off nuclei through Z exchange is totally drop out, therefore in Eq. 5.29 only the Higgs mediated process survives, with a consequent reduction of  $\xi \sigma_{\text{nucleon}}^{(\text{scalar})}$ , see Fig. 5.2.

Finally the last plot in Fig. 5.14 shows the sneutrino nucleon cross section in terms of the sneutrino mass  $m_1$ : the blue band represents configurations in the sneutrino parameter space (see Sec 4.3 for the parameter values), considering 18 MeV the neutrino mass bound. We see that light sneutrinos are compatible with the upper bound of CDMS, in the mass range from 10 GeV up to the Z pole scale. This is due to the large mass splitting of the two sneutrino states which effectively suppresses direct detection mediated by the Z boson. Such configurations provide viable dark matter candidates, even if subdominant, only by taking into account the tau neutrino mass bound. Assuming the more reliable electron neutrino mass bound it is recovered the minimal MSSM case. Heavy sneutrino,  $m_1 > m_Z/2$  are ruled out by direct detection if the annihilation cross section does not match the Higgs poles conditions, as discussed for the standard case.

## 5.7 Majorana models and direct detection rates

See-saw models, including a Majorana mass term, provide naturally a mass splitting in the sneutrino mass eigenstates, diagonal in the CP basis, and introduce right handed sneutrino  $\tilde{N}$  fields with a consequent mixing between left and right handed sneutrinos. Therefore, as discussed in the case of L-number violating models, also in Majorana models the direct detection rate is suppressed from the inelasticity of the sneutrino

nucleon scattering. Thus the definition of the scattering cross section on nuclei is given by Eq. 5.29.

### 5.7.1 TeV scale Majorana mass term

In Fig 5.15 we shown the suppression factor for Germanium and Iodine as a function of the one loop contributions to the neutrino mass. In this case values of the order of  $10^{-5}$  for the suppression factors are viable even if we consider the neutrino mass bound to be 2 eV. Again the Ge nuclei show a greater suppression respect to the Iodine nuclei.

Direct detection is shown in Fig 5.16, where the sneutrino nucleon coherent scattering  $\xi\sigma_{nucleon}^{(scalar)}$  is plotted as a function of the sneutrino mass  $m_1$  and the scan is done over all the parameter space of the SUSY model, as explained in Appendix B. The blue dots refers to subdominant halo components, while the red crosses denote dominant sneutrino configurations. We clearly notice that sneutrinos may be divide in three different classes, depending on the values of  $\xi\sigma_{nucleon}^{(scalar)}$ . Configurations on the top of the plot are certainly excluded by direct detection. On the left corner light sneutrinos may not only explain the annual modulation region but appear the dominant component of dark matter. Heavy sneutrinos on the right are not compatible with the DAMA/NaI region but are acceptable if we consider the CDMS upper bounds; in this case they can be either dominant or subdominant halo dark matter components.

In Fig 5.17 we report the sneutrino nucleon scattering  $\xi\sigma_{nucleon}^{(scalar)}$  in correlation with the sneutrino relic abundance  $\Omega h^2$ : almost all the cosmologically relevant configurations are under investigation or under reach of direct detection studies. Majorana models (with a TeV scale Majorana mass) provide a more rich phenomenology compared to the LR models, where dominant sneutrinos were mainly excluded by direct detection or possess very low values of the coherent cross section of nucleon.

### 5.7.2 Large scale Majorana mass term

In Sec. 4.4.2, we have seen that large mass splitting are allowed, interesting for the inelasticity properties [106, 107, 108, 109].

In these models direct detection comes back as a very stringent bound, as we can see in Fig 5.19: almost all the sneutrino configurations are excluded. There is very marginally room only for subdominant halo components in the intermediate mass range around 100 GeV.

Fig. 5.19 shows an inverse correlation between the inelastic scattering  $\xi\sigma_{nucleon}^{(scalar)}$  and the relic abundance  $\Omega h^2$ : sneutrinos in the relevant interval of WMAP are excluded by direct detection bounds. Only a small fraction of subdominant sneutrinos may account for the annual modulation signal.

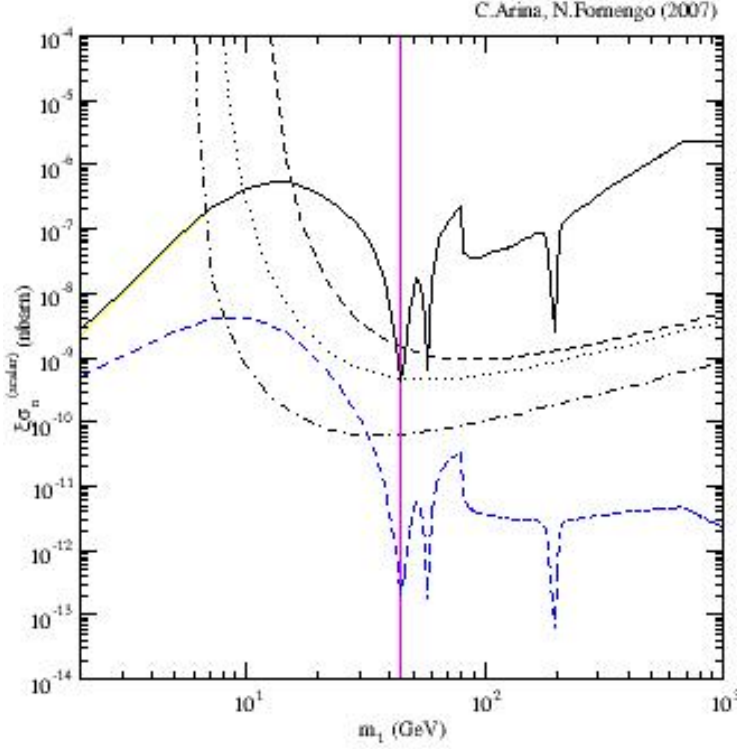


Figure 5.2: Contributions to the sneutrino nucleon cross section  $\xi \sigma_{nucleon}^{(scalar)}$  as function of the sneutrino mass  $m_1$ . The solid [black] curve denote the Z mediated t channel, while the dashed [blue] curve refers to the Higgs exchange channel. The vertical dashed line represent the Z width bound. The experimental curves which refer here to the upper limit from the CDMS experiment [143, 144, 148] (presented in the next section 5.3), as re-evaluated in Ref. [148] for three different galactic halo models which delimit the uncertainty band. The dotted line refers to the standard isothermal sphere with  $v_0 = 220 \text{ km s}^{-1}$  and  $\rho_0 = 0.3 \text{ GeV cm}^{-3}$ . The upper dashed line refers to a cored-isothermal sphere with a core radius of 5 Kpc (model B1 in Ref. [148]) and with  $v_0 = 170 \text{ km s}^{-1}$  and  $\rho_0 = 0.2 \text{ GeV cm}^{-3}$ . The lower dashed-dotted line refers to an axisymmetric density profile with a power-law potential (model C3 in Ref. [148]) with  $v_0 = 270 \text{ km s}^{-1}$  and  $\rho_0 = 1.66 \text{ GeV cm}^{-3}$ .

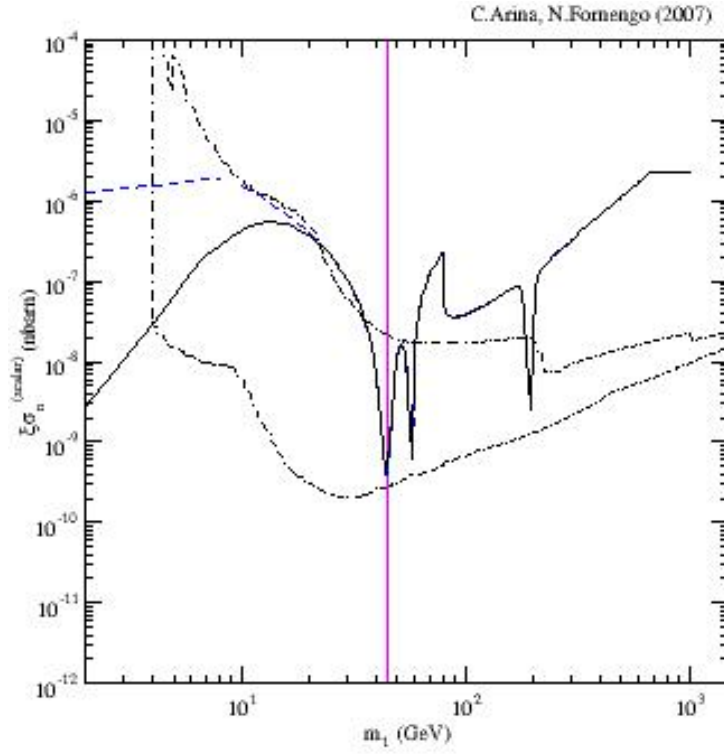


Figure 5.3: STD model – Sneutrino–nucleon scattering cross section  $\xi\sigma_{\text{nucleon}}^{(\text{scalar})}$  as a function of the sneutrino mass  $m_1$ , for the same set of parameters of Fig. 4.1. The solid (dashed) curves refer to models with (without) gaugino universality. The vertical line denotes the lower bound on the sneutrino mass coming from the invisible  $Z$ -width. The dashed-dotted curve shows the DAMA/NaI region, compatible with the annual modulation effect observed by the experiment [137, 138, 139, 140, 141].

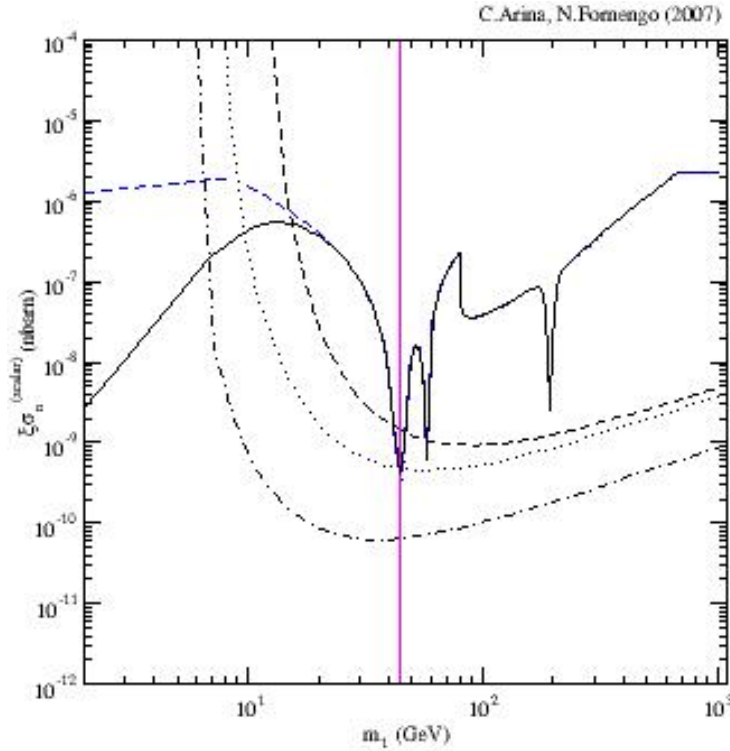


Figure 5.4: STD model – Sneutrino–nucleon scattering cross section  $\xi\sigma_{\text{nucleon}}^{(\text{scalar})}$  as a function of the sneutrino mass  $m_1$ . Notations are as in Fig. 5.3, except for the experimental curves which refer here to the upper limit from the CDMS experiment [143, 144, 148], as re-evaluated in Ref. [148] for three different galactic halo models which delimit the uncertainty band. The dotted line refers to the standard isothermal sphere with  $v_0 = 220 \text{ km s}^{-1}$  and  $\rho_0 = 0.3 \text{ GeV cm}^{-3}$ . The upper dashed line refers to a cored–isothermal sphere with a core radius of 5 Kpc (model B1 in Ref. [148]) and with  $v_0 = 170 \text{ km s}^{-1}$  and  $\rho_0 = 0.2 \text{ GeV cm}^{-3}$ . The lower dashed–dotted line refers to an axisymmetric density profile with a power–law potential (model C3 in Ref. [148]) with  $v_0 = 270 \text{ km s}^{-1}$  and  $\rho_0 = 1.66 \text{ GeV cm}^{-3}$ .

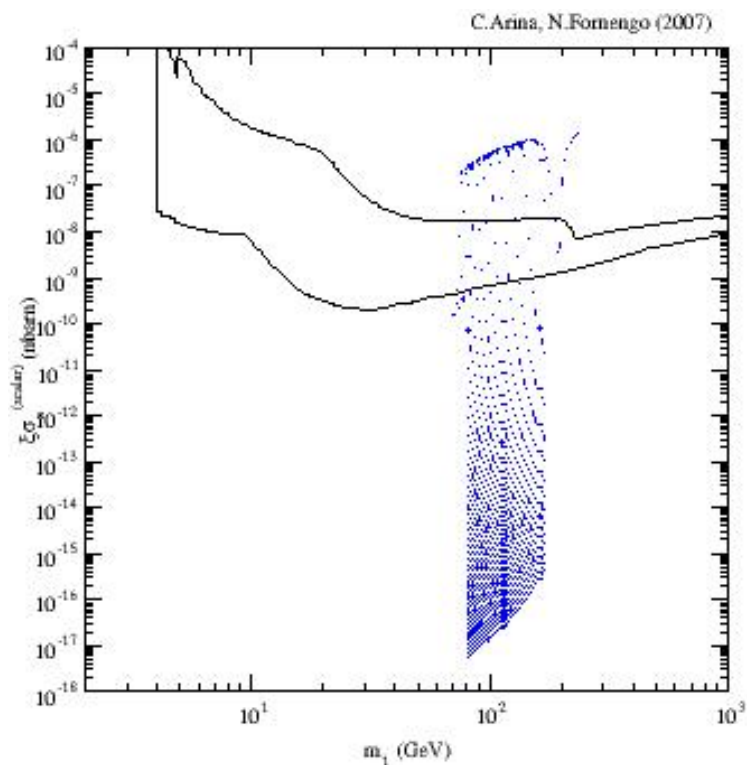


Figure 5.5: LR model – Sneutrino–nucleon scattering cross section  $\xi\sigma_{nucleon}^{(scalar)}$  as a function of the sneutrino mass  $m_1$ , for  $F^2 = 10^2 \text{ GeV}^2$  and for a scan of the soft mass parameters  $m_L$  and  $m_N$  in the ranges:  $120 \text{ GeV} < m_L < 1 \text{ TeV}$  and  $1 \text{ GeV} < m_N < 1 \text{ TeV}$ . The higgs and neutralino masses are defined as Fig. 4.1. The dot-dashed region shows the DAMA/NaI region [137, 138, 139, 140, 141], as Fig 5.3. All the configurations have a relic abundance compatible with the WMAP bound.

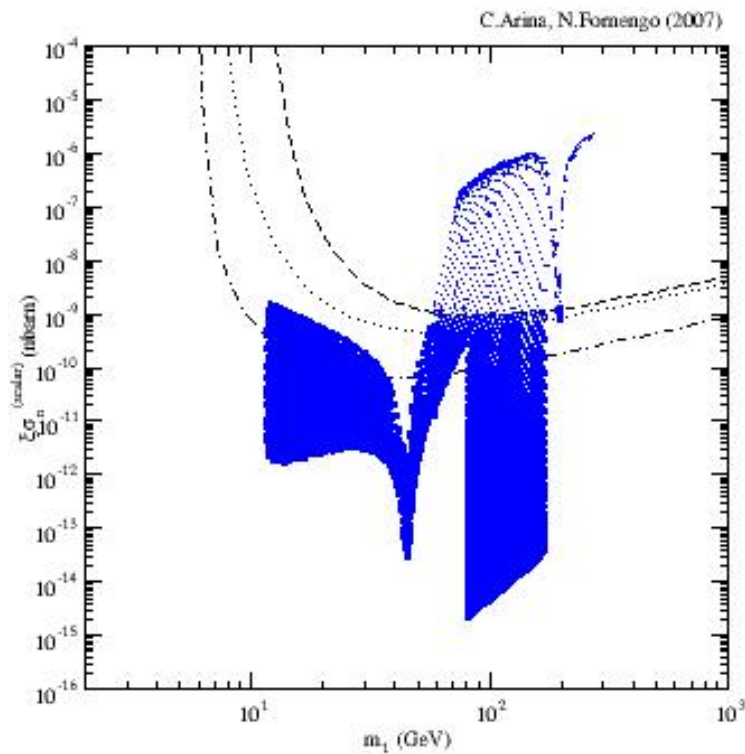


Figure 5.6: LR model – Sneutrino–nucleon scattering cross section  $\xi \sigma_{nucleon}^{(scalar)}$  as a function of the sneutrino mass  $m_1$ , for  $F^2 = 10^3 \text{ GeV}^2$  and for a scan of the soft mass parameters  $m_L$  and  $m_N$  in the ranges:  $120 \text{ GeV} < m_L < 1 \text{ TeV}$  and  $1 \text{ GeV} < m_N < 1 \text{ TeV}$ . The higgs and neutralino masses are defined as Fig. 4.1. The dashed, dotted and dot-dashed curves denote the CDMS upper bounds [143, 144, 148], as in Fig 5.4. All the configurations have a relic abundance compatible with the WMAP bound.

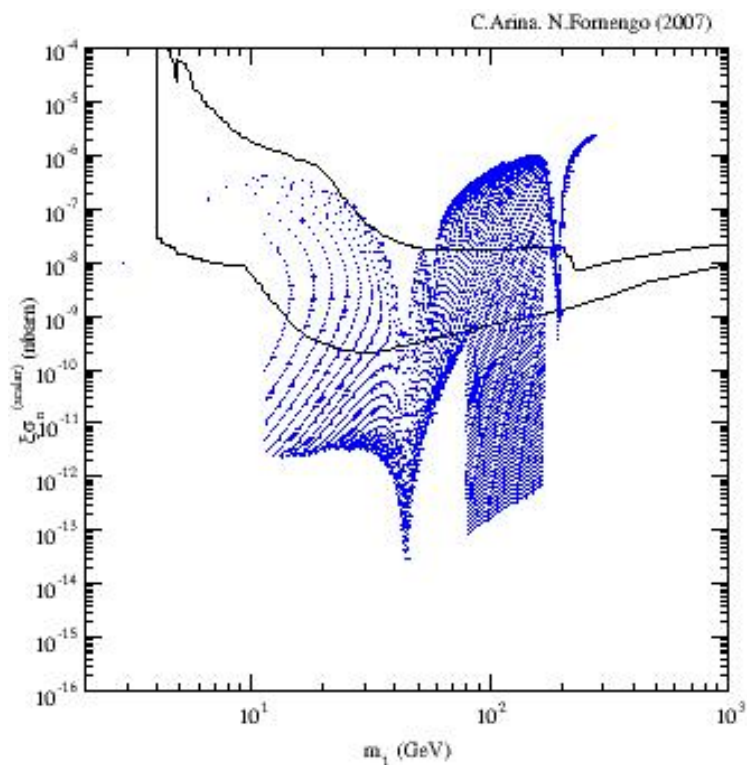


Figure 5.7: LR model – Sneutrino–nucleon scattering cross section  $\xi\sigma_{nucleon}^{(scalar)}$  as a function of the sneutrino mass  $m_1$ , for  $F^2 = 10^4 \text{ GeV}^2$  and for a scan of the soft mass parameters  $m_L$  and  $m_N$  in the ranges:  $120 \text{ GeV} < m_L < 1 \text{ TeV}$  and  $1 \text{ GeV} < m_N < 1 \text{ TeV}$ . The higgs and neutralino masses are defined as Fig. 4.1. The dot-dashed region shows the DAMA/NaI region[137, 138, 139, 140, 141], as Fig 5.3. All the configurations have a relic abundance compatible with the WMAP bound.

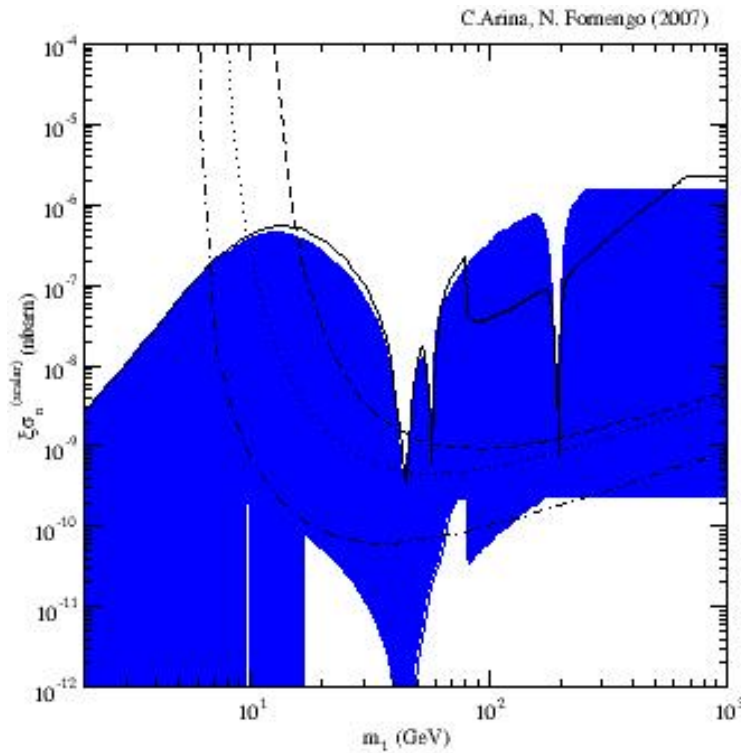


Figure 5.8: LR model – Sneutrino–nucleon scattering cross section  $\xi\sigma_{nucleon}^{(scalar)}$  as a function of the sneutrino mass  $m_1$ . The solid [black] curve denotes the standard MSSM cross section, while the band [blue] refers to all viable sneutrino configurations varying the sneutrino left–right mixing angle  $\theta$  in the range  $0.1 < \sin\theta < 1$ , for  $m_L$  fixed at 120 GeV. The higgs and neutralino masses are defined as Fig. 4.1. The dashed, dotted and dot-dashed curves denote the CDMS upper bounds [143, 144, 148], as in Fig 5.4.

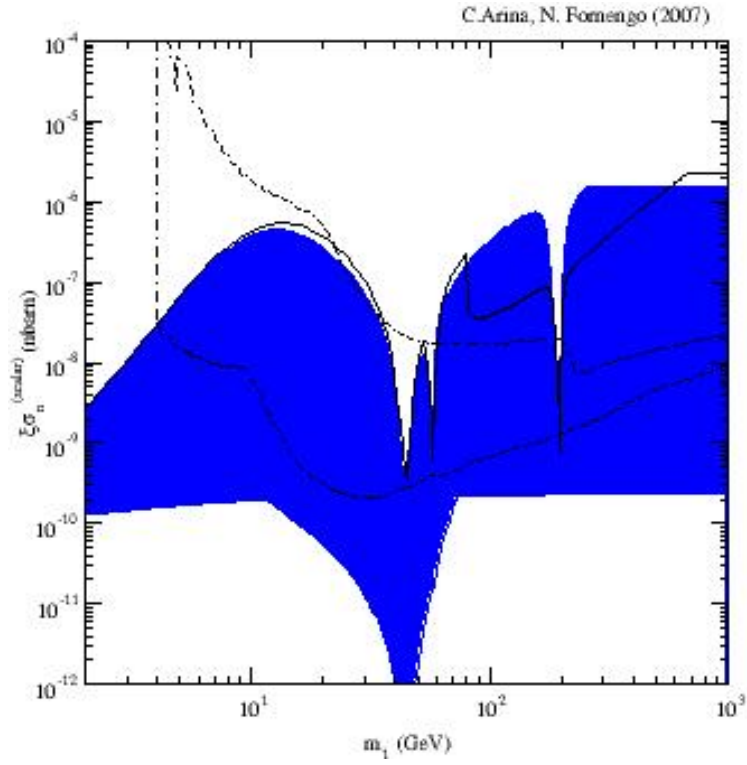


Figure 5.9: LR model – Sneutrino–nucleon scattering cross section  $\xi\sigma_{nucleon}^{(scalar)}$  as a function of the sneutrino mass  $m_1$ . The solid [black] curve denotes the standard MSSM cross section, while the band [blue] refers to all viable sneutrino configurations varying the sneutrino left–right mixing angle  $\theta$  in the range  $0.1 < \sin \theta < 1$ , for  $m_L$  fixed at 1 TeV. The higgs and neutralino masses are defined as Fig. 4.1. The dot-dashed region shows the DAMA/NaI region [137, 138, 139, 140, 141], as Fig 5.3.

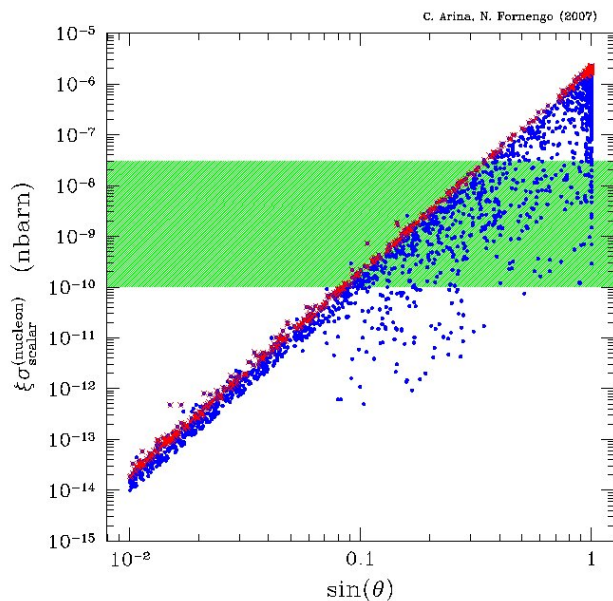


Figure 5.10: LR model – Sneutrino–nucleon cross section  $\xi\sigma_{nucleon}^{(scalar)}$  as a function of the left right mixing angle  $\sin\theta$  for a full scan in the SUSY parameter space. The sneutrino parameters are varied as follows:  $100 \text{ GeV} < m_L < 3 \text{ TeV}$ ,  $1 \text{ GeV} < m_N < 1 \text{ TeV}$  and  $1 \text{ GeV}^2 < F^2 < 10^6 \text{ GeV}^2$ . Crosses [red] refer to models with sneutrino relic abundance in the cosmologically relevant range; open circles [blue] denote sneutrino configurations cosmologically subdominant. The horizontal [green] band represents the sensitivity of the current direct detection experiments.

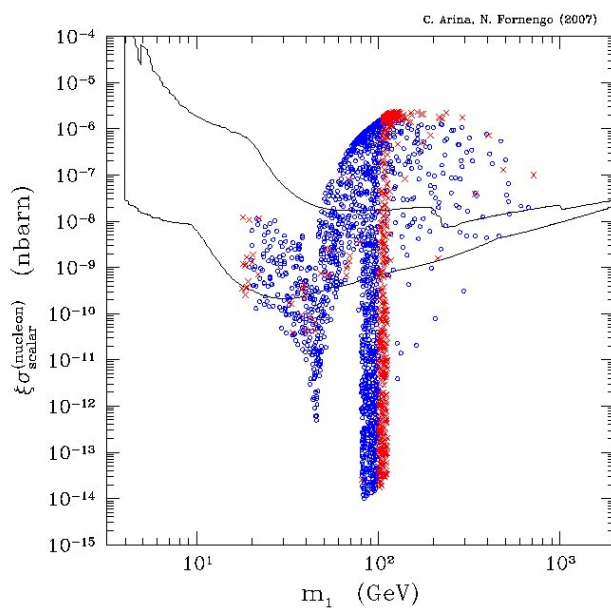


Figure 5.11: LR model – Sneutrino–nucleon cross section  $\xi\sigma_{nucleon}^{(scalar)}$  as a function of the sneutrino mass  $m_1$  for a full scan in the SUSY parameter space. The sneutrino parameters are varied as in Fig 5.10. Crosses [red] refer to models with sneutrino relic abundance in the cosmologically relevant range; open circles [blue] denote sneutrino configurations cosmologically subdominant. The dot-dashed region shows the DAMA/NaI region[137, 138, 139, 140, 141], as Fig 5.3.

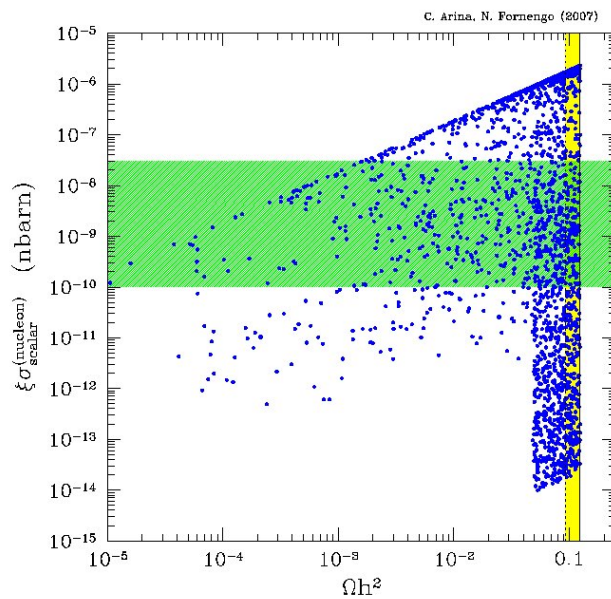


Figure 5.12: LR model – Sneutrino–nucleon cross section  $\xi\sigma_{nucleon}^{(scalar)}$  versus the sneutrino relic abundance  $\Omega h^2$  for a full scan in the SUSY parameter space. The sneutrino parameters are varied as in Fig 5.10. Crosses [red] refer to models with sneutrino relic abundance in the cosmologically relevant range; open circles [blue] denote sneutrino configurations cosmologically subdominant. The horizontal [green] band represents the sensitivity of the current direct detection experiments. The vertical [yellow] band denotes the WMAP interval for cold dark matter.

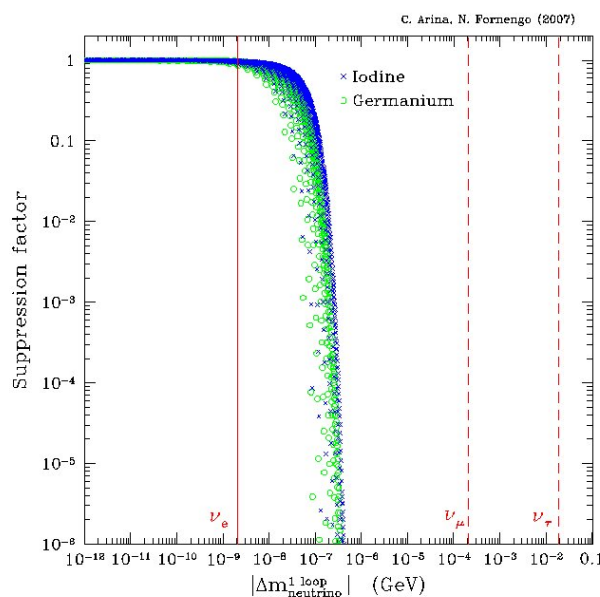
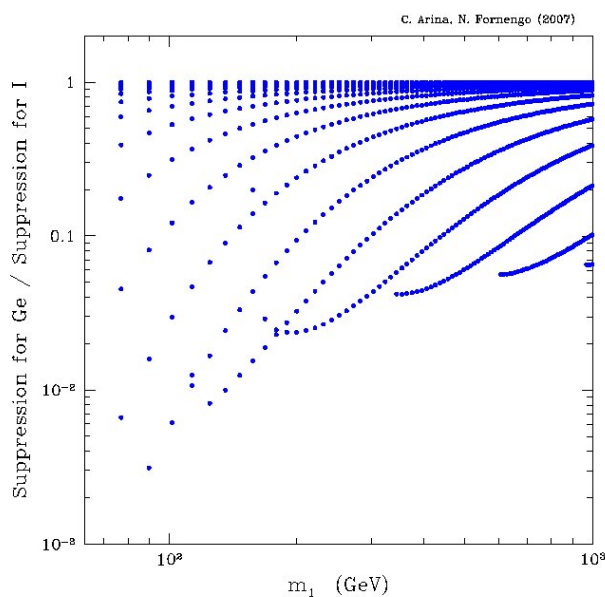


Figure 5.13:  $\mathcal{L}$  model – Upper panel: Ratio of the suppression factor for Germanium and Iodine as a function of the sneutrino mass  $m_1$ . The sneutrino mass parameters are varied in the ranges:  $10^{-4} \text{ GeV} < m_B < 10^2 \text{ GeV}$  and  $10^2 \text{ GeV} < m_L < 10^3 \text{ GeV}$ . Lower panel: Suppression factor of the direct detection rate as a function of the absolute value of the one loop contribution to the neutrino mass. The sneutrino mass parameters are varied as  $10^{-4} \text{ GeV} < m_B < 10^2 \text{ GeV}$  and  $10^2 \text{ GeV} < m_L < 10^3 \text{ GeV}$ . Crosses [blue] refer to the Iodine nucleus, open circles [green] to Germanium nucleus. The vertical lines denote the upper limit on the neutrino masses, as labelled.

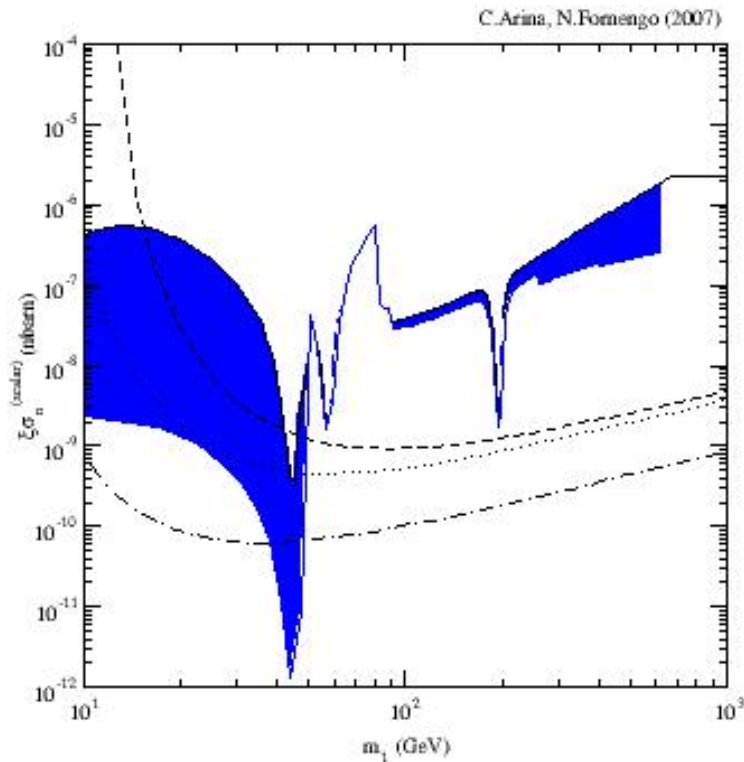


Figure 5.14:  $\mathcal{L}$  model – Sneutrino–nucleon scattering cross section  $\xi\sigma_{nucleon}^{(scalar)}$  as a function of the sneutrino mass  $m_1$ . The solid [black] curve denotes the standard MSSM cross section, while the band [blue] refers to the sneutrino–nucleon cross section for a scan of the sneutrino parameters,  $10^{-4} \text{ GeV} < m_B < 10^2 \text{ GeV}$  and  $80 \text{ GeV} < m_L < 1000 \text{ GeV}$ . The higgs and neutralino masses are defined as Fig. 4.1. The dashed, dotted and dot-dashed curves denote the CDMS upper bounds [143, 144, 148], as in Fig 5.4.

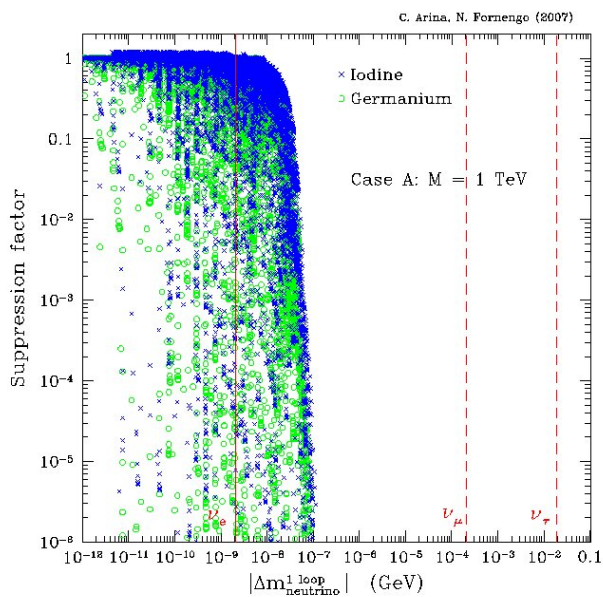


Figure 5.15: Maj[A] model – Suppression factor of the direct detection rate as a function of the absolute value of the one loop contribution to the neutrino mass for a Majorana mass parameter  $M = 1$  TeV. The sneutrino mass parameters are varied as  $1 \text{ GeV} < m_B < 10^3 \text{ GeV}$ ,  $10^2 \text{ GeV} < m_N < 10^3 \text{ GeV}$  and  $1 \text{ GeV}^2 < F^2 < 10^4 \text{ GeV}^2$ . Crosses [blue] refer to the Iodine nucleus, open circles [green] to Germanium nucleus. The vertical lines denote the upper limit on the neutrino masses, as labelled.

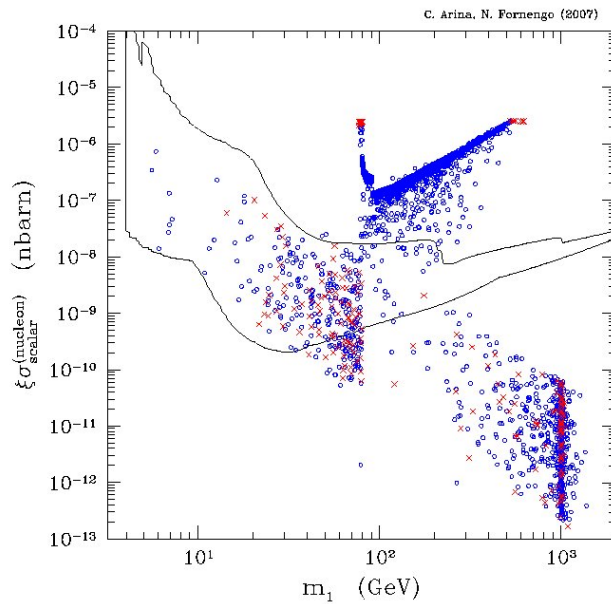


Figure 5.16: Maj[A] model – Sneutrino–nucleon cross section  $\xi\sigma_{nucleon}^{(scalar)}$  as a function of the sneutrino mass  $m_1$  for a full scan in the SUSY parameter space with a Majorana mass scale  $M = 1$  TeV. The sneutrino parameters are varied as:  $10^2 \text{ GeV} < m_N < 10^3 \text{ GeV}$ ,  $1 \text{ GeV} < m_B < 10^3 \text{ GeV}$  and  $1 \text{ GeV}^2 < F^2 < 10^4 \text{ GeV}^2$ . Crosses [red] refer to models with sneutrino relic abundance in the cosmologically relevant range; open circles [blue] denote sneutrino configurations cosmologically subdominant. The dot-dashed region shows the DAMA/NaI region[137, 138, 139, 140, 141], as Fig 5.3.

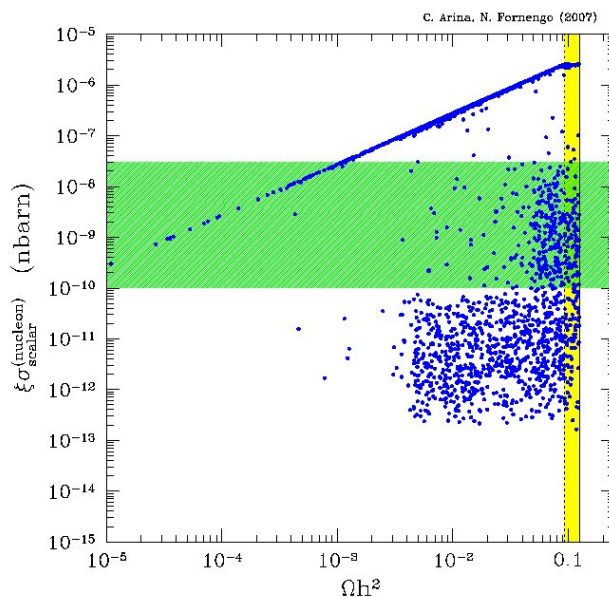


Figure 5.17: Maj[A] model – Sneutrino–nucleon cross section  $\xi\sigma_{nucleon}^{(scalar)}$  versus the sneutrino relic abundance  $\Omega h^2$  for a full scan in the SUSY parameter space with a Majorana mass scale  $M = 1$  TeV. The sneutrino parameters are varied as in Fig 5.16. Crosses [red] refer to models with sneutrino relic abundance in the cosmologically relevant range; open circles [blue] denote sneutrino configurations cosmologically subdominant. The horizontal [green] band represents the sensitivity of the current direct detection experiments. The vertical [yellow] band denotes the WMAP interval for cold dark matter.

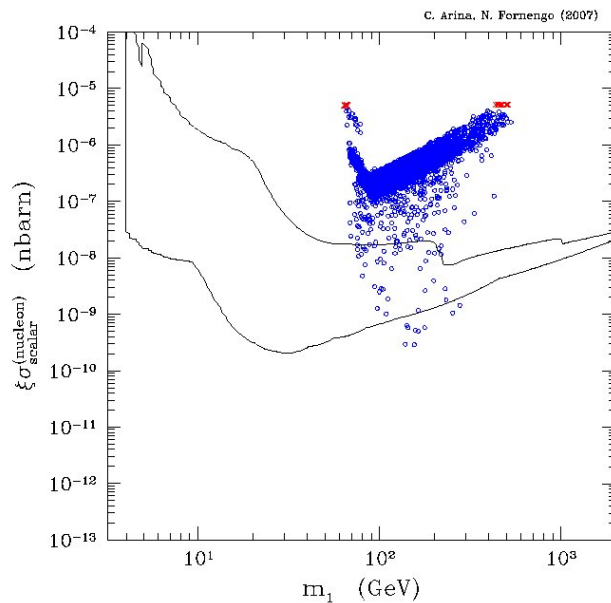


Figure 5.18: Maj[B] model – Sneutrino–nucleon cross section  $\xi\sigma_{nucleon}^{(scalar)}$  as a function of the sneutrino mass  $m_1$  for a full scan in the SUSY parameter space with a Majorana mass scale  $M = 10^9 \text{ GeV}$ . The sneutrino parameters are varied as follows:  $m_N = 0$ ,  $10^3 \text{ GeV} < m_B < 10^8 \text{ GeV}$  and  $1 \text{ GeV}^2 < F^2 < 10^4 \text{ GeV}^4$ . Crosses [red] refer to models with sneutrino relic abundance in the cosmologically relevant range; open circles [blue] denote sneutrino configurations cosmologically subdominant. The dot-dashed region shows the DAMA/NaI region[137, 138, 139, 140, 141], as Fig 5.3.

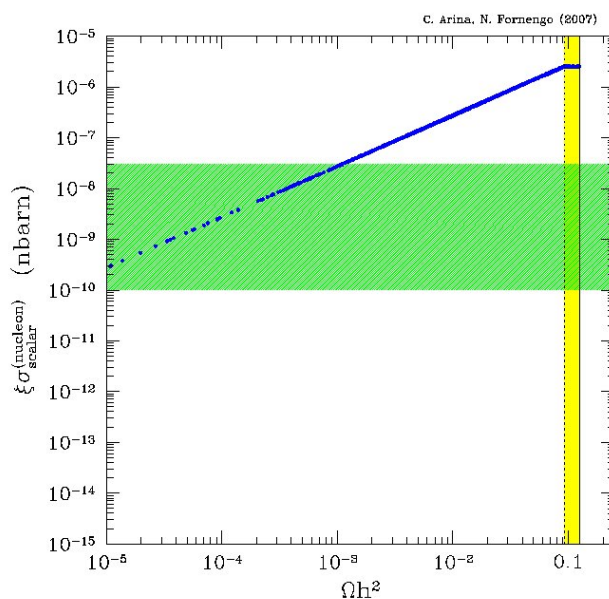


Figure 5.19: Maj[B] model – Sneutrino–nucleon cross section  $\xi\sigma_{nucleon}^{(scalar)}$  versus the sneutrino relic abundance  $\Omega h^2$  for a full scan in the SUSY parameter space with a Majorana mass scale  $M = 10^9$  GeV. The sneutrino parameters are varied as in Fig 5.18. Crosses [red] refer to models with sneutrino relic abundance in the cosmologically relevant range; open circles [blue] denote sneutrino configurations cosmologically subdominant. The horizontal [green] band represents the sensitivity of the current direct detection experiments. The vertical [yellow] band denotes the WMAP interval for cold dark matter.

# Chapter 6

## Sneutrino in the light of indirect dark matter searches

Dark matter particles are distributed in the Galactic halo and may annihilate in pairs producing a bunch of possible signals. Among these signals, antimatter, in particular antiprotons and antideuterons, and gamma rays may be produced. During the process of formation of the solar system, dark matter particles could be captured by gravitational attraction into heavy bodies, like the Sun and the Earth and there annihilate. The only annihilation products which can escape are neutrinos. The energy scale of the annihilation products is determined by the mass of the dark matter particles.

In the following sections we briefly summarize the main features of the antimatter, gamma rays and neutrino fluxes originating from dark matter annihilation. In Section 6.4 we discuss the theoretical expected indirect signals from sneutrino interactions in our Galaxy, in the minimal and extended supersymmetric scenarios of Chapter 4.

### 6.1 Antiproton and antideuterium signals

In general antimatter production is expected from dark matter particles annihilation in our Galaxy: positrons  $e^+$ , antiprotons  $\bar{p}$  and antideuterons  $\bar{D}$  are produced. In this Section we will consider the two latter type of antiparticles. Referring to antiprotons, many data have been collected by BESS [149, 150] and will be soon improved by the large statistics provided by the PAMELA satellite [151] and by the AMS [152] collaboration on board of the ISS. The  $\bar{D}$  signal is very weak, therefore antideuterium nuclei have not yet be found by the balloon experiment BESS, but more promising searches will be offered once more by AMS and by the GAPS [153, 154] spectrometers.

Secondary antiprotons are naturally produced by spallation of primary nuclei, mostly cosmic ray protons and helions, on the diffuse gas of the Milky Way ridge. If sneutrinos pervade our Galaxy a primary component adds up to that secondary distribution. The spectral distortion that ensues is expected a priori in the low energy region for mere kinematic reasons: unlike for a sneutrino annihilation, the center of mass frame for

spallation event is not at rest with respect to the Galaxy. In principle an excess of low energy antiprotons is a signature of an unconventional production, such as sneutrino annihilation.

The antiproton production differential rate [155] per unit volume and time is a function of space coordinates ( $r, z$  defined in the Galactic rest frame) and of antiproton kinetic energy  $T_{\bar{p}}$ :

$$q_{\bar{p}}^{\text{SUSY}}(r, z, T_{\bar{p}}) = \frac{1}{2} \langle \sigma v \rangle_0 g(T_{\bar{p}}) \left( \frac{\rho_{\tilde{\nu}}(r, z)}{m_{DM}} \right)^2 \quad (6.1)$$

where  $\langle \sigma v \rangle_0$ , defined in Eq. 2.54, denotes the average over the Galactic velocity distributions of the dark matter particle (which are highly non relativistic since their average velocity is of the order of  $\beta \sim 10^{-3}$ ) annihilation cross section and  $\rho_{\tilde{\nu}}(r, z)$  denotes the sneutrino density distribution, which is assumed to be proportional to the total dark matter density distribution as  $\rho_{\tilde{\nu}}(r, z) = \xi \rho_{DM}(r, z)$  (with  $\xi$  defined in Eq. 5.23), in order to take into account both dominant and subdominant sneutrino relics. Finally the second term in Eq. 6.1, denotes the antiproton differential spectrum per annihilation event:

$$g(T_{\bar{p}}) = \frac{1}{\sigma_{ann}} \frac{d\sigma_{ann}(\tilde{\nu}\tilde{\nu} \rightarrow \bar{p} + X)}{dT_{\bar{p}}} = \sum_f BR_f \left( \frac{dN_{\bar{p}}^f}{dT_{\bar{p}}} \right) \quad (6.2)$$

where  $f$  lists all the sneutrino annihilation final state particles which can subsequently produce antiprotons with a branching ratio  $BR_f$  and  $\frac{dN_{\bar{p}}^f}{dT_{\bar{p}}}$  denotes the differential energy distribution of the antiprotons generated by  $f$ . The production and decay chain of each final state follows semi-analytic calculations, until a quark is produced [155]. We use detailed fits and interpolations over the results of PYTHIA [156] simulations for the treatment of the processes involved in the quark hadronization and the subsequent hadron decays.

The source term  $q_{\bar{p}}^{\text{SUSY}}(r, z, T_{\bar{p}})$  is therefore a combination of astrophysical factors and of particle physics properties (the sneutrino self annihilation cross section and the hadronization into antiprotons of the annihilation products), and can be factored out.

Once the  $\bar{p}$  are produced they diffuse throughout the Galaxy: the propagation is affected by many physical processes, such as diffusion, scattering, energy losses, annihilation and reacceleration. The antiproton source spectra are therefore propagated in the galactic environment to determine the antiproton flux at the local position in the Galaxy  $\Phi(R_{\odot}, 0, T_{\bar{p}})$ :

$$q_{\bar{p}}^{\text{SUSY}}(r, z, T_{\bar{p}}) \longrightarrow \Phi^{\text{IS}}(R_{\odot}, 0, T_{\bar{p}}) \quad (6.3)$$

The propagation of cosmic rays antiprotons has been considered in the framework of a two-zone diffusion model, which has been described at length in Refs. [155]. We notice that the antiproton signal does not depend strongly on the critical behavior of the dark matter density profiles [155]; therefore respect to an isothermal cored profile a NFW density distribution produces fluxes which are only 20% higher. The main uncertainty,

relevant for the antiproton signals, comes from the lack of knowledge of the shape of the diffusion zone and which affects the propagation parameters. The diffusion model has five free parameters  $\delta$ ,  $K_0$ ,  $L$ ,  $V_c$  and  $V_A$ . The disk of the Galaxy is described as a thin disk of radius  $R = 20$  Kpc, which contains the interstellar gas and is embedded in a thicker diffusive halo, supposed to have a cylindrical shape with the same radius  $R$  as the disk and height  $L$  which is not well known. The matter density is much lower in the diffusion halo so that spallation of the charged nuclei occur only in the disk. Moreover the standard sources also happen to be located in the disk. The spatial diffusion of cosmic rays is assumed to occur uniformly in the whole (disk and halo) diffusion volume, with the same strength. The corresponding diffusion coefficient has been defined as  $K(E) = k_0 \beta (\mathcal{R}/1\text{GV})^\delta$ , where  $\mathcal{R}$  stands for the particle rigidity and  $K_0$  and  $\delta$  are free parameters of the model. We also consider the possibility that a Galactic wind blows the particles away from the disk in the  $z$  vertical direction, with a constant speed  $V_c$ . It induces an adiabatic dilution of the energy of the particles in the disk due to the sudden change in  $V_c$ . One of the processes that modify the antiproton energy distribution is a minimal reacceleration on random hydrodynamics waves, i.e. diffusion in momentum space. This process is assumed to occur only in the disk and is related to the velocity of disturbances in the hydrodynamical plasma  $V_A$ , called Alfvén velocity. The sets of diffusion parameters are constrained by analysing stable nuclei (mainly by fitting the boron to carbon ratio  $B/C$ ). The predictions for secondary antiprotons in this thesis are done using the astrophysical parameters reported in [155]:  $\delta = 0.70$ ,  $K_0 = 0.0112 \text{ kpc}^2/\text{Myr}$ ,  $L = 4 \text{ Kpc}$ ,  $V_c = 12 \text{ km/s}$  and  $V_A = 52.9 \text{ km/s}$  provide the median supersymmetric antiproton flux, while  $\delta = 0.46$ ,  $K_0 = 0.0765 \text{ kpc}^2/\text{Myr}$ ,  $L = 15 \text{ Kpc}$ ,  $V_c = 5 \text{ km/s}$  and  $V_A = 117.6$  lead to the maximal antiproton signal.

The fluxes we obtain after propagation are the interstellar fluxes of antiprotons at the Sun's position in the Galaxy. We have to further propagate them inside the heliosphere where the cosmic ray particles which eventually reach the Earth are affected by the presence of the solar wind; the top-of-atmosphere (TOA) antiproton flux  $\Phi_{\bar{p}}^{\text{TOA}}$  is obtained as in Ref. [155]. The solar modulation has the effect of depleting the low energy tail of the antiproton flux. The effect is clearly more pronounced for periods of strong solar activity, when the solar wind is stronger. In our analysis we have considered the minimum of the solar activity.

We mentioned before that an excess of antiprotons is in principle expected in the low energy tail of the antiproton spectrum, since sneutrinos are highly non relativistic in the Galaxy and therefore annihilate almost at rest. However because secondary antiprotons undergo inelastic yet non annihilating collisions in the interstellar medium, the high energy particles tend to lose energy and to populate the low energy tail of the spectrum that consequently is much flatter than previously estimated. This motivates the search of other cosmic ray signatures such as antideuterium  $\bar{D}$  [157]. The nuclei of antideuterium are less sensitive to such problems. As for the antiprotons, light antinuclei result from the interaction of high-energy cosmic-ray protons with the interstellar gas of the Milky Way disk. They form when an antiproton and an antineutron merge. The two antinucleons must be at rest with respect to each other in order that fusion takes place successfully.

For kinematic reasons, spallation reactions create very few low-energy particles. Low-energy secondary  $\bar{D}$  are even further suppressed. Energy loss mechanisms are also less efficient in shifting the antideuteron energy spectrum towards low energies. On the other hand, supersymmetric antideuteron nuclei are manufactured at rest with respect to the Galaxy. In sneutrino annihilations, antinucleons are predominantly produced with low energies. This feature is further enhanced by their subsequent fusion into antideuterons, hence a fairly flat spectrum arises [157]. Below a kinetic energy per nucleon of  $T_{\bar{D}} = 1 - 3 \text{ GeV}/n$ , secondary antideuterons are quite suppressed with respect to their supersymmetric partners. That low-energy suppression is orders of magnitude more effective for  $\bar{D}$  than for  $\bar{p}$ , but antideuteron fluxes are quite small with respect to antiproton fluxes. The production of antideuterons is more involved than antiprotons production, the calculation of the probability for the formation of an antideuteron can proceed in two steps [157]. We first need to estimate the probability for the creation of an antiproton-antineutron pair. Then, those antinucleons merge to yield an antinucleus of deuterium. The  $\bar{D}$  propagation and the T.O.A. flux are evaluated in Ref. [157].

## 6.2 Gamma rays

Dark matter would be not so dark after all, since  $\tilde{\nu} - \tilde{\nu}$  annihilation in the galaxies is expected to lead, among other final states previously described, to a  $\gamma$ 's signal which could in principle be detected above known backgrounds. Moreover the  $\gamma$  do not interact with the galactic magnetic field, therefore they trace the source. Since the dark matter annihilation rate is proportional to the square of its density, a signal enhancement is expected in high density regions like the center of our Galaxy. Such gamma rays might be identified by forthcoming or just operating atmospheric Cerenkov telescope such as MAGIC [158], HESS [159] or satellite detectors like EGRET [160, 161] and GLAST [162].

The diffuse photon flux from dark matter annihilation in the galactic halo, coming from a given direction in the sky defined by an angle of view  $\psi$  from the galactic center, and observed by a detector with angular resolution  $\theta$  can be written as [163]:

$$\frac{d\Phi_{\gamma}}{dE_{\gamma}}(E_{\gamma}, \psi, \theta) = \frac{d\Phi^{\text{SUSY}}}{dE_{\gamma}}(E_{\gamma}) \times \Phi(\psi, \theta) \quad (6.4)$$

The energy dependence in the  $\gamma$  differential flux, is given by the annihilation spectrum:

$$\frac{d\Phi^{\text{SUSY}}}{dE_{\gamma}}(E_{\gamma}) = \frac{1}{4\pi} \frac{\langle \sigma_{ann} v \rangle_0}{2m_{DM}^2} \sum_f \frac{dN_{\gamma}^f}{dE_{\gamma}} BR_f \quad (6.5)$$

where, once again,  $\langle \sigma_{ann} v \rangle_0$  is the dark matter self-annihilation cross section times the relative velocity of the two annihilating particles,  $\frac{dN_{\gamma}^f}{dE_{\gamma}}$  is the differential photon spectrum for a given  $f$  annihilation final state with branching ratio  $BR_f$ . The geometry dependence for the diffuse emission of our Galaxy is given by the line-of-sight integral:

$$\Phi(\psi, \theta) = \int_{\Delta\Omega(\psi, \theta)} d\Omega' \int_{l.o.s.} \rho_{DM}^2(r(\lambda, \psi')) d\lambda(r, \psi') \quad (6.6)$$

where  $r$  is the galactocentric distance, related to the distance  $\lambda$  from us by the relation  $r = \sqrt{\lambda^2 + R_\odot^2 - 2\lambda R_\odot \cos \psi}$  and  $\Delta\Omega(\psi, \theta)$  is the solid angle of observation pointing in the direction of observation  $\psi$  and for angular resolution of the detector  $\theta$ . Notice that Eq. 6.4 is factorized into two distinct terms: a cosmological factor  $\Phi$  which takes into account the geometrical distribution of DM in the galaxy and a supersymmetric factor  $\Phi^{\text{SUSY}}$  which contains the information about the nature of dark matter.

Assessing the size of such signals depends on many uncertain aspects of both astrophysics, related to  $\Phi$ , and particle physics, related to  $\Phi^{\text{SUSY}}$ . For instance the central structure of the DM halo is far from being well determined, as mentioned in Sec. 1.2 and this can lead to uncertainties on the calculation of expected gamma rates spanning several orders of magnitude. A sensitive issue is the presence of substructures in galactic halos, which can change predictions as compared to a smooth mass distribution. Also important and rather unknown are effects of baryons on the inner part of galaxies, as described in Sec. 1.2 taking into account baryon dissipation processes, that may enhance the gamma ray signals. This in general holds for gamma rays coming from the galactic center, while  $\gamma$  rays coming from large galactic latitudes, if substructures are not taken into account, are less strongly dependent on the halo density profile. We will comment further these uncertainties in the discussion of the theoretical predictions for sneutrinos, together with the choice of the dark matter density model for the galactic halo.

The diffuse photon spectrum is contained into the supersymmetric factor  $\Phi^{\text{SUSY}}$  and originates from the production of fermions, gauge bosons, Higgs bosons and gluons. Both gauge bosons and Higgs bosons eventually decay into fermions. The hadronization of quarks and gluons, in addition to radiative processes, can produce gamma rays. The main channel of  $\gamma$  rays production goes through the production and subsequent decay of neutral pions,  $\tilde{\nu}\tilde{\nu} \rightarrow q\bar{q} \rightarrow [\text{fragmentation}] \rightarrow \pi^0 \rightarrow 2\gamma$ . Sneutrino annihilation into lepton pairs can also produce gamma ray from electromagnetic showering of the final state leptons. In the case of the  $\tau$  lepton production, their semihadronic decays also produce neutral pions, which further contribute to the  $\gamma$  rays flux. We have evaluated the diffuse photon spectrum originating from hadronization and radiative processes by means of a Monte Carlo simulation with the PYTHIA package [156].

## 6.3 Neutrino flux

Among the indirect methods for searches of DM, a promising signal consists in neutrinos with energy  $E_\nu \lesssim m_{\text{DM}}$  produced by annihilations of dark matter particles accumulated in the core of the Earth and of the Sun looked for by large neutrino telescopes. MACRO [164], SuperKamiokande [165] and AMANDA [166] already obtained constraints on such neutrino fluxes, while experiments that are under construction, like ANTARES [167] and ICECUBE [168], or that are planned, like NEMO [169] will offer improved sensitivities.

A flux of neutrinos is produced inside the Earth or the Sun as a consequence of annihilation of dark matter particles which have been gravitationally captured inside

these celestial bodies [170, 171, 172]. The differential neutrino flux is given by [173]:

$$\frac{dN_\nu}{dE_\nu} = \frac{\Gamma_{ann}}{4\pi d^2} \sum_f BR_f \frac{dN_f}{dE} \quad (6.7)$$

where  $f$  runs over the different final states of the DM annihilations with branching ratios  $BR_f$ ,  $d$  is the distance of the neutrino source from the detector (e.g. the Earth radius) and  $dN_f/dE$  is the differential distribution of the neutrinos generated by the hadronization of quarks and gluons and the subsequent hadronic semileptonic decays and by the tau decays. The dark matter particles are highly non relativistic, therefore their annihilations occur almost at rest and the main phenomenological parameters that determine the neutrino spectra are the DM mass, the annihilation rates and the branching ratios of the basic channels into which the DM particles annihilate:  $q\bar{q}, \ell\bar{\ell}, \nu\bar{\nu}, W^+W^-, ZZ$  and Higgs particles and mixed gauge bosons Higgs final states. For sneutrinos in the presented supersymmetric models the  $\nu\nu$  channels are due to  $t$  channel neutralino and chargino exchange, and as discussed before are very efficient.

The annihilation rate  $\Gamma_{ann}$  depends on the rate of captured particles and therefore linearly on the dark matter nucleus scattering cross section  $\xi\sigma_{\mathcal{N}}^{(scalar)}$  and on the local dark matter density  $\rho_\odot$ .

Also the neutrino flux suffers from astrophysical uncertainties, mainly due to the poor knowledge of the local dark matter density and of the local dark matter velocity distribution function. The local density plays a role in the setup of capture and annihilation equilibrium in the Earth, while the velocity distribution affects mainly the capture process: capture is driven by the relation between the DM velocity and the escape velocity of capturing body.

Neutrinos escape from the center of the Earth and of the Sun passing through matter and regions at different densities. Therefore the propagation affects the flavor and the energy spectra of the neutrinos [173]. Referring to the Earth, the main distortion effect is due to neutrino oscillations with a length comparable to the radius of the Earth,  $R_\oplus$ .

Neutrinos may produce up-going muons  $\mu^\pm$  generated by the scattering with the rock below the detector and that run across the detector. This is traduced into a clear signature in the neutrino telescope, since the atmospheric background can be suppressed exploiting directionality. The muon flux at the detector depends on the neutrino energy spectrum and spatial distribution, the differential  $\nu - \mathcal{N}$  charged current cross section for the muon production and the energy losses and the multiple scattering of the muon in the rock or water surrounding the detector.

## 6.4 Sneutrino in supersymmetric models and indirect detection signals

In this Section we will present the expected signals from sneutrino annihilation into gamma rays and antimatter in the galactic halo and predicted neutrino fluxes from the

center of the Earth. We will consider only the SUSY models more relevant for the sneutrino cosmological properties, namely LR models and Majorana models (as defined in Chapter 4, we recall that Maj[A] models refer to a Majorana mass at the TeV scale, while Maj[B] models denote a Majorana mass at the scale  $10^9$  GeV). Indeed these models provide sneutrinos as good dark matter components and with direct detection signals compatible with the current experimental bounds. Thus it is interesting to go further in a deep investigation and study the possible indirect annihilation signals.

We will not discuss the standard MSSM and the  $\tilde{L}$  models, since the expected signals do not differ from the Maj[B] case and do not provide interesting results.

### 6.4.1 Indirect detection rates in right-handed models

Let us start with the theoretical prediction for antiproton fluxes in LR supersymmetric models, from mixed sneutrino annihilation in the galactic halo. In Fig. 6.1 the antiproton fluxes are evaluated at the kinetic energy of the antiproton of  $T_{\bar{p}} = 0.23$  GeV, while in Fig 6.2 at  $T_{\bar{p}} = 37.5$  GeV. In the plots only the cosmologically viable configurations are shown: the crosses [red] refer to dominant dark matter sneutrino, while the dots [blue] denote subdominant sneutrinos. The grey points refer to configurations which are excluded by direct detection searches. In Fig 6.1 the antiproton fluxes have been evaluated in a low energy bin, where the antiproton signals have a better chance to be disentangled by the background produced by the spallation of cosmic rays over the galactic medium. The yellow shaded area denotes the amount of the exotic antiprotons which can be accommodated in the BESS data in that energy bin. This has been established on the basis of the theoretical calculation of the antiproton background [174] and on BESS measurements, by determining the maximal amount of exotic antiproton flux which can be accommodated on the top of the background, without entering in conflict with the BESS data and its experimental error, at 90% C.L. Notice that none of the sneutrino configurations, in the mass range from 30 GeV up to 200 GeV, are excluded by the BESS data but are one order of magnitude below the current experimental sensitivities. A change in the parameters which enter in the diffusion equation can lead to an increase of about a factor of 8 or a decrease of up to a factor 10 in the predicted fluxes [155]. Therefore our predictions may be altered by these factors depending on the choice of the parameters in their allowed ranges [175]. In the case of the choice of astrophysical parameters which produce the maximal antiproton signal, the scatter plot in Fig. 6.1 would be enhanced by a factor of 8, therefore still BESS data would not exclude any sneutrino configuration. These will be detectable with just a small increase in the experimental sensitivity.

Prospects for the future are shown by the dashed and dotted horizontal lines, which denote our estimated sensitivity of the PAMELA [151] (dashed line) and AMS [152] (dotted line) detectors to exotic antiprotons after a run of 3 years: the sensitivities are determined as admissible excess within the statistical experimental uncertainty if the measured antiproton flux consists only in the background (secondary) component. The estimate has been performed by using the background calculation of Ref. [174], and refers

to a  $1\text{-}\sigma$  statistical uncertainty. All the supersymmetric configurations in Fig. 6.1 above the dashed or dotted lines can be potentially identified by PAMELA or AMS as a signal over the secondaries, while those which are below the dashed or dotted lines will not contribute enough to the total flux in order to be disentangled from the background. We therefore see that, in the case of the median antiproton flux, namely a median choice of the parameters of the two-zone diffusion model, shown in the Figure, only AMS will have the possibility to detect a signal from sneutrino dark matter, for masses around 60 GeV or for masses in the range 100–200 GeV. We notice that most of these configurations refer to subdominant sneutrinos: this justifies the approach to consider relic particle candidates also when they are not dominant dark matter components, since a signal from relic particles in the galaxy may well be discovered. In the case of astrophysical propagation parameters close to the values which provide the maximal antiproton signal, both PAMELA and AMS will have good chances to detect sneutrinos with masses in the range 50 – 200 GeV.

Notice that in a mass range of 65–130 GeV a large fraction of configurations, potentially detectable by AMS, are excluded by the direct detection upper bounds. This shows a nice interplay between different dark matter searches techniques. In Fig. 6.3 we plot the antiproton flux against the direct detection cross section  $\xi\sigma_{nucleon}^{(scalar)}$ , as well as the foreseen capabilities of PAMELA and AMS together with the current direct detection sensitivity region. Notice that a fraction of the configurations which are excluded by direct searches would be reached by PAMELA and AMS sensitivities. Direct detection and antiproton searches offer a good deal of complementarity: direct detection is sensible to configurations which provide very low antiproton signals and viceversa.

From these figures it appears to be not only a stronger probe to sneutrino dark matter but also a good chance of antiproton detection.

We come back to Fig 6.2: the antiproton flux is evaluated at an higher energy, at which CAPRICE [176] reports the detection of a flux potentially in excess of the theoretical background. The band refers to a signal which would fill the CAPRICE excess. At this energy bin sneutrino signals are not able to reach the level of the CAPRICE excess for a median choice of the propagation parameters. In the case of a maximal antiproton signal, namely a signal produced with the set of diffusion parameters which enhance the antiproton flux, a marginal compatibility would arise, for sneutrino in the mass range from 200 to 500 GeV. The dashed and dotted lines denote the sensitivities of PAMELA and AMS respectively: for a median choice of astrophysical parameters only AMS will potentially be able to investigate a small fraction of sneutrino configurations, while for a maximal choice both AMS and PAMELA will probe configurations in the mass range of 200–500 GeV. Light sneutrinos are not probed at this antiproton energies: they can not produce antiprotons at energies above their mass, since annihilations occur almost at rest.

In Fig 6.4 we show the predicted antideutrium fluxes at the kinetic energy per nucleon of  $T_{\bar{D}} = 0.23 \text{ GeV}/n$ . The dashed and dotted lines refer to the expected sensitivities of GAPS and AMS, evaluated as described previously for the antiproton flux. The  $\bar{D}$  produced by sneutrino annihilation provide fluxes which are below the current

experimental sensitivities, but are of the same order of the ones of the future experiments. We see that antideuteron searches will offer a sensitivity to sneutrino dark matter comparable to the antiproton searches. A signal detectable in one channel by two different detectors, will be detectable also in the other channels, again in two different experiments. Moreover, one of the detector, AMS, has the capabilities to detect a signal in both channels. The possibility to cross correlate different signals and to complement their information would be an extraordinary opportunity for dark matter searches. This is further complemented by direct detection: the light grey points, near the AMS sensitivity, are configurations discarded by direct searches. The signals are below the current experiment sensitivities.

Also the gamma ray signal provides good configuration for left-right handed mixed sneutrinos. In Fig. 6.5 we show the expected  $\gamma$  flux at  $E_\gamma = 1.5$  GeV coming from the center of the Galaxy in an angular bin which corresponds to the EGRET [160, 161] field of view. The choice of the energy bin refers to the case where EGRET detects an excess of gamma rays over the background from the galactic center. The yellow shaded area refers to this excess: exotic gamma rays into the yellow band are compatible with the EGRET data and those close to the solid horizontal line are able to explain the excess.

As noticed in Sec. 6.2, the geometry of the sneutrino distribution in the Universe strongly affects the gamma ray signals. In Fig. 6.5 we have used the Moore *et al.* [21, 19] strongly peaked profile ( $r^{-1.5}$ ), see Tab. 1.1. For a NFW profile behavior of  $r^{-1}$  [18], Tab. 1.1, the sneutrino predicted gamma ray flux would decrease by a factor of 60 and an additional factor of 10 for cored profile [163]. However for a  $r^{-1.5}$  profile, which are typical also for baryon dissipation effect [27, 28] in the galaxy and/or are due to the growth of a black hole [23, 24, 25, 26], sneutrino dark matter is at the level of explaining the EGRET excess, in a range mass from 65 up to 250 GeV. Clearly the cored profiles lead to a very low gamma flux and therefore are not able to fill the EGRET excess.

In Fig 6.5 we show our estimate for the capabilities of GLAST, for one year data taking. We have taken into account the GLAST effective area as in Ref. [162] and we have derived our predictions for the same angular energy bin of EGRET. Notice that GLAST will be sensitive to sneutrino configurations of masses between 30 GeV and 600 GeV, and will be close to detect also very light sneutrinos with further live time of data. Again for milder profiles, the sensitivity of GLAST will be reduced to a small range of masses (60-300 GeV) but nevertheless some configurations are still viable. We comment also that the angular resolution of GLAST will be much better than the EGRET one and therefore the capabilities of GLAST would be even more promising than the predicted ones in Fig. 6.5.

Let us now turn to the possible neutrino flux produced from annihilation of sneutrinos trapped by gravitational capture in the center of the Earth. In Fig. 6.6 we show the prediction for the flux of upgoing muons from the Earth as a function of the sneutrino mass  $m_1$ . The results are compared with the upper bound of Superkamiokande, MACRO and AMANDA. Notice that neutrino telescopes are sensitive to many viable sneutrino dominant and subdominant configurations, in particular for sneutrino in the mass range from 50 GeV up to 100 GeV. In Fig. 6.7 we have reported the upgoing muon flux with

the sneutrino nucleon scattering cross section  $\xi\sigma_{nucleon}^{(scalar)}$ : we see that the two signals are strongly correlated, as mentioned previously. Neutrino detectors upper bounds exclude regions which are mainly discarded already by direct detection searches.

### 6.4.2 Majorana models and indirect detection rates

In Fig 6.8 it is shown the antiproton flux at the antiproton kinetic energy  $T_{\bar{p}} = 0.23$  GeV for Maj[A] sneutrino models. Contrary to the LR models, here some configurations are excluded by the BESS data. Moreover configurations excluded by direct searches would have produced very low antiproton signals, practically undetectable by AMS and PAMELA. Also in these models, antiproton searches and direct detection experiments denote a high level of complementarity, both in the ability to exclude model configurations and in the prospects of detection. This is clearly summarized in Fig. 6.9 where the antiproton fluxes are correlated with the sneutrino nucleon scattering cross section. Notice that a fraction of configurations which are currently under study by direct detection experiments (either just inside the CDMS sensitivity range or inside the DAMA/NaI annual modulation region) have a chance of detection by the future PAMELA and AMS flight or by some highly sensitive future experiments.

The antideuteron signal, shown in Fig 6.10 at the kinetic energy per nucleon of  $T_{\bar{D}} = 0.23$  GeV/ $n$ , has a behavior similar to the antiprotons signal: also in this case direct detection searches and indirect detection in different channels are complementary. The configurations for lighter sneutrinos above the GAPS sensitivity line are almost excluded by the BESS data on antiprotons, but those under the GAPS and AMS sensitivity lines are under reach.

Notice that, for Maj[A] models, antimatter searches are not sensitive to heavy sneutrinos.

We turn now to the gamma ray expected flux from the Galactic center, shown in Fig 6.11, at the energy  $E_{\gamma} = 1.5$  GeV for a EGRET-like angular resolution. Contrary to the LR models, the predicted flux can be detected from EGRET and GLAST also if we take into account a NFW dark matter profile. Only light sneutrinos ( $m_1 < 80$  GeV) produce configurations able to explain the EGRET excess. GLAST will be sensitive to a large fraction of the sneutrino configurations.

Fig. 6.12 shows the upgoing muon flux from the Earth and the sneutrino nucleon scattering cross section. Contrary to the LR models, all the configurations are below the sensitivities of the current experiment and some of them are discarded by direct detection upper limits. However sneutrino in Maj[A] models may be detectable by an increase of sensitivity, although the increase should be sizeable.

The antiproton fluxes at the antiproton kinetic energy of 0.23 GeV for Maj[B] models are shown in the scatter plot of Fig. 6.13: the sneutrino configurations provided by these models are subdominant in the dark matter halo and practically undetectable by current and future antiproton searches. The antideuteron and gamma rays fluxes denote the same characteristics, therefore for these models indirect detections are not very appealing.

Fig. 6.14 refers to the upgoing flux from the Earth predicted for Maj[B] models; we clearly see that also for these signals the indirect searches are not very appealing. Most of the configurations are discarded by direct detection upper limits or are much below current neutrino detectors sensitivities.

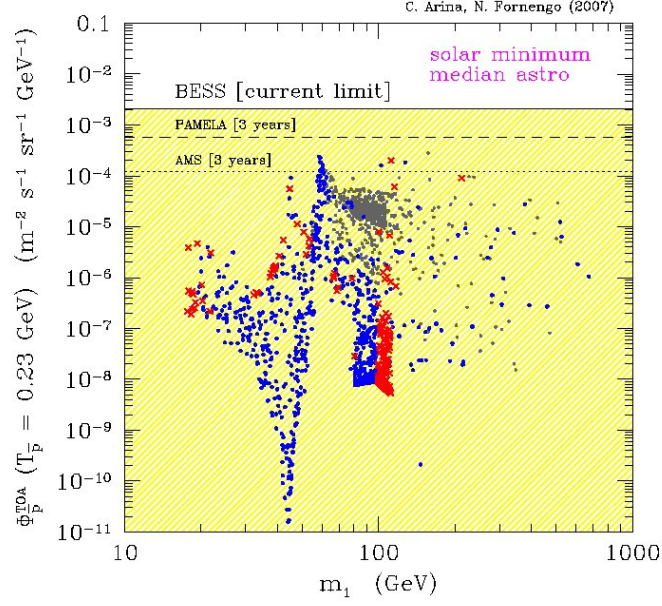


Figure 6.1: LR model – Antiproton flux at the antiproton kinetic energy  $T_{\bar{p}} = 0.23$  GeV as a function of the sneutrino mass  $m_1$ , for the galactic propagation parameters which provide the median value of antiproton flux and for a solar activity at its minimum. Crosses [red] refer to models with sneutrino relic abundance in the cosmologically relevant range; open circles [blue] denote sneutrino configurations cosmologically subdominant and light grey points are excluded by direct detection searches. The [yellow] shaded area denotes the amount of exotic antiprotons which can be accommodated in the BESS data [149, 150]. The dashed and dotted lines show the PAMELA [151] and AMS [152] sensitivities to exotic antiprotons for 3 years missions, respectively.

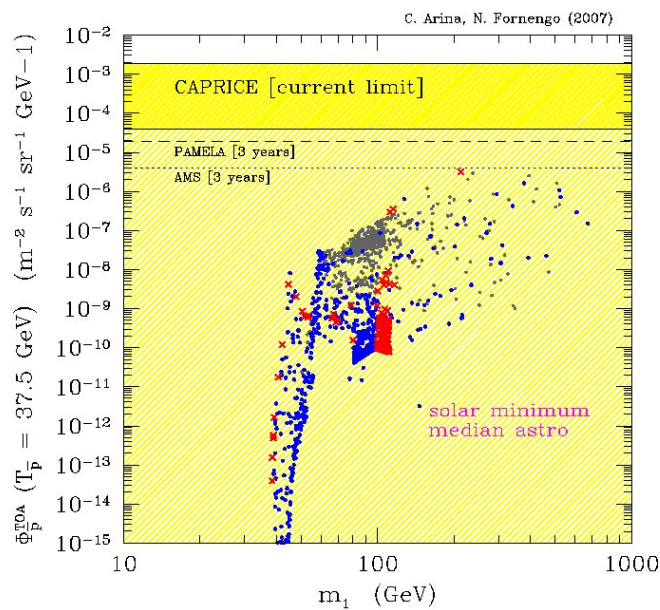


Figure 6.2: LR model – Antiproton flux at the antiproton kinetic energy  $T_{\bar{p}} = 37.5$  GeV as a function of the sneutrino mass  $m_1$ , for the galactic propagation parameters which provide the median value of antiproton flux and for a solar activity at its minimum. Notation are as in Fig 6.1, except for the upper [dark yellow] band which refers to the possible excess over the background measured by CAPRICE [176]. The lower area [yellow] denote fluxes compatible with the CAPRICE data.

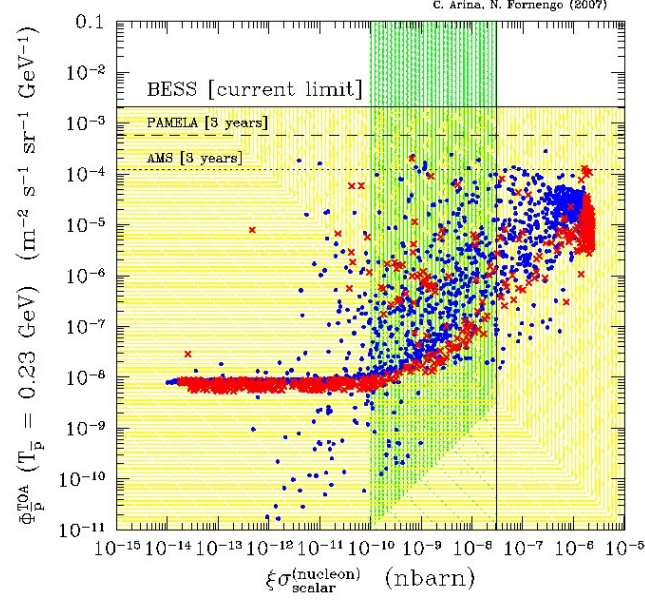


Figure 6.3: LR model – Antiproton flux at the antiproton kinetic energy  $T_{\bar{p}} = 0.23$  GeV correlated with the sneutrino nucleon cross section  $\xi\sigma_{nucleon}^{(scalar)}$ . Crosses [red] refer to models with sneutrino relic abundance in the cosmologically relevant range; open circles [blue] denote sneutrino configurations cosmologically subdominant. The horizontal line denote the upper limit from BESS [149, 150] and the shaded area [yellow] shows the amount of exotic antiprotons which can be accommodated in the BESS data. The dashed and dotted horizontal lines show the PAMELA [151] and AMS [152] sensitivities to exotic antiproton for 3 years missions, respectively. The vertical solid line denotes a conservative upper bound for direct detection searches and the vertical band [green] refers to the current sensitivities of the direct detection experiments.

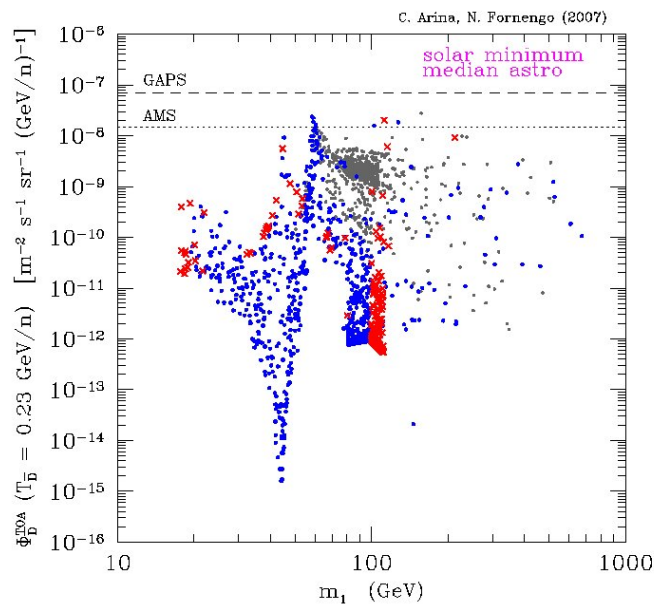


Figure 6.4: LR model – Antideuteron flux at the antideuteron kinetic energy per nucleon  $T_{\bar{d}} = 0.23 \text{ GeV/n}$  as a function of the sneutrino mass  $m_1$ . Notation are as in Fig 6.1. The dashed and dotted lines denote the GAPS [153] and AMS [152] sensitivities, respectively.

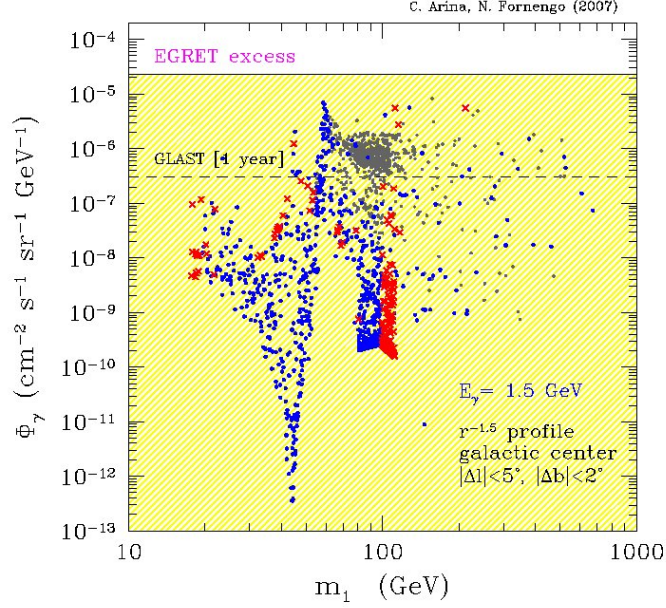


Figure 6.5: LR model – Gamma ray flux from the galactic center at the photon energy  $E_\gamma = 1.5 \text{ GeV}$ , as a function of the sneutrino mass  $m_1$ , for a Moore halo density profile [21, 19] and for the angular resolution of EGRET [160, 161]. Crosses [red] refer to models with sneutrino relic abundance in the cosmologically relevant range; open circles [blue] denote sneutrino configurations cosmologically subdominant and light grey points are excluded by direct detection searches. The shaded area [yellow] denotes the amount of exotic gamma rays compatible with the EGRET excess [160, 161]. The dashed line shows the GLAST [162] sensitivity for 1 year data taking and for the same EGRET angular bin.

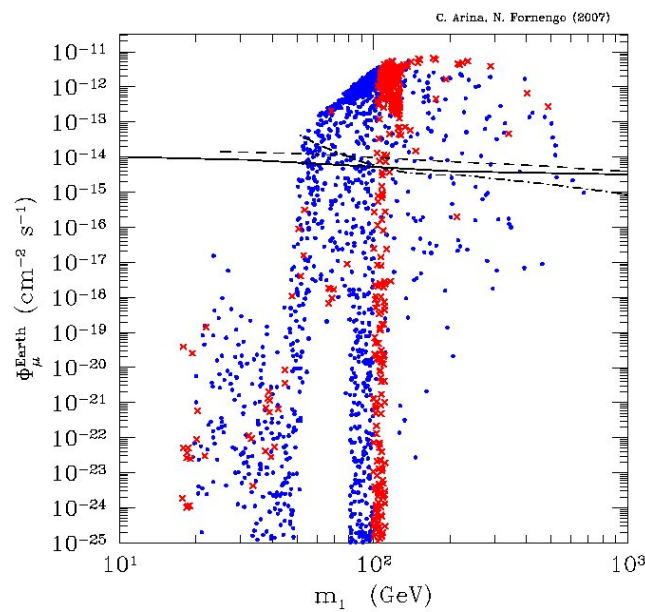


Figure 6.6: LR model – Upgoing muon flux from sneutrino pair annihilation in the center of the Earth  $\Phi_{\mu}^{Earth}$  as a function of the sneutrino mass  $m_1$ . Crosses [red] refer to models with sneutrino relic abundance in the cosmologically relevant range; open circles [blue] denote sneutrino configurations cosmologically subdominant. The solid, dashed and dotted lines denote the upper limit from SuperKamiokande [165], MACRO [164] and AMANDA [166], respectively.

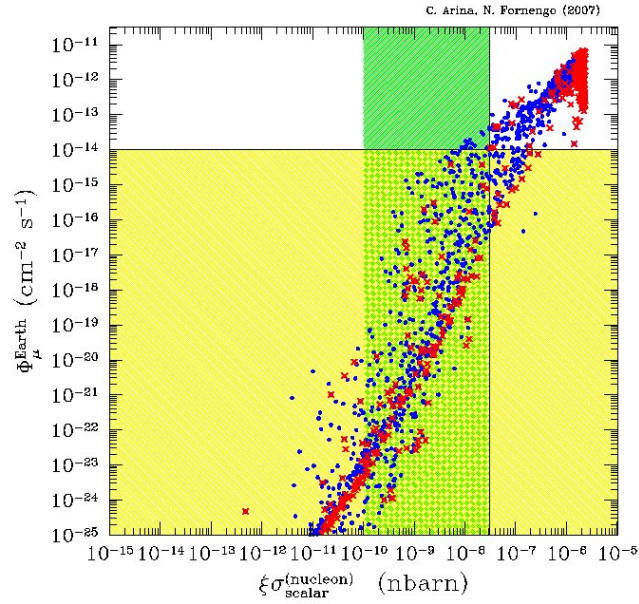


Figure 6.7: LR model – Upgoing muon flux from sneutrino pair annihilation in the center of the Earth  $\Phi_{\mu}^{Earth}$  correlated with the sneutrino nucleon cross section  $\xi \sigma_{nucleon}^{(scalar)}$ . Crosses [red] refer to models with sneutrino relic abundance in the cosmologically relevant range; open circles [blue] denote sneutrino configurations cosmologically subdominant. The horizontal line denotes the current upper bound from neutrino telescopes. The vertical solid line denotes a conservative upper bound for direct detection searches and the vertical band [green] refers to the current sensitivities of the direct detection experiments.

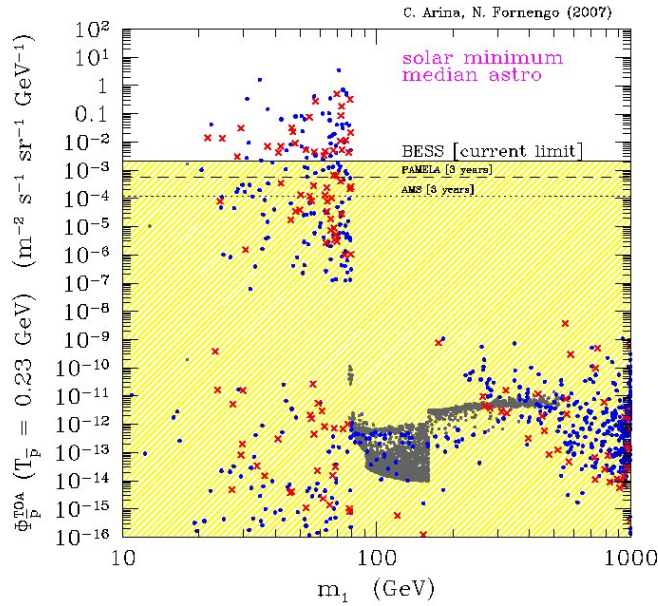


Figure 6.8: Maj[A] model – Antiproton flux at the antiproton kinetic energy  $T_{\bar{p}} = 0.23$  GeV as a function of the sneutrino mass  $m_1$ , for the galactic propagation parameters which provide the median value of antiproton flux and for a solar activity at its minimum. The Majorana mass is  $M = 1$  TeV and a full scan in the supersymmetric parameter space as in Fig 4.4.2. Crosses [red] refer to models with sneutrino relic abundance in the cosmologically relevant range; open circles [blue] denote sneutrino configurations cosmologically subdominant and light grey points are excluded by direct detection searches. The [yellow] shaded area denotes the amount of exotic antiprotons which can be accommodated in the BESS data [149, 150]. The dashed and dotted lines show the PAMELA [151] and AMS [152] sensitivities to exotic antiprotons for 3 years missions, respectively.

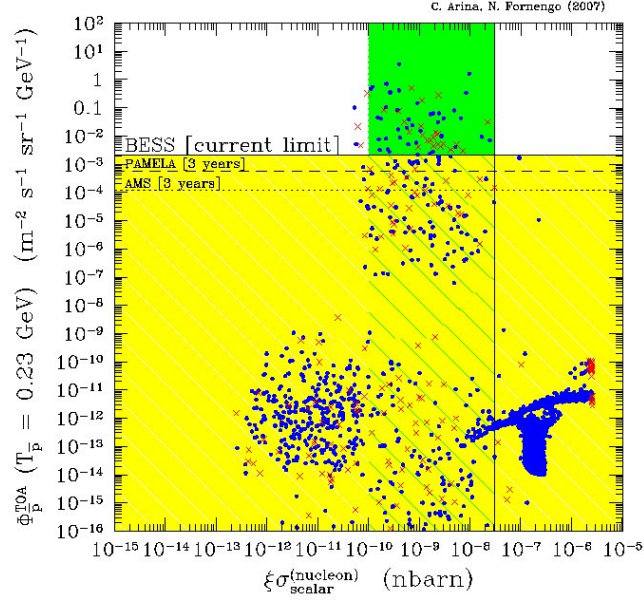


Figure 6.9: Maj[A] model – Antiproton flux at the antiproton kinetic energy  $T_{\bar{p}} = 0.23$  GeV correlated with the sneutrino nucleon cross section  $\xi \sigma_{\text{nucleon}}^{(\text{scalar})}$ , for a Majorana mass scale of 1 TeV and a full scan in the supersymmetric parameter space as in Fig 4.4.2. Crosses [red] refer to models with sneutrino relic abundance in the cosmologically relevant range; open circles [blue] denote sneutrino configurations cosmologically subdominant. The horizontal line denote the upper limit from BESS [149, 150] and the shaded area [yellow] shows the amount of exotic antiprotons which can be accommodated in the BESS data. The dashed and dotted horizontal lines show the PAMELA [151] and AMS [152] sensitivities to exotic antiproton for 3 years missions, respectively. The vertical solid line denotes a conservative upper bound for direct detection searches and the vertical band [green] refers to the current sensitivities of the direct detection experiments.

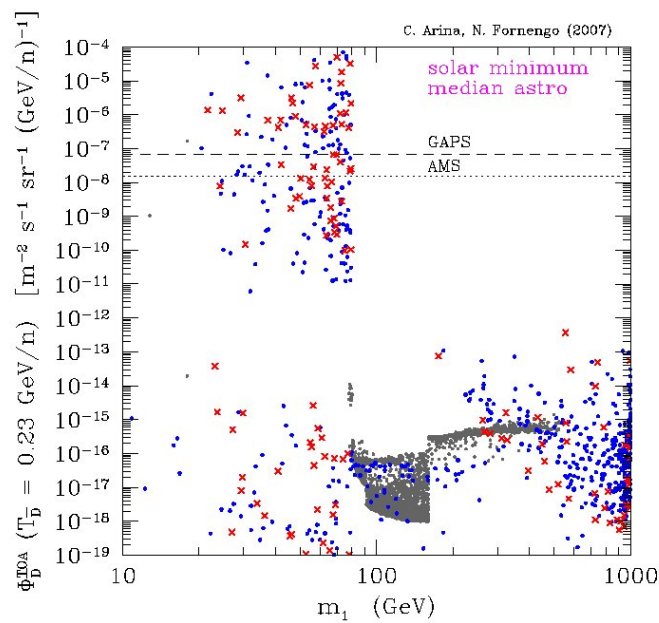


Figure 6.10: Maj[A] model – Antideuteron flux at the antideuteron kinetic energy per nucleon  $T_{\bar{d}} = 0.23$  GeV/n as a function of the sneutrino mass  $m_1$ , for a Majorana mass scale of 1 TeV and a full scan in the supersymmetric parameter space as in Fig 4.4.2. Notation are as in Fig 6.1. The dashed and dotted lines denote the GAPS [153] and AMS [152] sensitivities, respectively.

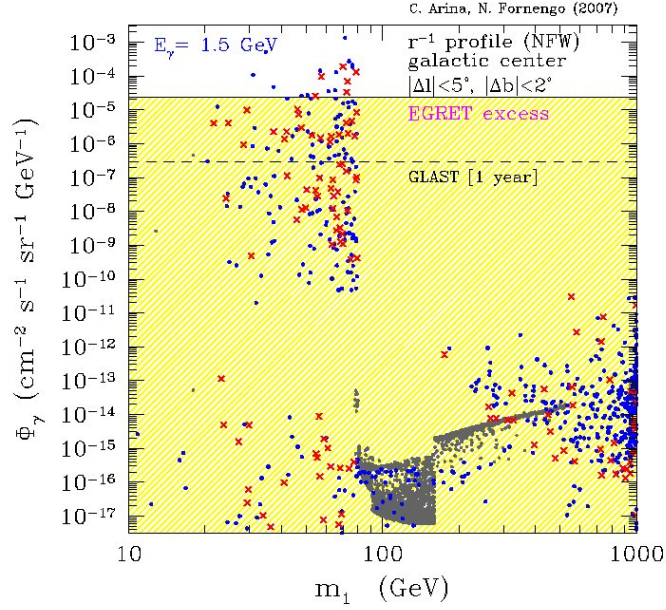


Figure 6.11: Maj[A] model – Gamma ray flux from the galactic center at the photon energy  $E_\gamma = 1.5$  GeV, as a function of the sneutrino mass  $m_1$ , for a Moore halo density profile [21, 19] and for the angular resolution of EGRET [160, 161]. The Majorana mass is  $M = 1$  TeV and a full scan in the supersymmetric parameter space as in Fig 4.4.2. Crosses [red] refer to models with sneutrino relic abundance in the cosmologically relevant range; open circles [blue] denote sneutrino configurations cosmologically subdominant and light grey points are excluded by direct detection searches. The shaded area [yellow] denotes the amount of exotic gamma rays compatible with the EGRET excess [160, 161]. The dashed line shows the GLAST [162] sensitivity for 1 year data taking and for the same EGRET angular bin.

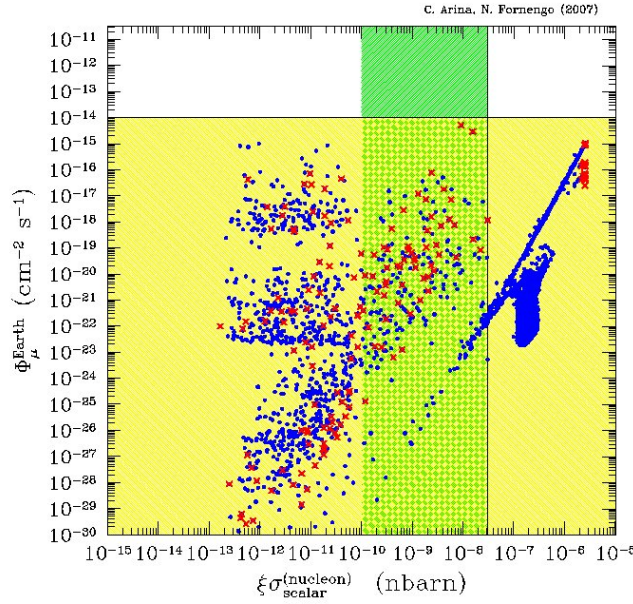


Figure 6.12: Maj[A] model – Upgoing muon flux from sneutrino pair annihilation in the center of the Earth  $\Phi_{\mu}^{\text{Earth}}$  correlated with the sneutrino nucleon cross section  $\xi \sigma_{\text{nucleon}}^{(\text{scalar})}$ . The Majorana mass is  $M = 1$  TeV and a full scan in the supersymmetric parameter space as in Fig 4.4.2. Crosses [red] refer to models with sneutrino relic abundance in the cosmologically relevant range; open circles [blue] denote sneutrino configurations cosmologically subdominant. The horizontal line denotes the current upper bound from neutrino telescopes. The vertical solid line denotes a conservative upper bound for direct detection searches and the vertical band [green] refers to the current sensitivities of the direct detection experiments.

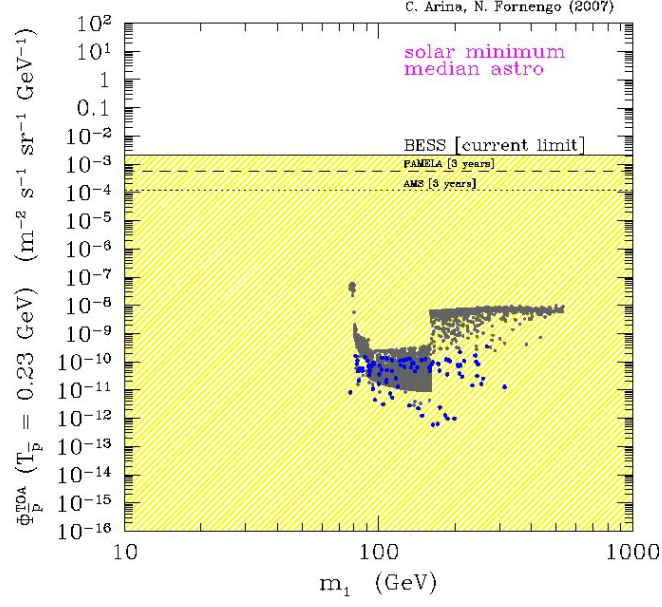


Figure 6.13: Maj[B] model – Antiproton flux at the antiproton kinetic energy  $T_{\bar{p}} = 0.23 \text{ GeV}$  correlated with the sneutrino nucleon cross section  $\xi\sigma_{nucleon}^{(scalar)}$ , for a Majorana mass scale of  $10^9 \text{ GeV}$  and a full scan in the supersymmetric parameter space as in Fig 4.4.2. Crosses [red] refer to models with sneutrino relic abundance in the cosmologically relevant range; open circles [blue] denote sneutrino configurations cosmologically subdominant. The horizontal line denote the upper limit from BESS [149, 150] and the shaded area [yellow] shows the amount of exotic antiprotons which can be accommodated in the BESS data. The dashed and dotted horizontal lines show the PAMELA [151] and AMS [152] sensitivities to exotic antiproton for 3 years missions, respectively. The vertical solid line denotes a conservative upper bound for direct detection searches and the vertical band [green] refers to the current sensitivities of the direct detection experiments.

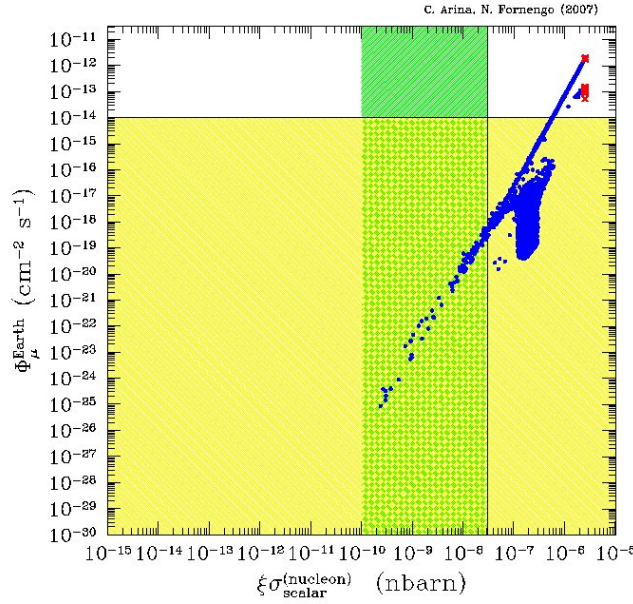


Figure 6.14: Maj[B] model – Upgoing muon flux from sneutrino pair annihilation in the center of the Earth  $\Phi_{\mu}^{Earth}$  correlated with the sneutrino nucleon cross section  $\xi \sigma_{\text{nucleon}}^{(\text{scalar})}$ . The Majorana mass is  $M = 10^9$  GeV and a full scan in the supersymmetric parameter space as in Fig 4.4.2. Crosses [red] refer to models with sneutrino relic abundance in the cosmologically relevant range; open circles [blue] denote sneutrino configurations cosmologically subdominant. The horizontal line denotes the current upper bound from neutrino telescopes. The vertical solid line denotes a conservative upper bound for direct detection searches and the vertical band [green] refers to the current sensitivities of the direct detection experiments.

# Conclusions

In this thesis we have re-analyzed the sneutrino phenomenology in the standard minimal supersymmetric model and in extensions of it, which can account for the neutrino masses. All the considered supersymmetric models conserve  $R$ -parity, thus the LSP is stable and by assumption is the sneutrino, the superpartner of the neutrino. Therefore sneutrinos turn out to be stable, neutral, weakly interacting: they may account for the cold dark matter content of the Universe.

Sneutrinos as particle candidates for DM have been studied in the past in a number of interesting papers, as mentioned in chapter 4, where their relic abundance and scattering cross section off nucleons, relevant for the direct detection searches of dark matter, have been calculated and discussed. Typically, in MSSM models, the sneutrino relic abundance is very low and the direct detection rate is a very stringent experimental bound to sneutrino dark matter. Some models, which extend the minimal standard SUSY models, have been proposed in order to circumvent the character of exclusion of sneutrino dark matter. However a thorough analysis with a global study in the full parameter space of the supersymmetric models has not been performed. Indirect detection signals, especially those coming from dark matter annihilation in the Galaxy, have not been typically discussed in the literature. We aimed to reconsider in a consistent way sneutrinos as cold relic from the early Universe and study their phenomenology relevant both for Cosmology and for relic particle detection. We have explicitly considered both cosmologically dominant and subdominant sneutrino configurations: in fact, we were interested not only in those configurations which are able to solve the CDM problem, but also those which provide a smaller amount of cosmological relic abundance but which could be potentially detectable by means of various astrophysical signals.

We have first re-analyzed the minimal standard MSSM. Sneutrinos are here typically subdominant dark matter components, with low values of the relic abundance in all the mass range from 50–70 GeV (their lower mass bound in MSSM from negative collider searches and constraints on the invisible Z decay width) up to 600–700 GeV (Sec. 4.1). They may account for CDM in the restricted mass range of 600–700 GeV, where the relic abundance values are in the WMAP interval for cold dark matter. This possibility is actually excluded by direct searches (Sec. 5.4), which allow sneutrinos to be a subdominant dark matter component only very marginally and for fine tuned conditions, that pose the sneutrino annihilation cross section on one of the Higgs pole or the Z pole.

The first extension of the minimal standard supersymmetric model we introduced

includes a right-handed neutrino superfield and allows for a much richer phenomenology (Sec. 4.2). The sneutrino fields result as a superposition of right-handed and left-handed fields: this mixing suppresses the  $Z$  coupling, since the right-handed fields are sterile respect to the  $Z$  boson. This is an interesting feature of the models, the relic abundance increases and the elastic cross section diminishes. Moreover the reduced  $Z$  coupling is also instrumental in allowing light sneutrinos, by circumventing the invisible  $Z$  width bound. From a full scan in the supersymmetric parameter space, we find that cosmologically dominant relic sneutrinos are present in the mass range from 15 GeV up to 1 TeV (where we stop our scan). We find that 15 GeV is actually the mass lower bound, induced by the cosmological limit on the relic abundance. The direct detection rate is acceptable for all the allowed mass range (Sec. 5.5). We also find that cosmologically dominant sneutrinos are not only accepted by the limits on direct searches but also that a large fraction of the supersymmetric configurations predict direct detection rates at the level of the current experimental sensitivities, including the possibility to explain the DAMA/NaI annual modulation signal. Indirect detection rates offer good possibilities (Sec. 6.4.1): antiproton fluxes are under reach of the PAMELA and AMS detectors in the mass range from 50 GeV up to 200 GeV. The antideuterium signals are accessible by GAPS and AMS in the same mass range of the antiproton signals. This offer a great opportunity for dark matter searches: a signal detectable in one antimatter channel by two different detectors, will be detectable also in other channels, again by two different detectors. The configurations accessible to indirect searches are typically cosmologically subdominant. Gamma rays from the galactic center do not provide very large signals: we predict fluxes not too far from the EGRET excess in the 50–200 GeV mass range, but the assumption of a very steep density profile toward the center of the galaxy is needed. GLAST will be sensitive to configurations in the same mass range, again assuming a  $r^{-1.5}$  density profile.

The second supersymmetric extension of the MSSM introduces a non renormalizable 5 dimensional operator, which violates the lepton number by two units (Sec. 4.3). The phenomenology of the sneutrino turns out to be related with the neutrino mass properties. The  $L$  violating terms in the SUSY and soft breaking lagrangians split the two sneutrino mass eigenstates and lead to an off-diagonal coupling to the  $Z$  boson. Despite the weakened coupling with the  $Z$  boson, which may modify the relic abundance values and the expected direct detection rates, these models do not lead to a phenomenology very different from the standard minimal supersymmetric models (Sec. 4.1), once one consider a neutrino mass bound of 2 eV on the one loop correction. Only for a neutrino mass bound of 18 MeV, which correspond to the kinematical mass bound for the tau neutrino, some increase of the relic abundance is possible. However, the direct detection limit (Sec. 5.6) strongly bounds these models, making them almost marginal.

The last class of extension of supersymmetric standard models leads to a renormalizable lagrangian, which incorporates both right-handed neutrino superfields and  $L$ -number violating terms (Sec. 4.4). Moreover these models offer the possibility to include neutrino masses via the see-saw mechanism. They provide a rich sneutrino phenomenology, again related to neutrino physics by one loop corrections to the neutrino

mass. The lagrangian includes a Majorana mass term, proportional to the mass  $M$ : depending on the scale of  $M$ , the phenomenology and the cosmological properties of the sneutrinos change. In the case of a TeV-scale Majorana mass parameter (Sec 4.4.1), sneutrinos may be the dominant dark matter component for masses in the range from 5 GeV up to 1 TeV (where we stop our scan), also for a neutrino mass bound of 2 eV: indeed the effects of the off-diagonal coupling with the Z boson and the mixing between left and right handed components add up. The direct detection (Sec. 5.7.1) is evaded in all the mass range and most of the configurations fall inside the current sensitivity range, including the possibility to provide the annual modulation signal detected by DAMA/NaI. The indirect detection rates (Sec. 6.4.2) provide bounds and constraints which are complementary to the direct searches: the former constraint light sneutrino configuration, while the latter are more severe for heavy sneutrinos. Antiproton fluxes are stringent bound for light sneutrinos, many configurations for masses below 80–90 GeV will be explored by PAMELA and AMS, while for masses above 90 GeV antiproton searches loose sensitivity. Also for antideuterons, AMS and GAPS will have sensitivity to probe a fraction of the configurations for masses below 80–90 GeV. For these light sneutrinos, also gamma rays provide a significant probe, even in the case of NFW density profiles: GLAST will have sensitivity to a fraction of those configurations with mass below 80–90 GeV. Finally models with a large scale Majorana mass parameter (Sec. 4.4.2) are strongly bounded by direct detection (Sec. 5.7.2): configurations with masses in the range 90–300 GeV are not excluded by direct detection, but they all refer to cosmologically subdominant sneutrinos. Indirect detection rates are typically very suppressed (Sec. 6.4.2).

We therefore conclude that sneutrinos offer a rich phenomenology as dark matter candidates, and they provide a viable alternative to relic neutralinos in a wide class of supersymmetric models. The predicted antimatter and gamma ray fluxes and the direct detection rates offer a good deal of complementarity in the sneutrino searches, since they are sensitive to different sneutrino configurations. Their phenomenology is also linked and constrained by neutrino physics through the problem of the neutrino mass origin.

# Appendix A

## Interaction Lagrangians

In this Appendix we report all the interaction vertices useful for the calculations in this thesis, which involve the sneutrino fields. We present first the interaction lagrangians in the standard minimal supersymmetric framework, then we discuss the derivation of the interaction vertices in the extended supersymmetric models, considered in this work. We consider the interaction between sleptons and Higgs bosons, sleptons and gauge bosons and finally sleptons and fermions.

The quantity  $T_{3l}$  refers to the third isospin component of the (s)lepton  $l$  belonging to a  $SU(2)_W$  doublet. All the quantities related to the neutralino and chargino sector are defined in Sec. 3.5.2, while the relevant Higgs parameters are described in Sec. 3.5.1. The slepton sector is discussed in Sec. 3.5.3, then the relevant sneutrino parameters are introduced in Chapter 4.

The interaction vertices among the other supersymmetric particles may be found in Refs. [55, 83]. We use the four component formalism for the fermionic spinors.

### A.1 Scalar leptons–Higgs bosons

Standard MSSM

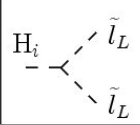
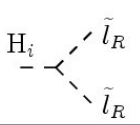
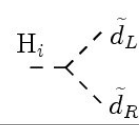
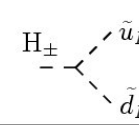
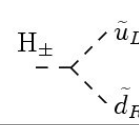
				
(a)	(b)	(c)	(d)	(e)
$H_i = h, H$	$H_i = h, H$	$H_i = h, H, A$		

Table A.1: Scalar leptons and Higgs vertices

The interaction lagrangians corresponding to the vertices in Tab. A.1 have the following

expressions:

$$\begin{aligned}
 (a1) \quad \mathcal{L}_{\tilde{l}_L \tilde{l}_L h} &= \left\{ \frac{g_2 m_Z}{\cos \theta_W} (T_{3L} - e_L \sin^2 \theta_W) \sin(\alpha + \beta) \right\} \tilde{l}_L^* \tilde{l}_L h + \frac{g_2 m_d^2}{m_W} \frac{\sin \alpha}{\cos \beta} \tilde{d}_L^* \tilde{d}_L h \\
 &\quad + \frac{g_2 m_u^2}{m_W} \frac{\sin \alpha}{\cos \beta} \tilde{u}_L^* \tilde{u}_L h \\
 (a2) \quad \mathcal{L}_{\tilde{l}_L \tilde{l}_L H} &= -\left\{ \frac{g_2 m_Z}{\cos \theta_W} (T_{3L} - e_L \sin^2 \theta_W) \right\} \cos(\alpha + \beta) \tilde{l}_L^* \tilde{l}_L H - \frac{g_2 m_d^2}{m_W} \frac{\cos \alpha}{\cos \beta} \tilde{d}_L^* \tilde{d}_L H \\
 &\quad - \frac{g_2 m_u^2}{m_W} \frac{\cos \alpha}{\cos \beta} \tilde{u}_L^* \tilde{u}_L H \\
 (b1) \quad \mathcal{L}_{\tilde{l}_R \tilde{l}_R h} &= \left\{ \frac{g_2 m_Z}{\cos \theta_W} e_R \sin^2 \theta_W \sin(\alpha + \beta) \right\} \tilde{l}_R^* \tilde{l}_R h + \frac{g_2 m_d^2}{m_W} \frac{\sin \alpha}{\cos \beta} \tilde{d}_R^* \tilde{d}_R h \\
 (b2) \quad \mathcal{L}_{\tilde{l}_R \tilde{l}_R H} &= -\left\{ \frac{g_2 m_Z}{\cos \theta_W} e_R \sin^2 \theta_W \cos(\alpha + \beta) \right\} \tilde{l}_R^* \tilde{l}_R H - \frac{g_2 m_d^2}{m_W} \frac{\cos \alpha}{\cos \beta} \tilde{d}_R^* \tilde{d}_R H \\
 (c1) \quad \mathcal{L}_{\tilde{l}_L \tilde{l}_R h} &= \frac{g_2 m_d}{2 m_W \cos \beta} (\mu \cos \alpha - A_d \sin \alpha) (\tilde{d}_L^* \tilde{d}_R + h.c.) h \\
 (c2) \quad \mathcal{L}_{\tilde{d}_L \tilde{d}_R H} &= -\frac{g_2 m_d}{2 m_W \cos \beta} (-\mu \sin \alpha + A_d \cos \alpha) (\tilde{d}_L^* \tilde{d}_R + h.c.) H \\
 (c3) \quad \mathcal{L}_{\tilde{d}_L \tilde{d}_R A} &= -\frac{i g_2 m_d}{2 m_W} (\mu + A_d \tan \beta) (\tilde{d}_R^* \tilde{d}_L - \tilde{d}_L^* \tilde{d}_R) A
 \end{aligned}$$

In Tab A.2 we have reported the 4-point interaction vertices:

$$\begin{aligned}
 (f1) \quad \mathcal{L}_{\tilde{l}_L \tilde{l}_L h h} &= \frac{g_2^2}{2} \left\{ \cos 2\alpha \left( \frac{T_{3l} - e_l \sin^2 \theta_W}{\cos^2 \theta_W} \right) - \frac{m_l^2}{m_W^2} D_l \right\} \tilde{l}_L^* \tilde{l}_L h h \\
 D_u &= \frac{\cos^2 \alpha}{\sin^2 \beta} \quad D_d = \frac{\sin^2 \alpha}{\cos^2 \beta} \\
 (f2) \quad \mathcal{L}_{\tilde{l}_L \tilde{l}_L H H} &= -\frac{g_2^2}{2} \left\{ \cos 2\alpha \left( \frac{T_{3l} - e_l \sin^2 \theta_W}{\cos^2 \theta_W} \right) - \frac{m_l^2}{m_W^2} D_l \right\} \tilde{l}_L^* \tilde{l}_L H H \\
 D_u &= \frac{\sin^2 \alpha}{\sin^2 \beta} \quad D_d = \frac{\cos^2 \alpha}{\cos^2 \beta} \\
 (f3) \quad \mathcal{L}_{\tilde{l}_L \tilde{l}_L A A} &= \frac{g_2^2}{2} \left\{ \cos 2\beta \left( \frac{T_{3l} - e_l \sin^2 \theta_W}{\cos^2 \theta_W} \right) - \frac{m_l^2}{m_W^2} D_l \right\} \tilde{l}_L^* \tilde{l}_L A A \\
 D_u &= \cot^2 \beta \quad D_d = \tan^2 \beta \\
 (g1) \quad \mathcal{L}_{\tilde{l}_R \tilde{l}_R h h} &= \frac{g_2^2}{2} \left\{ \cos 2\alpha \left( \frac{e_l \sin^2 \theta_W}{\cos^2 \theta_W} \right) - \frac{m_l^2}{m_W^2} D_l \right\} \tilde{l}_R^* \tilde{l}_R h h \\
 D_u &= \frac{\cos^2 \alpha}{\sin^2 \beta} \quad D_d = \frac{\sin^2 \alpha}{\cos^2 \beta} \\
 (g2) \quad \mathcal{L}_{\tilde{l}_R \tilde{l}_R H H} &= -\frac{g_2^2}{2} \left\{ \cos 2\alpha \left( \frac{e_l \sin^2 \theta_W}{\cos^2 \theta_W} \right) - \frac{m_l^2}{m_W^2} D_l \right\} \tilde{l}_R^* \tilde{l}_R H H \\
 D_u &= \frac{\sin^2 \alpha}{\sin^2 \beta} \quad D_d = \frac{\cos^2 \alpha}{\cos^2 \beta} \\
 (g3) \quad \mathcal{L}_{\tilde{l}_R \tilde{l}_R A A} &= \frac{g_2^2}{2} \left\{ \cos 2\beta \left( \frac{e_l \sin^2 \theta_W}{\cos^2 \theta_W} \right) - \frac{m_l^2}{m_W^2} D_l \right\} \tilde{l}_R^* \tilde{l}_R A A \\
 D_u &= \cot^2 \beta \quad D_d = \tan^2 \beta
 \end{aligned}$$

(f)	(g)	(h)
$H_i = h, H, A$	$H_i = h, H, A$	
(i)	(l)	(m)
(n)	(o)	(p)
$H_i = h, H, A$		

Table A.2: Scalar leptons and Higgs 4-point vertices

$$(h) \quad \mathcal{L}_{\tilde{l}_L \tilde{l}_L h H} = \frac{g_2^2 \sin 2\alpha}{2} \left\{ \frac{T_{3l} - e_l \sin^2 \theta_W}{\cos^2 \theta_W} - \frac{m_l^2}{2m_W^2} D_l \right\} \tilde{l}_L \tilde{l}_L h H$$

$$D_u = \frac{1}{\sin^2 \beta} \quad D_d = \frac{-1}{\cos^2 \beta}$$

$$(i) \quad \mathcal{L}_{\tilde{l}_R \tilde{l}_R h H} = \frac{g_2^2 \sin 2\alpha}{2} \left\{ \frac{e_l \sin^2 \theta_W}{\cos^2 \theta_W} - \frac{m_l^2}{2m_W^2} D_l \right\} \tilde{l}_R \tilde{l}_R h H$$

$$D_u = \frac{1}{\sin^2 \beta} \quad D_d = \frac{-1}{\cos^2 \beta}$$

$$(l) \quad \mathcal{L}_{\tilde{l}_L \tilde{l}_L H^+ H^-} = \frac{g_2^2 \cos 2\beta}{2} \left\{ -2T_{3l} + \left( \frac{T_{3l} - e_l \sin^2 \theta_W}{\cos^2 \theta_W} \right) \right\} \tilde{l}_L^* \tilde{l}_L H^+ H^- - \frac{g_2^2}{2m_W^2} D_l \tilde{l}_L^* \tilde{l}_L H^+ H^-$$

$$D_u = m_u^2 \tan^2 \beta \quad D_d = m_d^2 \cot^2 \beta$$

$$(m) \quad \mathcal{L}_{\tilde{l}_R \tilde{l}_R H^+ H^-} = \frac{g_2^2 \cos 2\beta}{2} \left\{ \frac{e_l \sin^2 \theta_W}{\cos^2 \theta_W} \right\} \tilde{l}_R^* \tilde{l}_R H^+ H^- - \frac{g_2^2}{2m_W^2} D_l \tilde{l}_R^* \tilde{l}_R H^+ H^-$$

$$D_u = m_u^2 \cot^2 \beta \quad D_d = m_d^2 \tan^2 \beta$$

$$(n1) \quad \mathcal{L}_{\tilde{l}_L \tilde{l}_L h H^-} = -\frac{g_2^2}{2\sqrt{2}} \left\{ \cos(\alpha + \beta) - \frac{m_u^2}{m_W^2} \frac{\cos \alpha \cos \beta}{\sin^2 \beta} + \frac{m_d^2}{m_W^2} \frac{\sin \alpha \sin \beta}{\cos^2 \beta} \right\} \tilde{u}_L^* \tilde{d} h H^-$$

$$(n2) \quad \mathcal{L}_{\tilde{l}_L \tilde{l}_L H H^-} = -\frac{g_2^2}{2\sqrt{2}} \left\{ \sin(\alpha + \beta) - \frac{m_u^2}{m_W^2} \frac{\sin \alpha \cos \beta}{\sin^2 \beta} - \frac{m_d^2}{m_W^2} \frac{\cos \alpha \sin \beta}{\cos^2 \beta} \right\} \tilde{u}_L^* \tilde{d} H H^-$$

$$\begin{aligned}
 (n3) \quad \mathcal{L}_{\tilde{l}_L \tilde{l}_L \text{AH}^-} &= \frac{ig_2^2}{2\sqrt{2}} \left\{ \cos 2\beta - \frac{m_u^2}{m_W^2} \cot^2 \beta + \frac{m_d^2}{m_W^2} \tan^2 \beta \right\} \tilde{u}_L^* \tilde{d} \text{AH}^- \\
 (o) \quad \mathcal{L}_{\tilde{l}_R \tilde{l}_R \text{hH}^-} &= \frac{g_2^2 m_u m_d \cos(\beta - \alpha)}{\sqrt{2} m_W^2 \sin 2\beta} \tilde{l}_R^* \tilde{l}_R \text{hH}^- \\
 (p) \quad \mathcal{L}_{\tilde{l}_R \tilde{l}_R \text{HH}^-} &= \frac{g_2^2 m_u m_d \sin(\beta - \alpha)}{\sqrt{2} m_W^2 \sin 2\beta} \tilde{l}_R^* \tilde{l}_R \text{hH}^-
 \end{aligned}$$

### $\tilde{\nu}$ models

The sneutrino-higgs boson lagragian has the form  $\tilde{\nu}^* \tilde{\nu} \text{H}_i$  or  $\tilde{\nu}^* \tilde{\nu} \text{H}_i \text{H}_i$ , therefore substituting the  $\tilde{\nu}_1$  mass eigenstate of Eq. 4.14, one obtains:

$$\begin{aligned}
 \tilde{\nu}^* \tilde{\nu} \text{H}_i &= \frac{1}{2} (\tilde{\nu}_+ + i\tilde{\nu}_-) (\tilde{\nu}_+ - i\tilde{\nu}_-) \text{H}_i \\
 &= \frac{1}{2} (\tilde{\nu}_+ \tilde{\nu}_+ - i\tilde{\nu}_- \tilde{\nu}_+ + i\tilde{\nu}_- \tilde{\nu}_+ \tilde{\nu}_- \tilde{\nu}_-) \text{H}_i \\
 &= \frac{1}{2} (\tilde{\nu}_+ \tilde{\nu}_+ + \tilde{\nu}_- \tilde{\nu}_-) \text{H}_i
 \end{aligned} \tag{A.1}$$

Notice that the coupling is diagonal and acquires a factor of 1/2.

## A.2 Scalar leptons–Gauge boson vectors

### Standard MSSM

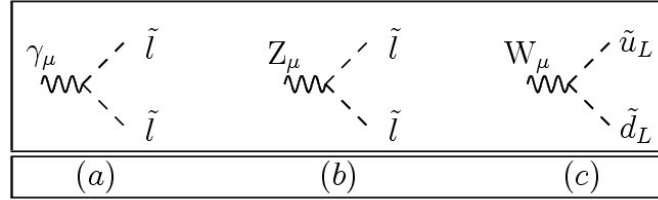


Table A.3: Scalar leptons and gauge bosons vertices

The slepton–gauge boson lagrangians corresponding to the diagrams in Tab. A.3 are given by:

$$\begin{aligned}
 (a) \quad \mathcal{L}_{\tilde{l} \tilde{l} \gamma_\mu} &= -e_l \gamma^\mu \tilde{l}^* \overleftrightarrow{\partial}_\mu \tilde{l} \\
 (b) \quad \mathcal{L}_{\tilde{l} \tilde{l} Z_\mu} &= -\frac{g_2}{\cos \theta_W} (T_{3l} - e_l \sin^2 \theta_W) Z^\mu \tilde{l}^* \overleftrightarrow{\partial}_\mu \tilde{l}
 \end{aligned}$$

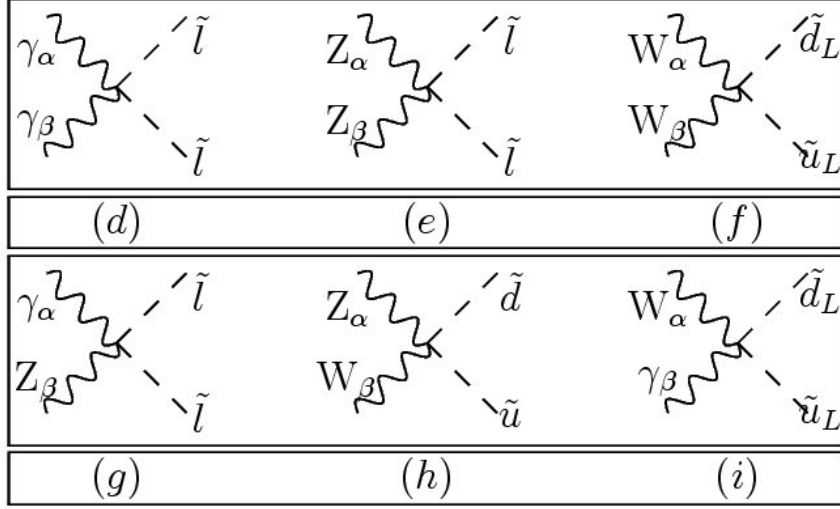


Table A.4: Scalar leptons and gauge bosons 4–point vertices

$$(c) \quad \mathcal{L}_{\tilde{u}\tilde{d}W_\mu} = -\frac{g_2}{\sqrt{2}} \{W^{+\mu} \tilde{u}_L^* \overleftrightarrow{\partial}_\mu \tilde{d}_L + W^{-\mu} \tilde{d}_L^* \overleftrightarrow{\partial}_\mu \tilde{u}_L\}$$

The slepton–gauge boson 4–point vertices in Tab. A.4 derive from the following interaction lagrangians:

$$(d) \quad \mathcal{L}_{\tilde{l}\tilde{l}\gamma_\alpha\gamma_\beta} = 2e^2 e_l^2 g_{\alpha\beta} \gamma_\alpha \gamma_\beta \tilde{l}^* \tilde{l}$$

$$(e) \quad \mathcal{L}_{\tilde{l}\tilde{l}Z_\alpha Z_\beta} = \frac{2g_2^2}{\cos^2 \theta_W} (T_{3l} - e_l \sin^2 \theta_W) g_{\alpha\beta} Z_\alpha Z_\beta \tilde{l}^* \tilde{l}$$

$$(f) \quad \mathcal{L}_{\tilde{l}\tilde{l}W_\alpha W_\beta} = \frac{g_2^2}{2} g_{\alpha\beta} W_\alpha W_\beta \tilde{l}^* \tilde{l}$$

$$(g) \quad \mathcal{L}_{\tilde{l}\tilde{l}\gamma_\alpha Z_\beta} = \frac{2g_2 e_l}{\cos \theta_W} (T_{3l} - e_l \sin^2 \theta_W) g_{\alpha\beta} Z_\alpha Z_\beta \tilde{l}^* \tilde{l}$$

$$(h) \quad \mathcal{L}_{\tilde{l}\tilde{l}Z_\alpha W_\beta} = -\frac{g_2^2 \sin^2 \theta_W}{\sqrt{2} \cos \theta_W} (e_u + e_d) g_{\alpha\beta} W_\alpha W_\beta \tilde{l}^* \tilde{l}$$

$$(i) \quad \mathcal{L}_{\tilde{l}\tilde{l}W_\alpha \gamma_\beta} = -\frac{g_2 e}{\sqrt{2}} (e_u + e_d) g_{\alpha\beta} W_\alpha W_\beta \tilde{l}^* \tilde{l}$$

### LR models

The scalar  $\tilde{\nu}_L$  field turns out to be multiplied by a factor of  $\sin \theta$ , Eq. 4.9; therefore the lagrangian acquires a  $\sin^2 \theta$  factor:

$$\mathcal{L}_{\tilde{\nu}_1 \tilde{\nu}_1 V_\alpha} \longrightarrow \sin^2 \theta \mathcal{L}_{\tilde{\nu}_L \tilde{\nu}_L V_\alpha} \quad (A.2)$$

with  $V_\alpha$  a generic gauge vector.

### $\mathcal{L}$ models

The sneutrino-Z lagrangian is reported in (b). Again substituting  $\tilde{\nu}_1$  from Eq 4.14:

$$\begin{aligned}
 \tilde{\nu}^* \overleftrightarrow{\partial} \tilde{\nu} Z^\mu &= \tilde{\nu}^* \partial_\mu \tilde{\nu} Z^\mu - \tilde{\nu} \partial_\mu \tilde{\nu}^* Z^\mu \\
 &= \frac{1}{2}(\tilde{\nu}_+ + i\tilde{\nu}_-) \partial_\mu (\tilde{\nu}_+ - i\tilde{\nu}_-) Z^\mu - \frac{1}{2}(\tilde{\nu}_+ - i\tilde{\nu}_-) \partial_\mu (\tilde{\nu}_+ + i\tilde{\nu}_-) Z^\mu \\
 &= (\tilde{\nu}_+ \partial_\mu \tilde{\nu}_+ - \tilde{\nu}_- \partial_\mu \tilde{\nu}_-) Z^\mu
 \end{aligned} \tag{A.3}$$

The coupling turns out to be off-diagonal; this is the one of the main features of the introduction of L-violating terms in the supersymmetric and soft breaking lagrangians. The sneutrino- $W^\pm$  lagrangian is reported in (c); after the substitution of the  $\tilde{\nu}_1$  mass eigenstate expression acquires a phase but remains diagonal:

$$\begin{aligned}
 \tilde{\nu}^* \overleftrightarrow{\partial}_\mu d W^{+\mu} &= \tilde{\nu}^* \partial_\mu d W^{+\mu} - d \partial_\mu \tilde{\nu}^* W^{+\mu} \\
 &= \frac{1}{\sqrt{2}}(\tilde{\nu}_+ - i\tilde{\nu}_-) \partial_\mu d W^{+\mu} - \frac{1}{\sqrt{2}} d \partial_\mu (\tilde{\nu}_+ - i\tilde{\nu}_-) W^{+\mu} \\
 &= \frac{1}{\sqrt{2}}(\tilde{\nu}_+ \partial_\mu d - i\tilde{\nu}_- \partial_\mu d) W^{+\mu} + h.c.
 \end{aligned} \tag{A.4}$$

## A.3 Scalar leptons–Fermions

### Standard MSSM

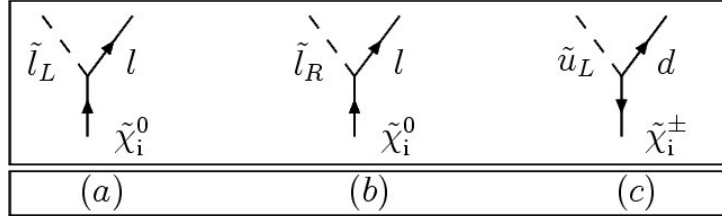


Table A.5: Scalar leptons and fermions vertices

We report the slepton–fermion interaction lagrangians of Tab A.5:

$$\begin{aligned}
 (a) \quad \mathcal{L}_{\tilde{l}_L l \tilde{\chi}_i^0} &= -\frac{g_2}{\sqrt{2}} \bar{l} \{ \alpha_L - \gamma_5 \beta_L \} \tilde{\chi}_i^0 \tilde{l}_L + h.c. \\
 \alpha_L &= \sqrt{\epsilon_i} \left( \epsilon_i \frac{m_l Z_{i,5-l}}{2m_W B_l} + T_{3l} Z_{i2} + \tan \theta_W (e_l - T_{3l}) Z_{i1} \right) \\
 \beta_L &= \sqrt{\epsilon_i} \left( \epsilon_i \frac{m_l Z_{i,5-l}}{2m_W B_l} - T_{3l} Z_{i2} - \tan \theta_W (e_l - T_{3l}) Z_{i1} \right) \\
 B_u &= \sin \beta \quad B_d = \cos \beta
 \end{aligned}$$

$$(b) \quad \mathcal{L}_{\tilde{l}_R \bar{l} \tilde{\chi}_i^0} = -\frac{g_2}{\sqrt{2}} \bar{l} \{ \alpha_R - \gamma_5 \beta_R \} \tilde{\chi}_i^0 \tilde{l}_R + h.c.$$

$$\alpha_R = \sqrt{\epsilon_i} (\epsilon_i e_l \tan \theta_W Z_{i1} + \frac{m_l Z_{i,5-l}}{2m_W B_l})$$

$$\beta_R = \sqrt{\epsilon_i} (\epsilon_i e_l \tan \theta_W Z_{i1} - \frac{m_l Z_{i,5-l}}{2m_W B_l})$$

$$B_u = \sin \beta \quad B_d = \cos \beta$$

$$(c) \quad \mathcal{L}_{\tilde{l}_L \bar{l} \tilde{\chi}_i^\pm} = -g_2 \{ U_{i1}^* \tilde{\chi}_i^\pm P_L u \tilde{d}_L^* + \bar{u} P_R U_{i1} \tilde{\chi}_i^\pm \tilde{d}_L + V_{i1} \tilde{\chi}_i^{\pm c} P_L d \tilde{u}^* + \bar{d} P_R V_{i1} \tilde{\chi}_i^{\pm c} \tilde{u} \}$$

### LR models

The interaction lagrangians acquire a  $\sin \theta$  factor (from Eq. 4.9):

$$\mathcal{L}_{\tilde{\nu}_l \bar{l} F} \longrightarrow \sin \theta \mathcal{L}_{\tilde{\nu}_L \bar{l} F} \quad (\text{A.5})$$

with  $F$  a generic fermionic field and  $\bar{l}$  the neutral or charged fermion, belonging to the same  $SU(2)$  supersymmetric doublet of the sneutrino.

### $\underline{L}$ models

The sneutrino- $\tilde{\chi}_i^0$  lagrangian is reported in (a), therefore using Eq. 4.14:

$$\begin{aligned} & -\frac{g_2}{\sqrt{2}} \bar{l} \{ \alpha_L - \gamma_5 \beta_L \} \tilde{\chi}_i^0 \tilde{\nu} + h.c. = \\ & -\frac{1}{\sqrt{2}} \frac{g_2}{\sqrt{2}} \bar{l} \{ \alpha_L - \gamma_5 \beta_L \} \tilde{\chi}_i^0 (\tilde{\nu}_+ + i\tilde{\nu}_-) + h.c. \end{aligned} \quad (\text{A.6})$$

The coupling is diagonal and acquires a phase. The same holds for the chargino interactions.

# Appendix B

## The supersymmetric model

We analyse the phenomenology of the sneutrino in an effective low-energy supersymmetric framework, with few free parameters, see Sec 3.5. In the next section we report the choice we made for the full scan in the parameter space. In Sec. B.2 we briefly discuss the experimental constraints we impose to the supersymmetric models.

### B.1 Scan over the SUSY parameter space

The full scans of the parameter space are performed over the following ranges of the MSSM parameters:  $1 \leq \tan\beta \leq 50$ ,  $100 \text{ GeV} \leq |\mu| \leq 3000 \text{ GeV}$ ,  $100 \text{ GeV} \leq M_2 \leq 3000 \text{ GeV}$ ,  $100 \text{ GeV} \leq m_Q \leq 3000 \text{ GeV}$ ,  $90 \text{ GeV} \leq m_A \leq 1000 \text{ GeV}$ ,  $-3 \leq A \leq 3$ . As for the  $R$  parameter (we recall here its definition,  $R \equiv M_1/M_2$ ), we use either its mSUGRA (a minimal gravity mediated supersymmetric scenarios) value  $R = 0.5$  or we scan over the interval  $0.005 \leq R \leq 0.5$ , depending on the case at study. In order to have the sneutrino as a dark matter candidate, we accept only parameter configurations for which the lightest sneutrino is also the lightest among all the supersymmetric particles.

The scans hold also for the extended supersymmetric models, since we introduce new parameters only in the sneutrino/neutrino sectors, the other MSSM parameters remain unchanged. The new parameters for the sneutrino are widely analysed in Chapter 4.

### B.2 Experimental constraints

All the masses of the supersymmetric particles are constrained by the accelerator limits: we use the bounds coming by negative searches at CERN  $e^+e^-$  collider LEP2 [177, 178, 179] and at the D0 collider detector at Fermilab. The invisible Z width constraint is also imposed on neutralinos lighter than  $m_Z/2$  which occur in the gaugino non universal models. The sneutrino mass bounds have been discussed in Chapter 4. The Higgs sector is bounded by Higgs searches at colliders, also from LEP2 working groups following [84], and from the limits found by the Collider Detectors CDF at Fermilab [85].

At present, only lepton number conserving processes have been observed in current experiments and there are no indications of FNCN processes. We summarize the constraints on SUSY models from current experiments on the muon anomalous magnetic moment  $a_\mu \equiv (g_\mu - 2)/2$ , on the measurements of the  $b \rightarrow s + \gamma$  decay process and on the branching ratio  $BR(B_s^0 \rightarrow \mu^+ + \mu^-)$ .

The most recent experimental measurement [180] of the muon anomalous magnetic moment  $a_\mu^{exp}$  exhibits a slight discrepancy relative to the predicted value of the Standard Model  $a_\mu^{th}$ . A recent theoretical review [181] of the computation of the Standard Model prediction yielded for the deviation  $\Delta a_\mu \equiv a_\mu^{exp} - a_\mu^{th}$  the values  $-98 \leq \Delta a_\mu \times 10^{11} \leq 565$ . Thus, we use this range in order to constraint the contribution to the muon anomalous magnetic moment from physics beyond the Standard Model.  $a_\mu$  is sensitive mostly to the overall mass scale of the sleptons, gauginos and light sneutrinos.

The branching ratio for the flavor changing neutral current  $BR(B_s^0 \rightarrow \mu^+ + \mu^-)$  is  $3 \times 10^{-9}$  with an upper bound measured by CDF and DO colliders detectors of  $1.2 \times 10^{-7}$  at 90% C.L. [182]. The upper bound is large because in a supersymmetric scenarios this process could be enhanced since  $BR(B_s^0 \rightarrow \mu^+ + \mu^-) \propto \tan\beta^6$ , due to higgsino and possibly gluino contributions [183].

From measurements of the process  $b \rightarrow s + \gamma$  [184], we adopt the interval  $2.89 \leq B(b \rightarrow s + \gamma) \times 10^{-4} \leq 4.21$ , which is larger by 25% with respect to the experimental determination [184] in order to take into account theoretical uncertainties in the SUSY contributions [185] to the branching ratio of the process (for the Standard Model only we employ the recent NNLO results from [186]).

There is no experimental evidence of an nonzero Electric Dipole Moment (EDM) for the electron ( $d_e$ ). The most stringent upper bound, obtained in Ref. [187], is  $d_e \leq 1.6 \times 10^{-27}$  e cm at 90% C.L. Likewise, there is no experimental evidence for radiative flavor-changing charged lepton decays. The 90% C.L. upper limits to the branching ratios for the muon and tau-lepton radiative decays are given by:  $BR(\mu \rightarrow e\gamma) \leq 1.2 \times 10^{-11}$ ,  $BR(\tau \rightarrow e\gamma) \leq 1.1 \times 10^{-7}$  and  $BR(\tau \rightarrow \mu\gamma) \leq 6.8 \times 10^{-8}$  [72]. These processes in principle can set bound on the sneutrino parameters in the extended supersymmetric models. However it turns out that the EDM is insensitive to the sneutrino sector at one loop [111].

# Bibliography

- [1] A. Liddle and D. Lyth, *Cosmological inflation and large-scale structure*. Cambridge, Uk: Univ. Pr., 2000. 400 p.
- [2] G. Jungman, M. Kamionkowski, and K. Griest, *Supersymmetric dark matter*, *Phys. Rept.* **267** (1996) 195–373, [[hep-ph/9506380](#)].
- [3] L. Bergstrom, *Non-baryonic dark matter: Observational evidence and detection methods*, *Rept. Prog. Phys.* **63** (2000) 793, [[hep-ph/0002126](#)].
- [4] G. Bertone, D. Hooper, and J. Silk, *Particle dark matter: Evidence, candidates and constraints*, *Phys. Rept.* **405** (2005) 279–390, [[hep-ph/0404175](#)].
- [5] **WMAP** Collaboration, D. N. Spergel *et. al.*, *Wilkinson Microwave Anisotropy Probe (WMAP) three year results: Implications for cosmology*, *Astrophys. J. Suppl.* **170** (2007) 377, [[astro-ph/0603449](#)].
- [6] S. Perlmutter and B. P. Schmidt, *Measuring cosmology with supernovae*, [astro-ph/0303428](#).
- [7] A. A. Penzias and R. W. Wilson, *A measurement of excess antenna temperature at 4080-mc/s*, *Astrophys. J.* **142** (1965) 419–421.
- [8] G. Gamow, *Expanding universe and the origin of elements*, *Phys. Rev.* **70** (Oct, 1946) 572–573.
- [9] C. L. Bennett *et. al.*, *Cosmic temperature fluctuations from two years of cobe differential microwave radiometers observations*, *Astrophys. J.* **436** (1994) 423–442, [[astro-ph/9401012](#)].
- [10] E. W. Kolb and M. S. Turner, *The early universe*, *Front. Phys.* **69** (1990) 1–547.
- [11] **Supernova Cosmology Project** Collaboration, R. A. Knop *et. al.*, *New constraints on  $\Omega_M$ ,  $\Omega_\Lambda$ , and  $w$  from an independent set of Eleven High-Redshift Supernovae Observed with HST*, *Astrophys. J.* **598** (2003) 102, [[astro-ph/0309368](#)].

- [12] M. Tegmark, *Cosmological Parameters*, Seattle, USA, September 5-9, 2003. Talk given at the Eighth International Workshop on Topics in Astroparticle and Underground Physics (Taup 2003).
- [13] D. M. Wittman, J. A. Tyson, D. Kirkman, I. Dell’Antonio, and G. Bernstein, *Detection of weak gravitational lensing distortions of distant galaxies by cosmic dark matter at large scales*, *Nature* **405** (2000) 143–149, [[astro-ph/0003014](#)].
- [14] SDSS Collaboration, M. Tegmark *et al.*, *The 3D power spectrum of galaxies from the SDSS*, *Astrophys. J.* **606** (2004) 702–740, [[astro-ph/0310725](#)].
- [15] M. L. Balogh *et al.*, *Galaxy ecology: groups and low-density environments in the SDSS and 2dFGRS*, *Mon. Not. Roy. Astron. Soc.* **348** (2004) 1355, [[astro-ph/0311379](#)].
- [16] J. J. Dalcanton and C. J. Hogan, *Halo cores and phase space densities: Observational constraints on dark matter physics and structure formation*, *Astrophys. J.* **561** (2001) 35–45, [[astro-ph/0004381](#)].
- [17] U. Seljak, A. Slosar, and P. McDonald, *Cosmological parameters from combining the Lyman- $\alpha$  forest with CMB, galaxy clustering and SN constraints*, *JCAP* **0610** (2006) 014, [[astro-ph/0604335](#)].
- [18] J. F. Navarro, C. S. Frenk, and S. D. M. White, *A universal density profile from hierarchical clustering*, *Astrophys. J.* **490** (1997) 493–508, [[astro-ph/9611107](#)].
- [19] B. Moore, T. Quinn, F. Governato, J. Stadel, and G. Lake, *Cold collapse and the core catastrophe*, *Mon. Not. Roy. Astron. Soc.* **310** (1999) 1147–1152, [[astro-ph/9903164](#)].
- [20] J. F. Navarro, C. S. Frenk, and S. D. M. White, *The structure of Cold Dark Matter halos*, *Astrophys. J.* **462** (1996) 563–575, [[astro-ph/9508025](#)].
- [21] B. Moore *et al.*, *Dark matter substructure within galactic halos*, *Astrophys. J.* **524** (1999) L19–L22.
- [22] P. Belli, R. Cerulli, N. Fornengo, and S. Scopel, *Effect of the galactic halo modeling on the DAMA/NaI annual modulation result: An extended analysis of the data for WIMPs with a purely spin-independent coupling*, *Phys. Rev.* **D66** (2002) 043503, [[hep-ph/0203242](#)].
- [23] P. Ullio, H. Zhao, and M. Kamionkowski, *A dark-matter spike at the galactic center?*, *Phys. Rev.* **D64** (2001) 043504, [[astro-ph/0101481](#)].
- [24] P. Gondolo and J. Silk, *Dark matter annihilation at the galactic center*, *Phys. Rev. Lett.* **83** (1999) 1719–1722, [[astro-ph/9906391](#)].

- 
- [25] D. Merritt, M. Milosavljevic, L. Verde, and R. Jimenez, *Dark matter spikes and annihilation radiation from the galactic center*, *Phys. Rev. Lett.* **88** (2002) 191301, [[astro-ph/0201376](#)].
- [26] D. Merritt, *Evolution of the dark matter distribution at the galactic center*, *Phys. Rev. Lett.* **92** (2004) 201304, [[astro-ph/0311594](#)].
- [27] F. Prada, A. Klypin, J. Flix, M. Martinez, and E. Simonneau, *Astrophysical inputs on the susy dark matter annihilation detectability*, [astro-ph/0401512](#).
- [28] O. Y. Gnedin, A. V. Kravtsov, A. A. Klypin, and D. Nagai, *Response of dark matter halos to condensation of baryons: cosmological simulations and improved adiabatic contraction model*, *Astrophys. J.* **616** (2004) 16–26, [[astro-ph/0406247](#)].
- [29] B. W. Lee and S. Weinberg, *Cosmological lower bound on heavy-neutrino masses*, *Phys. Rev. Lett.* **39** (1977) 165–168.
- [30] A. D. Dolgov, *Neutrinos in cosmology*, *Phys. Rept.* **370** (2002) 333–535, [[hep-ph/0202122](#)].
- [31] K. Griest and M. Kamionkowski, *Unitarity limits on the mass and radius of dark matter particles*, *Phys. Rev. Lett.* **64** (1990) 615.
- [32] S. Dodelson and L. M. Widrow, *Sterile-neutrinos as dark matter*, *Phys. Rev. Lett.* **72** (1994) 17–20, [[hep-ph/9303287](#)].
- [33] K. Abazajian, G. M. Fuller, and M. Patel, *Sterile neutrino hot, warm, and cold dark matter*, *Phys. Rev.* **D64** (2001) 023501, [[astro-ph/0101524](#)].
- [34] R. D. Peccei and H. R. Quinn, *CP conservation in the presence of pseudoparticles*, *Phys. Rev. Lett.* **38** (Jun, 1977) 1440–1443.
- [35] R. D. Peccei and H. R. Quinn, *Constraints imposed by CP conservation in the presence of pseudoparticles*, *Phys. Rev. D* **16** (Sep, 1977) 1791–1797.
- [36] L. J. Rosenberg and K. A. van Bibber, *Searches for invisible axions*, *Phys. Rept.* **325** (2000) 1–39.
- [37] H.-C. Cheng, J. L. Feng, and K. T. Matchev, *Kaluza-klein dark matter*, *Phys. Rev. Lett.* **89** (2002) 211301, [[hep-ph/0207125](#)].
- [38] K. Agashe and G. Servant, *Warped unification, proton stability and dark matter*, *Phys. Rev. Lett.* **93** (2004) 231805, [[hep-ph/0403143](#)].
- [39] K.-m. Cheung and G. L. Landsberg, *Kaluza-klein states of the standard model gauge bosons: Constraints from high energy experiments*, *Phys. Rev.* **D65** (2002) 076003, [[hep-ph/0110346](#)].

- [40] G. Servant and T. M. P. Tait, *Is the lightest kaluza-klein particle a viable dark matter candidate?*, *Nucl. Phys.* **B650** (2003) 391–419, [[hep-ph/0206071](#)].
- [41] E. W. Kolb, D. J. H. Chung, and A. Riotto, *Wimpzillas!*, [hep-ph/9810361](#).
- [42] C. Boehm, P. Fayet, and J. Silk, *Light and heavy dark matter particles*, *Phys. Rev.* **D69** (2004) 101302, [[hep-ph/0311143](#)].
- [43] A. Birkedal-Hansen and J. G. Wacker, *Scalar dark matter from theory space*, *Phys. Rev.* **D69** (2004) 065022, [[hep-ph/0306161](#)].
- [44] H.-C. Cheng and I. Low, *Tev symmetry and the little hierarchy problem*, *JHEP* **09** (2003) 051, [[hep-ph/0308199](#)].
- [45] M. Srednicki, R. Watkins, and K. A. Olive, *Calculations of relic densities in the early universe*, *Nucl. Phys.* **B310** (1988) 693.
- [46] S. Kolb, M. Hirsch, H. V. Klapdor-Kleingrothaus, and O. Panella, *Collider signatures of sneutrino cold dark matter*, *Phys. Lett.* **B478** (2000) 262–268, [[hep-ph/9910542](#)].
- [47] J. Bernstein, *Kinetic theory in the expanding universe*, . CAMBRIDGE, USA: UNIV. PR. (1988) 149p.
- [48] S. H. Hansen, G. Mangano, A. Melchiorri, G. Miele, and O. Pisanti, *Constraining neutrino physics with bbn and cmb*, *Phys. Rev.* **D65** (2002) 023511, [[astro-ph/0105385](#)].
- [49] P. Gondolo and G. Gelmini, *Cosmic abundances of stable particles: Improved analysis*, *Nucl. Phys.* **B360** (1991) 145–179.
- [50] K. Griest and D. Seckel, *Three exceptions in the calculation of relic abundances*, *Phys. Rev.* **D43** (1991) 3191–3203.
- [51] J. Edsjo and P. Gondolo, *Neutralino relic density including coannihilations*, *Phys. Rev.* **D56** (1997) 1879–1894, [[hep-ph/9704361](#)].
- [52] A. Hsieh and E. Yehudai, *HIP: Symbolic high-energy physics calculations*, *Comput. Phys.* **6** (1992) 253–261.
- [53] I. Wolfram Research, *Mathematica Edition: Version 5.2*, wolfram research, inc. ed., 2005. Champaign, Illinois.
- [54] **CompHEP** Collaboration, E. Boos *et. al.*, *Comphep 4.4: Automatic computations from lagrangians to events*, *Nucl. Instrum. Meth.* **A534** (2004) 250–259, [[hep-ph/0403113](#)].
- [55] H. E. Haber and G. L. Kane, *The search for supersymmetry: probing physics beyond the standard model*, *Phys. Rept.* **117** (1985) 75.

- 
- [56] S. Weinberg, *A model of leptons*, *Phys. Rev. Lett.* **19** (1967) 1264–1266.
- [57] S. L. Glashow, *Partial symmetries of weak interactions*, *Nucl. Phys.* **22** (1961) 579–588.
- [58] A. Salam, *Weak and electromagnetic interactions*, . Originally printed in \*Svartholm: Elementary Particle Theory, Proceedings Of The Nobel Symposium Held 1968 At Lerum, Sweden\*, Stockholm 1968, 367-377.
- [59] S. Dimopoulos and S. Raby, *Supercolor*, *Nucl. Phys.* **B192** (1981) 353.
- [60] E. Witten, *Dynamical breaking of supersymmetry*, *Nucl. Phys.* **B188** (1981) 513.
- [61] M. Dine, W. Fischler, and M. Srednicki, *Supersymmetric technicolor*, *Nucl. Phys.* **B189** (1981) 575–593.
- [62] S. Dimopoulos and H. Georgi, *Softly broken supersymmetry and  $su(5)$* , *Nucl. Phys.* **B193** (1981) 150.
- [63] N. Sakai, *Naturalness in supersymmetric guts*, *Zeit. Phys.* **C11** (1981) 153.
- [64] R. K. Kaul and P. Majumdar, *Cancellation of quadratically divergent mass corrections in globally supersymmetric spontaneously broken gauge theories*, *Nucl. Phys.* **B199** (1982) 36.
- [65] L. E. Ibanez and G. G. Ross,  *$Su(2)_l \times u(1)$  symmetry breaking as a radiative effect of supersymmetry breaking in guts*, *Phys. Lett.* **B110** (1982) 215–220.
- [66] J. R. Ellis, D. V. Nanopoulos, and K. Tamvakis, *Grand unification in simple supergravity*, *Phys. Lett.* **B121** (1983) 123.
- [67] L. Alvarez-Gaume, J. Polchinski, and M. B. Wise, *Minimal low-energy supergravity*, *Nucl. Phys.* **B221** (1983) 495.
- [68] U. Amaldi, W. de Boer, and H. Furstenuau, *Comparison of grand unified theories with electroweak and strong coupling constants measured at lep*, *Phys. Lett.* **B260** (1991) 447–455.
- [69] J. R. Ellis, S. Kelley, and D. V. Nanopoulos, *Probing the desert using gauge coupling unification*, *Phys. Lett.* **B260** (1991) 131–137.
- [70] C. Giunti, C. W. Kim, and U. W. Lee, *Running coupling constants and grand unification models*, *Mod. Phys. Lett.* **A6** (1991) 1745–1755.
- [71] P. Langacker and M.-x. Luo, *Implications of precision electroweak experiments for  $m(t)$ ,  $\rho(0)$ ,  $\sin^2\theta(w)$  and grand unification*, *Phys. Rev.* **D44** (1991) 817–822.

- [72] **Particle Data Group** Collaboration, W. M. Yao *et. al.*, *Review of particle physics*, *J. Phys.* **G33** (2006) 1–1232. and 2007 partial update (<http://pdg.lbl.gov>).
- [73] S. P. Martin, *A supersymmetry primer*, [hep-ph/9709356](https://arxiv.org/abs/hep-ph/9709356).
- [74] J. D. Lykken, *Introduction to supersymmetry*, [hep-th/9612114](https://arxiv.org/abs/hep-th/9612114).
- [75] H. P. Nilles, *Supersymmetry, supergravity and particle physics*, *Phys. Rept.* **110** (1984) 1.
- [76] S. R. Coleman and J. Mandula, *All possible symmetries of the s matrix*, *Phys. Rev.* **159** (1967) 1251–1256.
- [77] R. Haag, J. T. Lopuszanski, and M. Sohnius, *All possible generators of supersymmetries of the s matrix*, *Nucl. Phys.* **B88** (1975) 257.
- [78] J. Wess and J. Bagger, *Supersymmetry and supergravity*, . Princeton, USA: Univ. Pr. (1983) 259 p.
- [79] J. Wess and B. Zumino, *Supergauge invariant extension of quantum electrodynamics*, *Nucl. Phys.* **B78** (1974) 1.
- [80] P. Fayet and J. Iliopoulos, *Spontaneously broken supergauge symmetries and goldstone spinors*, *Phys. Lett.* **B51** (1974) 461–464.
- [81] L. O’Raifeartaigh, *Spontaneous symmetry breaking for chiral scalar superfields*, *Nucl. Phys.* **B96** (1975) 331.
- [82] L. Girardello and M. T. Grisaru, *Soft breaking of supersymmetry*, *Nucl. Phys.* **B194** (1982) 65.
- [83] J. F. Gunion and H. E. Haber, *Higgs bosons in supersymmetric models. 1*, *Nucl. Phys.* **B272** (1986) 1.
- [84] **ALEPH, DELPHI, L3 and OPAL** Collaboration, *Search for the standard model higgs boson at LEP*, [hep-ex/0107029](https://arxiv.org/abs/hep-ex/0107029). LEP Higgs Working Group for Higgs boson searches.
- [85] **CDF** Collaboration, A. A. Affolder *et. al.*, *Search for neutral supersymmetric higgs bosons in  $p\bar{p}$  collisions at  $\sqrt{s} = 1.8$  TeV*, *Phys. Rev. Lett.* **86** (2001) 4472–4478, [[hep-ex/0010052](https://arxiv.org/abs/hep-ex/0010052)].
- [86] B. C. Allanach, A. Djouadi, J. L. Kneur, W. Porod, and P. Slavich, *Precise determination of the neutral higgs boson masses in the mssm*, *JHEP* **09** (2004) 044, [[hep-ph/0406166](https://arxiv.org/abs/hep-ph/0406166)].

- 
- [87] G. Degrossi, S. Heinemeyer, W. Hollik, P. Slavich, and G. Weiglein, *Towards high-precision predictions for the mssm higgs sector*, *Eur. Phys. J.* **C28** (2003) 133–143, [[hep-ph/0212020](#)].
- [88] T. Han and R. Hempfling, *Messenger sneutrinos as cold dark matter*, *Phys. Lett.* **B415** (1997) 161–169, [[hep-ph/9708264](#)].
- [89] T. Han, D. Marfatia, and R.-J. Zhang, *A gauge-mediated supersymmetry breaking model with an extra singlet higgs field*, *Phys. Rev.* **D61** (2000) 013007, [[hep-ph/9906508](#)].
- [90] D. Hooper, J. March-Russell, and S. M. West, *Asymmetric sneutrino dark matter and the  $\Omega(b)/\Omega(DM)$  puzzle*, *Phys. Lett.* **B605** (2005) 228–236, [[hep-ph/0410114](#)].
- [91] T. Asaka, K. Ishiwata, and T. Moroi, *Right-handed sneutrino as cold dark matter*, *Phys. Rev.* **D73** (2006) 051301, [[hep-ph/0512118](#)].
- [92] H.-S. Lee, K. T. Matchev, and S. Nasri, *Revival of the thermal sneutrino dark matter*, *Phys. Rev.* **D76** (2007) 041302, [[hep-ph/0702223](#)].
- [93] S. Gopalakrishna, A. de Gouvea, and W. Porod, *Right-handed sneutrinos as nonthermal dark matter*, *JCAP* **0605** (2006) 005, [[hep-ph/0602027](#)].
- [94] S. Dimopoulos, G. F. Giudice, and A. Pomarol, *Dark matter in theories of gauge-mediated supersymmetry breaking*, *Phys. Lett.* **B389** (1996) 37–42, [[hep-ph/9607225](#)].
- [95] T. Bringmann, F. Borzumati, and P. Ullio, *Dark matter from late decays and the small-scale structure problems*, [hep-ph/0701007](#).
- [96] L. E. Ibanez, *The scalar neutrinos as the lightest supersymmetric particles and cosmology*, *Phys. Lett.* **B137** (1984) 160.
- [97] J. S. Hagelin, G. L. Kane, and S. Raby, *Perhaps scalar neutrinos are the lightest supersymmetric partners*, *Nucl. Phys.* **B241** (1984) 638.
- [98] J. R. Ellis, J. S. Hagelin, D. V. Nanopoulos, K. A. Olive, and M. Srednicki, *Supersymmetric relics from the big bang*, *Nucl. Phys.* **B238** (1984) 453–476.
- [99] T. Falk, K. A. Olive, and M. Srednicki, *Heavy sneutrinos as dark matter*, *Phys. Lett.* **B339** (1994) 248–251, [[hep-ph/9409270](#)].
- [100] K. Freese, *Can scalar neutrinos or massive dirac neutrinos be the missing mass?*, *Phys. Lett.* **B167** (1986) 295.
- [101] **ALEPH** Collaboration, A. Heister *et. al.*, *Absolute lower limits on the masses of selectrons and sneutrinos in the MSSM*, *Phys. Lett.* **B544** (2002) 73–88, [[hep-ex/0207056](#)].

- [102] A. Djouadi, J. Kalinowski, and P. M. Zerwas, *Two- and three-body decay modes of susy higgs particles*, *Z. Phys.* **C70** (1996) 435–448, [[hep-ph/9511342](#)].
- [103] G. Belanger, F. Boudjema, A. Pukhov, and S. Rosier-Lees, *A lower limit on the neutralino mass in the MSSM with non- universal gaugino masses. ((t)) ((u))*, [hep-ph/0212227](#).
- [104] J. R. Ellis, T. Falk, G. Ganis, K. A. Olive, and M. Srednicki, *The CMSSM parameter space at large  $\tan\beta$* , *Phys. Lett.* **B510** (2001) 236–246, [[hep-ph/0102098](#)].
- [105] L. Roszkowski, R. Ruiz de Austri, and T. Nihei, *New cosmological and experimental constraints on the CMSSM*, *JHEP* **08** (2001) 024, [[hep-ph/0106334](#)].
- [106] N. Arkani-Hamed, L. J. Hall, H. Murayama, D. R. Smith, and N. Weiner, *Small neutrino masses from supersymmetry breaking*, *Phys. Rev.* **D64** (2001) 115011, [[hep-ph/0006312](#)].
- [107] D. R. Smith and N. Weiner, *Inelastic dark matter*, *Phys. Rev.* **D64** (2001) 043502, [[hep-ph/0101138](#)].
- [108] D. R. Smith and N. Weiner, *Inelastic dark matter at DAMA, CDMS and future experiments*, *Nucl. Phys. Proc. Suppl.* **124** (2003) 197–200, [[astro-ph/0208403](#)].
- [109] D. Tucker-Smith and N. Weiner, *The status of inelastic dark matter*, *Phys. Rev.* **D72** (2005) 063509, [[hep-ph/0402065](#)].
- [110] Y. Grossman and H. E. Haber, *Sneutrino mixing phenomena*, *Phys. Rev. Lett.* **78** (1997) 3438–3441, [[hep-ph/9702421](#)].
- [111] A. Dedes, H. E. Haber, and J. Rosiek, *Seesaw mechanism in the sneutrino sector and its consequences*, [0707.3718](#).
- [112] L. J. Hall, T. Moroi, and H. Murayama, *Sneutrino cold dark matter with lepton-number violation*, *Phys. Lett.* **B424** (1998) 305–312, [[hep-ph/9712515](#)].
- [113] M. Hirsch, H. V. Klapdor-Kleingrothaus, and S. G. Kovalenko, *B-l violating masses in softly broken supersymmetry*, *Phys. Lett.* **B398** (1997) 311–314, [[hep-ph/9701253](#)].
- [114] H. V. Klapdor-Kleingrothaus, S. Kolb, and V. A. Kuzmin, *Light lepton number violating sneutrinos and the baryon number of the universe*, *Phys. Rev.* **D62** (2000) 035014, [[hep-ph/9909546](#)].
- [115] M. Hirsch, H. V. Klapdor-Kleingrothaus, and S. G. Kovalenko, *Sneutrino oscillations and neutrinoless double beta decay*, *Phys. Lett.* **B403** (1997) 291–296.

- 
- [116] G. 't Hooft and M. J. G. Veltman, *Scalar one loop integrals*, *Nucl. Phys.* **B153** (1979) 365–401.
- [117] P. Minkowski,  $\mu \rightarrow e\gamma$  at a rate of one out of 1-billion muon decays?, *Phys. Lett.* **B67** (1977) 421.
- [118] M. Gell-Mann, P. Ramond, and R. Slansky, *Supergravity*, p. 135. North Holland, Amsterdam, 1979.
- [119] T. Yanagida, *Proceedings of the Workshop on Unified Theory and Baryon Number in the Universe*, p. 95. KEK, Tsukuba, Japan, 1979.
- [120] R. N. Mohapatra and G. Senjanovic, *Neutrino mass and spontaneous parity nonconservation*, *Phys. Rev. Lett.* **44** (1980) 912.
- [121] R. N. Mohapatra and G. Senjanovic, *Neutrino masses and mixings in gauge models with spontaneous parity violation*, *Phys. Rev.* **D23** (1981) 165.
- [122] J. Schechter and J. W. F. Valle, *Neutrino masses in  $SU(2) \times U(1)$  theories*, *Phys. Rev.* **D22** (1980) 2227.
- [123] J. R. Ellis, R. A. Flores, and J. D. Lewin, *Rates for inelastic nuclear excitation by dark matter particles*, *Phys. Lett.* **B212** (1988) 375.
- [124] G. D. Starkman and D. N. Spergel, *Proposed new technique for detecting supersymmetric dark matter*, *Phys. Rev. Lett.* **74** (1995) 2623–2625.
- [125] A. K. Drukier, K. Freese, and D. N. Spergel, *Detecting Cold Dark Matter candidates*, *Phys. Rev.* **D33** (1986) 3495–3508.
- [126] K. Freese, J. A. Frieman, and A. Gould, *Signal modulation in Cold Dark Matter detection*, *Phys. Rev.* **D37** (1988) 3388.
- [127] R. H. Helm, *Inelastic and elastic scattering of 187-mev electrons from selected even-even nuclei*, *Phys. Rev.* **104** (Dec, 1956) 1466–1475.
- [128] A. Bottino, F. Donato, N. Fornengo, and S. Scopel, *Size of the neutralino nucleon cross-section in the light of a new determination of the pion nucleon sigma term*, *Astropart. Phys.* **18** (2002) 205–211, [[hep-ph/0111229](#)].
- [129] J. R. Ellis, K. A. Olive, Y. Santoso, and V. C. Spanos, *Update on the direct detection of supersymmetric dark matter*, *Phys. Rev.* **D71** (2005) 095007 and references therein, [[hep-ph/0502001](#)].
- [130] R. Bernabei *et al.*, *Investigating the DAMA annual modulation data in the framework of inelastic dark matter*, *Eur. Phys. J.* **C23** (2002) 61–64.
- [131] M. W. Goodman and E. Witten, *Detectability of certain dark-matter candidates*, *Phys. Rev.* **D31** (1985) 3059.

- [132] G. F. Giudice and E. Roulet, *Energetic neutrinos from supersymmetric dark matter*, *Nucl. Phys.* **B316** (1989) 429.
- [133] M. Drees and M. M. Nojiri, *New contributions to coherent neutralino - nucleus scattering*, *Phys. Rev.* **D47** (1993) 4226–4232, [[hep-ph/9210272](#)].
- [134] M. Drees and M. Nojiri, *Neutralino - nucleon scattering revisited*, *Phys. Rev.* **D48** (1993) 3483–3501, [[hep-ph/9307208](#)].
- [135] P. Belli, *Review of direct searches for wimps (non-cryogenic detectors)*, Sendai, Japan, September 11-15, 2007. Talk given at the Tenth International Conference on Topics in Astroparticle and Underground Physics (Taup 2007).
- [136] G. Gerbier and D. Bauer, *Review of direct searches for wimps (cryogenic detectors)*, Sendai, Japan, September 11-15, 2007. Talk given at the Tenth International Conference on Topics in Astroparticle and Underground Physics (Taup 2007).
- [137] R. Bernabei *et al.*, *Dark matter search*, *Riv. Nuovo Cim.* **26N1** (2003) 1–73, [[astro-ph/0307403](#)].
- [138] R. Bernabei *et al.*, *Dark matter particles in the galactic halo: Results and implications from DAMA/NaI*, *Int. J. Mod. Phys.* **D13** (2004) 2127–2160, [[astro-ph/0501412](#)].
- [139] R. Bernabei *et al.*, *Investigating pseudoscalar and scalar dark matter*, *Int. J. Mod. Phys.* **A21** (2006) 1445–1470, [[astro-ph/0511262](#)].
- [140] R. Bernabei *et al.*, *Investigating halo substructures with annual modulation signature*, *Eur. Phys. J.* **C47** (2006) 263–271, [[astro-ph/0604303](#)].
- [141] R. Bernabei *et al.*, *On electromagnetic contributions in WIMP quests*, *Int. J. Mod. Phys.* **A22** (2007) 3155–3168, [[0706.1421](#)].
- [142] R. Bernabei *et al.*, *Particle dark matter: From dama/naï to dama/libra*, *Phys. Atom. Nucl.* **69** (2006) 2056–2067.
- [143] **CDMS** Collaboration, M. S. Armel-Funkhouser *et al.*, *Exclusion limits on the WIMP nucleon cross-section from the first run of the Cryogenic Dark Matter Search in the soudan underground lab*, *Phys. Rev.* **D72** (2005) 052009, [[astro-ph/0507190](#)].
- [144] **CDMS** Collaboration, D. S. Akerib *et al.*, *Limits on spin-independent WIMP nucleon interactions from the two-tower run of the Cryogenic Dark Matter Search*, *Phys. Rev. Lett.* **96** (2006) 011302, [[astro-ph/0509259](#)].
- [145] **XENON** Collaboration, J. Angle *et al.*, *First results from the XENON10 dark matter experiment at the Gran Sasso National Laboratory*, [0706.0039](#).

- [146] G. Belanger, F. Boudjema, A. Cottrant, A. Pukhov, and A. Semenov, *WMAP constraints on SUGRA models with non-universal gaugino masses and prospects for direct detection*, *Nucl. Phys.* **B706** (2005) 411–454, [[hep-ph/0407218](#)].
- [147] M. Beck *et. al.*, *Searching for dark matter with the enriched detectors of the heidelberg - moscow double beta decay experiment*, *Phys. Lett.* **B336** (1994) 141–146.
- [148] A. Bottino, F. Donato, N. Fornengo, and S. Scopel, *Do current WIMP direct measurements constrain light relic neutralinos?*, *Phys. Rev.* **D72** (2005) 083521, [[hep-ph/0508270](#)].
- [149] **BESS** Collaboration, S. Orito *et. al.*, *Precision measurement of cosmic-ray antiproton spectrum*, *Phys. Rev. Lett.* **84** (2000) 1078–1081, [[astro-ph/9906426](#)].
- [150] **BESS** Collaboration, T. Maeno *et. al.*, *Successive measurements of cosmic-ray antiproton spectrum in a positive phase of the solar cycle*, *Astropart. Phys.* **16** (2001) 121–128, [[astro-ph/0010381](#)].
- [151] **PAMELA** Collaboration, M. Boezio *et. al.*, *The space experiment PAMELA*, 2004.
- [152] **AMS** Collaboration, M. Aguilar *et. al.*, *The Alpha Magnetic Spectrometer (AMS) on the International Space Station. I: Results from the test flight on the space shuttle*, *Phys. Rept.* **366** (2002) 331–405.
- [153] K. Mori *et. al.*, *A novel antimatter detector based on X-ray deexcitation of exotic atoms*, *Astrophys. J.* **566** (2002) 604–616, [[astro-ph/0109463](#)].
- [154] J. Koglin, Fermilab, May 10-12, 2007. Talk given at the The Hunt for Dark Matter.
- [155] F. Donato, N. Fornengo, D. Maurin, P. Salati, and R. Taillet, *Antiprotons in cosmic rays from neutralino annihilation*, *Phys. Rev.* **D69** (2004) 063501, [[astro-ph/0306207](#)].
- [156] T. Sjostrand *et. al.*, *High-energy-physics event generation with pythia 6.1*, *Comput. Phys. Commun.* **135** (2001) 238–259, [[hep-ph/0010017](#)].
- [157] F. Donato, N. Fornengo, and P. Salati, *Antideuterons as a signature of supersymmetric dark matter*, *Phys. Rev.* **D62** (2000) 043003, [[hep-ph/9904481](#)].
- [158] **MAGIC** Collaboration, C. Baixeras, *The magic telescope*, *Nucl. Phys. Proc. Suppl.* **114** (2003) 247–252.
- [159] **HESS** Collaboration, <http://www.mpi-hd.mpg.de/hfm/HESS/HESS.html>, see references therein.

- [160] S. Hunter *et al.*, *EGRET observations of the diffuse gamma-ray emission from the galactic plane*, *Astrophys. J.* **481** (1997) 205.
- [161] H. A. Mayer-Hasselwander *et al.*, *High-energy gamma ray emission from the galactic center*, *Astron. Astrophys.* **335** (1998) 161–172.
- [162] **GLAST** Collaboration, A. Morselli, A. Lionetto, A. Cesarini, F. Fucito, and P. Ullio, *Search for dark matter with GLAST*, *Nucl. Phys. Proc. Suppl.* **113** (2002) 213–220, [[astro-ph/0211327](#)].
- [163] N. Fornengo, L. Pieri, and S. Scopel, *Neutralino annihilation into gamma-rays in the milky way and in external galaxies*, *Phys. Rev.* **D70** (2004) 103529, [[hep-ph/0407342](#)].
- [164] **MACRO** Collaboration, M. Ambrosio *et al.*, *Limits on dark matter WIMPs using upward-going muons in the MACRO detector*, *Phys. Rev.* **D60** (1999) 082002, [[hep-ex/9812020](#)].
- [165] **Super-Kamiokande** Collaboration, A. Habig, *An indirect search for WIMPs with Super-Kamiokande*, [hep-ex/0106024](#).
- [166] **IceCube** Collaboration, A. Achterberg *et al.*, *The IceCube collaboration: Contributions to the 29th international cosmic ray conference (ICRC 2005), Pune, India, Aug. 2005*, [astro-ph/0509330](#).
- [167] **ANTARES** Collaboration, <http://antares.in2p3.fr/index.html>, see references therein.
- [168] **IceCube** Collaboration, J. Ahrens *et al.*, *Sensitivity of the icecube detector to astrophysical sources of high energy muon neutrinos*, *Astropart. Phys.* **20** (2004) 507–532, [[astro-ph/0305196](#)].
- [169] **NEMO** Collaboration, <http://nemo.web.lal.in2p3.fr/>, see references therein.
- [170] A. Gould, *Resonant enhancements in wimp capture by the earth*, *Astrophys. J.* **321** (1987) 571.
- [171] A. Gould, *Wimp distribution in and evaporation from the sun*, *Astrophys. J.* **321** (1987) 560.
- [172] J. Lundberg and J. Edsjo, *Wimp diffusion in the solar system including solar depletion and its effect on earth capture rates*, *Phys. Rev.* **D69** (2004) 123505, [[astro-ph/0401113](#)].
- [173] M. Cirelli *et al.*, *Spectra of neutrinos from dark matter annihilations*, *Nucl. Phys.* **B727** (2005) 99–138, [[hep-ph/0506298](#)].
- [174] F. Donato *et al.*, *Antiprotons from spallation of cosmic rays on interstellar matter*, *Astrophys. J.* **536** (2001) 172–184, [[astro-ph/0103150](#)].

- [175] D. Maurin, F. Donato, R. Taillet, and P. Salati, *Cosmic rays below  $Z=30$  in a diffusion model: new constraints on propagation parameters*, *Astrophys. J.* **555** (2001) 585–596, [[astro-ph/0101231](#)].
- [176] **WiZard/CAPRICE** Collaboration, M. Boezio *et. al.*, *The cosmic-ray anti-proton flux between 3-GeV and 49-GeV*, *Astrophys. J.* **561** (2001) 787–799, [[astro-ph/0103513](#)].
- [177] A. Colaleo, “*Search for MSSM topologies at LEP and lower limit on LSP mass.*” Prepared for 9th International Conference on Supersymmetry and Unification of Fundamental Interactions (SUSY01), Dubna, Russia, 11-17 Jun 2001.
- [178] **DELPHI 2001-085 CONF 513** Collaboration, J. Abdallah *et. al.*, *Searches for supersymmetric particles in  $e+e-$  collisions up to 208 GeV and interpretation of the results within the MSSM*, 2001.
- [179] **LEP2 Joint SUSY Working Group** Collaboration.  
<http://lepsusy.web.cern.ch/lepsusy/>.
- [180] **Muon G-2** Collaboration, G. W. Bennett *et. al.*, *Final report of the muon  $E821$  anomalous magnetic moment measurement at BNL*, *Phys. Rev.* **D73** (2006) 072003, [[hep-ex/0602035](#)].
- [181] J. Bijnens and J. Prades, *The hadronic light-by-light contribution to the muon anomalous magnetic moment: Where do we stand?*, *Mod. Phys. Lett.* **A22** (2007) 767–782, [[hep-ph/0702170](#)].
- [182] **D0** Collaboration, V. M. Abazov *et. al.*, *Search for  $B_s \rightarrow \mu^+ \mu^-$  at D0*, **0707.3997**.
- [183] A. Dedes, H. K. Dreiner, U. Nierste, and P. Richardson, *Trilepton events and  $b/s \rightarrow \mu^+ \mu^-$ : No-lose for  $msugra$  at the tevatron?*, [hep-ph/0207026](#).
- [184] **Heavy Flavor Averaging Group (HFAG)** Collaboration, E. Barberio *et. al.*, *Averages of  $b$ -hadron properties at the end of 2005*, [hep-ex/0603003](#).
- [185] M. Ciuchini, G. Degrassi, P. Gambino, and G. F. Giudice, *Next-to-leading QCD corrections to  $B \rightarrow X_s \gamma$  in supersymmetry*, *Nucl. Phys.* **B534** (1998) 3–20, [[hep-ph/9806308](#)].
- [186] M. Misiak *et. al.*, *The first estimate of  $BR(B \rightarrow X_s \gamma)$  at  $\mathcal{O}(\alpha(s)^2)$* , *Phys. Rev. Lett.* **98** (2007) 022002, [[hep-ph/0609232](#)].
- [187] B. C. Regan, E. D. Commins, C. J. Schmidt, and D. DeMille, *New limit on the electron electric dipole moment*, *Phys. Rev. Lett.* **88** (2002) 071805.